A GENERAL FRAMEWORK FOR INFERRING THE DEVELOPMENTAL CAUSES OF MODULARITY OF MORPHOLOGICAL VARIATION WITH APPLICATIONS TO THE CRANIOMANDIBULAR COMPLEX IN RODENTS

by

Eladio J. Márquez

A dissertation submitted in partial fulfillment
of the requirements for the degree of
Doctor of Philosophy
(Biology)
in The University of Michigan
2009

Doctoral Committee:

Associate Research Scientist Miriam L. Zelditch, Co-Chair
Professor Philip Myers, Co-Chair
Professor William L. Fink
Professor Daniel C. Fisher
Professor H. David Sheets, Canisius College

© Eladio J. Márquez
2009

To Rosa
To my parents, Gustavo and Emma

ACKNOWLEDGEMENTS

For their unconditional support, love and infinite patience throughout these years, I thank my family, and especially my wife, Rosa, my children, Samuel and Veronica, and my parents, Gustavo and Emma, whose effort and sacrifice has made it possible for me to get this far. For her hard work and rigorousness, and her unequalled dedication to her advisor's role, I thank Miriam Zelditch, who is largely responsible for this dissertation not being just about statistical methods. For being a friend and a colleague, a voice and hand of support when I needed them the most, I thank Lacey Knowles, whose rapid comprehension of my personal and academic circumstances opened doors for me that, on hindsight, were quite instrumental for my arriving at this stage of my career. For their prompt advise when it was needed, saving me from weeks, sometimes months, of futile pursuit, I thank the other members of my committee, Phil Myers, Dave Sheets, Dan Fisher, and Bill Fink. For their frequent support and assistance on academic and personal grounds, I thank my friends at the Museum of Zoology and EEB, too many to name in this space. Special thanks to UMMZ and EEB personnel, for making my life through school easier, even possible: Norah Daugherty, Steve Hinshaw, Jane Sullivan, Christy Byks-Jazayeri, Julia Eussen, LaDonna Walker, and Lisa Herring. Collection of museum samples for this work was made possible thanks to the assistance of Phil Myers and Steve Hinshaw from UMMZ, Michael Carleton and Helen Kafka from USNM, Mark Hafner from LSUMZ, Craig Ludwig from MVZ, and Bruce Patterson from FMNH. Many of the ideas and innovations discussed in this dissertation were inspired and/or encouraged by conversations with many colleagues, notably Benedikt Hallgrímsson, Dean Adams, Jim Rohlf, Fred Bookstein, Günter Wagner, Chris Klingenberg, Markus Bastir, Jesús Marugán-Lobón, Neus Martínez-Abadías, Rebecca Young, Philip Mitteroecker, Leandro Monteiro, Brian Hall, Doug Futuyma, David Houle, Arnold Kluge, Scott Steppan, and Marcelo Weksler. Funding for my early years in the program was provided by Universidad Simón Bolívar (Caracas, Venezuela). This research was partially supported by the National Science Foundation under Doctoral Dissertation Improvement Grant No. 0407570. Financial support was also provided by a Hinsdale Fellowship from the UM Museum of Zoology, and by a Travel Scholarship from the Society for Integrative and Comparative Biology. Any opinions, findings, and conclusions or recommendations expressed in this material are those of the author and do not necessarily reflect the views of any of these people or institutions.

TABLE OF CONTENTS

DEDICATION ii

ACKNOWLEDGEMENTS iii

LIST OF FIGURES v

LIST OF TABLES vii

ABSTRACT viii

CHAPTER I: A GEOMETRIC FRAMEWORK FOR TESTING HYPOTHESES OF VARIATIONAL MODULARITY 1

- Abstract 1
- Introduction 2
- A Novel Statistical Framework for Studies of Variational Modularity 13
- Visualizing Modularity in Morphometric Data 25
- Relationship to Alternative Methods 27
- Correlations vs. Covariances in Studies of Modularity 32
- Conclusions 34
- Appendix 49

CHAPTER II: CAN MODULARITY EXPLAIN PATTERNS OF INTERSPECIFIC DISPARITY? A STUDY OF DEVELOPMENTAL CONSTRAINTS IN THE CRANIOMANDIBULAR COMPLEX OF ORYZOMYINE RODENTS 53

- Abstract 53
- Introduction 53
- Materials and Methods 56
- Results 81
- Discussion 98
- Appendices 152

BIBLIOGRAPHY 157

LIST OF FIGURES

Figure I.1. Schematic representation of pleiotropic interactions in the genotype-phenotype map 41
Figure I.2. Model of the effects of pleiotropic variation on phenotypic integration 42
Figure I.3. Simple example illustrating the overlap of successive patterns of modularity as postulated by the palimpsest model (Hallgrímsson et al. 2007) 43
Figure I.4. Partitions of the mandible used in simulations of modular covariation structure 44
Figure I.5. Relationship between number of fixed parameters (i.e., number of zeros in covariance matrices) and γ value computed for each model 45
Figure I.6. Example of visualizations of modular variation using part-whole PLS 46
Figure I.7. Results from application of Mitteroecker and Bookstein (2007) approach using simulated data 47
Figure I.8. Effect of incorrectly delimiting partitions as modules in PLS 48
Figure II.1. Phylogenetic relationships among species included in this study 118
Figure II.2. Diagrammatic representation of the lateral (top), mandible (middle), and ventral (bottom) views of the skull analyzed in this study 119
Figure II.3. Modules used to define hypotheses of modularity 120
Figure II.4. Most-highly supported models for *Holochilus chacarius* 130
Figure II.5. Part-whole PLS analysis based on best-supported modules for *Holochilus chacarius* for cranial and mandibular data sets 131
Figure II.6. Most-highly supported models for *Melanomys caliginosus* 132
Figure II.7. Part-whole PLS analysis based on best-supported modules for *Melanomys caliginosus* for cranial and mandibular data sets 133
Figure II.8. Most-highly supported models for *Microryzomys minutus* 134
Figure II.9. Part-whole PLS analysis based on best-supported modules for *Microryzomys minutus* for cranial and mandibular data sets 135

Figure II.10. Most-highly supported models for *Nectomys squamipes* 136
Figure II.11. Part-whole PLS analysis based on best-supported modules for *Nectomys squamipes* for cranial and mandibular data sets 137
Figure II.12. Most-highly supported models for *Oligoryzomys nigripes* 138
Figure II.13. Part-whole PLS analysis based on best-supported modules for *Oligoryzomys nigripes* for cranial and mandibular data sets 139
Figure II.14. Most-highly supported models for *Oryzomys couesi* 140
Figure II.15. Part-whole PLS analysis based on best-supported modules for *Oryzomys couesi* for cranial and mandibular data sets 141
Figure II.16. Most-highly supported models for *Oryzomys palustris* 142
Figure II.17. Part-whole PLS analysis based on best-supported modules for *Oryzomys palustris* for cranial and mandibular data sets 143
Figure II.18. Most-highly supported models for *Oryzomys xantheolus* 144
Figure II.19. Part-whole PLS analysis based on best-supported modules for *Oryzomys xantheolus* for cranial and mandibular data sets 145
Figure II.20. Most-highly supported models for *Sigmodontomys alfari* 146
Figure II.21. Part-whole PLS analysis based on best-supported modules for *Oryzomys xantheolus* for cranial and mandibular data sets 147
Figure II.22. Dendrograms showing similarity of oryzomyine species in model space 148
Figure II.23. Principal component analyses of mean shapes of craniomandibular data from nine species of oryzomyines 149
Figure II.24. Principal component analyses of mean shapes of skull shape data from seven species of oryzomyines 150
Figure II.25. Difference between (A) *H. chacarius* and (B) *S. alfari* and the mean of other seven oryzomyine species, computed after superimposing each pair of means using ordinary Procrustes superimposition 151

LIST OF TABLES

Table I.1. Modules of modularity used to simulate data with known patterns of covariation 37

Table I.2. Results from simulations, showing the measure of fit (γ^* values) obtained from fitting models H_0-H_{12} (Table I.1) to the data sets simulated assuming each of these models model (Table I.1) 38

Table I.3. Results from simulations, showing models supported by at least one jackknife sub-sample of each simulated data set, among the 620 models that include all possible combinations of models H_1-H_{12} (see Table I.2) 39

Table I.4. Results from application of Mitteroecker and Bookstein (2007) approach to simulated data 40

Table II.1. List of oryzomyine species and sample sizes (*N*) used in this study 108

Table II.2. Tests of homogeneity of samples included in this study 109

Table II.3. List of secreted and transcription factors used to build hypotheses of "mutational targets" tested in this study 110

Table II.4. Models used in initial tests 111

Table II.5. Best supported models for each species 112

Table II.6. List of a priori modules of the mandible supported by each species 116

Table II.7. Partial disparities contributed by each species to the total disparity among mean shapes of nine species of oryzomyines included in this study 117

ABSTRACT

Modularity is a principle of construction whereby individual units are internally cohesive and relatively autonomous from other such units. Modularity thus confers a degree of evolutionary autonomy to the sets of traits integrating a module, a feature hypothesized to enhance evolvability by allowing selection to optimize individual parts without interfering with others. Detecting modularity in morphological traits requires analyzing the structure of covariation because traits integrated by development into modules are expected to show stronger mutual covariation. However, unambiguous patterns of modularity are rare. That is because the developmental processes underlying most phenotypic traits share regulatory elements and/or have spatially overlapping effects. Pervasive interactions can produce the appearance of statistical integration among biologically modular traits. Herein, a statistical framework is provided that confronts these limitations on methods for inferring modularity from morphological data. The theoretical basis of this new method states that modules are subsets of dimensions embedded in phenotypic space, an approach that differs from previous ones by not defining modules as anatomical parts but rather as aspects of the variation of these parts. This abstraction allows traits to be integrated into more than one module and also suggests a natural approach for testing a priori hypotheses of modularity by fitting competing hypotheses to observed covariance matrices, searching for the best-supported causal explanations. A comprehensive method is developed and tested using simulated data, then used to address a major outstanding issue in evolutionary biology: whether the developmental processes that structure variation within populations bias the direction of long-term divergence. This hypothesis is tested by fitting multiple developmental models to both intraspecific and interspecific craniomandibular data obtained from a clade of ecologically diverse rodents. Results reveal a remarkable congruence among patterns within and between species, and they also suggest that there are different mechanisms by which modular variation arises within different parts of the skull, i.e., cranium and

mandible. That these structures have different dynamics both within and among species suggests that whether intraspecific variation constrains the direction of divergence may depend on mechanisms structuring modularity within populations.

CHAPTER I

A GEOMETRIC FRAMEWORK FOR TESTING HYPOTHESES OF VARIATIONAL MODULARITY

ABSTRACT

Modularity is defined as the relative autonomy (i.e., background-independence) of genetic interactions, the developmental processes regulated by these interactions, and the phenotypic traits produced by these processes. In morphological traits, modularity is evinced as strength of covariation (i.e., integration) within anatomical regions, and it is caused by common developmental pathways or genetic factors shared by these regions. Because distinct pathways may interact, share genetic components, and influence overlapping anatomical regions, it is not generally expected for variational (i.e., morphological) modules to display a simple pattern of strong integration within and weak or no integration outside modules. This does not necessarily imply that most morphological variation is integrated and non-modular, because most phenotypic traits are highly multidimensional, so that different sets of dimensions may show distinct patterns of integration. This section elaborates on this idea to propose a geometric framework in which variational modules are defined as subspaces embedded within the space occupied by the entire phenotype. Although this is perhaps an unorthodox idea in that it seeks to re-interpret pervasive integration as complex modularity, it is consistent with developmental and quantitative genetic explanations for the origin of variational modules. A statistical methodology is then proposed to deal with the difficult problem of inferring individual modules from morphometric covariation structure. The proposed approach uses the standard formalism of goodness of fit tests to compare observed and expected covariance matrices, where the latter are obtained by partitioning the original data set into modules as predicted by one or more theories, thus allowing testing hypotheses of modularity of any conceivable complexity. The utility of this approach is confirmed using a simulated data set based on a real anatomical structure (the rodent mandible). The relationship of this approach to current methodologies is also discussed.

INTRODUCTION

Heritable variation is essential for most forms of evolutionary sorting, including natural selection, and, for that reason, variation is arguably the central concept in evolutionary biology (Hallgrímsson and Hall 2005). Yet, the processes producing and patterning variation are remarkably complex, and thus remain poorly understood. Whereas the primary sources of variation can be broadly categorized as "environmental" or "mutational," the magnitude and pattern of variation is a function of a combination of population-genetic dynamics and the array of processes collectively known as the "genotype-phenotype map" (Wagner and Altenberg 1996). The genotype-phenotype map encompasses the network of epigenetic and epistatic interactions among genes and gene products through which genetic variation is transduced to phenotypic variation (Wagner 1984), and the complexity of this map means that there is usually no direct correspondence between different levels of variation. Therefore, the causes of phenotypic variation cannot be inferred given only knowledge about correlations between genotype and phenotype (Mackay 2001; Klingenberg 2008): Additional information about developmental processes underlying the map is also needed (Houle 1991; Cowley and Atchley 1992; Steppan et al. 2002). The properties of the map that are currently receiving most attention include phenotypic integration (Olson and Miller 1958; Pigliucci and Preston 2004), modularity (Wagner and Altenberg 1996), developmental instability (Markow 1993), canalization (Waddington 1942; Hallgrímsson et al. 2002; Dworkin 2005; Zelditch 2005), plasticity (Pigliucci 2001; West-Eberhard 2003), and robustness (de Visser et al. 2003). These properties channel, alter or mold genetic and environmental variation, and therefore are all causally related to the magnitude and structure of phenotypic variation (Nijhout and Davidowitz 2003). Whereas it is undisputed that these properties interact, the precise nature of the relationships among them is much debated (Hallgrímsson et al. 2002). For example, it is presently unclear whether the mechanisms of canalization are the same as those that stabilize development against random noise (Klingenberg and McIntyre 1998; Debat et al. 2000; Réale and Roff 2003).

Not all properties of genotype-phenotype map have a similar effect on variation. Whereas canalization and stabilization regulate its magnitude, either increasing it systematically as a response to specific cues (i.e., plasticity) or keeping it low in the presence of perturbations (i.e., robustness), modularity and integration structure variation by distributing it unequally among traits. Modules are usually defined as relatively integrated components of the developmental system, dissociable from and capable of interacting with other such units without losing their integrity (Bolker 2000). Modules are also referred to as the building blocks of complex morphological structures (Atchley and Hall 1991), and more generally, modules are often regarded as hierarchical structures, in that modules can be nested within larger modules (Raff 1996). Finally, as units of the genotype-phenotype map, modules are expected to exhibit certain degree of evolutionary autonomy (Riedl 1977; Raff 1996; Wagner and Altenberg 1996; Wagner and Cheverud 2007). Although all types of modules share these general properties, modules can be distinguished with respect to their general functions within the genotype-phenotype map. Wagner and Mezey (2004) distinguish three general types of modules: (1) developmental modules, (2) genetic process modules, and (3) variational modules. Developmental modules consist of morphogenetic processes that can be deployed relatively independently from their background and that interact to form an individual, locally restricted component of a complex system. Genetic process modules are broadly defined as any subset of the genome consisting of relatively constant secreted and transcription factors that jointly perform a typical regulatory function and can be deployed with little modification in disparate tissues or developmental processes (Gerhart and Kirschner 1997; Kirschner and Gerhart 1998). Genetic process modules are commonly associated with *cis*-regulatory activity (Carroll et al. 2004), and most of the best characterized cases correspond to generic cell-cell and matrix-cell signaling pathways comprising highly conserved genes, such as the Delta-Notch signaling pathway (Henrique et al. 1995; De Celis 2004). Variational modules are sets of phenotypic traits characterized by tighter statistical associations, or phenotypic integration, with respect to their background (Chernoff and Magwene 1999; Magwene 2000). The strength of integration within a variational module is commonly attributed to shared pleiotropic effects (Cheverud 1995), and is thought to result from shared developmental and

functional processes (Olson and Miller 1958; Cheverud 1982, 1996; Zelditch and Carmichael 1989; Klingenberg 2005, 2008).

From its onset, the study of morphological integration has consisted of attempts to infer developmental and functional processes from observed patterns of phenotypic covariation (Olson and Miller 1958; Van Valen 1965; Cheverud 1982; Zelditch 1987). Albeit implicitly, the concept of variational module has figured prominently in these efforts, in that the strength and structure of integration among phenotypic traits is thought to result from the interactions among underlying developmental and functional. Consequently, most studies of integration have focused on identifying variational modules by analyzing the distribution of covariances or correlations under the general premise that traits conforming a module should covary more strongly than traits in separate modules. As most studies acknowledge, however, inferring developmental interactions from phenotypic covariation is a methodologically and conceptually difficult problem because of the complexity of the developmental networks that comprise the genotype-phenotype map (Klingenberg 2008). This difficulty is largely due to the fact that developmental processes interact so that variational modules are rarely, if ever, truly statistically independent. This lack of independence among modules often invalidates the assumption of a simple covariation structure, in which traits are grouped in independent, non-overlapping modules (Magwene 2000; Mitteroecker and Bookstein 2007; Zelditch et al. 2009). Instead, variational modules can be correlated by sharing subsets of common traits, which means that modules cannot generally be directly inferred from covariance or correlation matrices.

Despite the complex structure of covariation it is nevertheless possible to test causal developmental hypotheses that predict patterns of modularity by fitting them to observed covariance matrices (Zelditch 1987; Zelditch and Carmichael 1989). Herein I present a statistical framework for testing alternative hypotheses of variational modularity, one rooted in the biological principles underlying that concept. This approach treats modules as targets of specific developmental processes, so the definition of a module encompasses both the phenotypic traits spanning the module and the epigenetic and functional interactions causing their integration. Thus, when

hypothesizing a variational module spanning, for example, the braincase, the same module is also assumed to comprise the specific set of processes that are responsible for integrated variation within the braincase, e.g., growth of the brain (Moss and Young 1960). This focus on causes of covariation means that expectations derived from hypotheses of modularity do not necessarily have to be expressed in terms of sets of phenotypic traits, but instead as sets of variational properties (i.e., dimensions) of these traits. To accomplish this, I treat modules as *subspaces embedded in phenotypic space*. Although a rather abstract formalism, this is consistent with both the cases in which modules possess a simple covariation structure, forming non-overlapping cliques of variables (e.g., Zelditch and Carmichael 1989; Cheverud 1982, 1995; Klingenberg et al. 2003), and the more complex ones in which modules are correlated and spatiotemporally overlapping (Magwene 2000; Zelditch et al. 2008; Mitteroecker and Bookstein 2007; Márquez 2008). In the following sections, this abstraction is further developed in more intuitive terms, and a statistical method is proposed to implement this framework in the study of variational modularity in multivariate morphological data.

Causes of variational modularity

Integration within variational modules results from the cumulative effect of pleiotropic effects on the traits forming a module (Cheverud 1996; Wagner and Altenberg 1996; Klingenberg 2008). The fact that pleiotropy is a pervasive phenomenon, however, means that pleiotropic effects can be commonly found both within and among modules (Cheverud 2004; Albertson et al. 2005; Kenney-Hunt et al. 2008). Consequently, variational modules can be treated as discrete entities to the extent that they display a *relatively* high degree of morphological integration compared to extra-modular integration: integration within modules arises from the aggregation of relatively many or strong pleiotropic interactions whereas integration between modules arises from relatively few or weak pleiotropic interactions (Fig. I.1). This model expresses both intra- and inter-modular integration in terms of the same general kind of interactions (i.e., pleiotropy), which in practice means that it is possible to uncover the genetic basis of individual modules by studying the distribution of pleiotropic effects across a complex phenotype (e.g., using Quantitative Trait Loci analysis; Mezey et al. 2000). Although

such analyses concentrate on the genetic correlates of phenotypic covariation, seemingly placing development in a "black box" (Riska 1986; Houle 1991; Hall 2003), most studies of modularity attempt to explain the distribution of pleiotropic effects in the context of the developmental or functional processes underlying modules (e.g., Zelditch and Carmichael 1989; Cheverud et al. 1997; Monteiro et al. 2005; Klingenberg et al. 2003; Albertson et al. 2005, Zelditch et al. 2009). To this end, a substantial body of theory has accumulated that attempts to formalize the role of pleiotropy in structuring the variation that is transduced from genotype to phenotype during development (e.g., Lande 1979; Cheverud 1982; Wagner 1984, 1988; Burger 1986; Atchley and Hall 1991; Wolf et al. 2005), generally supporting the hypothesis that patterns of pleiotropic associations will evolve to match individual-level demands imposed by functional coupling among body parts (e.g., Cheverud 1982; Wagner 1988; Leamy et al. 1999). Tests comparing genetic covariances to patterns of functional association have broadly supported this hypothesis (Cheverud et al. 1997; Leamy et al. 1999; Mezey et al. 2000; Klingenberg et al. 2004), although most of these comparisons have assumed rather simple patterns of modularity in which only one or a limited set of modules are tested and where modules are not allowed to overlap.

Determining the precise genetic and developmental factors underlying pleiotropic effects on covariation structure remains a challenge. One approach is to examine the effects on covariation structures of mutations that disrupt known developmental processes in experimental systems with controlled genetic backgrounds (Hallgrímsson et al. 2006). But determining the effects of a single mutation is only a first step toward understanding the role that a developmental network plays in producing modular variation because the magnitude and spatial extent of pleiotropic effects transduced through developmental networks may vary among loci and among alleles of single loci (Klingenberg 2008). Another approach, which relies on a more literal interpretation of the model of pleiotropy (Fig. I.1), searches for Quantitative Trait Loci (QTLs) that map to sets of morphological traits, and quantifies pleiotropic loci as those simultaneously affecting two or more traits (Cheverud et al. 1997; Leamy et al. 1999; Mezey et al. 2000; Klingenberg et al. 2004; Albertson et al. 2005). Patterns of pleiotropic effects quantified in this manner have been used to show that variational modularity in regions of the skull

can be explained by an excess of pleiotropic interactions within, as opposed to between, these modules (Mezey et al. 2000). Of special interest to theories regarding the evolutionary origin of modules is a particular class of QTLs that can reveal variation among individuals in the pleiotropic relations among traits, namely relationship QTLs (rQTLs). rQTLs are mapped loci that are associated with variation in one trait when controlling for a second trait (i.e., a covariate). In this approach, genetic variation in pleiotropic effects is evinced by differences among genotypes in the relationship between the trait and the covariate (i.e., differential epistasis; Pavlicev et al. 2008). Application of rQTLs has revealed variation in the allometric relationships between bone lengths and overall size; such variation reveals differential epistatic effects among alleles (Pavlicev et al. 2008), and it is this variation that enables selection to modify pleiotropic associations among traits (Wagner and Cheverud 2007) and also provides a mechanistic basis for the evolution of patterns of modularity.

The developmental causes of pleiotropy have also been a major focus of research. Klingenberg (2005, 2008) summarizes two general mechanisms through which pleiotropic variation can arise: (1) direct interactions and (2) parallel variation. The major distinction between these two causes of pleiotropy is the relationship between the causes of variation and the cause of the covariation. In the case of direct interactions (Fig. I.2A), these need not be the same; the covariation structure results from the interactions along pathways that transmit the variation, whatever its cause. Examples of this type of pleiotropy are induction pathways, in which regulatory signals are sequentially transduced so that variation arising within any component is transmitted along the pathway (e.g., induction of the zone of polarizing activity in vertebrate limbs by *shh*; Riddle et al. 1993), and pathways in which morphological traits are derived by partitioning a limited pool of certain precursor (Riska 1986; Houle 1991; Nijhout and Emlen 1998). In contrast, pleiotropic effects due to parallel variation result from variation in common factors that affect otherwise independent pathways (Fig. I.2B). These sources of variation, which include both allelic effects and environmental factors, are external to the individual organisms (Klingenberg 2008), and are expected to cause covariation among traits even if there are no direct interactions between their developmental processes. This effect, however, may depend on the complexity of the

affected traits (see below). While both forms of pleiotropy are theoretically able to produce variational modularity, only direct interactions produce variational patterns that reflect developmental and functional causes of modularity.

A feature common to all these hypotheses is that they treat modules as defined entities, produced by knowable sets of epigenetic interactions that are susceptible to delimitation in anatomical terms. Given that variational modules can be thought of as specific morphological aspects whose covariation structure may reflect the history of all the developmental interactions leading up to them, the precise nature of modules might be as complex as the interactions that produce them. This complexity is the reason for referring to these modules vaguely as morphological "aspects" instead of as traits, characters, variables, or parts. It is this idea that covariation structures will rarely display a clear-cut pattern of individual modules with fixed anatomical boundaries that motivates the methods described herein. The present approach is premised on the idea that interactions among developmental pathways and spatiotemporal overlap of variational modules will produce complex patterns of covariation from which it is difficult to extract information about modularity. Despite the obscuring effect of these factors, variational modules produced from the processes described above should still be embedded in the phenotypic covariance structure. Therefore, it should be possible to investigate support for a particular array of modules by comparing hypothetical matrices derived from these hypotheses to observed covariance matrices (e.g., Márquez 2008). This approach, described below, requires that covariance matrices have a degree of predictability, a requirement that is largely determined by the intrinsic dimensionality of the modules embedded in them. But modules derived from complex patterns of pleiotropic interactions should be highly multidimensional, which means that neither the accumulation of disparate pleiotropic effects from multiple loci or the overlap among module boundaries will necessarily reduce the information about modularity contained in covariance structures. That is because each module could reside in its own region of the phenotypic space.

Consequences of multidimensionality of variational modules

Variational modularity (i.e., morphological integration) is normally expected to reduce the dimensionality of *overall* phenotypic variation relative to its theoretical maximum (e.g., Cheverud 1995; Chernoff and Magwene 1999; Hallgrímsson et al. 2002). Considerably less attention has been paid to the structure of variation *within* individual modules. However, understanding intra-modular variation is important not only because modules are expected to be internally integrated but also because the evolutionary consequences of modular variation depend critically on the covariation structure of each module (Hansen et al. 2003), just as the evolution of individual one-dimensional traits depends on the variances of those traits. As discussed above, integration within modules results from the aggregated effect of pleiotropic interactions, which are transduced through developmental pathways (Fig. I.2A). This general process implies that more complex pathways should tend to produce more complex intra-modular variation patterns, where "complexity" refers to the number of components of that pathway (e.g., signal transducers, membrane receptors, transcription factors, etc.) and the interactions among them. For variational modules, complexity refers to the dimensionality of their variation structure, which is a consequence of the variation of pleiotropic effects both within and among the loci involved in their development (Klingenberg 2005, 2008). In conclusion, the dimensionality of a variational module is a function of the number of different sources of pleiotropic variation because each of these sources (i.e., loci and their interactions) is expected to affect a different aspect of the variation.

This conclusion suggests that the structure of covariation among the phenotypic aspects that form a module depends on both the number of developmental elements and the functional characteristics they share. Thus, bilateral structures that develop as separate developmental modules (e.g., limbs) are expected to covary highly because they share the same developmental program, thus jointly forming a variational module (Wagner and Mezey 2004). Elements shared by developmental networks that have little else in common should account for a smaller portion of the covariation among the corresponding traits, especially when the effects of shared elements are context-dependent (e.g., Notch-Delta cell-cell signaling pathway; De Celis 2004). Consequently,

to the extent that the developmental networks leading to phenotypic modules share fewer elements in common with other such networks, the structure of covariation in the affected modules should tend to be unique, and thus occupy its own set of dimensions within phenotypic space. An important methodological consequence of this reasoning is that the likelihood of observing a strong correlation among traits that have developed independently should be inversely proportional to the complexity of the developmental pathways for these traits, so that this complexity should limit the ability of parallel pleiotropic effects (Fig. I.2B) to produce a measurable covariation among independent modules. It is also valuable to notice that statistical independence among variational modules may be obscured by effects of processes shared by all modules, such as growth, and thus it is more likely to be valid for integration caused by local developmental processes (Mitteroecker and Bookstein 2007).

The preceding discussion refers to the origin of multidimensional variation of a single module, but, as noted above, covariation structure rarely consists of a collection of isolated modules that can be independently analyzed. Instead, as noted by Hallgrímsson et al. (2007), the sequential superimposition of effects of developmental and functional processes through ontogeny produces extensive functional and morphological overlap among variational modules, resulting in covariation structures from which it may be impossible to deduct patterns of modularity (Fig. I.3). However, as proposed above, a sufficiently complex developmental process may map onto the variational structure of the phenotype with a set of unique dimensions defining a variational module, providing that the process has enough overall variance (Hallgrímsson et al. 2007). As a result, while a covariance matrix may contain a "patchwork" of disparate and only partially independent modules (Cowley and Atchley 1992), these modules may still conserve their integrity while they become embedded within phenotype space. The fact that these modules are composed of overlapping anatomical features (Hallgrímsson et al. 2007; Fig. I.3), however, implies that they cannot be identified as sets of physical variables, their identification instead requires a rather abstract approach, namely defining variational modules as sets of *dimensions*, i.e., subspaces embedded in the space occupied by the whole phenotype. In this approach, anatomical features *contribute* to modules, so that only a certain portion of the variation of said features may be causally attributed to the

variation of specific modules, therefore facilitating a conceptual image in which overlapping modules can be mathematically disentangled by assigning each overlapping feature to a putative module. Unfortunately, any mathematical procedure that could be used to approximately extract modules embedded in this way (e.g., Structural Equation Modeling) would require making a tremendous number of strong assumptions about observed covariation structures (Fornell and Bookstein 1982), and thus an alternative, more heuristic procedure seems desirable. The approach described in this study seeks to infer patterns of modularity by comparing observed and expected patterns of covariation. To accomplish this, patterns are derived from theories of integration and from models derived from heuristic searches; modules postulated by these models are used to build hypothetical covariance matrices that are directly compared to observed phenotypic covariance matrices.

Evolutionary implications

The idea that variational modules are subspaces embedded within a phenotypic space has important implications for the evolutionary consequences of modularity. Morphological integration is often considered to be both a source of evolutionary constraints—i.e., the reduction of heritable variation along one or more dimensions of variation (Maynard Smith et al. 1985)—and a medium to facilitate evolvability—i.e., the ability to produce selectively useful variation (Hansen 2003). That the same structural feature (modularity/integration) can be a cause of both constraint and evolvability may seem contradictory, but this dual role results from the fact that integration limits the independent component of variation of traits so that selection cannot optimize each one individually, but, at the same time, integration allows suites of functionally coupled traits to be selected as a unit, without interfering with other such units (Wagner 1988). Like any other feature of the phenotype, patterns of integration/modularity can evolve, although whether there are any general predictors for the evolutionary versatility of modules is an open question (Wagner and Cheverud 2007; Klingenberg 2008). Multivariate evolution theory predicts that in order for selection to alter prevailing patterns of modularity, there should be allelic variation in the effects of pleiotropic interactions (Cheverud 1996; Hansen 2006; Pavlicev et al. 2008), and Klingenberg (2005,

2008) has argued that since allelic variation is a cause of covariation among modules, this form of integration should generally be more evolutionarily labile. These observations suggest that independent developmental modules can become integrated into larger variational "super-modules" if pleiotropic effects shared by their respective pathways transduce enough variation for correlating selection to act upon. Similarly, the opposite process, i.e., parcellation (i.e., splitting) of super-modules (Wright 1932; Wagner and Altenberg 1996; Mezey et al. 2000) is possible if the independent component of variation of the resulting modules is selected upon (Beldade et al. 2002; Hansen et al. 2003), and/or if the pleiotropic effects linking both modules are epistatically modified under certain genetic backgrounds (Wagner and Altenberg 1996; Leamy et al. 1997; Wolf et al. 2006).

In addition to modularization and parcellation, there is no theoretical limit for how modules can be subdivided and rejoined as long as there is autonomous variation along these directions of variation. The question of whether there is a basic level of modularity beyond which parcellation is impossible without requiring a trait re-definition or, perhaps, innovation (Müller and Wagner 1991), is clearly an empirical question whose answer would depend on the nature of the trait and the developmental network behind it. In an often-cited argument, Hall and Atchley (1991; Hall and Miyake 2000; Hall 2003) have advocated a definition of developmental modules, i.e., mesenchymal condensations, as the basic morphogenetic units upon which morphological features are built, analogous to the units of evolution proposed by Lewontin (1970). Variation of these units, which consist of the earliest aggregate of cells formed during an organ's morphogenesis, arises from variation in certain basic parameters such as cell division and death rates, in turn controlled by knowable regulatory pathways. The idea that there is a basic level of modular organization that is relatively free to autonomously become a variational module or to combine into integrated higher-order modules is attractive because it explains both the conservativism of basic developmental rules (Riedl 1977; Müller and Wagner 1991; Raff 1996; von Dassow and Munro 1999) and the prevailing divergence of covariation structures (e.g., Steppan et al. 2002). Despite its obvious appeal, this hypothesis remains to be properly tested. Thus far, comparative analyses of patterns of variational modularity have provided circumstantial evidence supporting the conservation of putative developmental units, showing that the subspaces (i.e., modules)

of the mandible that are shared by the members of a clade of rodents with widely different covariation patterns resemble the pattern of modularity that would be expected should covariances induced by mesenchymal condensations dominate the phenotypic covariation structure later in ontogeny (Márquez 2008).

A NOVEL STATISTICAL FRAMEWORK FOR STUDIES OF VARIATIONAL MODULARITY

Conveying the full complexity of the conceptualization described in the preceding section for the developmental origin of variational modularity in tests of *a priori* hypotheses of modularity and integration requires the implementation of similarly complex statistical methods. To this end, the present work describes a general approach in which ordinary multivariate techniques are used to mirror the multidimensional geometry implied by the model described above. This model assumes that intra-modular trait covariation results from the cumulative effect of successive layers of genetic and epigenetic interactions, whose combined effect ultimately leads to the partitioning of the phenotypic space into modular but non-independent subspaces. These techniques are then used to build hypotheses and their expectations based on knowledge of developmental and functional interactions, which are tested for goodness of fit against the observed covariance structure of a set of phenotypic traits. As in any standard statistical test, the approach presented herein consists of (1) an internal logic for translating hypotheses based on developmental and functional interactions into quantitative structures with the desired geometry, (2) the ability to represent expectations from hypotheses and data in commensurable forms (i.e., covariance matrices) to make them comparable, (3) a goodness of fit statistic that measures the similarity between expected and observed patterns of modularity, and (4) a null distribution for this statistic under the hypothesis that expected and observed patterns diverge only by chance. Following it is a description of each of these components, as implemented in this approach.

Formulation of hypotheses

Traditionally, *a priori* hypotheses of morphological integration and modularity have consisted of arrays of blocks (modules) of traits jointly defined according to a

common explanatory principle, such as, for instance, the effect of muscle function or tooth eruption on the development of the skull form. In this approach, postulated modules reflect the underlying covariation structure that is expected to result from the spatiotemporal organization of said principle, which is assumed to be known, so that testing among alternative hypotheses amounts to contrasting among fully defined self-contained sets of putative modules. For example, muscular function, a commonly tested explanatory principle for skeletal covariation patterns, can be invoked to formulate a model in which skeletal traits that interact with the same muscular units are hypothesized to be integrated as a module, and therefore expected to be mutually interconnected by stronger covariances than traits interacting with disparate muscular units (Young and Badyaev 2006). In this approach, intra-modular covariation is seen both as a by-product of shared functional and developmental interactions among the component traits, and proportional to the *variance* of the shared processes (Zelditch 1987; Hallgrímsson et al. 2007), such that independent subsets of interactions are expected to lead to statistically independent modules. In the example of effects of muscle function on skeletal covariation patterns, those independent subsets of interactions may correspond to separate muscles or muscle groups carrying out distinct functions (e.g., mastication, deglutition, locomotion), which can be modeled by partitioning the structure under study (the skull) into modules matching the morphological regions hypothesized to be influenced by each of these subsets of muscle. Additional explanatory principles commonly tested in studies of craniofacial integration and modularity include, among others, embryonic tissue and cell lineage origin, and influence of functional matrices. The approach for building hypotheses is usually focused on the same question, namely what is the principle or family of processes (e.g., cellular origin, function) that best explain the covariation structure of a set of traits.

A clear advantage of this approach is that it allows establishing a transparent link between causal processes and statistical patterns when formulating hypotheses of modularity. However, its reliance on general principles to define putative modules seems rather artificial in many instances, because alternative principles are rarely mutually exclusive. Consequently, this approach can only adequately test whether a single principle is more important than others. For example, asking whether the covariation

structure induced by muscle function is more relevant than the covariation induced by morphogenetic processes is less informative than decomposing the relative contributions of these processes to covariances among traits. This limitation is particularly problematic for analyses of interspecific divergence of patterns of modularity, where this approach could lead to situations in which different causal factors are supported for the covariation patterns of two species, which is a rather uninformative result because it cannot be accurately construed as if the species are actually affected by different sets of developmental or functional processes. Instead, the two supported processes are likely to influence covariation patterns of both species to some extent. Consequently, by treating alternative models as exclusive explanations, interspecific differences are likely to confound complex patterns of interactions among ontogenetic processes, thus requiring the elaboration of critical tests that explicitly take these interactions into account.

In the alternative framework proposed herein, any developmental or functional process that affects more than one anatomical region or trait is theoretically capable of producing a variational module, provided that this process is capable of transducing sufficient variation. The simplest pattern that may result from this system, aptly termed *simple structure* (e.g., Mitteroecker and Bookstein 2007), occurs when the developmental and functional processes affecting separate modules do not interact, or if they do, such interactions are invariant, and therefore do not contribute to the covariance among traits that belong to distinct modules. More complex situations occur when multiple developmental processes influence the covariation structure of a single morphological trait, either because these processes interact or by wielding their influence during different ontogenetic stages. Similarly, many morphological structures carry out multiple functions, each associated to different subsets of traits (Moss 1968). The mammalian frontal bone, for example, is functionally associated to the braincase, orbit, sinuses, ethmoid, nasal bones, and masticatory apparatus (Moss and Young 1960), and each of these structures is in turn functionally coupled with different subsets of skull structures.

From these considerations, overlap among variational modules is expected to be common, so that some of the traits or regions that belong to a module will often belong to other modules as well (Moss 1968). Overall, the picture that emerges is one of a complex

patchwork of interacting but approximately distinct processes that is capable of producing an equally complex pattern of phenotypic covariation. Within this patchwork, covariances result from the additive effect of all of the processes linking two traits, so that a particularly high covariance may indicate traits that recurrently belong to the same modules, and not necessarily that they actually form a single module. This process-oriented interpretation of covariance patterns suggests that purely phenomenological approaches to infer modularity from covariances or correlations may tend to overestimate the number of modules defined within a complex structure, or even support modules which are inexplicable in terms of actual processes.

This situation is further complicated by the addition of evolutionary considerations. Even though selection directly acts on phenotypic variation, actual selective responses will affect the processes underlying the covariation structure of the phenotype (Cowley and Atchley 1992). From a methodological standpoint, the major difficulty that this poses is that the processes responsible for intra-modular integration can be evolutionarily conserved and yet show spatiotemporal divergence with respect of the morphological regions that they affect. The vagueness of variational modules that this situation entails implies that both evolutionary conservation and correlated divergence within modules may be easily obscured by divergence of the anatomical boundaries of these modules. This divergence may simply take the form of shifting boundaries or, as discussed above, to involve the coalescence or rupture of formerly independent or joined modules. For example, effects of a large masticatory muscle group like the temporalis, which loads on both the mandible ramus and the temporal region of the calvarium, may be still considered as stereotypical for a large group of related taxa (e.g., Muroid rodents), even if the attachment sites and specific loading patterns are not the same in all species; the same modules are still present in all species, even if the cranio-mandibular regions they span diverge.

In order to take these observations into consideration, tests of hypotheses of modularity must in practice satisfy three basic conditions: first, hypotheses should be based on *a priori* expectations of modular variation derived from functional and developmental theories, not only to ensure interpretability of patterns supported by tests,

but also to avoid treating groups of traits that share a recurrent set of processes as single modules; second, given the non-exclusivity of the processes responsible for morphological integration, tests should include hypotheses containing modules expected from multiple explanatory principles (e.g., muscle function and developmental origin of skull tissues), in addition to the more traditional approach in which only instances of a single principle are included; and finally, hypothetical modules should be defined as to have flexible boundaries, making tests more conservative by acknowledging that module boundaries may be more diverse than modules are, a major concern particularly when carrying out interspecific comparisons, as shown in this study.

Generation of expectations from data

The covariances among observed coordinates are computed in the conventional way (Dryden and Mardia 1998), but the expected covariances are obtained by transforming each data set to match the covariation structure implied by the models. Specifically, Procrustes residuals are partitioned into anatomical regions corresponding to the modules specified by each model, and these partitions are each assigned to their own subspace, orthogonal to all other partitions. That is achieved by the following steps: 1) make as many copies of the original data set as there are modules in the hypothetical matrix; 2) within each copy, assign a value of zero to each coordinate that does not belong to the module; 3) combine all copies into a single matrix by stacking them vertically, so that the resulting matrix has dimensions $nm \times 2k$, where n is sample size, m is the number of modules in the model being considered, and k is the number of (2-D) landmarks and semi-landmarks. For example, if we wish to compute an expectation from a model with three modules containing the pairs of coordinates for landmarks 1-8:

[**1 2 3**] [**4 5 6**] [**7 8**]

we first partition the full data set with n observations and eight variables into three subspaces, by forming the extended data matrix

$$X_0 = \begin{bmatrix} \mathbf{1} & \mathbf{2} & \mathbf{3} & \mathbf{0} & \mathbf{0} & \mathbf{0} & \mathbf{0} & \mathbf{0} \\ \mathbf{0} & \mathbf{0} & \mathbf{0} & \mathbf{4} & \mathbf{5} & \mathbf{6} & \mathbf{0} & \mathbf{0} \\ \mathbf{0} & \mathbf{0} & \mathbf{0} & \mathbf{0} & \mathbf{0} & \mathbf{0} & \mathbf{7} & \mathbf{8} \end{bmatrix}$$

in which each element corresponds either to one of the variables (vectors **1**-**8**) or to a vector of zeros, each of length *n*.

The expected covariance matrix, namely $\mathbf{S_0}$, can be computed from the columns of $\mathbf{X_0}$. For models of modularity (see above), $\mathbf{S_0}$ will equal the observed covariance matrix after between-module covariances are replaced by zeros. However, that does not take into account the covariances among Procrustes residuals induced by GLS superimposition (Walker 2000), which are estimated and included into $\mathbf{X_0}$ by performing a Procrustes superimposition of the rows in the extended data matrix ($\mathbf{X_0}$) prior to computing covariance matrices. This factorization also does not account for covariances induced by the geometry of sampled shapes, the general expectation being that landmark coordinates that are more proximate to each other will tend to bear higher covariances than more distant landmarks (Roth 1996; Mitteroecker and Bookstein 2007). The present approach, however, tests for relative support among competing models sharing a common geometry (see below), and thus this "spatial packaging" (Roth 1996) effect should not affect their relative goodness of fit.

When combining alternative models of modularity as described above, it is possible to obtain models in which some modules overlap, i.e., share landmarks. While module overlap may be biologically reasonable in that two or more processes can affect the same anatomical region, assigning one variable to more than one subspace presents a methodological challenge because that will multiply its variance and its covariances with other variables within the region of overlap by the number of instances that the variable is replicated. Therefore, the expected values must be adjusted so that the model does not excessively depart from observed values. To that end, a possibility is to model landmarks within an overlapping region as contributing equally to the variation of each of the overlapping modules by dividing the Procrustes residuals in matrix $\mathbf{X_0}$ by $\sqrt{s}$, were s equals the number of modules sharing the corresponding landmark. For example, if the model being tested is

[1 2 3] [3 4 5] [3 5 6 7 8]

in which variable 3 is shared by three modules, and variable 5 is shared by two, $\mathbf{X_0}$ would equal

$$\begin{bmatrix} \mathbf{1} & \mathbf{2} & \mathbf{3/\sqrt{3}} & \mathbf{0} & \mathbf{0} & \mathbf{0} & \mathbf{0} & \mathbf{0} \\ \mathbf{0} & \mathbf{0} & \mathbf{3/\sqrt{3}} & \mathbf{4} & \mathbf{5/\sqrt{2}} & \mathbf{0} & \mathbf{0} & \mathbf{0} \\ \mathbf{0} & \mathbf{0} & \mathbf{3/\sqrt{3}} & \mathbf{0} & \mathbf{5/\sqrt{2}} & \mathbf{6} & \mathbf{7} & \mathbf{8} \end{bmatrix}$$

Application of this correction makes the simplifying assumption that variance within regions spanned by more than one module is homogeneously distributed among these modules. A number of alternatives seem more suitable for different applications, such as partitioning this variance according to the ontogenetic period in which each overlapping module is developmentally or functionally active—more recent modules could account for a larger share of the variation in the region. Also, a more analytical approach could be used by estimating the proportion of the variance of the shared landmarks that is accounted for by each overlapping module. Clearly, this aspect of the present approach offers ample room for improvement. Irrespective of the method used to partition this variation, however, it is interesting to notice that overlapping modules are no longer orthogonal, allowing thus the definition and testing of biologically informed patterns that could not possibly be obtained by conventional eigenanalysis techniques, such as PCA or CPCA, which not only are constrained to produce orthogonal axes with no *a priori* biological meaning, but also offer no way to group variables into hypothetical modular subspaces.

Estimating goodness of fit

Goodness of fit between expected and observed patterns can be assessed using a variety of metrics that measure the similarity between covariance matrices such as trace correlations (Klingenberg et al. 2003), Procrustes distances (Peres-Neto and Jackson 2001), matrix correlations (Cheverud 1982; Dietz 1983), Common Principal Component Analyses (Phillips and Arnold 1999; Mezey and Houle 2003), angles between subspaces (Zelditch et al. 2006), and γ (Richtsmeier et al. 2005). The present study uses that last metric (γ), which is computed as:

$$\gamma = \text{trace } \{(\mathbf{S} - \mathbf{S_0})(\mathbf{S} - \mathbf{S_0})^T\}$$

(Richtsmeier et al., 2005), where **S** and $\mathbf{S_0}$ are the observed and modeled covariance matrices, respectively, and the *T* superscript is the transpose symbol.

The similarity between the data and a model is always affected by the number of fixed and estimated parameters; consequently, models having more "zero-covariance" elements will regularly appear to be less similar to the data than those having fewer orthogonal subspaces (Fig. I.5). To control for this artifact, γ values were regressed on the number of fixed parameters contained in each model (i.e., the number of zeros in their respective covariance matrices). Since the total number of parameters is fixed for all models (= number of distinct elements in the covariance matrices), this is equivalent to control for the number of estimated parameters, such as done in more familiar techniques for correction of model support statistics (e.g., Akaike Information Criterion). Residuals from this regression were added to the expected value (mean) of γ, yielding γ^*, the test statistic for the evaluation of the models. The smallest values of γ^* correspond to the best supported models. This procedure is appropriate for γ, which is linearly related to the number of fixed parameters in the model, but simulations demonstrate that more complex methods will be needed when using test statistics that have a non-linear relationship to the number of fixed parameters (e.g., angles between subspaces). The core aspect of the Matlab® code used to carry out these tests is included in the Appendix.

Significance tests

To test the hypotheses of modularity, the expected distributions of γ^* were obtained using a parametric Monte Carlo approach in which the model covariance matrix ($\mathbf{S_0}$) and the original sample size (*n*) of each model and species were used to parameterize a Wishart distribution (Krzanowski 2000). This is the distribution of covariance matrices, or, more precisely, sums of squares and cross-products (SSCP matrices) of a multivariate normal population. A random variate generator (Krzanowski 2000), implemented in the function WISHRND of Matlab® (The Mathworks 2006) was used to generate 1,000 random covariance matrices from this distribution, and γ^* was computed between $\mathbf{S_0}$ and these random covariances, giving a probability value for the hypothesis that this value of γ^* is no larger than that between two matrices produced from the same

model. A low (< 0.05) *P*-value corresponds to large values of γ^*, indicating a large difference between data and model and thus a poorly fitting model.

Random permutations of the original data can also be used as an alternative to this parametric approach. Those permutations generate a distribution of covariance matrices under the model being tested. In this case, specimen coordinates are randomly permuted within each module postulated by the model, thus preserving the intra-modular while destroying the inter-modular covariation structure. As in the Monte Carlo approach, covariances from permuted data sets are used to generate a distribution of γ^* under each model, that can be compared to the original value of γ^*.

Determining model support

Given many models, the procedure outlined above might fail to reject two or more competing hypotheses merely because of inadequate statistical power; in cases, as in this study, when several similar models are simultaneously tested, distinguishing statistically between them demands very large samples. Therefore, a more informative approach is to rank models by the strength of their support (i.e., γ^*). Confidence intervals for γ^* were obtained using a jackknife resampling method (Manly 2006) in which a randomly chosen subset of 10% of the specimens were dropped from each sample to produce 500 subsamples, from which 95% confidence intervals were computed as the 2.5 and 97.5 percentiles for each model-data comparison (Klingenberg 1996). Finally, a measure of model support (namely 'jackknife support') was computed by counting the proportion of jackknife samples in which a model ranks first (i.e., has the lowest value of γ^*).

The definitions provided above for $\mathbf{X_0}$ and $\mathbf{S_0}$ represent the expected values for a covariance structure with a known modular pattern, and as such they do not include an estimate of measurement error. Whereas it is customary for goodness of fit and other techniques to account for measurement error by computing model support after minimizing the difference between data and model using, for example, a Least Squares approach, the use of γ^* to compute model support does not need to implement any of such approaches for two reasons, namely (1) expected covariances from each model are directly obtained from the data, so that it is assumed that data are measured without error,

and (2) only relative support is used to find the best-fitting model, so that it is implicitly accepted that a better model could always be found if the entire parameter space could be explored (something unfeasible for most data sets given current computational capabilities). In using this approach, it is thereby implicitly assumed that the measurement error structure remains constant throughout a study, so that error variance can be safely ignored when determining relative support.

All of the methods described herein have been included in the software application MINT (Márquez 2008), which has been made publicly available at the author's website.

Evaluating the method via simulations

To assess how accurately the approach described herein estimates model support under a variety of controlled situations, the method was applied to a series of simulated data sets created according to twelve hypothetical patterns of modularity based on proposed models for the development of the mammalian mandible. These models (see Table I.1) were also tested in a comparative study of anatomical modularity in the mandible of oryzomyine rodents on a subset of the data analyzed in the following chapters (Márquez 2008). Mandibles were simulated to include the same landmarks used in the present study of skull modularity (see Fig. II.2), and modules included in each model (Fig. I.4) vary in number and coverage, and thus in their intrinsic dimensionality, providing a useful benchmark against which to compare results obtained from actual morphometric data.

To simulate landmark data with a known covariation structure, random vectors were sampled from a multivariate normal distribution (Krzanowski 2000) with mean vector zero (i.e., to simulate Procrustes residuals) and covariance matrices derived from each of the twelve developmental models plus a null model describing complete absence of covariance. These covariance matrices were obtained by arranging another data set comprising a randomly sampled multivariate normal distribution with mean vector zero and covariance matrix I (the identity matrix) to follow the structure described by each model, using the same approach described above to build expected covariance matrices

from each model. Simulated data were computed for the minimum (39) and maximum (77) sample sizes available in this study for the mandibles of oryzomyine species (see Table II.1). Application of this procedure produced 26 data sets sampled from two sets of 13 multivariate normal distributions corresponding to each of the 12 models of modularity plus a null model. For each, γ^* values, their confidence intervals, and their jackknife support were computed as described above to determine whether the best supported model is the one from which the data were derived. Finally, model support statistics were also computed for each of the 620 models resulting from combining the modules hypothesized by the same set of 12 models, to assess the sensitivity of test results to the increase in resolution introduced by adding multiple similar models to the correct one.

Analysis of simulated data sets confirms that the methods used herein can detect the correct model of modularity if it is included among tested alternatives (Tables I.2, I.3). This is the case for analyses of the 13 original models (Table I.2) and also for the 620 models formed by combining them. Because the γ^* values are obtained by regressing model-specific γ values on the number of fixed parameters (Fig. I.5), results are expected to depend on the number of models being evaluated. As in any least-squares procedure, the larger the number of observations (models, in this case), the more stable the results. Not surprisingly, resolution is improved when all 620 models are simultaneously compared, particularly for model H_0, which predicts a total absence of integration across the mandible (Table I.3).

These simulations show that the methods are typically robust to variation in the number of models being examined, but the signal is sometimes obscured for the most highly modular models, i.e., those that predict weak or no covariances across the mandible. Similarly, the methods are reasonably robust to small sample sizes, with the correct model being supported above the others in all but two cases (i.e., the highly modular H_0 and H_1, Table I.2) even when samples are as small as $N = 39$. Jackknife support for the correct model from the analysis of 620 models exceeds 75% for all but one model (H_1), and exceeds 90% for all but four models (Table I.2). Again, the models that predict a larger number of smaller modules tend to produce a weaker signal at $N =$

39. As might be expected, the signal is improved when analyses are based on large sample sizes (data not shown); thus, at $N = 200$, jackknife support is 100% even for model H_1.

Although both γ^* and jackknife support must be interpreted with caution when sample sizes are small, the purpose of these statistics is limited to finding the best supported hypothesis. However, the pattern of support for the full set of hypotheses, not simply the best one, is a function of the covariation structure in the data, so even though a large sample size may be required when assessing a highly modular model, its support relative to other models will generally be higher when it is true than when it is not. Hence, with $N = 39$, H_0 ranks first out of 620 when the data are simulated according to H_0, whereas it ranks between 306th and 596th when the data are simulated using other models. In contrast, H_1 ranks fifth when data actually follow H_1, just below models {1,2}{3}{5}{4,6} (first), {1,2}{3}{4}{5}{6}, {1,2}{4}{5}{3,6}, and {1}{2}{3}{5}{4,6} (fourth), but it ranks between 48th and 293rd when data follow every other model except H_0 and H_5. In those cases, H_1 ranks second and eighth, respectively. Note that a higher rank for H_1 when data are simulated based on H_0 rather than H_1 does not imply that H_0 is more strongly supported by these data because ranks are relative measures and the regressions are independent from each other. In fact, H_0 ranks 533rd when data are simulated using H_1.

Simulations show that the methods used herein are reasonably robust at small sample sizes, although robustness seems partly dependent on the dimensionality of the data; when there are a large number of modules, sample sizes need to be proportionally increased to facilitate their detection. These simulations, however, represent worst-case scenarios because (1) intra-module covariances were derived from data simulated using an isotropic distribution (i.e., using an identity matrix as covariance matrices), which means that covariation within modules had a large random component, whereas modular variation is normally expected to show much more intra-modular integration, and (2) each of the 52 pairs of coordinates in the simulated samples was treated as a landmark, producing a 100-dimensional space. Actual data rarely have such high dimensionality. The oryzomyine mandible data upon which these simulations were based, for instance,

occupy a space with substantially fewer degrees of freedom, as only 18 of the 69 sampled coordinates correspond to landmarks, with the remaining being semi-landmarks, each of which contribute only one dimension to the space (Bookstein 1997). Consequently, the sample size requirements should be correspondingly smaller.

Robustness of results depends also on the total number of models being tested, including the original hypotheses and the models that result from combining them. That dependence arises from the fact that the main test statistic, γ^*, is computed by a least-squares regression (of γ on the number of zero-covariance elements within each model). Each point in that regression represents the value for an individual model. Yet, these results also appear to be highly robust to variation in the number of tested models based on the simulations using 13 versus 620 models (Tables I.2 and I.3, respectively). The results differ only in their adjustment of the γ value for the model having the greatest number of zero-covariances i.e., H_0, the null model that predicts a total absence of integration. This model behaves as an outlier only when the regression is based on 13 models. When the number of models to be tested is insufficient, outliers such as this one can either be removed or the γ statistic can be adjusted using a robust regression.

VISUALIZING MODULARITY IN MORPHOMETRIC DATA

One of the major strengths of geometric morphometrics is, as the name implies, the ability to graphically illustrate the geometric differences resulting from the comparison of two shapes (Bookstein 1991; Dryden and Mardia 1998). Consequently, applications based on these methods are usually accompanied by a number of techniques for visualization of patterns of variation. For instance, variation implied by an eigenvector can be shown as the shape difference between two endpoints along this vector, or, more commonly between the corresponding differences between these endpoints and their middle point (Dryden and Mardia 1998). Therefore, we wish to produce a visualization of modularity that reflects modules in a way that contrasts their increased internal integration with respect to their background. In other words, a visualization that shows both intra-modular and inter-modular variation is preferred to either of these views alone.

To this end, a variant of Partial Least Squares (PLS; Wold 1966; Rohlf and Corti 2000; Bookstein et al. 2003) is proposed in which each putative multivariate module is compared to the entire structure to which it belongs. This visualization technique is termed part-whole PLS. PLS is a technique that computes the linear combinations of two or more blocks of variables (e.g., modules) that maximize the covariance between the sets. Like Principal Component Analysis (PCA), PLS produces sets of orthogonal axes on which each variable set can be projected; unlike PCA, PLS axes are oriented so that the first vector of one block maximally covaries with the second block; as usual, the second and successive vectors are constrained to be orthogonal to every other vector in the basis (Rohlf and Corti 2000). Changes in shape implied by these vectors are then readily computed using standard geometric morphometrics techniques (Bookstein et al. 2003).

Part-whole PLS is more consistent with the philosophy of the present approach than the alternative (i.e., visualizing the variation of isolated parts), for two reasons. First, it offers a more realistic interpretation of a part's variation by ensuring that it lies along axes of variation actually displayed by the whole structure (e.g., the entire mandible), that is, a module subspace is assumed to be embedded within the entire space occupied by the morphological complex under study. Second, it allows for visualizing regional variation within the context of the variation of the whole, making it possible to detect patterns of covariation both between and within parts. PLS axes corresponding to the full mandible for some of the models used in the simulations described above are shown in Figure I.6. In these illustrations, the signal produced by modules is clearly appreciated as dimensions where only one module loads within the space spanned by the whole structure. These analyses and visualizations can also be carried out using the MINT software (Márquez 2008). In addition to allowing the visualization of hypothetical or known modular patterns, part-whole PLS has proven effective as an exploratory technique, and it has been used as a heuristic to derive additional models of modularity with more support than models derived from the theory (Márquez 2008).

RELATIONSHIP TO ALTERNATIVE METHODS

Even though the conceptualization of variational modules as subspaces embedded within phenotypic spaces may appear novel, most traditional and current methods have implicitly treated modules as multivariate subspaces. The present approach differs from these methods in multiple ways, but the main features that distinguish it from most of these are (1) its emphasis on analyzing the entire space spanned by observed covariance matrices, as opposed to rely on pairwise comparisons among *a priori* partitions, (2) its emphasis on both intra- and inter-modular covariation in the definition and test of patterns of modularity, and (3) its ability to handle models of modularity that hypothesize a spatiotemporal overlap among modules.

A similar set of principles to the basic decomposition of phenotypic spaces into modular subspaces has been recently proposed by Mitteroecker and Bookstein (2007) in an attempt to formalize the definition of variational modules in term of latent causal factors (Jöreskog and Wold 1982; Bookstein 1986). In their approach, a phenotypic covariance matrix $\mathbf{\Sigma}$ is modeled as

$$\mathbf{\Sigma} = \mathbf{\Sigma_c} + \begin{pmatrix} \boldsymbol{\sigma}_\mathbf{a} & \cdots & \mathbf{0} \\ \vdots & \ddots & \vdots \\ \mathbf{0} & \cdots & \boldsymbol{\sigma}_\mathbf{k} \end{pmatrix} + \mathbf{\Psi}$$

where the $\mathbf{\Sigma_c}$ matrix accounts for integration among all of the measured variables, namely *common* or *global* factors (e.g., allometric variation),$\boldsymbol{\sigma}_\mathbf{a}$, with $\mathbf{a} = 1 \ldots k$, are the covariance matrices among the variables comprising each module, and $\mathbf{\Psi}$ is a matrix of measurement errors (Mitteroecker and Bookstein 2007). Despite differences in nomenclature, this equation is almost identical to the formulation used in the present study, with each $\boldsymbol{\sigma}_\mathbf{a}$ matrix corresponding to a different modular subspace. An important distinction is the treatment of the common factor, which Mitteroecker and Bookstein prefer to remove in order to obtain "proper" modularity information. In the present approach, allometric variation is removed by regressing the original variables onto centroid size and using the residuals from this regression for further analyses (Zelditch et al. 2003). The choice to remove allometric variation is a matter of convenience, since the observation that allometry produces integration is rather trivial and potentially capable to

obscure patterns of local modularity (Mitteroecker and Bookstein 2007). Should allometric variation be considered among the models being tested, it would be more consistent within the philosophy of the present approach to include a size vector within each module, thus effectively transforming each subspace into a size-shape space (Mitteroecker et al. 2004). In Mitteroecker and Bookstein (2007) approach, however, common factors affecting the phenotype in a global manner are treated as external covariates with respect to individual modules, following the customary approach used in path analysis (Wright 1932; Zelditch 1987; Zelditch et al. 2008; Jepsen et al. 2009). When interpreted in this way, indeed it appears necessary to control for such common factors if local modules are to be uncovered, a task that is complicated by the authors' assertion that allometric variation, which can be readily removed from phenotypic data, is only one of the possible common factors, such that other factors, most likely unavailable for direct measurement, must also be removed from the covariation structure. To solve this problem, Mitteroecker and Bookstein propose to use the component of the total variation that is *outside* of the putative modules to estimate the common factor. This is computed as the first axes of a Singular Value Decomposition of the matrix of cross-products between two modules, i.e., PLS (Bookstein 1991; Rohlf and Corti 2000). In other words, a common factor is estimated as the between-module component of the variation.

The approach proposed by Mitteroecker and Bookstein is notably different from the one described in this study for two major reasons. First, the suggestion that there is a unique global factor other than allometric variation seems at odds with the conventional definition of modules as hierarchical and/or reticulated sets of factors, whereby the concept of "common" or "local" are not absolute, but relative to the specific traits under consideration. In agreement with this premise, within the present approach any non-allometric common factor would be considered as a hypothesis of modularity in its own right, and tested accordingly. In fact, some of the models tested in the following chapters include factors that treat the entire mandible as a single module. In turn, no model in the study treats the entire skull (i.e., cranium plus mandible) as a module, simply because there is no known developmental process to account for such pattern of variation. Second, any method that uses PLS to estimate variation between putative modules

necessarily requires a rigid definition of modules, because this technique offers no statistic that is capable of distinguishing among the relative support for alternative hypotheses of modularity.

In order to explore the potential problems posed by removing a common factor in order to retrieve local patterns of modularity, PLS was used as described by Mitteroecker and Bookstein (2007, 2008) to estimate the common factor from data sets simulated assuming a known model of modularity. Simulations were carried out as described above, using two of the models of the mandible shown in Table I.4, specifically model H_3 ({1,2,4}{3,5,6}) and H_8 ({1,2}{3,4,5,6}), each consisting of two non-overlapping modules comprising a distal and a proximal region of the mandible, respectively. Two sets of simulations were obtained for each module, (1) including, and (2) excluding a common factor. The common factor was computed as the first principal component of the covariance matrix of another data set, also simulated as above, in which the entire mandible was hypothesized as a single module. This principal component (**a**) was expanded into a Sums of Squares and Cross-Product matrix $\mathbf{\Sigma_c} = \mathbf{a}^{\mathrm{T}}\mathbf{a}$ and added to the modular covariance matrix to obtain $\mathbf{\Sigma}$ (see equation above). This procedure guarantees that the common factor will be one-dimensional, and thus it should be captured by the first PLS axis. In order to examine the approach, each of these four data sets was submitted to two PLS analyses, in which (1) the correct and (2) the incorrect model was used to partition the landmarks into blocks prior to computation of the common factor. It is expected from these analyses that a common factor should be identified only in the data sets to which such factor was added. This is tested by computing the probability that the squared covariance between the putative modules (i.e., the singular value of the first PLS axis) is higher than expected from random permutations within the modules (Rohlf and Corti 2000): only those samples in which a common factor was included should produce PLS axes that account for a significant portion of the covariance among the sets, because in absence of a common factor, these sets should be statistically independent. The results of this exercise show that most of these expectations are fulfilled, with an exception (Table I.4, highlighted rows): partitioning a data set according to the incorrect modules seems to produce a signal that leads one to conclude that there is a common factor when in fact there is none. Comparing plots of PLS scores from these situations

suggests that inter-modular patterns of covariation computed with the *incorrect* model in *absence* of a common factor are more similar to patterns computed with the *correct* model in *presence* a common factor than to those patterns that use the *correct* model and *do not include* a common factor (Fig. I.7). These results suggest that support for an incorrect common factor does not require a substantial change in the percent covariance accounted for the incorrect partition. The significant *P*-values for the first PLS axis obtained in these cases must then result from a translation of the distribution of random permutations towards a lower range of values for the proportion of the covariance explained by this factor, so that randomly permuted data sets show relatively more independence among partitions than the observed PLS axes. This could be explained by an effect on the intra- and inter-modular covariation patterns caused by incorrectly partitioning a data set in which those variables that are incorrectly allocated tend to covary with the partition to which they actually belong, causing random permutations to effectively treat both inter- and intra-modular associations as exchangeable, instead of only inter-modular associations as assumed by the tests. This issue could be addressed using Klingenberg et al.'s (2003) landmark permutation technique to test for module integrity, although this procedure also has its own limitations (see below).

In general, these results indicate that whenever modules are incorrectly defined so that variables that belong to the same module are wrongly assigned to different partitions, removing a common factor will also remove or distort the intra-modular components of the variation of the modules that are incorrectly defined. This effect is illustrated in Figure I.8, in which part-whole PLS reveals integration patterns that tend to follow the true pattern of modularity irrespective of the partitioning scheme used to compute PLS axes. This does not imply that PLS can accurately reveal true patterns of modularity, because incorrectly partitioning a data set has an obscuring effect on the underlying covariation structure, as evident from comparing Figure I.8 to Figure I.6, which reveals a much stronger modular association when the postulated modules agree with the true modules. It remains to be explored whether this consequence of the method would prevent its application to situations in which modules overlap, which by definition share a subset of variables. Furthermore, results suggest that when there is in fact a common factor, this is correctly computed irrespective of whether variables are partitioned

according to the correct modules (Table I.4, Fig. I.7), which is expected because this approach assumes that common factors are effectively independent from the modular structure in the data. Therefore, should common (global) factors be measurable, controlling for them using PLS should be equivalent to removing them using ordinary regression techniques, as customarily done for allometric variation (e.g., Zelditch et al. 2003).

As mentioned above, Mitteroecker and Bookstein approach can only test for the strength, or lack thereof, of integration among modules, being limited in its ability to compare among alternative modules in terms of intra-modular integration, even though the concept of modularity stresses both of these components (Bolker 2000). This limitation is shared by most approaches for studying modularity using PLS or other forms of pairwise comparisons among modules (e.g., Monteiro et al. 2005). Along similar lines, Klingenberg et al. (2003) have proposed testing for the strength of association within putative modules with respect to their background by comparing their pairwise correlation to the distribution of correlation values computed from blocks of random sets of variables. Although this approach treats modules in a way that is compatible with conventional definitions in that it assumes that modules are minimally correlated, it is unclear how it can be used to rigorously test among alternative hypotheses, how can it deal with models including more than two modules, and whether it can be used to test hypotheses including overlapping modules.

A different approach that is not based on pairwise comparisons has been proposed by Magwene (2000). In this approach, graph theory statistics are used to test for the strength of association among groups of variables defining semi-independent modules, a module being defined as a set of traits which are conditionally independent from other variables. Although this conceptualization seems superficially reasonable in that it considers both intra- and inter-modular variation, it is weakened by the fact that in practice the variation of each variable is conditioned on every other variable, including those within the same putative module, effectively destroying or distorting any information about modularity in the data (Mitteroecker and Bookstein 2007). This is similar to the effect shown above resulting from using PLS to estimate a common factor

from modules with incorrectly defined boundaries (Mitteroecker and Bookstein 2007). In the case of graph theory, this issue is not a flaw of the general approach, but only of this particular implementation. In fact, if implemented by conditioning variation of a module only on variables outside the module, this approach is largely equivalent to the one advocated in this study, in that both conceptualize modules as (conditionally) independent components of variation of traits, not as traits per se. It seems worthwhile to further explore the methodological implications of graph theory (Whittaker 1990) to formulate and tests hypotheses of modular subspaces in phenotypic and genetic covariance matrices.

Another conceptual advantage of the method described herein is its ability to postulate and test non-orthogonal models, overcoming a major limitation of traditional eigenanalysis techniques (Steppan et al. 2002). Other methods allow for non-orthogonal modules, such as Confirmatory Factor Analysis (Jöreskog and Wold 1982; Zelditch and Carmichael 1989), but the approach presented herein differs from them by not relying on assumptions about the expected structure of variation (Fornell and Bookstein 1982; Bookstein 1986). However, a methodological limitation that arises when modules are allowed to be non-independent is that non-orthogonal factors cannot be easily combined to compute their joint effects. This limitation can be overcome by extracting axes of maximum covariation among separate modules, using methods such as PLS or canonical correlations (Rohlf and Corti 2000). However, as discussed above, these methods ignore within-module covariances. The alternative presented here, namely part-whole PLS regression, can find the directions of both within- and between-module covariation using the entire covariance matrix. Despite the large number of part-whole comparisons required by this approach, this is a useful tool for detecting patterns of inter-module covariation as well as for testing the internal integrity of putative modules.

CORRELATIONS VS. COVARIANCES IN STUDIES OF MODULARITY

As noted above, numerous methods have been proposed to measure integration and test hypotheses regarding its causes and consequences since Olson and Miller (1958) and Berg (1960) popularized the use of correlation structure to understand phenotypic integration (for a recent review, see Mitteroecker and Bookstein 2007). With few

exceptions, most of these approaches have focused on finding ways to obtain accurate statistical representations of underlying patterns of integration, and less attention has been paid to ensure that these representations can be incorporated into the mathematics of general evolutionary theory (Lande 1979; Wagner 1984; Hansen and Houle 2008). Thus, for example, Olson and Miller (1958) and later researchers (e.g., Cheverud 1982, 1995; Monteiro et al. 2005) have chosen to use correlation matrices and indexes derived from them to analyze patterns of morphological integration. Correlation matrices standardize the covariation structure in a multivariate data set by equating the variances of the individual variables to one, and this is an appropriate standardization when the variables under study are measured in different scales with incommensurable variances (Wagner 1984). Although it is clear that some standardization is needed whenever data cannot be directly compared (Hansen and Houle 2008), morphological integration studies have advocated the use of correlation matrices even when variables are measured in the same scale. This is justified by a definition of integration that emphasizes common direction of variation irrespective of the magnitude of variation (e.g., Cheverud 1989). An undesirable consequence of using correlations instead of covariances, however, is that results from these methods can only be verbally connected to methods and questions posed by general evolutionary theory, which is mathematically expressed in terms of covariances (Lande 1979; Lynch and Walsh 1998). In contrast to most studies of morphological integration/variational modularity, the approach proposed herein is not suitable for correlation data, and in its present form it should only be applied to covariance matrices. This is because each correlation value is standardized independently from other traits, and thus its relevance within a module would be inconsistent among alternative models of modularity. Although this property of the method limits its applicability only to commensurable variables, it also has two important advantages. First, as suggested above, by being based on covariance matrices, models and results derived from the present approach should be applicable to general quantitative genetics methods. Second, and perhaps more importantly, the operational definition of integration used by this method assumes that intra-modular variation is a function of pleiotropic variation accumulated through defined developmental networks, implying that in order to decompose observed variation in terms of hypothetical contributions from

separate developmental pathways, it must be assumed that variances remain in the same scale throughout the mapping of genetic onto phenotypic variation. Transforming covariances into correlations would have the undesirable effect of distorting the pleiotropic effects of shared developmental pathways to a point that the corresponding modular subspaces could no longer be recovered.

The present approach seeks to formalize the generally undisputed notion that phenotypic and genetic covariance matrices contain the cumulative effects of multiple epigenetic interactions during the mapping from genotype to phenotype (e.g., Wagner 1984; Cowley and Atchley 1992; Klingenberg 2005). By explicitly testing hypotheses of modularity as causes of covariation among phenotypic variables, it could facilitate the incorporation of mechanistic explanations for observed phenotypic and genetic covariances, thus potentially allowing establishing functional connections between developmental interactions and short-term divergence. Thus, for example, it should be possible to estimate the autonomy of a given module (i.e., the proportion of its genetic variance that is independent of other aspects of the phenotype; Hansen and Houle 2008) and thus, for a given selection gradient, the potential contribution of this module to the evolvability of a genotype (Hansen and Houle 2008). A promising aspect of this approach is the possibility to explain some of the correlates of evolvability in terms of specific developmental processes. Overall, given the appropriate data (e.g., genetic variants with known phenotypic effects and strictly controlled genetic backgrounds), it seems theoretically possible to decompose a G- or P-matrix as a function of the contributions from different epigenetic interactions, which would clearly constitute a highly informative framework for understanding and predicting evolutionary divergence under a wide variety of mutational scenarios.

CONCLUSIONS

The general approach used in this study rests on the idea that individual modules are affected by local processes, which means that the structure of covariation is shaped partly by the accumulation of local effects even when they partially overlap (Cowley and Atchley 1992). Mathematically, the regions where modules intersect are therefore modeled by assuming that their (co)variances result from the cumulative effect of

overlapping processes. This view of modules shifts the focus of studies of modularity away from asking whether a particular module exists, or whether a given phenotypic part is a module, to asking about the degree to which specific genetic and epigenetic factors contribute to the distinction of modules and, more generally, to the patterning of phenotypic covariances.

Analyzing modularity in terms of both the within- and between-module associations, within the span of full covariance matrices, may seem directly contrary to the idea that modules are defined as independent subsets of variables. However, the present approach reconciles these apparently conflicting views by treating modules as self-contained multidimensional subspaces that are embedded within the full space occupied by the data. This geometric interpretation of modules makes it straightforward to derive and test explicit hypotheses based on developmental and functional theories because the expectations derived from them are merely reorganizations, not modifications of the geometric characteristics (e.g., degrees of freedom) of the original space. In fact, it is this commensurability between data and models, as well as among models, which allows for testing multiple competing hypotheses simultaneously in terms of a unique goodness of fit statistic (Richtsmeier et al. 2005). Furthermore, because all hypotheses are directly compared to the data, results can be continually reexamined by adding new hypotheses or by refining the old ones. An important consequence of this is that there is no penalty for testing novel or even unrealistic hypotheses along with familiar ones, which means that this can simultaneously be applied as an inferential and heuristic tool.

The representation of variational modules as semi-independent subsets of variables (i.e., subspaces) is consistent with their definition as dissociable parts of the phenotype (Raff 1996; Magwene 2000; Mitteroecker and Bookstein 2007). This representation assumes that modules, like most phenotypic features, are inherently multidimensional, which means that individual vectors (e.g., Principal Components) rarely can correspond to an entire module. As a result, methods that extract such vectors are likely to fail to find modules, especially when the modules are not statistically independent. In general, non-independence (i.e., non-orthogonality) of modules can be

due to the spatiotemporal overlap of their causal factors. Therefore, defining modularity in terms of an array of strictly orthogonal subspaces should be decided in light of developmental and functional considerations rather than methodological limitations (Steppan et al. 2002; Mezey and Houle 2003). We clearly need methods that can detect intersecting modules if the structure of modularity and integration regularly arises from multiple, spatially overlapping processes.

Model		Description
H_0:	No modules	"Null" model, predicting absence of modular structure; all covariances are hypothesized to be zero.
H_1:	{1}{2}{3}{4}{5}{6}	Partitions map to mesenchyme condensations, the developmental modules of the mandible, based on whether partition {4} is associated to the ramal bone (H_1) or to the incisor alveolus (H_2) (Atchey and Hall 1991; Hall and Miyake 2000; Hall 2003).
H_2:	{1,4}{2}{3}{5}{6}	
H_3:	{1,2,4}{3,5,6}	Partitions distinguish the processes of the mandible from the ramus and alveoli, which undergo endochondral and membranous ossification, respectively. This model also addresses timing of ossification as a source of integration, since membranous ossification precedes endochondral ossification (Kaufman and Bard 1999)
H_4:	{1,4$^+$}{2}{5}{3,4$^-$,6}	Molar and incisor alveoli defined as separate partitions to represent developmental and functional interactions with their respective teeth (Boughner and Hallgrimsson 2008). In the proximal half of the mandible, the condyle (as part of the condyloid process) is assigned a individual partition to contrast its role as component of the TMJ, distinguished from the other regions, which are the main attachment and loading sites for masticatory muscles (Rinker 1954).
H_5:	{1}{2}{3}{5}{4,6}	Partitions defined to reflect localized functional interactions: {1,4$^+$}/{1} and {2} span incisor and molar alveoli, whereas {3} and {4,6}/{4$^-$,6} span attachment sites and loading regions of the temporalis, and lateral masseter and pterygoid muscles, respectively (Rinker 1954); {5} includes the condyle, which is functionally related to the TMJ. The two models are distinguished by the allocation of the ascending portion of the ramus (sampled by partition {4$^+$}) as part of the incisor alveolus (H_5) or as a masseter attachment (H_6).
H_6:	{1,4$^+$}{2}{3}{5}{4$^-$,6}	
H_7:	{1,2}{5}{3,4,6}	Partitions defined to reflect broad functional interactions distinguishing tooth-bearing portions of the rostral half of the mandible from the muscle-bearing proximal half and the articular region.
H_8:	{1,2}{3,4,5,6}	The mandible is divided into tooth-and muscle-bearing parts. The two versions of this model are distinguished according to whether the ascending ramus is interpreted as insertion site of the masseter (H_8) or as the posterior portion of the incisor alveolus (H_9). This two-part model has been used in quantitative genetics of the mouse mandible (Cheverud et al. 1997; Klingenberg et al. 2004), and in studies of morphological integration (Klingenberg et al. 2003).
H_9:	{1,2,4$^+$}{3,4$^-$,5,6}	
H_{10}:	{1,2,5}{3,4,6}	Partitions predict integration between condyle and dental alveoli due to the effect of rotation at the TMJ on occlusion patterns (Björk 1969; Björk and Skieller 1972). Models differ in whether the ramus is affected, and whether an effect is predicted for both molar and incisor alveoli or for molar alveolus only.
H_{11}:	{1}{2,4,5}{3,6}	
H_{12}:	{1,2,4,5}{3,6}	

Table I.1. Modules of modularity used to simulate data with known patterns of covariation. Modules correspond to regions of the mandible hypothesized to be affected by a common process. Partitions are: {1} anterior (rostral) portion of incisor alveolus; {2} molar alveolus; {3} coronoid process; {4} posterior portion of incisor alveolus and attachment site of lateral masseter muscles, decomposable into partitions {4+} and {4-}; {5} condyloid process; {6} angular process. See Figure I.4 for a pictorial representation of each partition.

Simulated model	Model support												
	H_0	H_1	H_2	H_3	H_4	H_5	H_6	H_7	H_8	H_9	H_{10}	H_{11}	H_{12}
H_0	0.589	0.589	0.585	0.573	0.577	0.588	0.588	0.576	0.588	0.574	0.580	**0.569**	0.572
H_1	0.621	0.463	0.467	0.470	0.501	0.459	0.496	**0.456**	0.477	0.508	0.458	0.475	0.477
H_2	0.634	0.472	**0.348**	0.380	0.439	0.474	0.427	0.481	0.529	0.473	0.509	0.512	0.411
H_3	0.619	0.525	0.477	**0.383**	0.497	0.537	0.525	0.509	0.502	0.448	0.536	0.506	0.469
H_4	0.622	0.515	0.435	0.472	**0.412**	0.514	0.438	0.495	0.541	0.459	0.515	0.545	0.487
H_5	0.620	0.468	0.473	0.499	0.483	**0.445**	0.487	0.452	0.456	0.499	0.465	0.479	0.502
H_6	0.620	0.512	0.446	0.465	0.434	0.481	**0.432**	0.505	0.520	0.452	0.510	0.527	0.472
H_7	0.596	0.521	0.547	0.533	0.497	0.492	0.539	**0.404**	0.421	0.515	0.420	0.512	0.540
H_8	0.595	0.520	0.555	0.515	0.495	0.490	0.545	0.403	**0.364**	0.470	0.433	0.504	0.555
H_9	0.610	0.547	0.512	0.439	0.461	0.552	0.496	0.506	0.504	**0.408**	0.529	0.534	0.493
H_{10}	0.592	0.527	0.543	0.546	0.517	0.508	0.544	0.445	0.481	0.538	**0.413**	0.525	0.504
H_{11}	0.616	0.518	0.538	0.513	0.514	0.517	0.551	0.494	0.483	0.520	0.511	**0.431**	0.487
H_{12}	0.613	0.532	0.483	0.473	0.500	0.547	0.521	0.526	0.539	0.514	0.514	0.480	**0.416**

Table I.2. Results from simulations, showing the measure of fit (γ^* values) obtained from fitting models H_0-H_{12} (Table I.1) to the data sets simulated assuming each of these models model (Table I.1). Lowest γ^* value (in boldface) indicates the most supported model. Only shown data set with $N = 39$ simulated individuals.

Simulated model	Best ranked models	Jackknife support
H_0	H_0	100%
H_1	{1,2}{3}{5}{4,6} {1,2}{3}{4}{5}{6} {1}{2}{3}{5}{4,6} (H_6) {1}{2}{3}{4}{5}{6} (H_1) {1}{2}{4}{5}{3,6} {1,2}{4}{5}{3,6}	46% 42% 6% 3% 2% 1%
H_2	{1,4}{2}{3}{5}{6} (H_2) {1,2,4}{3}{5}{6}	94% 6%
H_3	{1,2,4}{3,5,6} (H_3)	100%
H_4	{1,4^+}{2}{5}{3,4^-,6} (H_4) {1,4}{2}{5}{3,4^-,6}	98% 2%
H_5	{1}{2}{3}{5}{4,6} (H_5) {1}{2}{5}{3,4,6}	81% 19%
H_6	{1,4^+}{2}{3}{5}{4^-,6} (H_6) {1,4}{2}{3}{5}{4^-,6} {1,4^+}{2}{5}{3,4^-,6} (H_4)	75% 24% 1%
H_7	{1,2}{5}{3,4,6} (H_7) {1}{2}{5}{3,4,6}	94% 6%
H_8	{1,2}{3,4,5,6} (H_8) {1}{2}{3,4,5,6}	78% 22%
H_9	{1,2,4^+}{3,4^-,5,6} (H_9) {1,2,4^+}{5}{3,4^-,6}	99% 1%
H_{10}	{1,2,5}{3,4,6} (H_{10})	100%
H_{11}	{1}{2,4,5}{3,6} (H_{11})	100%
H_{12}	{1,2,4,5}{3,6} (H_{12})	100%

Table I.3. Results from simulations, showing models supported by at least one jackknife sub-sample of each simulated data set, among the 620 models that include all possible combinations of models H_1-H_{12} (see Table I.2). Jackknife support measures the proportion of jackknife sub-samples in which each model ranks best. 100 jackknife runs used in each case. Only shown data set with $N = 39$ simulated individuals.

Models used for simulations	Modules used for PLS	% squared covariance captured by common factor	*P*-value
{1,2,4}{3,5,6}	{1,2,4}{3,5,6}	14.15	0.218
{1,2,4}{3,5,6} + common factor	{1,2,4}{3,5,6}	70.81	0.001
{1,2,4}{3,5,6}	**{1,2}{3,4,5,6}**	**16.55**	**0.001**
{1,2,4}{3,5,6} + common factor	{1,2}{3,4,5,6}	62.9	0.001
{1,2}{3,4,5,6}	{1,2}{3,4,5,6}	15.08	0.525
{1,2}{3,4,5,6} + common factor	{1,2}{3,4,5,6}	77.15	0.001
{1,2}{3,4,5,6}	**{1,2,4}{3,5,6}**	**12.34**	**0.011**
{1,2}{3,4,5,6} + common factor	{1,2,4}{3,5,6}	71.47	0.001

Table I.4. Results from application of Mitteroecker and Bookstein (2007) approach to simulated data. Common factors are extracted from simulated data sets based on two versions (i.e., with and without a common factor) of two distinct covariation structures. Analyses are designed to test the effects of (1) defining a modular structure in PLS analyses that differs from the true modular structure in the data, and (2) extracting a common factor when in fact there is no common factor in the data. *P*-value is the probability that the percentage of squared covariance accounted for by the first PLS vector is no larger than expected for two random matrices. Because simulations assume perfect modularity, this value is expected to be significant ($P < 0.05$) only in the presence of a common factor.

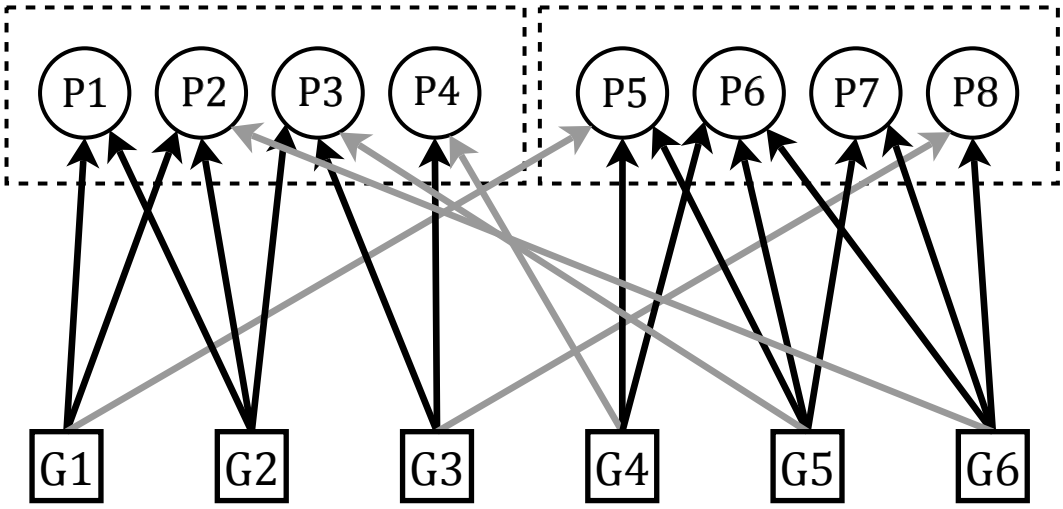

Figure I.1. Schematic representation of pleiotropic interactions in the genotype-phenotype map. The squares at the base of the arrows (G1-G6) represent individual loci, and arrows represent direct or indirect effects on phenotypic traits (P1-P8). More than one arrow indicates the presence of pleiotropy. Phenotypic traits appear integrated in two modules (delimited by dashed lines). Intra-modular effects are indicated by dark arrows, inter-modular effects by light arrows. Adapted from Wagner and Altenberg (1996).

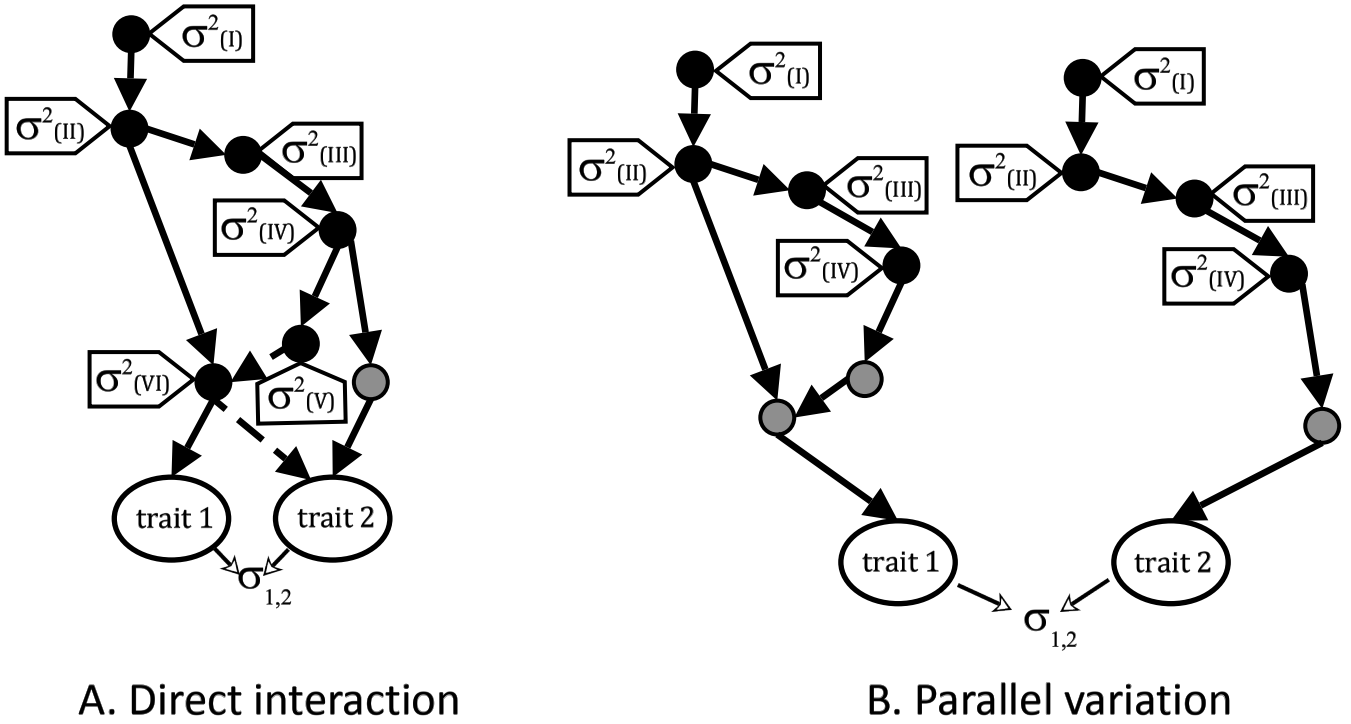

Figure I.2. Model of the effects of pleiotropic variation on phenotypic integration. A, direct interaction transduced through a single pathway shared by two traits; B, same components as in A, but decomposed into two independent pathways by deleting the interactions represented by dashed arrows in A and duplicating the remaining shared interactions among traits 1 and 2. In both cases, variation is introduced at each shared component (represented by dark circles). Variation at non-shared components (grey circles) is ignored as it does not contribute to the covariance among these traits. The symbols σ^2 and $\sigma_{1,2}$ represent, respectively, pleiotropic variation of the components of the traits' developmental pathways, and phenotypic covariation between traits 1 and 2. Distinct components of pathways are identified with numerals to illustrate patterns of shared loci. Connectors represent interactions among pathway elements, with arrows representing causal directions for these interactions, and the direction with which variation is transduced. Direct interaction produces covariation among traits that can be interpreted as developmental modularity. Parallel variation (e.g., allelic variation or environmental perturbations affecting the shared element) may produce covariation that can be interpreted as variational (but not developmental) modularity. The likelihood that parallel variation produces covariation among traits 1 and 2 is related to the number of shared components among the pathways, the dependence of the pleiotropic effects on the context where they occur, and the variation of pleiotropic effects among allelic variants of the shared components.

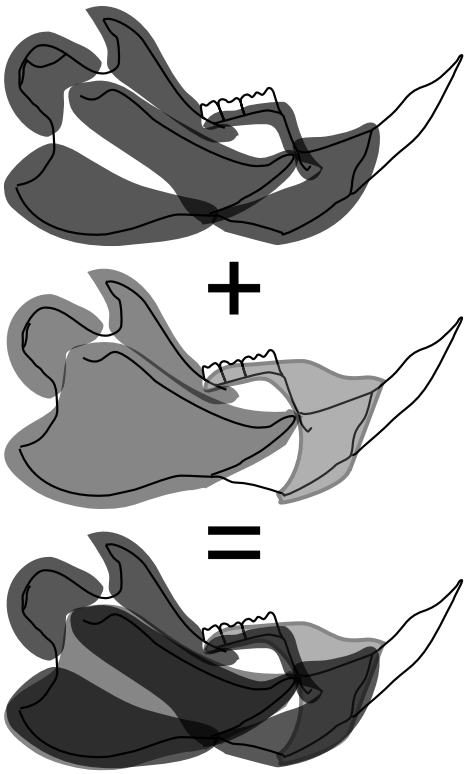

Figure I.3. Simple example illustrating the overlap of successive patterns of modularity as postulated by the palimpsest model (Hallgrímsson et al. 2007). The shaded areas in each model correspond to variational modules (top: areas of the mandible that approximately map to the mesenchymal condensations, middle: muscle attachment sites and tooth alveoli, bottom: superimposition of both models). Intensity of shading is proportional to the number of overlapping modules in a region. The idea behind the palimpsest model is that observed covariances will summarize the cumulative effects of multiple layers of modularity, represented by the model at the bottom.

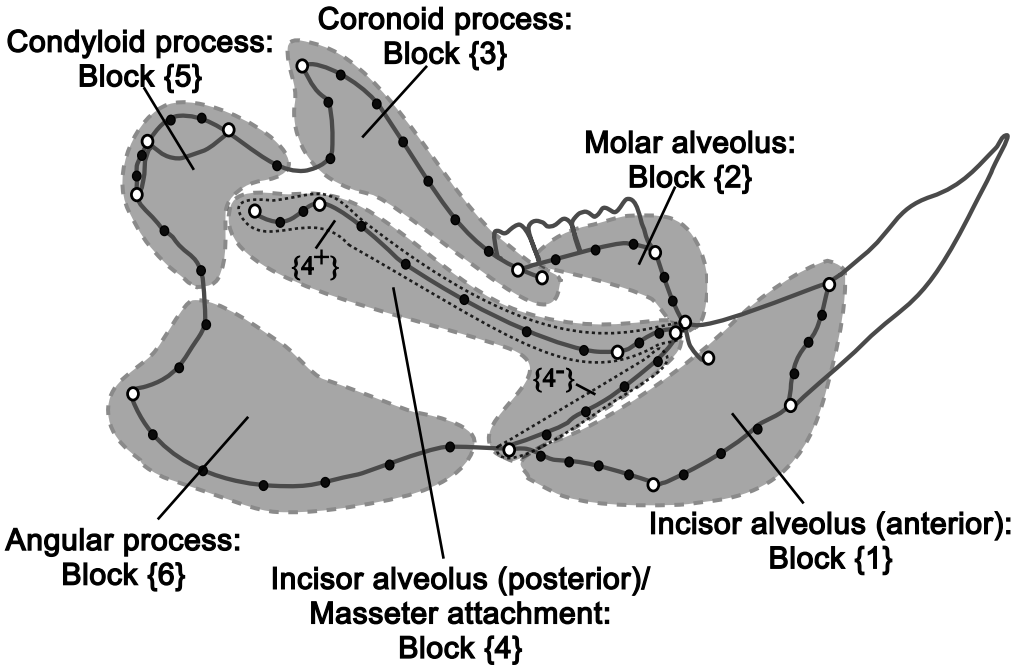

Figure I.4. Partitions of the mandible used in simulations of modular covariation structure.

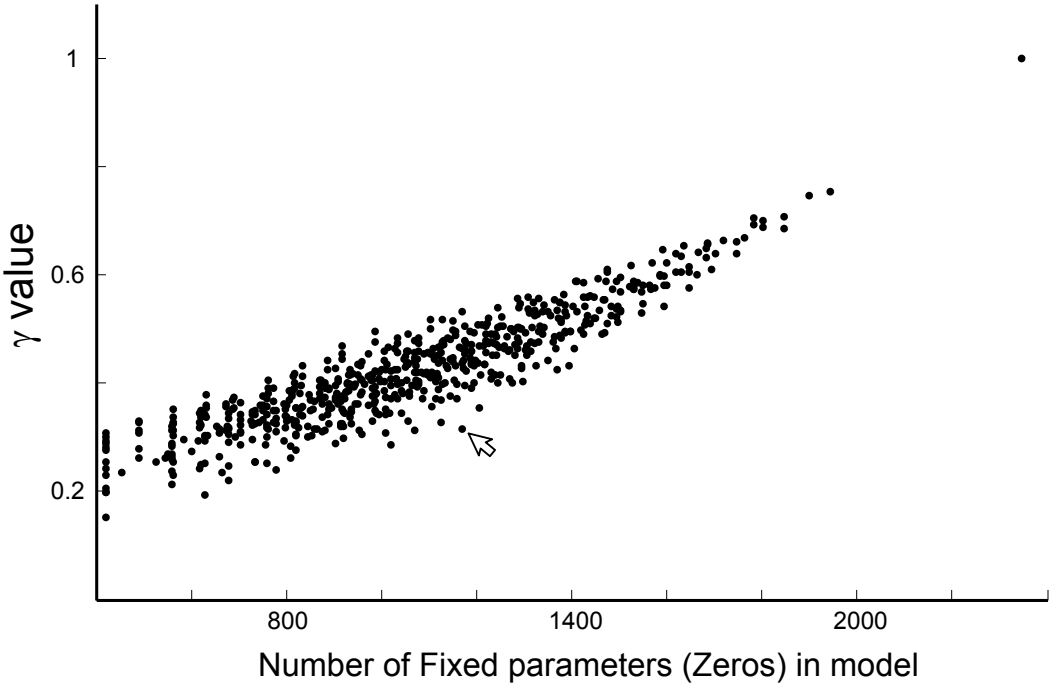

Figure I.5. Relationship between number of fixed parameters (i.e., number of zeros in covariance matrices) and γ value computed for each model. Plot includes the 620 models derived from the 12 hypotheses of modularity (H_1-H_{12}) used in simulations analyses. Arrow indicates the best-supported model in this example, i.e., model H_3 (see Table I.1 for details), after removing the effect of the number of parameters from γ (i.e., to obtain γ*). Outlier value in the top end of both axes is the 'null' model with zero covariances among landmarks (i.e., H_0).

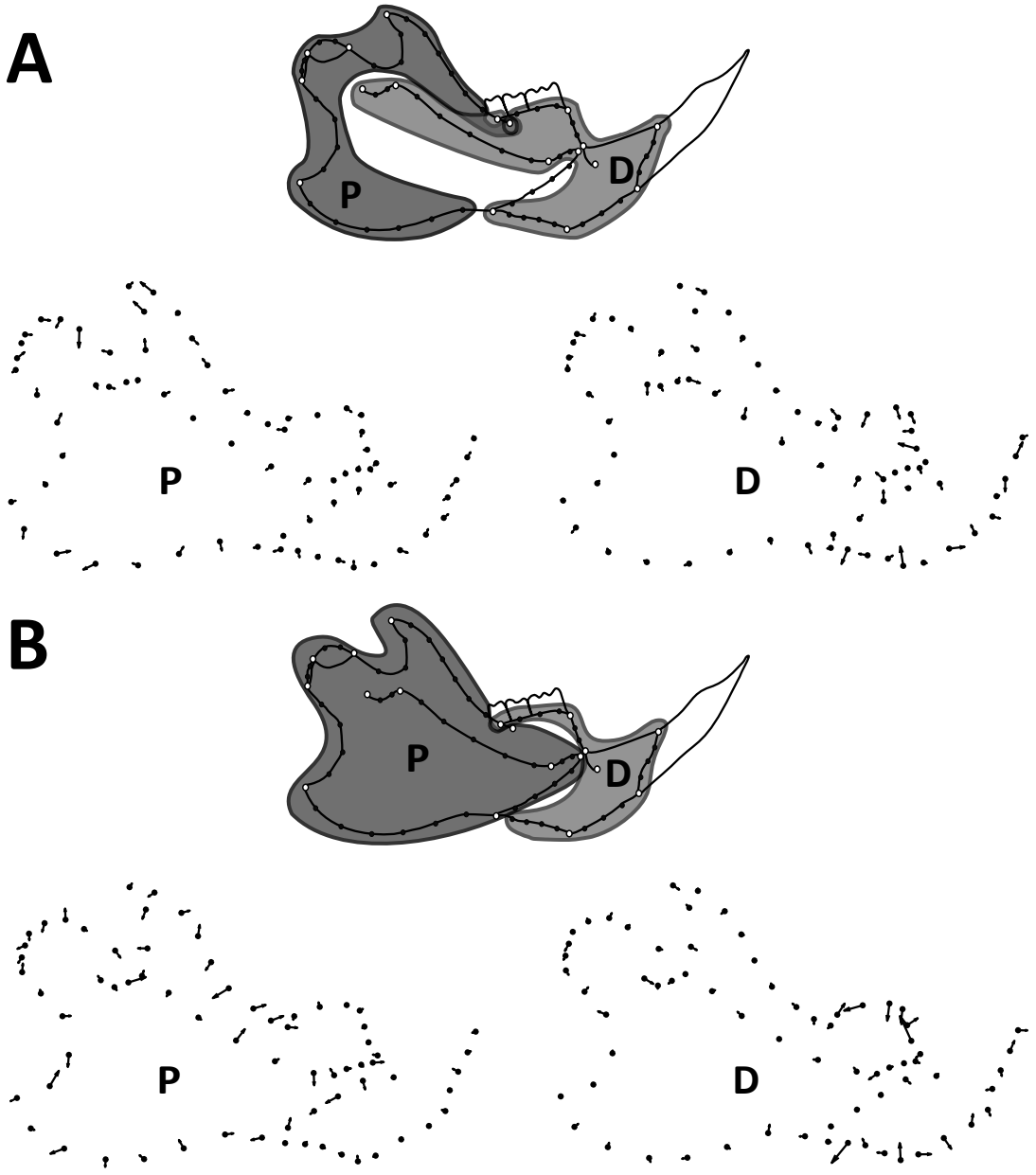

Figure I.6. Example of visualizations of modular variation using part-whole PLS. Data were obtained from simulations using models (A) H_3 and (B) H_8 (see Table I.2 for details). Each model contains a proximal (P) and distal (D) module which are projected onto the space occupied by the whole mandible using PLS. Implied deformations are shown for the first PLS axes (PLS1) obtained from both data sets. In A, PLS1 accounts for 13.91% and 15.28% of the squared covariance between the proximal and the whole and the distal and the whole, respectively, both significant at $P < 0.005$ based on 1,000 permutations. Corresponding values for case B are 14.18% and 17.48% for the proximal and distal modules, respectively, both significant at $P < 0.05$ based on 1,000 permutations. PLS axes above the first show further decomposition of the same patterns captured by PLS1.

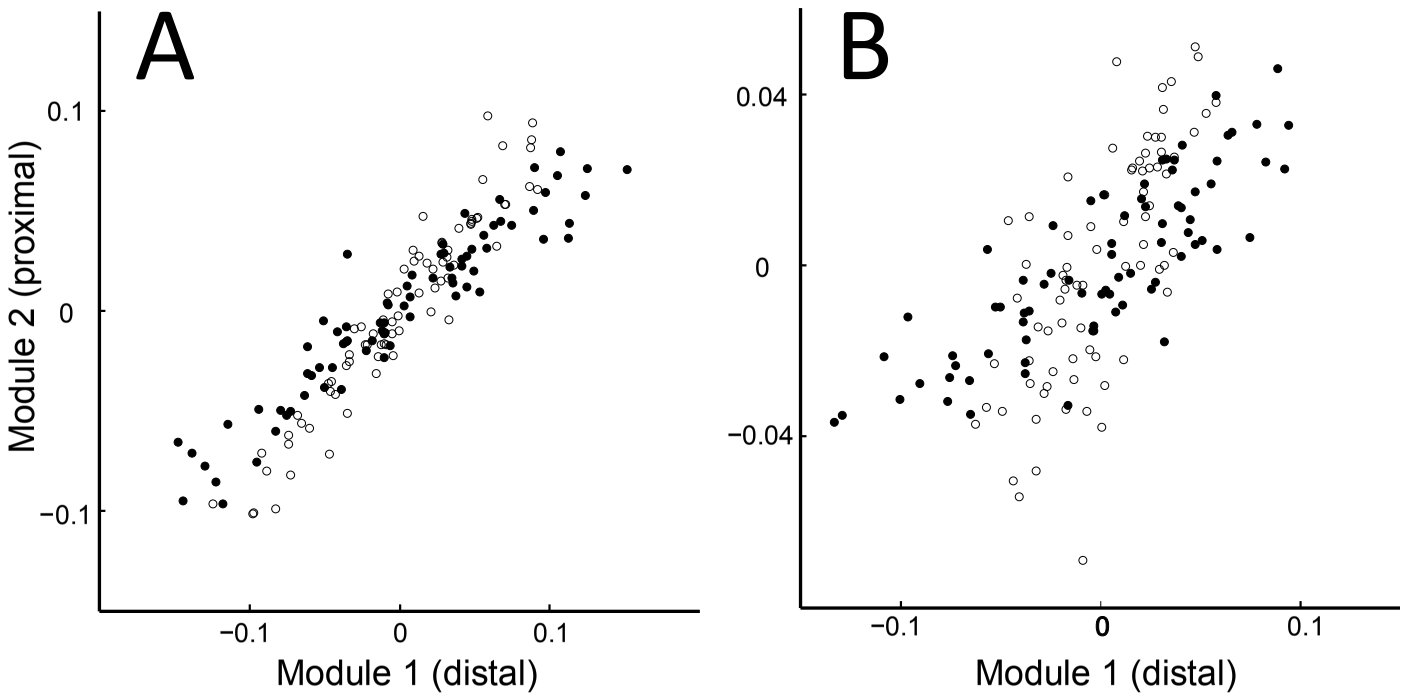

Figure I.7. Results from application of Mitteroecker and Bookstein (2007) approach using simulated data. Plots contain the scores of PLS1axes from simulations based a model of modularity specifying a proximal and a distal module of the mandible. A, simulated data includes a common factor, absent from B. In each plot, open circles indicate that the subdivision into proximal and distal partitions used in PLS analyses correspond to the partitions used to simulate the data ("correct" model); closed circles correspond to scores produced when partitions used in PLS analyses differ from the partitions used to simulate the data ("incorrect" model). Note that there is no effect of using the incorrect model when there is a common factor (A), but using the incorrect model when there is no common factor (B, closed circles) tends to resemble the pattern observed in A. See text for discussion.

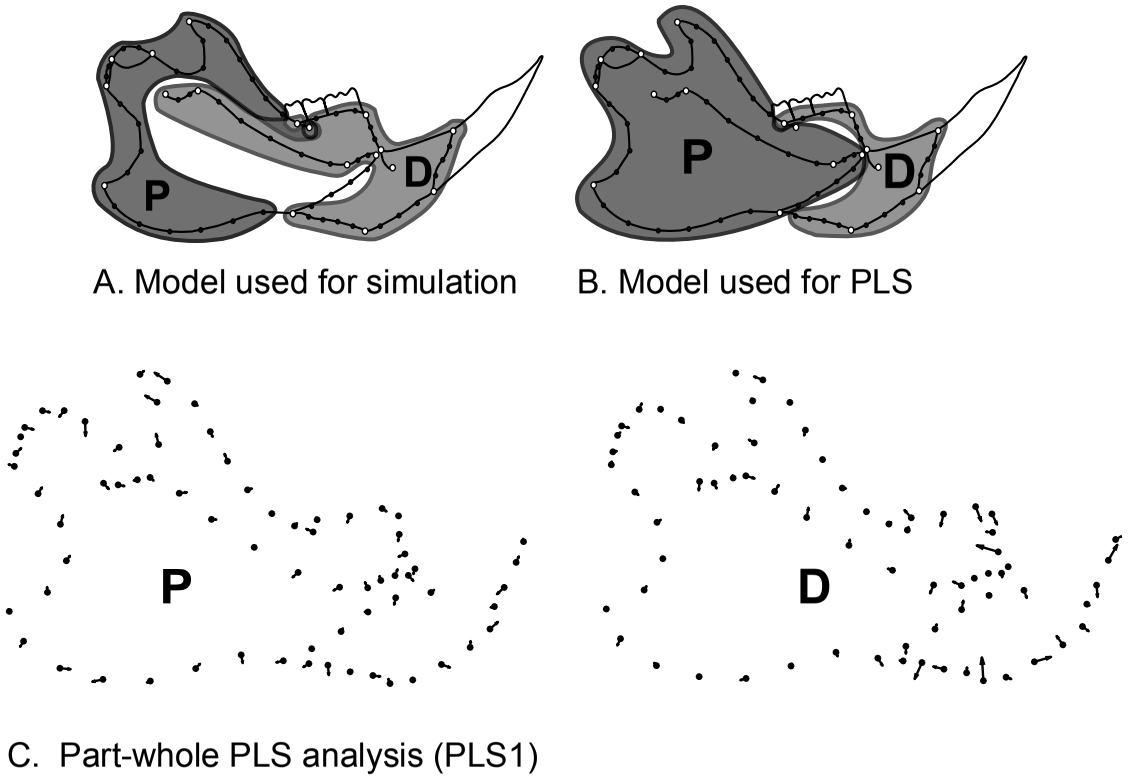

Figure I.8. Effect of incorrectly delimiting partitions as modules in PLS. A, model used for simulating data in absence of a common factor ("correct model"). B, partitions used for PLS analysis ("incorrect model"). C, deformations implied by the first axis of a part-whole PLS analysis based on the incorrect model. Notice that covariation within the proximal (P) partition (left panel) is weaker at the regions incorrectly assigned to this partition, whereas covariation within the distal (D) partition (right panel) shows covariation between the distal and proximal modules, as expected, given the model in A. PLS1 accounts for 10.48% and 20.70% of the squared covariance between proximal and distal partitions, respectively. Only the latter is significant at $P = 0.002$ based on 1,000 permutations.

APPENDIX

Annotated Matlab® code for tests of hypotheses of modularity based on 2-D landmark data using γ* as goodness of fit statistic. Annotations are preceded by the percent symbol ('% ').

```
function [d,P,summ]= mintcoretest(data,proto,centSize,disType,disWidth,disConf)

% MINTCORETEST is the core function for MINT--modularity and integration
% analysis software.  It accepts a data set and a protocol containing one or
% more modularity hypotheses and produces a distribution of covariance matrices
% for each hypothesis being tested, and a p-value for each hypothesis.
%
% Inputs:
%   - data: original landmark data (one data set only, in matrix form).
%   - proto: protocols for modularity hypotheses in a cell array, each
%     cell (in a row) containing a single hypothesis.  For each protocol, 1st
%     column = number of module, 2nd column = landmark included in each
%     module.  First protocol always corresponds to 'null model' (diag-only
%     non-zero entries).
%   - centSize: Column vector containing centroid sizes for each specimen.
%
% Parameters:
%   - disType: method used to generate null distributions: 'wish' or 'perm'
%    (Wishart/parametric and permutation/non-parametric methods)
%   - disWidth: number of covariance matrices to be included in null
%     distributions
%   - disConf: % confidence to report from output parameters.
%
% Outputs:
%   - P: P-values for each hypothesis
%   - d: value(s) of test statistic (gamma*)
%   - D: distribution of values of test statistic under each model
%   - DCI: limits of confidence of distribution as % disConf
%   - summ: cell array with full set of results
%   - datacova: covariance matrix of original data (in a cell array)
%   - nullcova: covariance matrix of null model (model #1 in 'proto')


% First, blank arrays are set up for outputs and other common structures

P = zeros(length(proto),1);
d = P;
dRaw = P;
dStd = P;
noZeros = P;
D = cell(length(proto),1);
DCI = D;
summ = cell(length(proto),8);

% Internal random-seed initialization

rand('state',sum(100*clock));

% Procrustes superimposition of data set under analysis.  Function COMPLEXFORM
% transforms a two-column set of [x,y] coordinates into a column complex
% vector.  Function XYFORMCONV transform a row coordinate vector into a
% two-column coordinate vector.  Function PROCRUSTES accepts a landmark
% data set in complex form and centroid size, and returns the data set
% after GLS superimposition, the GLS mean, and a vector with Procrustes
% distances (which remain unused in this algorithm).
```

```
for t = 1:size(data,1)
	dataC(t,:) = complexform(xyformconv(data(t,:))).';
end

[dataC,dataMean,dataProcdist] = procrustes(dataC,centSize,[]);
dataResC = dataC - repmat(dataMean,size(dataC,1),1);
dataRes = realco(dataResC); % dataRes are Procrustes residuals

% The following builds the covariance expected matrix for each model and
% compares it to the observed covariance matrix

for h = 1:length(proto)
	allPart = {};
	protoPart = proto{h};
	noPart = max(protoPart(:,1));
	for p = 1:noPart
		allPart{p,1} = dataResC;
	end

% this builds the expected value according to the model.  First,
% the original data are stacked as separate matrices whose non-zero
% entries correspond to data within (but not outside) modules:

	dataPart = [];
	for r = 1:noPart
		thisPart = zeros(size(allPart{r}));
		thisPart(:,protoPart(find(protoPart(:,1) == r),2)) =
		allPart{r}(:,protoPart(find(protoPart(:,1) == r),2));
		dataPart = [dataPart; thisPart];
	end

% this split the variance in equal parts among landmarks from overlapping
% regions (if any):

	for t = 1:size(dataPart,2)
		dataPart(:,t) =
		dataPart(:,t)./sqrt((length(find(dataPart(:,t)))/size(data,1)));
	end

% Procrustes superimposition of expected data under current model (h):

	[dataPartC,dataPartMean,dataProcdist] = procrustes(dataPart +
	repmat(dataMean,size(dataPart,1),1),repmat(centSize,noPart,1),[]);

% Computing Procrustes residuals:

	dataPart = realco(dataPartC - repmat(dataPartMean,size(dataPartC,1),1));

% The following computes gamma* value.
% First, for null model (h = 1), the for remaining models:

	if h == 1
		datacova = (dataRes.'*dataRes)./size(dataRes,1);
		nullcova = (dataPart.'*dataPart)./size(dataRes,1);
	end
	thisPartCova = (dataPart.'*dataPart)./size(dataRes,1);
	[thisStatRaw,thisStatStd,thisPartZeros] =
	mintstatstar(dataRes,dataPart,'dd',nullcova,protoPart);

% Above, MINTSTATSTAR computes gamma comparing the original matrix
% (dataRes) to the model matrix (dataPart).  Input 'dd' indicates that
% both matrices contain landmark/Procrustes residuals (as opposed to
```

```
% covariances), input nullcova is the covariance matrix of the null
% model, used to estimate gamma* from gamma, and input protoPart
% contains the protocol for the current model, used to compute the
% number of zeros (no.  of fixed parameters) in the model.

% Outputs of MINTSTATSTAR are thisStatRaw (gamma values), thisStatStd
% (gamma values standardized so that the largest value equals 1), and
% thisPartZeros (number of zeros in the current model)

      dRaw(h) = thisStatRaw;
      dStd(h) = thisStatStd;
      noZeros(h) = thisPartZeros;

% The following computes the distribution and P-values under the model,
% using the Monte Carlo approach (based on the Wishart distribution)
% or a permutation approach

      newStats = zeros(disWidth,1);
      switch disType
            case 'wish'
                  thisPartSSCP = thisPartCova*size(data,1);
                  for m = 1:disWidth
                        newMat = wishrnd(thisPartCova,size(data,1));
                        newMat = newMat*trace(cov(dataRes,1)*
                        size(dataRes,1))/trace(newMat);

% the step above rescales the SSCP matrix produced by WISHRND (a
% MATLAB function) so that variance in simulated covariances
% equals variances in observed/modeled covariance matrices

                        newStats(m) = mintstatstar(newMat/size(data,1),
                        dataPart,'cd',nullcova,protoPart);
                  end

            case 'perm'
                  for t = 1:size(dataRes,1)
                        dataResC(t,:) =
                        complexform(xyformconv(dataRes(t,:))).';
                  end

                  for p = 1:disWidth - 1
                        dataPermC = zeros(size(dataResC));
                        for m = 1:noPart
                              dataPermC(:,protoPart(protoPart(:,1) == m,2))=
                              dataResC(randperm(size(dataResC,1)),
                              protoPart(protoPart(:,1) == m,2));
                        end
                        [dataPermC,permMean,bleh] =
                        procrustes((dataPermC +
                        repmat(dataMean,size(data,1),1)));
                        dataPerm = realco(dataPermC -
                        repmat(permMean,size(dataPermC,1),1));
                        newStats(p) = mintstatstar(dataPerm,dataPart,
                        'dd',nullcova,protoPart);
                  end
      end

% The following collects gamma* values from each Monte Carlo/permutation
% as a distribution, and computes P-values

      D{h} = newStats;
      DCI{h} = [perctile(newStats,(100-disConf)/2),
      perctile(newStats,(100+disConf)/2)];
```

```
        if strcmp(disType,'wish')
                P(h) = (sum(newStats >= thisStatRaw))/disWidth;
        else
                P(h) = (1 + (sum(newStats >= thisStatRaw)))/(disWidth + 1);
        end

% Note that P-values are computed using gamma (instead of gamma*) values

end


% Computing gamma* from gamma and the number of zeros of each model

[dBeta,dIntercept,dResid] = regress(dStd,noZeros);
d = dResid + mean(dStd);

% Finally, the following builds a summary array with all results
% per model.  In order, these correspond to: #model, distribution
% of gamma values, raw gamma values, standardized gamma values,
% No.  of zeros in model, gamma* values, and P-values.

for k = 1:h
        [summ{k,:}] = deal(k,D{k},DCI{k},dRaw(k),dStd(k),noZeros(k),d(k),P(k));
end
```

CHAPTER II

CAN MODULARITY EXPLAIN PATTERNS OF INTERSPECIFIC DISPARITY? A STUDY OF DEVELOPMENTAL CONSTRAINTS IN THE CRANIOMANDIBULAR COMPLEX OF ORYZOMYINE RODENTS

ABSTRACT

Hypotheses of craniomandibular modularity were tested in nine species of oryzomyine rodents to determine whether the same causal factors shape covariance structures in all species. Such constancy is required if developmental processes are to constrain evolutionary divergence. I find that many of the same developmental modules are supported by all nine species, suggesting conservation of the factors underlying patterns of phenotypic covariation despite ample ecological diversity among these species. Moreover, a detailed examination of conserved and divergent patterns in whole-skull, cranial, and mandibular data sets suggests that different mechanisms of functional and developmental integration in crania and mandibles may result in qualitatively different patterns of modularity. While cranial modules might arise early in development and then become successively integrated, mandibular modules may be regularly maintained and integrated by distinct but overlapping aspects of masticatory function. I then address whether conserved patterns of intraspecific modularity have constrained craniomandibular diversification in this group, finding congruence between patterns of interspecific co-disparity and intraspecific modularity, a pattern that is more evident in cranial than mandibular traits. These results suggest that a causal link between intraspecific patterns of modularity and interspecific patterns of disparity may depend on the specific nature of the mechanisms responsible for modular variation.

INTRODUCTION

The primary question addressed in this study is whether developmental constraints bias evolutionary divergence, a question that has a long history(e.g., Maynard Smith et al. 1985; Arnold 1992; von Dassow and Munro 1999; Atchley et al. 1992; Beldade et al. 2002; Young and Badyaev 2006). However, few studies have examined the role that developmental processes play in directing morphological divergence (e.g.,

Jernvall et al, 2000), partly because the hypothesis only makes sense if these developmental processes are conserved (Zelditch et al. 1990; Nemeschkal 1999). If so, then it is possible to test whether directions of variation within species correspond to directions of divergence. It is commonly accepted, however, that whatever biases developmental constraints impose on evolutionary trajectories are transitory, perhaps lasting no longer than a few generations (Schluter 1996). Whether such constraints have long-term consequences has been much debated, especially whether the structure of covariation arising from developmental interactions among traits can bias evolutionary divergence at the expense of optimality of adaptation (e.g., Riedl 1977; Lande and Arnold 1983; Turelli 1988; Zeng 1988; Cowley and Atchley 1990; Houle 1991; Arnold 1992; Wagner and Misof 1993; Armbruster and Schwaegerle 1996; Schluter 1996; Armbruster et al. 1999; Badyaev and Hill 2000; Arnold et al. 2001; Sinervo and Svensson 2002; Jones et al. 2003; Wagner and Mezey 2004; Frankino et al. 2007; Walker 2007; Hunt et al. 2008; Blows and Walsh 2009). Most tests of this hypothesis focus on biases imposed by genetic covariances. But covariances are generally difficult to interpret in terms of the developmental processes underlying them (Riska 1986; Houle 1991), and a conserved developmental system can produce multiple different covariance structures (Hallgrímsson et al. 2007). Therefore, tests of the hypothesis that developmental interactions constrain divergence need to be complemented by analyses of the developmental factors that shape these covariances.

Identifying the factors underlying the structure of covariance is a serious methodological challenge because these factors can be multidimensional and non-independent. No multivariate techniques exist that can extract such structures from data without making a large number of questionable assumptions. In terms of processes, these factors correspond to developmental networks and pathways through which genetic and environmental variation is channeled and transduced (Klingenberg 2005, 2008), providing multiple opportunities for interactions among factors. These are then manifest as networks of traits that share dimensions of variation. Groups of traits that share all of their dimensions are defined as modules (Wagner and Mezey 2004), and, according to one hypothesis, it is modules that bias the directions of divergence, constraining directions of variation of traits integrated within the modules (e.g., Klingenberg 2005).

Therefore, testing this hypothesis amounts to asking three questions, namely (1) what developmental hypotheses predict the structure of modules?, (2) are those processes and resulting modules evolutionary conserved?, and (3) has morphological diversity preferentially accumulated along the same dimensions defining the conserved modules?

The present study addresses these questions using the craniomandibular complex of nine ecologically diverse species of oryzomyine rodents. To answer the first question, a novel approach is used to search for the most highly supported hypothesis among a large list of models derived from functional and developmental theories each postulating a particular modular arrangement (Márquez 2008; see also Chapter I of this dissertation). The second question is addressed by seeking the conserved modules, which are determined from the most-highly supported modules. This search yields a consensus model that specifies the anatomical regions consistently integrated into a single module within all sampled species. The third question is addressed by comparing the conserved patterns of modularity to the major directions of disparity in species means, and by fitting the hypotheses of modularity used for intraspecific data to these means.

The results support the hypothesis that patterns of modularity are highly conserved; seven species share one pattern while the other two species display unique patterns. Perhaps surprisingly, disparity among these seven species appears to be structured along the dimensions predicted by their conserved pattern of modularity. The remaining two species, again, appear to diverge in unique directions. While these results support the hypothesis of developmental constraints on evolutionary divergence, that hypothesis is more highly supported by cranial than mandibular data. The mandible appears to be more complex within species and less constrained in its divergence, thus suggesting that cranial and mandibular integration are caused by different mechanisms. These results therefore suggest that in order to answer the question initially posed in this study, i.e., whether modularity constrains divergence, it may be necessary first to consider the mechanisms whereby modular variation is generated because not all mechanisms of integration need be equally likely to produce constraints, even if they all are developmental in origin.

MATERIALS AND METHODS

Overview of methodological approach

In the present study, patterns of variational modularity are examined by testing alternative a priori models, each of which hypothesizes a distinct modular structure caused by specific functional or developmental mechanisms. In practice, the models are represented by a series of partitions, each of which delimits a region sampled by subsets of landmarks and semi-landmarks. Each anatomical subset of coordinates corresponds to a putative module and so ought to be characterized by high internal morphological integration and low integration with other such modules. The models selected for testing represent a diversity of factors including the effect of single-gene knockouts, and whole developmental and functional processes spanning morphogenesis (e.g., mesenchymal condensations; (Atchley and Hall 1991; Hall and Miyake 2000) through post-weaning growth and remodeling (e.g., effects of masticatory muscles on bone deposition and remodeling; Herring 1993). While the resulting hypotheses comprise the most exhaustive collection of models used in a study of modularity or morphological integration to date, the list is far from complete. Nonetheless, models tested in this study cover a substantial proportion of the developmental and functional processes capable of affecting covariation patterns in the mouse mandible.

The methodology for testing a priori hypotheses, described in detail in the preceding Chapter, consists of three basic steps: (1) compute the expected covariance matrix from the model, by assuming that each module resides in its own subspace within the space occupied by the entire structure, (2) compute a statistic measuring the distance between observed and expected covariances for each model, (3) determine the absolute and relative support for each model by both computing the probability that this distance is smaller than expected by chance and the frequency with which this model ranks as the best among models (i.e., jackknife support). Given that the objective is to find the best-supported model, the search is expanded to models with no known biological rationale to ensure that the entire space is sufficiently explored.

After steps 1-3 outlined above are complete, a data-to-model distance statistic (γ^*) and its confidence interval has been computed for each model, these are then sorted

to determine which model has the most support (i.e., the one with the lowest γ* value). Afterwards, the vicinity of this model is explored by listing the modules hypothesized by all of the models whose support falls within the confidence interval of the most supported one, and then searching for all possible combinations among these modules (as shown in Chapter I). In the present case, the large number of models being tested implies that it is not computationally feasible to search for all possible combinations, but a preliminary test using a subset of about 116,500 module combinations suggest that restricting the search to the vicinity of the best-supported models is a robust procedure to find the most supported models. In the following step, the models found from all possible module combinations in each of the species sampled for this study are pooled into a single set, along with all of the previously tested a priori hypotheses, and mode support is re-computed.

A final step consists of a heuristic search where the boundaries of the most supported modules found in the previous steps are modified, within individual species, to allow for the possibility that even though a particular pattern of modularity may be supported across an entire clade, the exact module boundaries need not be conserved, in the same way as the conserved causal factors of modularity (functional interactions and developmental interactions, gene expression) may be individually fine-tuned within each species, probably even suggesting the re-definition of supported modules due to extensive alteration of their boundaries. In this study, the heuristic search consisted of a basic algorithm in which the most-supported model (or model plus their module combinations, if more than one was supported by previous tests) was modified by adding and removing random landmarks to its putative modules until the resulting model could not be longer improved. Specifically, in each round of the algorithm, in five copies of the currently most supported model, a random landmark is added to a module (also randomly chosen), whereas a random landmark is removed from this module in five other copies of the model, in an attempt to avoid support for a locally (instead of globally) best model. The ten new models obtained in this way are then compared to the full set of models, and the most supported model is updated. This procedure is repeated until a better model is not found after five consecutive loops, and pilot tests suggest that the results do not change when this tolerance value is increased to 10. As is the case for any search algorithm, this

procedure has ample room for improvement, although the similarity of models independently found in individual species (see Results section) suggest that this algorithm is robust.

As in analyses carried out in the previous Chapter, model support was determined using the Matlab®-based program MINT (Márquez 2008). An unreleased of this program was used for these analyses, which includes the heuristic search algorithm and allows analyses on multiple views of a single structure (see below).

Data

Species sampling

The species sampled for present analyses belong to the oryzomyine clade of sigmodontine rodents (Table II.1; see photographs in Appendix A), which have experienced a remarkable ecological radiation and expansion throughout South, Central, and Southern North American (Carleton 1973; Voss 1988). Nine species were chosen based on phylogenetic proximity (Weksler 2003, 2006) and to ensure an appropriate representation of the ecological diversity of the clade (Table II.1). Figure II.1 shows the topology of the portion of the oryzomyine phylogeny encompassing the species sampled in this study (Weksler 2006). Although relevant ecological features such as dietary preferences are not known in detail for most species, their wide distribution, ranging from habitats as distinct as the Peruvian desert (e.g., *O. xantheolus*; Guabloche et al. 2002) to rainforest streams (e.g., *N. squamipes*; Hershkovitz 1944), strongly suggests that these species span a wide dietary spectrum (for detailed locality information, see Appendix B).

Samples were drawn from museum specimens (see Appendix B). Because this study was focused on population (co)variation patterns explicable in developmental and functional terms, it is important to control for extraneous sources of variation (e.g., geographical location, collection date, sex). Those might induce phenotypic covariances obscuring patterns of modularity. Specimens were thus chosen to maximize sample size while limiting geographical and temporal variation as much as possible. Only adult specimens, as determined by tooth eruption and wear, were used in the present study. To determine whether to pool samples from multiple geographical locations or collection

dates or sexes, the homogeneity of the sample was assessed by first comparing covariance matrices between groups (e.g., males vs. females). That comparison was done by measuring the angle between subspaces spanned by each sample (Zelditch et al. 2006); the number of dimensions used in this comparison was chosen to span at least 95% of the variation. Should that differ between samples, as might be expected when sample sizes differ, the smaller value was used. The null hypothesis that the covariance matrices differ by no more than expected by chance is tested by randomly assigning specimens to each sex, geographical location, and capture date, maintaining the original sample sizes. Angles between subspaces were computed for each of 1,000 random permutations produced in this way, and *P*-values for the null hypothesis were computed by dividing the number of permutations in which the angle equaled or exceeded the original value by the total number of permutations. After using the Bonferroni criterion to correct the *P*-values obtained from these comparisons, all supported pooling samples (see Table II.2). Final sample sizes (excluding specimens missing at least one skull view) range from 30 for *Sigmodontomys alfari* to 70 for *Nectomys squamipes* (Table II.1).

Data acquisition

Digital images of the skull were acquired from ventral and lateral views of the cranium and the right side of the mandible in lateral view (unless that side was severely damaged). Specimens were placed in standardized orientation, on a graduated rotating stage under a macro (60 mm Nikkor) camera lens (manufactured by Nikon®). A 635 nm laser level beam (manufactured by LaserMark®) was used to aid in the alignment of species in a standard orientation. In the resulting photographs, landmarks and points along curves (semi-landmarks) were digitized on a tablet PC using TpsDig2 (Rohlf 2006). Figure II.2 shows the selection of landmarks and semi-landmarks sampled for this study: 41 landmarks in the ventral view of the cranium, 54 landmarks in the lateral view of the cranium, and 18 landmarks and 51 semi-landmarks in the mandible. A full symmetric set of landmarks was digitized for the ventral view (totaling 74 landmarks), and the two sides averaged to produce the final set of 41 landmarks. The endpoints of a ruler were digitized to remove scaling artifacts produced by differences in focal distance Landmarks were transformed into Procrustes residuals by the conventional Procrustes superimposition (Rohlf and Slice 1990); semi-landmarks were superimposed by allowing

them to slide along curves bounded by landmarks to minimize the Procrustes distance among individuals, and then superimposed along with the landmarks (Bookstein 1997). Superimposition of semi-landmarks was done in Semiland6 (Sheets 2002a). Allometric variation within species was removed by calculating residuals from a regression of shape on the logarithm of centroid size using Standard6 (Sheets 2002b) separately for each species and view, adding the residuals to the mean configurations for each species/view.

The use of semi-landmarks and superimposition reduces the dimensionality of a sample because each semi-landmark supplies only one dimension; semi-landmarks can vary only in the direction perpendicular to the curve (Bookstein 1997). For that reason, there are $2k + l - 4$ dimensions, with k being the number of landmarks, l the number of semi-landmarks; the four other dimensions are lost by scaling, translation, and rotation (Bookstein 1991). This discrepancy between the dimensionality of the data and the number of coordinates is not problematic because the comparisons between hypothesized and observed covariance matrices are based on an integral metric (see below) that uses all the information in covariance matrices to produce a single scalar value. The results should therefore be invariant to geometric transformations of these matrices, differing only by scale. Therefore, ordinary Procrustes residuals (Dryden and Mardia 1998) were used to compute covariance matrices in all present analyses. The method produces the same results whether covariances are derived from Procrustes residuals or Partial Warp scores so long as the covariance (or SSCP) matrices being compared are properly scaled

Models

The initial set of hypotheses tested herein (i.e., prior to combining their modules) contains a total of 66 models (labeled H_0-H_{65}), including a "null" model (H_0) which states that there is no modularity (i.e., all covariances equal zero). These models were based on 84 modules (M_1-M_{84}), derived as predictions from the specific developmental, functional, and genetic factors detailed below (Fig. II.3). Most of these models specify non-overlapping sets of landmarks analogous to the hypotheses tested in similar studies (Klingenberg et al. 2003), which means that they have a simple structure (Mitteroecker and Bookstein 2007) of "strict modularity" in that modules are hypothesized to be statistically independent. While modules are orthogonal by design, they are not

statistically or biologically equivalent to the orthogonal vectors produced by eigenanalysis techniques (e.g., PCA, CPCA) because those eigenvectors are computed to maximize explained variance. They will therefore match a strictly modular structure only if the (orthogonal) modules account for decreasing proportions of variance. Some models, however, do not assume a simple structure but instead hypothesize anatomically overlapping modules owing to distinct processes that affect the same regions of the skull. Models that include overlapping modules contain general causal factors (e.g., masseter and pterygoid overlap in their attachment in the angular process of the mandible), and modules where multiple causal factors overlap due to their cumulative effect during ontogeny (Hallgrímsson et al. 2007). As noted in the previous chapter, overlapping modules are not statistically independent, even if they are biologically independent.

A novel approach is needed to test models that incorporate multiple views of the skull in a single analysis. This approach is needed because the variational properties pertain to the whole structure and disparate results from separate analyses of skull views may be difficult to interpret. This criterion can be relaxed in the case of the division between cranium and mandible even though these structures are affected by a number of common processes, particularly during early embryogenesis (see below). Nevertheless, each part undergoes a number of unique transformations (e.g., growth of the cranial vault affects the mandible only indirectly), and each is affected by unique functions (e.g., chewing). This combination of overlap and individuality is apparent from the definitions of modules tested herein, which may span only cranial or mandibular regions. Only in a few cases do regions within the mandible interact with regions within the cranium (Fig. II.3). Therefore, two sets of analyses were carried out in this study, the first assumes that the skull as an integrated unit comprising cranium and mandible, the second treating cranial and mandibular models separately. For the latter analyses, models including the entire structure within a single module were removed from analyses, yielding a total of 62 and 22 models for the cranium and mandible, respectively. The landmarks shared by both views of the cranium (represented as stars in Fig. II.2) were treated as if they belonged to the same module. This included situations where these landmarks were hypothesized to be independent from any other landmark (i.e., not belonging to any

module). Covariance matrices including these landmarks were computed as described in the previous chapter, i.e., after independently superimposing each configuration.

After briefly reviewing developmental and functional aspects of craniofacial ontogeny as they pertain to tests of modularity, the following sections detail the modules used to design the hypotheses of modularity tested on the oryzomyine data. Modules are classified according to their hypothesized origin into seven categories: (1) functional matrices, in which individual modules correspond to skeletal components of functional matrices, (2) differences in embryonic primordia giving rise to skull tissues, which contrast mesoderm- and neural crest-derived skull cells, (3) differences in mode of ossification (endochondral vs. intramembranous), (4) differences in embryonic tissue origin of regions of the chondrocranium mapping to the adult skull (neurocranium vs. splanchnocranium), (5) timing of developmental sequences of ossification, in which stage-specific events are hypothesized to produce integration, (6) mapping of mesenchymal condensations to postnatal skull regions as individual modules, and (7) anatomical targets of individual gene knock outs, in which regions affected by developmental gene mutations are hypothesized to be the morphological outcome of epigenetic cascades containing such genes.

Overview of craniofacial development in the context of variational modularity

The following description is primarily based on the extensive account of craniomandibular development compiled by de Beer (1985), Moore (1981), and Dixon et al. (1997), as well as reviews by Cheverud (1995) and Depew et al. (2002a).

The embryonic chondrocranium (endocranium) comprises two functionally and developmentally distinct divisions, namely the neurocranium and the splanchnocranium (viscerocranium). The neurocranium, which houses the central nervous system and sensory organs, in turn comprises a basal plate (floor) composed of a parachordal plate and a trabecular plate, and paired otic, optic, and nasoethmoidal capsules. The boundary between parachordal and trabecular plates broadly delimits the regions of the chondrocranium derived from mesenchymal condensations of cells originating from paraxial mesoderm (PM) and cranial neural crest (CNC) primordia, respectively. The parachordal cartilage develops in close association with the notochord, giving rise to

occipital cartilages and to the proximal portion of the basisphenoid. The trabecular plate originates from the fusion of two caudal (i.e., acrochordal and polar) and one rostral (i.e., trabecular) chondrification centers, which give rise, respectively, to the distal portion of the basisphenoid and the presphenoid. Parachordal cartilages are physically connected to the cartilages of the otic skeleton, whereas trabecular cartilages extend rostrally and dorsally, in structural continuity with the cartilaginous skeleton of the nasoethmoidal region (e.g., cribriform plate, nasal septum, turbinals), and the orbital region. The nasoethmoidal region forms the embryonic rostrum, whereas the orbital region both provides supports for the optic apparatus and forms the lateral walls of the braincase. The latter also structurally bridges the chondrocranium regions derived from CNC (i.e., nasal and trabecular neurocranium) and mesoderm (i.e., otic and parachordal neurocranium), thus containing cells derived from both primordia.

The splanchnocranium (viscerocranium) comprises the chondrocranial elements derived from the branchial arches and functionally and developmentally associated with the masticatory, pharyngeal, and laryngeal organs. Patterning within branchial arches is regulated by the combinatorial expression of *Dlx* genes (Depew et al. 2002b). Most relevant for the study of the adult cranium are the structures derived from the first branchial arch, which give rise to the masticatory, pharyngeal, and laryngeal apparatuses in mammals, as well as contributing to the otic skeleton (incus and malleus ossicles), orbital skeleton (lamina obturans, squamosal), basicranium (pterygoid, ala temporalis), and oral cavity (secondary palate, alveolar bone). The first branchial arch forms the primary craniomandibular joint between Meckel's cartilage (MC) and the incus, as well as, upon ossification of the dentary, the secondary and definitive craniomandibular joint, i.e., the temporomandibular joint (TMJ). The second through fourth branchial arches, although intimately linked to cephalic function, give rise to structures that are not part of the external adult cranium, and therefore are excluded from the present study, such as the stapes ossicles, and hyoid and thyroid cartilages.

The dermatocranium (exocranium) comprises discrete bones that form by dermal (intramembranous) ossification, usually as protective hard tissue surrounding a cartilaginous or otherwise "soft" element of the skull. Dermatocranial tissues are not

developmentally homogeneous, as they include bones derived from both PM and CNC cells. Thus, the parietal and most of the interparietal bones are PM-derived and ossify in association with the brain tissues around which they form, whereas remaining dermatocranial elements are derived from CNC cells and ossify around the neurocranial and splanchnocranial tissues functionally associated to the frontonasal, orbital, oral-alveolar, and dentary (mandible) regions. Development of the cranial vault structures is intimately linked to growth of the brain (Moss and Young 1960; Hoyte 1971), whereas normal development of orofacial structures requires the fusion of the facial prominences that condense around the oropharyngeal membrane (Hallgrímsson et al. 2007). Elements of the chondrocranium that do not become surrounded by dermatocranial bones instead undergo endochondral ossification, forming the postnatal sphenoid, occipital, and otic regions of the postnatal basicranium.

Following ossification of dermatocranial and chondrocranial elements of the skull, postnatal growth and development of skull bones are heavily influenced by locomotory and feeding functions, which are intimately associated to skeletal components. Of particular relevance are mastication and occlusion mechanisms, which involve a major muscle complex (i.e., masseter-pterygoid-temporalis), and teeth. Compressive and tensile forces generated by both of these processes can elicit osteoclastic and osteoblastic activity, and are primarily responsible for postnatal skull remodeling (Hoyte ad Enlow 1966; Herring 1993). Postnatal interactions between muscles, teeth, and cranial bone result in thickening of structures that serve as muscle attachment sites, such as the zygomatic arch and frontal, temporal, parietal, and occipital ridges, and thus are generally expected to have a strong influence on the structure of variation of the skull (Cheverud 1982; Zelditch 2005; Willmore et al. 2006).

The development of the skull is clearly a complex and multilayered set of processes with many potential sources of variation and covariation. As such, it may produce complex patterns of covariance in adult skulls that do not display the effects of a single process. That complexity is enhanced by the fact that the various phases described above are not discrete or hierarchically organized throughout ontogeny. Instead, they only partially overlap. Thus, for instance, the division of the embryonic chondrocranium

into trabecular and parachordal cartilages and sensory capsules does not exactly correspond to the distinction between dermally and chondrogenically ossified elements in the adult skull. Similarly, not all cranial musculature is derived from the PM, as bucco-nasal and labial muscles have a non-PM mesodermal origin. Moreover, PM-derived masticatory muscles functionally link developmentally disparate splanchnocranial (e.g., mandible ramus), calvarial (e.g., frontal ridge), and secondary cartilage (e.g., angular process of the mandible) elements. In general, an intricate pattern of intracranial associations is expected when cellular origins of the tissues and the distribution of mutational effects are taken into account. That intricacy increases when functional units of the skull are superimposed on cellular origin and the distribution of mutational effects. Consequently, any attempt to test mechanistic hypothesizes requires a careful identification of the critical predictions that can distinguish among competing hypotheses.

Developmental and Functional Hypotheses

1. FUNCTIONAL MATRICES

Attempts to partition the vertebrate skull into discernible subdivisions have a remarkably long history (e.g., van der Klaauw 1945) based on a variety of ontogenetic and functional considerations (de Beer 1985; van der Klaauw 1945). However, except for the rather coarse division into neurocranium, visceral and dermal components of the embryonic skull, there is little consensus regarding the number of basic skull components (Zelditch et al. 1992). The idea of partitioning the skull into distinct functional units dates at least to Van der Klaauw (1945), who identified 36 functional units. It was not until the "functional matrix" theory (Moss and Young 1960; Moss et al. 1972), however, that experimental manipulations were used to document the impact of individual functions on the skull's structural development. The outcome of these analyses is the view of the skull as a rigid support matrix for the soft tissues of the cephalic region, including cartilages, blood vessels, neural tissue and muscles. The functional matrix theory maintains that the dependence between structure and function is not simply due to parallel development (and evolution) of hard and soft parts but rather involves multiple interactions between these elements throughout the entire ontogeny of the skull: Bone

growth closely depends on the development of functional units. As predicted by this hypothesis, skeletal regions associated with atrophic or malformed functional units tend to become deformed or fail to develop. The distribution of skeletal effects caused by experimental manipulations of functional units has thus been used to delimit functional matrices. When results from these experiments are expressed as quantitative hypotheses (e.g., Cheverud 1982, 1995), it is easy to visualize the affected anatomical regions as the downstream targets of developmental perturbations. In terms of variational modularity, the regions of the skull affected by perturbations of a functional unit would be expected to covary under normal conditions by virtue of their close ontogenetic association to this unit, making them suitable candidates for both developmental modules and loci of evolutionary divergence. The putative modules described below are based as much as possible on reported results of experimental manipulations of functional matrices.

Two types of functional matrices have been distinguished (Moss and Salentjin 1969): (1) periosteal matrices and (2) capsular matrices. Periosteal matrices surround skeletal components and influence bone growth and remodeling via apposition and resorption. This type of matrix includes the skull musculature, most prominently the group of masticatory muscles (i.e., masseters, temporalis, and pterygoids), as well as blood vessels, glands, and cranial nerves. The specific orientation and magnitude of tensile and compressive forces on hard tissues (e.g., muscle attachment sites) and the adjacent buttresses upon which these forces load are complex and often context-dependent (Hoyte and Enlow 1966; Herring 1993). In general, however, some effect (resorption, apposition, or a mixture of both) is expected, making it possible to model variational modularity for periosteal matrices from which geometric data can be collected (e.g., bone edges and sutures serving as muscle insertion sites). In the case of muscle insertions, there is an additional element contributing to increased covariation *within* attachment sites, which is the joint migration of muscles and their associated bone-muscle connective tissues during condensation. These cell populations are derived, respectively from paraxial mesoderm and rhombencephalic neural crest (Köntges and Lumsden 1996).

Capsular matrices comprise structures enclosed within cavities surrounded by skeletal components, including the neural, nasal, otic, optic, oral, and pharyngeal matrices. According to the functional matrix theory, bone growth in capsular matrices occurs by means of passive translation of dermatocranial elements coupled with periosteal membranous ossification (Moss and Young 1960; Moss et al. 1972) and endosteal remodeling (e.g., Bruner and Ripani 2008). Therefore, we can predict modules comprising skeletal elements associated with individual matrices. By virtue of their association to major cephalic organs, capsular functional matrices have been a natural subject in many analyses of morphological integration (e.g., Cheverud 1982, 1995; Zelditch and Carmichael 1989). Five or six such matrices can be found in the cephalic region, namely calvarial, oral (sometimes including a dental-alveolar), nasal, optic, and otic matrices. In each case, development of a soft tissue stimulates and regulates the development of specific skeletal elements surrounding or providing structural support to the tissue. In this study, five capsular (oropharyngeal, nasal, orbital, otic, and neural) and two periosteal (masticatory and periosteal) matrices were hypothesized to be variational modules, each discussed individually, below.

Oropharyngeal matrix (Figs. II.3.2-II.3.5)

Development of the oral cavity is intimately linked to the nasal and pharyngeal functional matrices. Whereas the nasoethmoid complex contributes to the development of the roof of the mouth (herein treated as a component shared by the nasal and oral matrices), the pharyngeal airway plays a central role in the development of the oral cavity per se, so that skeletal elements supporting oral and pharyngeal matrices are henceforth treated as components of the same general functional matrix. The skeletal components of the oropharyngeal matrix comprise the elements surrounding the mouth, namely the palatine processes of the maxillary and palatine bones and both upper and lower alveoli, in addition to the cranial base elements that develop in conjunction with the pharynx, i.e., presphenoid and pterygoids (Bosma 1963).

A close functional link between pharyngeal and oral matrices is mediated by the tongue, whose proper development is a pre-condition for the normal development of the mandible, pharynx, and palate (Bosma 1963; Dixon 1997a; Schumacher 1997).

Removing the tongue inhibits proximo-distal growth of the mandible although it has no effect on the upper jaw, whereas collapse of the pharynx results in collapse of the mandible (Bosma 1963). Similarly, normal closure of the secondary palate requires that the tongue be displaced away from the palate (Seegmiller and Fraser 1977), which partly controls for the diameter of the pharyngeal canal, and hence the volume of the buccal cavity (Bosma 1963).

The oropharyngeal matrix is also functionally and developmentally linked to other skull elements. At the proximal end of the head, the connection between the pharyngeal airway and the trunk implies that body posture influences the orientation and diameter of the pharynx, and hence its attachment to nuchal muscles (i.e., semispinalis, longissimus, splenius, orbitoscapularis, and cleido-occipitalis; Rinker 1954), which establishes an association with the occipital attachment of such muscles (Bosma 1963). On the oral side, molar occlusion functionally links the mouth cavity with components of the masticatory apparatus in that masticatory forces tend to be dissipated through the fronto-maxillary, zygomatico-maxillary (including the maxillary-lacrimal intersection), and pterygoid-maxillary buttresses of the cranium. Removing teeth enlarges the sinus cavity owing to thinning of sinus walls (Dixon 1997b).

These observations are incorporated in present hypotheses as four distinct modules: (1) oral, including bones surrounding the buccal cavity (Fig. II.3.2); (2) oropharyngeal, comprising the oral partition plus the skeleton of the pharyngeal airway (Fig. II.3.3); (3) pharyngo-nuchal, comprising the pharyngeal capsular matrix and the head-neck periosteal matrix (Fig. II.3.4); and (4) oral-masticatory, adding the periosteal regions of dissipation of masticatory forces to the oral matrix (Fig. II.3.5).

Nasal matrix (Fig. II.3.6)

The skeletal components of the nasal matrix comprise the dermal bones surrounding the cartilaginous elements of the olfactory apparatus (nasal septum, ethmoid, cribriform plate, nasolacrimal canal, and turbinals), namely pre-maxilla, maxilla, nasals, and lacrimals. It is delimited ventrally by the roof of the mouth (pre-maxillary, maxillary surfaces surrounding the incisor foramen), and caudally by the frontonasal suture and the basis of the zygomatic process of the maxilla. To preserve the functional unity

championed by the functional matrix theory, the nasal matrix is treated herein as a single hypothetical module, even though experimental removal of internal structures (prominently the nasal septum) is accompanied of a collapse of the roof elements of the region (i.e., nasal bones) (Sarnat 1997). The nasal matrix is also related to lateral growth of the skull, particularly affecting the palatal process of the maxilla (Dixon 1997a), an effect embedded in the hypothesized oropharyngeal matrix for the purposes of present tests. Finally, the link between the rostrum and the frontonasal suture, whose synostosis causes a lateral bending of the snout (Huggare and Rönning 1997), is automatically considered by including this suture in the nasal module.

Orbital matrix (Fig. II.3.7)

The orbital region of the skull develops around the optic capsule and eye by elongation and cavitation of a number of bone processes that are also related to other functional matrices. The orbit is therefore only partially regulated by the growth and development of the eye (Hoyte 1997a), overlapping with other postulated modules. Although treated as a single putative module in this analysis, the orbital skeleton spans elements of the lateral wall of the braincase (lamina obturans, temporal process of the squamosal, and lateral process of the frontal) and elements associated with the nasal matrix (frontonasal complex, including lacrimal and maxillary bones), and with the zygomatic arch (zygomatic processes of squamosal and maxillary and jugal), which also has a major role in the masticatory apparatus.

Otic matrix (Fig. II.3.8)

The otic skeleton forms around the labyrinth and ossiculo-tympanic complex, and comprises, for the purpose of the present study, the auditory bulla, internal and external auditory meatus, and periotic bone. These elements are treated as a single functional unit, by virtue of their functional and physical detachment of the otic apparatus from the basicranium from which it is ventrally and laterally separated by the sphenotympanic and squamotympanic fissures. It is only postnatally fused at the periotic-mastoid interface (Baer et al. 1983).

Neural matrix (Figs. II.3.9-II.3.11)

According to Moss and Salentjin (1967), the effect of the growing brain on the development of the braincase is analogous to the effects of sensorial capsules (otic, optic, nasal), in that it is the volume of the soft tissue, irrespective of its actual functionality that stimulates and regulates the growth of calvarial bones. In this view, parietal, interparietal, and frontal bones, as well as the temporal processes of squamosals, which altogether form the calvarium, are passively translated on the external surface (ectomenix) of the growing brain and undergo compensatory appositional growth at their sutures (Moss et al. 1972). The main influence of this process on the cranial base occurs at the endocranial surface (Bruner and Mitani 2008) although basicranial growth parallel to calvarial growth is seen in the occipital region (Moss et al. 1972). Postnatally, the main orientation of braincase growth is along the antero-posterior axis, which is thought to orchestrate the major rotation of the skull in which the angle separating the basicranium from the rostrum is flattened, causing the foramen magnum to be dorsally displaced as well as the nasal bones to become more closely aligned to the frontals (Baer et al. 1972; Moss et al. 1987). This pattern of growth seems to be independent of posture, as noted below (Fanghanel 1974, cited by Schumacher 1997). In the present study, these observations are interpreted as indicating a subdivision of the entire cranium into three putative partitions: calvarium (Fig. II.3.9), basicranium (Fig. II.3.10), and rostrum (Fig. II.3.11).

Masticatory matrix (Figs. II.3.12-II.3.16)

The masticatory function of the skull is carried out by the group of four major muscles connecting the mandible to the cranium, namely medial and lateral pterygoid, temporalis, and masseters. Numerous experiments involving partial section and re-section of these muscles have demonstrated their individual contributions to the morphogenesis and postnatal shaping of the processes of the mandible as well as the cranial surfaces upon which they exert mechanical loads (e.g., Avis 1961; Hohl 1983; Brennan and Antonyshyn 1996). These experiments demonstrate a functional and developmental dependence between muscles and their areas of attachment and tensile loading in the mandible, specifically between: (1) temporalis muscle and the coronoid process (e.g., Washburn 1947; Hohl 1983; Brennan and Antonyshyn 1996), (2) lateral

pterygoid muscle and the condyloid process (e.g., Hinton 1990), and (3) medial pterygoid and masseter muscles and the angular process and proximal end of the mandible ramus (e.g., Avis 1961; Hohl 1983). More relevant for tests of mastication as an integrating factor, however, are the effects of these muscles on skull growth and development. In this sense, a central role in the development of the cranial vault has been demonstrated for the temporalis muscle in that either removing or paralyzing it causes substantial modifications of the temporal and supraorbital regions (e.g., Brennan and Antonyshyn 1996). In fact, it has been postulated that the rounded shape of the calvarium is maintained by a balance between the compressive outward forces exerted by the growth of the brain and tensile downward forces exerted by the temporalis. Unilateral sectioning of this muscle leads to overgrowth of the temporal region in the manipulated side in dogs (Köster and Mierzwa 1985, cited by Schumacher 1997). Similarly, significant alterations in the basicranium result from manipulation of masticatory muscles, most evident at synchondroses (Wieslander and Tandläkare 1963). These effects originate either at the attachment of the medial pterygoid muscle or the temporomandibular joint. In the latter case, variation in the articulation leads to variation in shape of the condyle (Kantomaa and Hall 1988). Finally, the masseter muscles influence the development of the zygomatic arch even though removal or paralysis of these muscles does not completely eliminate this structure, merely reducing it (Pratt and Loring 1943) perhaps because that arch also serves as a component of the ocular skeleton.

The following masticatory partitions are tested in present tests: (1) coronoid process plus temporal ridge, associated to the temporalis muscle (Fig. II.3.12); (2) proximal half of the mandible plus zygomatic arch, associated to the masseter muscles (Fig. II.3.13); (3) angular process plus pterygoid fossa, associated to external pterygoids (Fig. II.3.14); (4) condyloid process plus glenoid fossa, associated to the TMJ (Fig. II.3.15); and (5) a comprehensive module combining all of these four partitions, corresponding to the full "masticatory" matrix (Fig. II.3.16).

Postural (nuchal) matrix (Fig. II.3.17)

The final functional matrix considered in this study accounts for the effect of neck musculature, which is largely a function of body posture. A link has not been

demonstrated between angle of the foramen magnum relative to the cranial base and verticalization in mice; however, amputation of upper extremities appears to exert significant influence on the shape and relative orientation of both rostrum and mandible, leading to a brachycephalic skull characterized by a shorter snout, apparently as a result of a shortening of the palate and mandible (Fanghanel 1974, cited by Schumacher 1997). Elsewhere in the skull, the only noticeable effect of bisection of neck muscles is on the occipital ridge on which these muscles insert (Hoyte 1997b). This matrix is included in the present study for purposes of completeness even though postural effects seem relatively unimportant compared to other skull functions. This hypothesized module predicts integration among the distal half of the mandible ramus, the palate, and the occipital ridge.

2. TISSUE PRIMORDIA

The bone and cartilage of the skull is derived from two cell-lineages, paraxial mesoderm (PM) and cranial neural crest (CNC). Paraxial mesoderm comes from the somitomeres surrounding the distal portion of the notochord. The cells migrate to form the condensations that give rise to cranial muscles and parachordal elements of the embryonic neurocranium, including the proximal portion of the presphenoid, basisphenoid, and occipital segments that develop around the notochord, with basioccipitals forming the floor and the exoccipitals forming the lateral extensions joining dorsally to make the supraoccipital region (Noden 1978; Jiang et al. 2002). Parachordal elements condense as paired sets of chondrifications which later join medially as synchondroses or appositionally. Cells derived from the PM also give rise to the mesenchyme of the otic capsule, cartilages associated with vestibular and cochlear apparatuses and parts of the optic capsule, and the orbital region via mesodermally-derived portions of the sphenoid and parietals. Finally, mesenchyme of calvarial bones posterior to the coronal suture (i.e., parietals and most of the interparietal) also derive from PM (Couly et al. 1993; Jiang et al. 2002; Yoshida et al. 2008).

The CNC forms in the folds of the distal portion of the neural tube at the intersection between neural tube and ectoderm and is therefore regarded as ectodermal in origin (Baker and Bronner-Fraser 1997). The fate of cells migrating from the CNC is

varied, including mesenchyme of both chondrocranial and dermatocranial elements as well as the alveolar regions and teeth. In the chondrocranium, CNC-derived cells give rise to the trabecular, nasoethmoidal, and most of the orbital regions as well as the mesenchyme of the splanchnocranium. In the dermatocranium, CNC-derived cells are precursors of the dermal bones associated with the splanchnocranium (squamosals, jugal, maxillary, dentary) and dermal bones that develop in conjunction with the nasal apparatus (pre-maxillary, frontonasal complex, lacrimals), as well as upper and lower alveolar bone (Noden 1978).

The CNC primordium is segmented into three regions according to the region of the developing brain from which they are derived, i.e., forebrain (FB), midbrain (MB), and hindbrain (HB). Fate mapping has shown that CNC cells derived from these subdivisions contribute to distinct populations of cranial mesenchyme. Thus, cells from FB migrate to the orbital region and the frontonasal process, whereas cells from the rostral aspect of MB migrate to the mandibular extension of the first branchial arch and orbital and frontonasal regions, where they appear to mix with FB-derived cells. The HB, on the other hand, is clearly segmented into 7-8 rhombomeres which migrate along three clearly delimited cell streams that correspond to the first three branchial arches. Cells derived from rhombomeres 1 and 2 (R1 and R2), mixed with some cells derived from the caudal aspect of the MB, forming the first of these streams, condensing in the first branchial arch that had previously been colonized by MB-derived cells. A second stream, comprising cells derived from R4, condenses in the second branchial arch. Finally, cells derived from R6, R7, and R8, form a stream that condenses in the third branchial arch (Couly et al. 1993; Chai et al. 2000).

Hypotheses of modularity are constructed by assuming that tissues derived from a single primordium share a number of regulatory mechanisms, timing and physical location both before and after migration, any or all of which could cause covariation. Variation in cell population sizes, rates of cell division and cell death, and rates of migration of PM and CNC cells are expected to produce covariances among the "downstream" traits influenced by these processes. Present tests include a general hypothesis of modularity based on skull primordia, in which the skull is partitioned

according to the major source of mesenchyme, i.e., PM (Fig. II.3.18) vs. CNC (Fig. II.3.19).

3. Mode of ossification

The skull can be divided into chondrocranium (endocranium) and dermatocranium (exocranium), the first ossifying endochondrally, the second intramenbranously. Within the chondrocranium, neurocranial elements derived from parachordal cartilages, external elements of the otic complex, and proximal elements of the trabecular cartilages undergo endochondral ossification. A number of ossification centers later coalesce to form the bones of the basicranium. The rostral components of the cartilaginous neurocranium, in turn, disappear or persist as cartilages throughout ontogeny, being replaced or surrounded by dermal bone, a fate shared with elements of the cartilaginous viscerocranium and calvarial bones. Such bones develop from mesenchymal condensations that grow outwardly via intramembranous ossification until they meet, forming fibrous sutures, after which they continue to grow at their periosteal surface (Baer et al. 2003). As a result, the external bones of the adult skull can be categorized according to whether they result from endochondral ossification of primary cartilage or intramembranous ossification. This distinction could contribute to skull integration because the genetic and epigenetic factors involved in these two modes of ossification differ considerably in terms of (1) the involved developmental pathways, (2) their dependency on functional attributes of the skull in that the chondrocranium is traditionally seen as being less dependent on epigenetic interactions than the dermatocranium (Moss et al. 1972; van Limborgh 1982), (3) their responsiveness to endocrine factors such as growth hormones (Nilsson et al. 1986), and (4) their sensitivity to environmental fluctuations (Young and Badyaev 2007). Such differences thus make it possible to postulate that each subset of skull components is a separate module (endochondral ossification: Fig. II.3.20, membranous ossification: Fig. II.3.21). In addition, it is possible to consider an additional tissue type that does not undergo either form of ossification, namely the secondary cartilage that caps the periosteal surface of the condyle and angular process of the mandible (de Beer 1985), which is herein tested as an additional hypothetical module (Fig. II.3.22).

4. SPLANCHNOCRANIUM VS. NEUROCRANIUM

The distinction between the splanchnocranium and neurocranium is established early in skull ontogeny. Even though other hypotheses posit finer subdivisions of these components, a distinction between the two is justified by abundant evidence that the branchial arches rely on unique developmental pathways, including distinct axes (antero-posterior, medio-lateral, and dorso-ventral) of epithelial signaling for specification of arch-specific structures (e.g., teeth), and possibly even a unique Hox-code determination of arch identity (Depew et al. 1999). For the present study, the partitioning of the neurocranium is identical to that defined for the basicranium according to the functional matrix theory (Fig. II.3.10). The distinction between that model and this is the addition of the splanchnocranial partition, one that includes all dermatocranial elements derived from the first branchial arch, namely mandible, maxillary, squamosal, jugal, lacrimal, palatine, and alisphenoid bones (Fig. II.3.23).

5. TEMPORAL PATTERNS OF OSSIFICATION

Whereas most skull bones that undergo intramembranous ossification develop from one or a few ossification centers through periosteal accretion, over one hundred paired and unpaired endochondral ossification centers have been identified in the chondrocranial skeleton, which continue to expand until they fuse within individual elements or meet at synchondroses (Hoyte 1997b). The hypothesis that distinguishes intramembranous from endochondral, previously discussed, ignores the potential effects of chronological sequence of ossifications. The present model incorporates that timing effect which could result from epigenetic and micro-environmental signals that affect regions of the skull at particular developmental stages. Consequently, elements undergoing simultaneous ossification may be affected by the same signals. For the present study, information about ossification sequences is taken from that for the house mouse (*Mus musculus*; Kaufman and Bard 1999) to derive five putative models reflecting the relative timing and distribution of ossifying skull regions. The modules represented in this study correspond, respectively, to the following Theiler Stages/Embryonic age (in days) in the house mouse (Kaufman and Bard 1999): (1) TS 22-23/E 13.5-14.5 (Fig. II.3.24), (2) TS 23/E 14.5 (Fig. II.3.25), (3) TS 24/E 15.5 (Fig. II.3.26), (4) TS 25/E 16.5 (Fig. II.3.27), (5) TS 26/E 17.5 (Fig. II.3.28), and (6) perinatal (Fig. II.3.29).

6. MESENCHYMAL CONDENSATIONS

Mesenchymal condensations have been regarded both as the basic building blocks of complex morphological structures and as the most basic morphogenetic units capable of producing an evolutionary response (Atchley and Hall 1991). The interpretation of mesenchymal condensations as units of development and evolution has been based on the spatiotemporal distinctiveness of these cell aggregates, as well as on their potential to differentiate into many tissue types (Hall and Miyake 2000; Hall 2003). The distinction of mesenchymal condensations is argued on the grounds that this is the stage at which genes are selectively up- or down-regulated, preceding the onset of expression of genes specific to the differentiated tissue. In their general model for the development and evolution of complex structures (i.e., those derived from multiple condensations), Atchley and Hall define parameters of cell condensations as fundamental developmental units. These units include the number of stem cells, the timing of the initiation of condensation, the fraction of mitotic cells, the rate of mitosis, and the rate of apoptosis. Natural selection is presumed to operate on these parameters. The model does not rule out natural selection acting at later ontogenetic stages, but it does propose that condensations are the most basic units in morphological and developmental evolution.

For the most part, individual, suture-bound elements of the dermatocranium can be traced back to single condensation of either PM or CNC-derived cells (Noden 1978; Jiang et al. 2002). In contrast, synchondrosis-bound elements of the chondrocranium often result from the aggregation of more than one chondrogenic center (Kaufman and Bard 1999), making it impossible to trace actual condensations from adult specimens. However, single condensations are not split into separate (synchondrosis-bound) elements so treating each as a single unit is reasonable. The chondrocranial elements of interest for the purpose of this study are those that form the basicranium, which develop largely within the basal plate from parachordal or NC origin. Caudally, the occipital bone develops from paired basal chondrogenic centers that coalesce medially and give rise to the basioccipital, forming lateral extensions, i.e., the future exoccipitals, and meeting dorsally to give rise to the supraoccipital. Further rostrally, the basisphenoid is derived from the fusion of at least two condensation centers, one (caudal) of parachordal origin, the other (rostral) of trabecular origin, whereas the presphenoid, rostral to the

basisphenoid, forms from a condensation of NC origin. Both basisphenoid and presphenoid develop lateral projections. Basisphenoid projections extend into the greater temporal alae that fuse with the anterior lamina, which has a membranous origin and is derived from a separate condensation, to form the alisphenoid. This bone is therefore considered herein only cautiously as a putative module. For similar reasons, the external auditory complex, which includes the periotic bone, bulla an and auditory meatus, is split into two modules, one corresponding to the periotic, which condenses as a single cartilage surrounding the auditory labyrinth, and the mastoid-bulla complex, which develops in membrane from the endo- and ectodermal surfaces of the first pharyngeal pouch, respectively, from the coalescence of numerous bulbous projections.

The dentary bone is a special case, as it is the sole dermatocranial bone that develops from the coalescence of six morphogenetic condensations of CNC origin. One additional condensation forms the Meckel's cartilage, but this makes little contribution to the adult mandible. The other six condensations give rise to (1) the central ramus, (2) the odontogenetic incisor alveolus, (3) odontogenic molar alveolus, and the (4) coronoid, (5) condyloid, and (6) angular processes. Two processes develop from a combination of intramembranous and chondrogenic ossification with associated secondary cartilage (i.e., angular and condylar), and a membranous process (i.e., coronoid) that develop within the anlage of the temporalis muscle before attaching to the mandible ramus (Atchley and Hall 1991; Cheverud et al. 1991).

A total of 22 modules are defined in association with mesenchymal condensations in the craniomandibular complex, corresponding to the following structures: (1) basioccipital (Fig. II.3.30), (2) supraoccipital (Fig. II.3.31), (3) exoccipital (Fig. II.3.32), (4) basisphenoid plus ala temporalis (Fig. II.3.33), (5) presphenoid (Fig. II.3.34), (6) lamina obturans (Fig. II.3.35), (7) palatine plus pterygoid (Fig. II.3.36), (8) periotic (Fig. II.3.37), (9) tympanic bulla (Fig. II.3.38), (10) parietal (Fig. II.3.39), (11) interparietal (Fig. II.3.40), (12) squamosal (Fig. II.3.41), (13) maxilla plus lacrimal (Fig. II.3.42), (14) premaxilla (Fig. II.3.43), (15) nasal (Fig. II.3.44), (16) frontal (Fig. II.3.45), (17) molar alveolus of the mandible (Fig. II.3.46), (18) incisor alveolus of the mandible (Fig.

II.3.47), (19) mandible ramus (Fig. II.3.48), and (20) condyloid (Fig. II.3.49), (21) coronoid (Fig. II.3.50), and (22) angular (Fig. II.3.51) processes of the mandible.

7. MUTATIONAL TARGETS

Many of the secreted factors and signaling molecules involved in regulation of skull development are specific to particular types of processes (e.g., chondrification, osteoblast differentiation) but some participate in multiple disparate processes. Consequently, allelic variation of these factors is potentially able to produce covariation among traits influenced by multiple pathways, which would be evinced as variational modularity (Klingenberg 2005; see Chapter I for further discussion). The primary experimental approaches used to establish the anatomical targets of these signaling molecules and the associated transcription factors is to knock out specific genes in a systematic manner. The results are often sensitive to genetic background, and it can be difficult to determine the extent to which variation induced by these kinds of experiments mimics natural variation because the knocked out genes might be devoid of standing variation in natural populations. Therefore, mutational targets are better interpreted as modules in the sense that such mutations reveal the presence of an underlying epigenetic cascade affecting a particular anatomical region. However, one important caveat is that not every mutation within a developmental pathway will have the same effect on morphology. Thus, even though the epithelial factor *endothelin-1* regulates the transcription factors *dHAND* and *Msx1* (Thomas et al. 1998), knockouts of these individual genes produce notably distinct effects on the skull morphology (see Table II.3; Satokata and Maas 1994, Yaganisawa et al. 2003, Kurihara et al. 2004).

The hypothetical modules used in this study correspond to known mutational targets of regulatory genes of skull development (listed in Table II.3). Many of the genes included in this study have been compiled in a recent review by Depew et al. (2002a). The hypotheses are based on the photographs of mutants plus verbal descriptions of mutational effects by the original authors of each study. A total of 24 secreted factors and 24 transcription factors with diverse regulatory roles were considered during this study. After merging those mutations with identical effects into a single module and those mutations suggesting modules that were indistinguishable from other modules used

in the study, a total of 14 and 19 new modules were added, corresponding to secreted and transcription factors, respectively (see Table II.3).

Hypotheses of modularity

The initial set of hypotheses is based on certain combinations of individual modules illustrated in Fig. II.3. This gives a total of 66 models (listed in Table II.4), with H_0 corresponding to the null model of no modularity or integration (i.e., all covariances equal to zero). Models H_1 to H_{21} represent alternative versions of the hypotheses derived from the functional matrix theory. Model H_1 divides the skull in three partitions (calvarium, basicranium, and rostrum-mandible) to represent the skull-wide effect of brain growth. Antero-posterior growth of the braincase has a flattening effect on the angle between rostrum and basicranium (Moss et al. 1987), whereas lateral growth of the brain case exerts tensile forces onto the basicranium (Bruner and Ripani 2008). For purposes of this study, this effect is interpreted as three separate effects on regions spanned by the three modules defined in H_1. Models H_2 and H_3 seek to account for masticatory function. H_2 comprises modules M_{12}-M_{14} depicting the functional influence of the temporalis, masseters, and pterygoid muscles, respectively, and M_{15}, which links the cranial and condylar components of the temporomandibular joint; H_3, on the other hand, is based on module M_{16}, which combines the effects of the three major masticatory muscles in a single module. Models H_4 to H_9 depict several alternative versions of modules presumably associated with the same general function. Each includes M_6 (nasal capsule), M_7 (orbit), M_8 (otic capsule), and M_9 (calvarium) but they vary with respect to M_2, M_3, or M_5, each a different version of the oral matrix (oral-only, oropharyngeal, and oral-masticatory, respectively). Similarly, a postural (nuchal) matrix is included either by itself (M_{17}) or as integrated with an oral component (module M_4). Models H_{10} to H_{24} combine models H_4-H_9 with either model H_2 or H_3, adding masticatory function to those represented in other models.

Models H_{22}-H_{24} contrast the variational patterns expected according to the tissue-primordium hypothesis, including a PM-only module, a CNC-only module, and a combination of the two. Models H_{25} and H_{26} contrast endochondral and membranous

ossification, and endochondral ossification, membranous ossification, and secondary cartilage, respectively.

Models H_{27}-H_{30} contrast structures derived from splanchnocranium and neurocranium. Model H_{27} includes a single module (M_{23}) corresponding to splanchnocranial elements, whereas models H_{28}-H_{30} also include the neurocranium, represented either as the set of walls and roof of the braincase (frontals, parietals, interparietals, and squamosal process of the squamosals, M_9), or as a braincase-basicranium complex (parietals, interparietals, occipitals, and sphenoid, M_{18}). In addition, models H_{29} and H_{30} include module M_8, corresponding to the auditory bulla, given that this structure is derived from neither splanchnocranium nor neurocranium, being instead of endodermal origin (Depew et al. 2002a). Models H_{31} and H_{32} are based on the chronological sequence of ossification in *Mus* and the structures derived from mesenchymal condensations in the craniomandibular complex. Hypotheses H_{33} to H_{65} predict that a single mutational target (as defined in Table II.3) is a single module. Hypotheses H_{33} to H_{46} correspond to secreted factors whereas H_{47} to H_{65} correspond to transcription factors. Each mutational target is modeled separately because there is no obvious way in which they can be meaningfully combined. Analyzing all possible combinations—7672 and 84466 models from secreted and transcription factors, respectively, makes prohibitive computational demands. Furthermore, preliminary analyses of models that combined all secreted factors or all transcription factors in a single model produce models with extremely low empirical support, scoring among the worst of all competing hypotheses.

Comparative analysis of intraspecific patterns of modularity

Consensus model

Shared elements of supported models can be combined into a 'consensus' hypothesis, i.e., a model containing only modules supported in all or most species. Such a consensus could be obtained for each internal node on the phylogeny, but that phylogenetic approach would be better suited for analyses based on a larger number of species and clades. In the present study, a "horizontal" consensus was built by combining models from all sampled species, using theoretical and heuristic models. A

consensus built in this way should not be interpreted as an interspecific average or overall trend; instead, a consensus includes those modules that are common to all or nearly all species, and thus can potentially be interpreted as a set of phylogenetically conserved modules.

Interspecific comparisons in model space

When comparing species with respect to fit among competing models, the statistics γ and γ^* can be interpreted as the distance between each species' data and the model. However, when a single model fits two or more species equally well, it does not necessarily follow these species are separated by a short distance because two objects that are equally distant from a third need not occupy the same position, especially in high-dimensional spaces. To increase the precision with which a species' position is determined, it is useful to have a large number of reference points, i.e., additional models. In this study, this was accomplished by constructing a vector of γ^* values (one per model being tested) for each species. This vector has two interpretations. The first is as a set of distances between the observed covariation matrix and a large number of patterns with known pattern of modularity. The second is as the coordinates for the data in a 'model space' centered on a species' covariance pattern. Because each species' model space is potentially centered at a different position, only the direction of these vectors is comparable across species. In this study, those directions were compared by the correlation coefficients between γ^* vectors for pairs of species, providing an indirect comparative approach of their underlying patterns of integration.

RESULTS

Intraspecific patterns of modularity

Following is a detailed description of the results of tests of hypotheses for each of the nine oryzomyine species sampled for this study (summarized in Table II.5).

Holochilus chacarius

Of the 66 models initially tested for the skull data set, which spans the cranium and mandible, the most strongly supported is H_1, which partitions the skull into calvarium, basicranium, and rostrum (jackknife support for this model is 95%). Of the

models initially tested for the cranium-only data set, empirical support is split among three models: H_{24} (25%), which posits two modules, one the calvarium-basicranium, the other the calvarium-rostrum module; H_{60} (39%), which posits a single calvarium-rostrum module; and H_{48} (26%), which posits a single module containing elements of the basicranium, calvarium, and rostrum. Of the models initially tested for the mandible, one is most highly supported, H_{32} (100%), which posits partitions that correspond to mesenchymal condensations. In comparisons based on the full set of models (comprising the 66 initial models plus the module combinations from the most-supported among the initial set of models), one model was supported by each data set (Fig. II.4A). Both skull and cranium data sets supported a single model, comprising modules M_{11}, associated with the rostrum, and M_{18}, associated with the neurocranium. The mandible data support a model containing four modules: (1) molar alveolus, (2) incisor alveolus, (3) ramus, and (4) a module comprising the angular, coronoid, and condyloid processes.

These analyses suggest that integration of the posterior half of the cranium affects the entire braincase, forming a unit distinct from the anterior half, which also forms an integrated unit spanning certain splanchnocranial elements (i.e., maxilla, premaxilla, and zygomatic). The mandible seems to be associated with the rostrum, including the zygomatic, palate, and palatine, within the context of the craniomandibular complex. This pattern suggests a functional (i.e., mastication) explanation for the pattern of integration between cranium and mandible. However, when analyzed separately, a more complex pattern is revealed within the mandible, one that partially resembles expectations from the model of mesenchymal condensations. The distinction between that pattern and the one expected by the condensation hypothesis is that, in the data, the mandibular processes are mutually integrated but independent from the rest of the ramus. Only one model predicts this (H_{58}), but the integration among mandible processes is consistent with any set of modules that is nested within this pattern (e.g., mesenchymal condensations), because the independence of these processes is biological, not necessarily statistical. Although it is possible that this pattern is consistent with functional matrix theory (see models M_{12}, M_{14}, and M_{15}), that seems unlikely because the functional matrix model would also imply that integration is stronger between the condyloid and pterygoid

and the temporalis attachment site, than between the latter processes and the masseter attachment sites.

Heuristic optimization of module boundaries significantly improved the fit of the best-supported model (jackknife support = 100%; see Table II.5). The boundaries were adjusted to accommodate a larger extent of antero-posterior (AP) integration than suggested by a priori and combination models (Fig. II.4B). In the skull data set, this is apparent as a forward extension of the calvarium-basicranium module to include the fronto-maxillary suture and part of the nasal, and a backward extension of the rostral module toward the parietals. These extensions produce an overlap between modules in the frontal region. Such a pattern of AP integration may depend on treating the mandible as part of the rostrum, because without including the mandible, the model is not supported by data. Instead, for the cranium-only data set, there is a weak (but noticeable) increase in integration between modules in the squamosal-sphenoid intersection and the zygomatic spine. This discrepancy between the results for the two data sets might be due to a stronger integration between the zygomatic arch and mandible in the whole-skull data, which might be due to an interaction between these bones during mastication. Finally, in the mandible-only data set, there is an increase in AP integration, including integration between the angular process and both alveoli, and between the coronoid process and both molar alveolus and ramus. The ramus, in turn, appears somewhat integrated with the incisor alveolus. Overall, the patterns of integration supported by heuristic models seem to overlay regions presumably derived from different mesenchymal condensations, which seem to retain some individuality, onto elements the that evoke complex functional interactions between tooth-bearing and muscle-bearing skeletal components (Zelditch et al. 2008), i.e., between processes and alveoli.

Results from part-whole PLS are broadly consistent with patterns described above (Fig. II.5), especially for the mandible. They reveal strong integration between molar alveolus and mandible processes, particularly the coronoid process, and also integration among ramus, coronoid process, and incisor alveolus. For the cranium-alone data, when the rostrum is regressed onto the whole, PLS finds little integration between rostral and calvarium-basicranium modules. In contrast, if the calvarium-basicranium is regressed

onto the whole, the cranium as a whole appears to be integrated. This discrepancy suggests that covariation between anterior and posterior cranial regions spans multiple dimensions—they are approximately orthogonal only in some dimensions. This pattern is consistent with the concept of modularity as implemented herein, and, as seen below, is commonly observed in the species included in this study.

Melanomys caliginosus

Analyses based on initial models favor the same models for all three data sets. Both skull and cranium-only data sets support H_{34} (100%), which is based on the effects of the loss-of-function mutation in the *Tgfβ-2* gene (module M_{53}; Sanford et al. 1997). According to this model, the calvarium and lateral walls of the braincase are integrated with each other and with the palate and proximal half of the mandible (Fig. II.6A). The rostrum, basicranium, and mandibular alveoli are not integrated in any module. A second model, weakly supported when testing the full set of models, adds another module, M_6, to M_{53}. This added module comprises the anterior region of the snout, corresponding to the skeletal matrix of the nasal capsule (i.e., nasal and pre-maxillary bones)

For the mandible-only data, initial tests support two models: H_3 (53%) and H_{32} (33%). The first contains one module comprising the proximal half of the mandible, spanning insertion sites of all masticatory muscles (i.e., M_{16}). The second is based on mesenchymal condensations. When testing the full set of models, these two are also supported, but less so than the combined model $\{M_{46}\}\{M_{48}\}\{M_{77}\}$ (Table II.5), which is the model supported by *H. chacarius* except for the absence of an incisor alveolus module (Fig. II.6A). Other models whose γ * CI overlaps the CI of these two include H_{20} (=H_3 plus an alveolar module), H_2 (also based on attachment sites of masticatory muscles, assigning a module to each muscle group and adding an alveolar module), and H_{14} (=H_2 plus an alveolar module) (Fig. II.6A).

These results suggest that the covariation structure of *M. caliginosus* supports two distinct patterns of modularity. The first contrasts posterior and anterior regions of both mandible and cranium, whether they are considered jointly or separately, a result that is consistent with the pattern expected from the effect of *Tgfβ-2* gene knockout (i.e., model H_{34}). The second pattern posits integration internal to the mandible, which seems to

simultaneously support (1) a pattern in which tooth- and muscle-bearing regions are separated in distinct modules, and (2) a pattern consistent with expectations from the mesenchymal condensations model.

Heuristic models also support these two alternative patterns (Fig. II.6B). In the case of the cranium and skull data, AP integration is supported in both lateral and ventral views, affecting mainly the dermatocranial, zygomatic, and nasal regions. In the mandible data, a similar pattern to *H. chacarius* is observed, in that the mandible processes appear integrated with the molar alveolus, whereas the ramus appears integrated with the incisor alveolus.

These patterns are broadly supported by part-whole PLS analyses (Fig. II.7). PLS vectors, however, account for a considerably smaller magnitude of variation in the rostrum and palate regions than suggested by these models or than seen in *H. chacarius*, suggesting that the AP axis, or, as discussed in the case of *H. chacarius*, rostral structures, span a subspace approximately orthogonal to the subspace occupied by the calvarium.

Microryzomys minutus

The best supported modules are remarkably consistent regardless of the models included in tests. When analyses are based on 66 models, skull and cranium-only data support H_{34} (100%), the same one supported by *M. caliginosus*, whereas the mandibular data support model H_{32} (100%), i.e., mesenchymal condensations. Using the full set of models, two modules are supported by the whole-skull data: H_{34} and the combination of that plus M_6 (i.e., nasal plus pre-maxillary bones). The cranium-only data support H_{34} (Fig. II.8A), as in the case of *M. caliginosus*. For the mandible, the most supported of the a priori and combination models contains modules corresponding to mesenchymal condensations (i.e., H_{32}), excluding only the molar module (M_{46}). H_{32} is, however, the next best supported model, followed by H_2 and H_{14}, which can be interpreted as originally intended, namely as a superimposition of regions associated with individual attachments of masticatory muscles (plus an alveolar module in H_{14}), or it could also be interpreted as the superimposition of effects of muscle function on the structure derived

from mesenchymal condensations. That second alternative cannot be ruled out given the support found for this hypothesis in the mandible data.

In addition to the similarities between the a priori models supported by *M. caliginosus* and *M. minutus*, the heuristic models supported by both species suggest that there is relatively strong integration between calvarium and rostrum. *M. minutus,* however, shows that there is a high degree of integration within the rostrum, including the palatal region, which is either a separate module, or integrated with other regions of the skull (Fig II.8B). The basicranium in *M. minutus* appears unusually strongly integrated, sharing common partitions with either neurocranial or rostral elements. This pattern of two distinct (and distant) modules might mean that the basicranium in this species is associated with both regions, due perhaps to the pervasive effects of braincase growth (Baer 1954; Hoyte 1971; Bruner and Ripani 2008) or with the role that the basicranium is thought to play as the central integrator of the cranium (Lieberman et al. 2000). The heuristic model for the mandible shows little integration across the AP axis, and the regions related to mesenchymal condensations seem to remain approximately modular. Results from PLS analyses are consistent with those from the a priori tests (Fig. II.9). However, as found in the other species, integration along the AP axis that is hypothesized by heuristic models is not readily apparent in the first PLS vector. A clearer signal emerges from the mandibular data, which supports the heuristically modified a priori model, and suggests other associations (e.g., incisor-ramus, angular-ramus-coronoid) not supported by the heuristic search.

Nectomys squamipes

Analyses produce consistent results regardless of the models used in tests. In the case of the skull, the best-supported model is the one supported by data from *M. caliginosus* and *M. minutus* (see Table II.5). However, that similarity between species does not extend to the cranium or mandible data sets. The cranium data set supports model H_{60}, which posits a module spanning regions affected in *Otx2*-null mice. In homozygous form, this mutation affects neural-crest derived regions of the skull. Even though this hypothesized effect is different from that seen in all other species included in this study (except *S. alfari*, see below), it is consistent with the pattern of AP integration

observed in other heuristic models. In fact, heuristic models for the skull and cranium in *N. squamipes* are largely indistinguishable from those in *M. caliginosus*. For the mandible, both the masticatory model and the mesenchymal model are supported (Fig. II.10A).

Heuristic searches based on those models found strong proximo-distal integration in the cranium (Fig. II.10B) as well as some evidence of integration in the rostral region, like that seen in *M. minutus*. Integration is also detected in the basicranium (i.e., basioccipital, exoccipitals, and external auditory meatus), which appears to be integrated with both neurocranium and rostrum. For the mandible, heuristic searches support a model that is almost identical to the one on which the search was based, further supporting masticatory function as the main cause of integration (and modularity) in this species.

PLS supports most of these patterns, including the pattern of integration along the AP axis observed for cranial data (Fig. II.11). This suggests that in *N. squamipes*, unlike the other species, AP integration spans a subspace with lower dimensionality (i.e., stronger integration), which might mean that this region is a variational module or super-module. Additionally, PLS suggests that there might be integration between ramus and both alveoli, although it is not possible to determine whether that is due solely to chance. Additionally, PLS vectors show that the covariance between the posterior half and the whole mandible is no greater than expected by chance ($P = 0.049$). Given that the pattern described strongly resembles those expected from the best-supported model, it would appear that this module has a high dimensionality (i.e., its variation is distributed more or less homogeneously over several dimensions). In general, however, these results are not readily interpretable and there is less variation in the mandible of *N. squamipes* than seen in the other species.

Oligoryzomys nigripes

Relative support for models for the skull, cranium, and mandible does not depend on which sets of models are included in the tests. Once again, the best-supported models (Table II.5) for the skull and cranium data sets are H_{34} and $\{M_{53}\}\{M_6\}$, which include, respectively, a calvarium-palate-posterior mandible module, plus a module comprising

nasal and pre-maxillary bones. For the mandible, three types of models are supported: (1) a joint module comprising all mandible processes plus ramus and molar alveolus (2) one module per mesenchymal condensations, and (3) one module per region associated with attachment sites for masticatory muscles (Fig. II.12A).

Heuristic models for the skull and cranium suggest a higher degree of integration between calvarium and zygomatic arch than seen in the other species (Fig. II.12B), whereas integration among basicranial elements seems weaker. The heuristic model supported for the mandible indicates integration among mandibular processes and integration along the entire AP axis (Fig. II.12B). As also noticed in other species, the first PLS axis does not seem to recover the pattern of AP integration for skull and cranium. In contrast, PLS discerns the same modules supported by tests of *priori* models in the mandible, and finds particularly strong integration between molar alveoli and ramus (Fig. II.13).

Oryzomys couesi

The best-supported models for the skull and cranium are the same ones favored for *M. caliginosus*, *M. minutus*, and *O. nigripes* (Table II.5), regardless of the models used in these tests (Fig. II.14A). These include H_{34} (i.e., a calvarium-palate-posterior mandible module), and $\{M_{53}\}\{M_6\}$ (i.e., H_{34} plus a nasal and pre-maxillary bones). For the mandible, the only models that fit well are related to the effects associated with masticatory musculature, with modules concentrated in the posterior half of the mandible, each associated with a muscle attachment site. Interestingly, models for the mandible are consistent with those supported for the skull, which also show little support for integration within either alveolus.

A heuristic model for the skull was derived from model $\{M_{53}\}\{M_6\}$, which is nearly as well-supported as model $\{M_{53.}\}$ (see Table II.5). This model posits integration between calvarium and zygomatic arch, whereas the nasal capsule matrix is an individual module (Fig. II.14B). For the cranium data, however, a heuristic model derived from $\{M_{53}\}$ suggests that the rostral module may be integrated with the calvarium. These apparently conflicting inferences, like the discrepancies between heuristic models and PLS axes, might be due to integration among non-orthogonal modules such as an overlap

between modules at the fronto-nasal and fronto-parietal boundaries. In the case of the mandible, the model found by a heuristic search differs from the best-supported a priori mode in that it shows relatively strong integration (1) between ramus-angular module and the other two processes, (2) between coronoid process and incisor alveolus, and (3) between the condyloid process and the incisor alveolus, as predicted by functional effects associated with changes in direction of growth of the mandible due to rotation (i.e., change in posture) at the temporomandibular joint (Björk 1969). As seen in the other species, the first PLS vectors of both cranium and mandible data provide little evidence supporting the unique integration patterns depicted by heuristic models, and variation accounted for by these vectors does not reveal much integration beyond the module being regressed (Fig. II.15). This might mean that data have an unusually high dimensionality. However, because that lack of support applies to all views and modules, and because most PLS vectors account for no more covariance than expected by chance (Fig. II.15), it may be that the modules found by heuristic models are rather weakly defined and/or account for a relatively small portion of the variation in this species.

Oryzomys palustris

The best supported models (Table II.5) once again include models H_{34} (= M_{53}, i.e., a calvarium-palate-posterior mandible module), and $\{M_{53}\}\{M_6\}$ (i.e., H_{34} plus nasal and pre-maxillary bones), and H_{60} (=M_{79}, i.e., integration along the AP axis of the cranium, approximating a module of CNC-derived tissues (also supported by *N. squamipes* and *S. alfari*). For the mandible, the best-supported models propose that the mandibular processes are integrated, but there is support as well for the modules predicted from mesenchymal condensations and masticatory muscle attachment) (Fig. II.16A).

Heuristic models based on skull and cranium data sets support patterns similar to those seen in the other species (i.e., *M. caliginosus*, *N. squamipes*, *M. minutus*, *O. couesi*), in which there is strong integration along the AP axis through the zygomatic arch (Fig. II.16B). In addition, *O. palustris* shows strong integration within the rostrum, as found in *N. squamipes* and *M. caliginosus*. A heuristic model of the mandible, on the other hand, maintains support for a module comprising the mandible processes. This

module incorporates elements of the ramus, specifically the continuation of the superficial masseteric ridge rostral to the angular process. This addition suggests a dual role for masticatory function and development (e.g., chondrogenesis) in structuring the covariation of the ventral aspect of the mandible. Interestingly, a similar heuristic model is supported by *O. nigripes* which, as seen above, supports the same a priori models as *O. palustris*. This consistency of optimal, sub-optimal, and heuristic models further strengthens the argument that sub-optimal models contain relevant information regarding the underlying integration structure in a data set.

As seen in other species, most patterns detected by heuristic search are supported by PLS analyses. Particularly evident is the support for integration between the ramal portion of the superficial masseteric ridge and both the mandible processes and alveoli, as well as integration between both alveoli (Fig. II.17). An exception that was also seen in other species is the absence of AP integration in the first PLS vector of the cranium data. As discussed above, this suggests that the AP pattern results from non-orthogonality of neurocranial and rostral modules.

Oryzomys xantheolus

An unusually large number of models are supported by the data from this species, which might result from the low resolution caused by small sample size. This lack of resolution seems to affect the cranial data most. The skull data set supports the same models favored by the data from most other species (i.e., H_{34}: calvarium-palate-posterior mandible, and $\{M_{53}\}\{M_6\}$,: H_{34} plus nasal and pre-maxillary bones) (Table II.5; Fig. II.18A). The best-supported models for the cranial data set also include H_{34}. In addition, the cranial data support models based on tissue primordia (PM vs. CNC modules), model H_{60} (also supported by *N. squamipes*, *O. palustris*, and *S. alfari*) and other models that postulate some form of AP integration (see Table II.5). Mandible data support a model with three modules, comprising, respectively, the three processes, both alveoli, and the ramus. Other supported models include the partition of the mandible into posterior and anterior modules and a model based on mesenchymal condensations.

Heuristic models based on skull and cranial data show particularly widespread integration throughout the proximo-distal axis of the cranium, including strong

integration between rostral (i.e., nasal, premaxilla, maxilla, zygomatic) and basicranial (i.e., occipital, sphenoid, presphenoid, and external auditory meatus) elements (Fig. II.18B). Such widespread integration could explain the abundance of models supported by cranial data in this species (Fig. II.18A) because multiple models capture some local aspects of the integration of this apparently global pattern. In contrast, the heuristic model supported by the mandibular data is almost identical to the corresponding a priori model.

PLS discerns the same patterns predicted by the best-fitting a priori hypotheses (Fig. II.19). The first PLS vector from the cranium data set suggests AP integration, as seen in *N. squamipes*. As discussed above, this may indicate that the rostral and neurocranial modules have fused into a single module or, more likely, that the orientation of these modules is closer to being parallel in multidimensional space. It is also possible that the pattern is due to compressing multidimensional information into relatively few axes due to small sample size.

Sigmodontomys alfari

There are many well-supported models for the skull, probably due to small sample size, but these models consistently suggest the same general patterns of integration. However, many of these patterns are unique to this species. One recurrent pattern is that the mesoderm-derived tissues (i.e., M_{18}) form a module (Fig. II.20A). Other models supported by the data from this species are associated with late ossifying regions (M_{28}), or paraxial mesoderm-derived tissues (M_{19}), and *Tgfβ-1* (M_{53}) and *Prx* (M_{77}) mutational targets. In the case of the mandible, two basic models are supported: (1) all three processes jointly define one module, with the ramus and molar alveolus defining a module each and (2) one module spans the posterior half of the mandible. This combination of models is also seen in several other species.

Heuristic models are broadly consistent with patterns discerned from the best-supported a priori models for the skull, cranium, and mandible (Fig. II.20B). The only noticeable discrepancy suggests integration between CNC-derived tissues and elements of the occipital bone. This observation, however, is not confirmed by PLS analyses (Fig. II.21). PLS of cranial data show evidence of AP integration along the first PLS axis, as

also seen in *N. squamipes* and *O. xantheolus*, possibly due to stronger integration within this axis. PLS of the mandible data supports the hypothesis of integration between mandibular processes and ramus, consistent with suboptimal models which were excluded from the heuristic search (Fig. II.20A). In any case, the best-supported model (i.e., mandibular processes jointly forming a module) is nested within this pattern of integration within the posterior half of the mandible so results from these analyses are not inconsistent.

Summary of findings

Many of the same patterns are detected in all nine species, suggesting a remarkable conservation of phenotypic covariation structures despite the high degree of ecological diversity and phylogenetic divergence exhibited by these species. As expected, there is a greater diversity of patterns detected by heuristic searches, but that diversity seems mostly confined to small differences in the boundaries between conserved modules.

Comparative analysis of intraspecific patterns of modularity

The aim of this section is to explore the links between intraspecific patterns of modularity and morphological divergence.

Consensus model

A strict consensus model derived from the best-supported skull models (Table II.5) includes one module that spans the posterior half of the mandible plus glenoid fossa plus palatine and parietal bones. A consensus based on the model unanimously supported by all species other than *H. chacarius* and *S. alfari* (which are unique in their patterns of craniomandibular integration) includes module M_{53}, and possibly $M_{6.}$ For the cranium data set, *N. squamipes* and *O. xantheolus* also appear to support unique models, but the modules supported by these species do overlap those supported by the remaining five, i.e., spanning frontal, parietal, interparietal, squamosal (including the zygomatic process), exoccipital, and palatal process of the palatine. A consensus based on this set of anatomical regions is not changed by adding *S. alfari*, but if *H. chacarius* is included, that narrows the strict consensus to the pattern identical to that described above for the skull data set (minus the mandible).

Identification of a mandibular consensus based on a priori models is relatively straightforward. However, in this case it may not suffice to build a consensus from the optimal models alone; distinct models in the vicinity of the best-supported ones should also be taken into account. This, as discussed in detail in the next section, is because of the recurrent relatively high support observed for discrepant models, which does not seem an artifact of sampling issues, but a real pattern resulting from a high dimensionality of modularity in the mandible. Table II.6 lists modules supported by all species, highlighting those that belong to optimal models. From the columns of this table, it is apparent that the most commonly supported modules correspond to the mesenchymal condensations of the mandible. In cases where some of these modules are not supported, they appear to be embedded within larger modules. For example, even though the data from *O. couesi* do not support molar or incisor alveolus modules, those two modules are nested within the tooth-bearing module that is supported in this species. If the analysis is restricted only to the best-supported models, no single module is present in all species. In this case, some species do not support the hypothesis that one or both tooth alveoli are modules. Specifically, the hypothesis of an incisor alveolus module is not among the optimal models for *M. caliginosus*, *O. nigripes*, *O. palustris*, whereas the hypothesis of a molar alveolus module is not supported by *M. minutus,* and neither alveolus is a module in *O. couesi* and *S. alfari.* However, data from all species support the hypothesis that the posterior half of the mandible is either a single module, or two, one containing the ramus, the other the mandibular processes (or some other partitioning of the posterior mandible). The consensus from optimal plus suboptimal models (in the vicinity of the optimal ones) is identical to $H_{32:}$: each mesenchymal condensation is a module. A consensus based solely on the optimal models contains four modules, the three mandibular processes, plus a ramus module, i.e., a combination of M_{49}-M_{51} (Fig. II.3).

A consensus derived from the heuristic models of the skull and cranium is more consistent because most species share several common features, such as a module spanning most of the AP cranial axis. The boundaries do vary among species, with the most variable being (1) the inclusion of the zygomatic spine and other elements of the maxilla, as well as (2) elements of the occipital bone and other basicranial regions. As in

the case of the analyses based on a priori models, *H. chacarius* and *S. alfari* are exceptions, with the former showing a marked division of the cranium into calvarial and rostral regions, and the latter showing strong integration only anterior to the squamosal. In addition, both of these species are especially highly integrated in the palatal area. A strict consensus based on all nine species would then postulate integration of squamosal, frontal, dorsal aspects of pre-maxillary bones, and the entire mandible in a single module. Exclusion of these two species leads to a consensus model in which exoccipital, periotic, squamosal, interparietal, parietal, frontal, nasal, and alisphenoid bones, as well as the glenoid fossa and the entire mandible form one module.

Models based on heuristic searches for the mandibular data show increased integration across all partitions, mostly involving individual landmarks within one region being associated with spatially restricted modules, making it difficult to define the boundaries of the consensus. The most recurrent associations introduced by heuristic searches is between the ramus and incisor alveolus, which may be partially consistent with the Atchley-Hall model of developmental models tested in this study (Atchley 199), given that the ramus contains also the posterior portion of the incisor alveolus, and as such could be affected by variation associated to odontogenic processes. However, in all cases, only a few alveolar landmarks, and sometimes only one, are integrated with the ramus. That pattern is seen in all species other than *N. squamipes*, *O. couesi*, and *O. xantheolus*. It is important to note, however, that the heuristic search takes a single model as starting point, ignoring the possibility that multiple suboptimal models are among the valid alternatives. That may explain why the consensus for the mandible, based on heuristic models, is not distinct from that model built from modules defined a priori.

Interspecific comparisons in model space

The best 100 models, including the original ones and those combining modules of the best ones, were used for interspecific comparisons. This approach guarantees that all modules supported across all species (and views) are included in the comparisons, while also optimizing the signal to noise ratio. Comparisons were based on the results for each data set (i.e., γ^* for the whole-skull, cranium-only and mandible data sets).

Dendrograms and the interspecific correlations used to build them are shown in Fig. II.22. As expected, the skull and cranium data sets are more similar to each other than either is to the mandible data set. The only element shared by all data sets suggests relatively high similarity among the patterns of modularity seen in *M. caliginosus*, *O. nigripes*, and *O. palustris*. This group, in turn, is similar to *O. couesi* and *M. minutus* in the skull and to *M. minutus* in the cranium data set. Additionally, *N. squamipes*, *O. xantheolus*, and *S. alfari* appear to be correlated in the mandible data set, whereas *H. chacarius* and *N. squamipes*, and *N. squamipes* and *O. xantheolus* appear to be similar in skull and cranium data sets, respectively. *H. chacarius* and *S. alfari* emerge as the most divergent in the skull data set, whereas a comparable degree of divergence is seen only for *S. alfari*, and for *M. minutus* and *O. couesi* in the cranium and mandible data sets, respectively. These results do not correspond well to the patterns of model support exhibited by the different sets of skull traits and might result from differences among species in the covariance between mandible and cranium. Despite the similarity of the closely related *M. caliginosus*, *O. nigripes*, and *O. palustris* (see Appendix A) in patterns of mandibular integration, and among the semi-aquatic *N. squamipes*, *O. xantheolus*, and *S. alfari*, no known explanatory factor is strongly associated with these patterns of similarity.

Modularity and disparity

The first principal component of the skull, cranium, and mandible shape is associated primarily with interspecific size differences. It thus appears to be an evolutionary allometry axis. In order to compare patterns of interspecific divergence and intraspecific patterns of modularity, we need to remove that allometric component by regressing the mean shape for each species on its mean centroid size. This avoids the risk of confounding differences in shape due to differences in size, generally involving interspecific variation in the relative size and shape of the braincase with respect to the rostrum, with differences related to the pattern of (non-allometric) modularity supported for most of the species sampled herein, which also involve variation in the shape of the braincase. Figure II.23 shows PCA ordinations of skull data sets before and after allometric correction.

Interspecific differences are not homogeneously distributed (Fig. II.23B), and thus the overall covariation patterns are likely to be dominated by the extreme shapes. Analysis of the partial disparities of the whole-skull data set, which estimates the contribution that each species makes to the total disparity (Table II.7) reveals that nearly 36% of the disparity is due to two species: *H. chacarius* and *S. alfari*. The remaining species account for a similar proportion of the disparity (ranging from 8% to 12%) and are also (approximately) homogeneously distributed around their mean shape (Fig. II.24A). Because analyses that include the two outlier species will be dominated by them, these two are excluded from the remaining comparative analyses.

Tests of a priori models fitted to interspecific covariance matrices suggest that most of the morphological (co-)disparity is concentrated in the braincase, palate and posterior mandible. In contrast to the results from the intraspecific analyses, the same model fits all views of the skull. The module receiving the greatest support is M_{53}, with γ^* values equal to 0.506, 0.561, and 0.344, and jackknife support values of 87%, 53%, and 85% for the skull, cranium, and mandible data sets, respectively. This is the model supported by the intraspecific analysis as well. Another, less strongly supported module is M_{77}, with γ^* values of 0.541, 0.577, and 0.390 and jackknife support values of 13%, 32%, and 15% for skull, cranium, and mandible data sets, respectively. This model receives very limited support from the intraspecific analyses; the only support that those analyses offer comes from the cranial data of *S. alfari*. An additional module, M_{79} also receives some support from the cranium data set ($\gamma^* = 0.593$, jackknife support = 15%). This one is partially supported by intraspecific analyses of *N. squamipes*, *O. palustris*, and *O. xantheolus*.

Even though M_{53} and M_{77} span largely overlapping regions (including squamosal, parietal, interparietal, exoccipital, alisphenoid and palatine, glenoid fossa and mandibular processes), they differ in critical elements of the AP axis of the skull and mandible. M_{53} is unique in spanning the frontal and supraoccipital bones and mandible ramus, and M_{77} is unique in spanning the maxillary bone. Results of these interspecific analyses suggest the presence of separate caudal and rostral aspects of cranial divergence, a pattern approximately recovered by PC1 and PC2 of the skull and cranium data (Fig. II.24B).

PC1 of both data sets (which accounts for 41% of the skull and 38% of the cranial variation) is dominated in lateral view by variation at the parietal, interparietal, supraoccipital, squamosal (including the zygomatic process), and orbitosphenoid, and in ventral view by variation at the presphenoid, palatine, and glenoid fossa. In contrast, PC2 (skull: 6%, cranium: 7% of total variation) is dominated in lateral view by the frontal, maxilla (including the zygomatic process), lacrimals, and premaxilla, and in ventral view by palatine, palatal process of the maxilla, and the maxilla-premaxilla boundary. Notably, the morphological regions singled out by these axes overlap in the orbit/palatine region, just as the modules supported by this covariation structure do. Regarding the mandible, PC1 and PC2 computed from the skull and mandible-alone data sets differ, even though both of these views support the same models. In the skull data set (Fig. II.24B), PC1 (45% of the variance) shows variation at the ramus, molar alveolus, angular, and condylar regions, whereas PC2 (5%) shows variation at the molar and incisor alveoli, the ramus, and the condyloid process. In the mandible data set (Fig. II.24B), both PC1 and PC2 are dominated by variation at the ramus and all processes, which is consistent with the consensus module for the mandible based on optimal models (see above).

Ordinations using principal components are, as expected, almost identical for the skull and cranium, but slightly different for the mandible (Fig. II.24). In the ordinations based on skull and cranium data, PC1 accounts for interspecific differences among *O. palustris*, *O. couesi*, *N. squamipes*, and *M. minutus*, whereas PC2 accounts for differences among *M. caliginosus*, *O. xantheolus*, and *O. nigripes*. In contrast, in ordinations based on the mandible, both PCs account for variation in all seven species, although these ordinations are highly consistent with those that include the cranium. Geometrically, the discrepancy between skull/cranium and mandible data seems to reflect a rotation of the same axes (see Fig. II.24A). In anatomical terms, the discrepancy seems to result from co-disparity between ramus and alveoli in the former versus co-disparity among mandible processes in the latter. These two patterns reflect distinct aspects of mandibular disparity.

As mentioned above, *H. chacarius* and *S. alfari* make disproportionate contributions to disparity, hence including them in the PCA results in a dramatic increase in the perceived dimensionality of this group, with the proportion of disparity captured by

PC1 dropping from 41% to 10%, from 38% to 22%, and from 45% to 13% for the skull, cranium, and mandible data sets, respectively. Considering that these two species are also the ones with the most divergent patterns of modularity, it seems worth asking whether differences in mean shape have a similar structure as the intraspecific patterns of covariation, despite the fact that it is not possible to test developmental hypotheses for the species using only their means. Figures II.25A and B show these differences for *H. chacarius* and *S. alfari*, respectively, computed by subtracting the mean shape of each of these two species from the mean shape based on all others species combined, after rotating them using ordinary Procrustes superimposition (Dryden and Mardia 1998). From these figures, it appears that the two species differ from that mean in different characteristics, although some are common to both. One common feature is that both species show abundant differences in the ventral view of the cranium, particularly so in the palate-palatine region. Similarly, both species show marked differences in the relative position of the molar alveolus along the AP axis, which seems to be highly conserved in other species. Additionally, they differ along the lambdoid suture and zygomatic process of the squamosal. However, they are dissimilar in that *H. chacarius* seems to differ slightly in the posterior braincase (in the supra- and exoccipital and parietal) and also in the frontal and maxillary bones, including the zygomatic spine, whereas *S. alfari* differs primarily toward the anterior aspect of the rostrum (nasal and pre-maxillary bones). Major differences between these species relative to that mean are found only in the mandible: in *H. chacarius*, differences are observed in most aspects but the condyle and the mental side of the incisor alveolus, whereas in *S. alfari* differences are concentrated in the ramus, the least differences seen in the condyloid and molar alveolus.

DISCUSSION

Hypotheses of craniomandibular modularity were tested in nine ecologically diverse species of oryzomyine rodents to determine whether the same causal factors shape covariance structures in all species. Such constancy is required if developmental processes are to constrain evolutionary divergence over long time scales (Alberch 1980; Maynard Smith et al. 1985; Zelditch et al. 1990). Previous studies have compared covariance matrices to determine if they retain the same structure but few have asked

whether the developmental factors responsible for covariance structures are conserved and those that do have typically tested few developmental hypotheses (e.g., Zelditch et al. 1990; Nemeschkal 1999; Monteiro et al 2005). More importantly, prior studies did not take into account the complications due to the complex geometry of modules, particularly, the fact that they can be both biologically independent and yet capable of combining with each into "super-modules" (Nemeschkal 1999; Márquez 2008) and of evolving in concert (Wagner and Cheverud 2007). Whether individual modules persist and retain their internal structure has been an open question. In this study, I find that many of the same developmental modules are, in fact, detected in all nine species, suggesting that the internal structure of modules is conserved in this ecologically diverse group. Moreover, this detailed examination of both conserved and divergent patterns in the whole-skull plus cranial and mandibular data sets shows that different mechanisms responsible for functional and developmental integration in crania and mandibles may result in qualitatively different patterns of modularity. With regard to the evolutionary impact of these conserved modules, I find a high congruence between the patterns of conserved intraspecific modularity and interspecific co-disparity. Among species with relatively similar skull shapes, this congruence is manifest as support of the same hypotheses of modularity in both intra- and interspecific data. Species with highly divergent cranial shapes also have highly divergent patterns of cranial modularity. Taken together, these results reveal a strong link between the developmental mechanisms underlying intraspecific variation and the major directions of evolutionary diversification.

Intraspecific patterns of modularity

Widespread support for a conserved a priori model of craniomandibular modularity

Two models of craniomandibular modularity are best supported by the data from seven of the nine species. The one that fits most of the species includes a module that spans calvarium, basicranium and proximal mandible. This module comprises frontal, parietal, interparietal, exoccipital, supraoccipital, and squamosal plus alisphenoid, palatine-palatal, and proximal-mandibular regions (module M_{53}: Fig. II.3.53). The other model contains that broad craniomandibular module plus a nasal module (comprising the skeletal component of the nasal capsule: nasal, lacrimal, and premaxillary bones [module

M_6: Fig. II.3.6]). The two exceptional species are *S. alfari* and *H. chacarius*; in them, the mandible is integrated with the rostral cranium, including the zygomatic arch, and the oropharyngeal region (i.e., palatines, pterygoids, and floor of maxilla and premaxilla). In addition, in these two species, the oral cavity is strongly integrated. Taken together, the hypotheses of modularity supported by most species in this study suggest that there is typically one module spanning the braincase, palate, and proximal half of the mandible. The cranial part of that module is also supported by the cranium-only data for six of the nine species. Of the other three species, a hypothesized module that spans the entire cranium except the posterior basicranium fits two of them. This module comprises basioccipital, ala temporalis, basisphenoid, pterygoids, periotic, and internal and external auditory meatus (module M_{79}: Fig. II.3.79). In the remaining species, *H. chacarius*, the same cranial module is found as described above for the craniomandibular data.

Heuristically modifying modular boundaries yields a clear pattern common to most species: cranial elements are integrated along the AP axis, producing a super-module containing the calvarium and some combination of pre-maxillary, maxillary, and nasal bones. This super-module usually excludes ventral structures (i.e., basicranium, palate), although they are included in some cases. This same AP integration is found whether searches are initiated with a model containing a single calvarial module or separate calvarial and rostral modules. AP axial integration therefore does not appear to be an artifact of the model used to initiate the search. However, AP axial integration is not supported by PLS analyses, which suggest AP axial integration for only the three species (*N. squamipes*, *O. xantheolus*, and *S. alfari*) in which the best-fitting a priori models also predict AP integration. The weak support from PLS for integration between anterior and posterior cranial structures suggests that these regions are only partially integrated, that is, it is possible that only some dimensions of their respective subspaces covary. A pattern of partial integration is consistent with the idea that modules can be integrated because they interact with each other or because developmental processes structuring modularity have overlapping effects on two or more modules. For the AP axis, this geometric interpretation implies that there are autonomous as well as integrating factors affecting anterior and posterior structures. Interestingly, this also appears to be the case, but in the reverse direction, in *H. chacarius*, which does not support either a

priori or heuristic models of AP integration, but does partially support AP integration along the first PLS axis (Fig. II.5).

In contrast to the broadly shared patterns seen in the craniomandibular and cranial data, several disparate models fit the mandible-only data. That does not appear to be due to low resolution of the data because, unlike the other two data sets, the number of modules supported by the data does not fluctuate with sample size (see Tables II.1, II.5). One explanation for the disparity of models fitting the mandible-only data is that there are multiple "layers" of processes influencing integration of this structure. That possibility follows from the statistic used in this study to measure goodness of fit of a model (i.e., γ^*), which is a pairwise distance between model and empirical matrix; an empirical matrix can be equidistant from two model matrices that occupy different positions in a multidimensional space. Consequently, the equidistant model matrices may correspond to distinct but equally supported causal explanations. Should that be the case, suboptimal models in the vicinity of best-supported models should also be considered relatively well-supported.

Additional support for the hypothesis of multilayered mandibular variation is suggested by the observation that the pattern supported by the whole-skull data resembles that of the cranium-only data more closely than it does the mandible-only data. This might indicate that, in addition to the disparate hypotheses of modularity supported by the mandible, there is an additional level of mandibular integration caused by the interaction between cranium and mandible. This pattern can be interpreted as a hierarchy of causal factors, with the mandible nested within the skull (Kenney-Hunt 2007, cited by Wagner and Cheverud 2007). Cranio-mandibular interactions may be another source of modular variation for the mandible, an interpretation supported by cases in which mandibular and cranio-mandibular patterns of modularity are indistinguishable (e.g., in *O. nigripes*; Fig. II.12A). This is consistent with the explanations suggested above for integration within the AP axis of the cranium because it implies that there is a module spanning the posterior cranium and the proximal mandible distinct from other modules found within these structures. This module seems to account for relatively more variation in the cranium than in the mandible, which leads to the re-interpretation of *cranial* integration

as *craniomandibular* integration, one that could not be detected without the joint analysis of both structures.

Cranium vs. mandible

Modularity of crania and mandibles differ in several major aspects, perhaps the most evident being the higher degree of overall cranial integration, which is manifest as support for a super-module spanning the AP axis. This super-module, found in all but one species, is not predicted by any a priori model, and as suggested by PLS analyses, it might best be interpreted as partial integration between distinct modules (rather than as occupying a high level in a hierarchy of nested modules).The fact that this form of integration is found only in the cranium suggests that causes of modularity differ between cranium and mandible even though both form from developmentally independent cell condensations (Hall and Miyake 2000). One hypothesis to explain the discrepancy between these two skeletal complexes is that the structure of functional integration is essentially different between the two components (see Zelditch et al. 2009). In the cranium, functional units are highly localized and developmental integration arises, at least partly, by coordinated growth within these localized functional components (rather than function per se), as predicted by the functional matrix theory (Moss and Young 1969). In the mandible, as Zelditch et al. (2008, 2009) hypothesize, integration could arise from the relationship between forces generated by muscles and experienced at teeth during mastication, i.e., between the loading induced by muscular contraction and occlusion. Therefore, integration in the mandible is caused by function, rather than, as predicted by the functional matrix theory, by physical contact with a functional unit (Moss and Rankow 1968). The mechanism of integration, bone's response to tensile forces, is thus common to cranium and mandible, but the spatial structure of those forces and their degree of localization differs between cranium and mandible.

One possible explanation for the contrast that I find between the cranium and mandible takes into account differences in their sources of non-allometric integration. In the cranium, each skeletal module is influenced by at least four sources: (1) integration directly induced by growth of functional components, (2) integration by proximity among spatially adjacent skeletal elements, (3) integration among functionally coupled modules,

and (4) integration among tissues with similar cellular properties (e.g., cartilage, dermal bone, etc.). Of these sources, two of them (2, 4) also contribute to modularity in the mandible, but the first and third become indistinguishable because intra-modular (e.g., within the ramus) and inter-modular integration (e.g., between ramus and molar alveolus) originate as direct effects of masticatory function.

The main distinction between mandible and cranium is therefore not their complexity or the number of modules (or factors) affecting each (Caumul and Polly 2005) but rather how integration *among modules* originates in each. According to the principles laid out above, it would seem that cranial modules become integrated over ontogeny because early growth is the only source of modular cohesion or autonomy, whereas mandibular modules become integrated by on-going function. Consequently, we would expect that identifying individual modules of the cranium should become increasingly difficult through ontogeny, whereas mandibular modules should each account for a relatively high portion of the variation through adulthood. Note that this distinction does not predict that either of these structures will be more or less integrated. If mandibular functions integrate the entire mandible, as suggested by Zelditch et al. (2008, 2009), we would expect each of these functions to produce a variational module and widespread integration would then result from spatiotemporal overlap among these modules. The finding of a multilayered covariation structure in the mandible, characterized by high support for alternative, disparate models, could therefore be explained by different mandibular functions (e.g., gnawing, chewing, grinding) generating their own variational modules, each integrating different subsets of mandibular components into partially correlated subspaces.

Analyses of oryzomyines thus suggest that: (1) the cranium seems more integrated than the mandible but only because the modules embedded within the cranium are relatively more highly correlated; (2) the mandible appears to have a more complex structure of modularity than the cranium, comprising multiple layers of covariation (i.e., sets of subspaces), including those representing cranio-mandibular coupling and those accounting for intrinsic integration of the mandible. These two results are consistent with the hypothesis that there are different mechanisms of cranial and mandibular integration.

The function-driven growth that is postulated to integrate the latter would cause each functional interaction within the mandible (e.g., between teeth and bone, bone and muscle, muscle and secondary cartilage, and so forth) to imprint its own covariation structure; (3) in agreement with these observations, it is possible to conclude that the covariation structures of mandible and cranium are at least partly independent, both functionally and developmentally; finally, (4) also consistent with these results is the observation that heuristic models seem to be more variable in the mandible than in the cranium; given that these interspecific differences do not seem to be structured according to phylogenetic relatedness, explanations for the resulting integration patterns may be found in details of each species' ecology, possibly reflecting functional diversity.

Connections with similar studies

The patterns seen in most of these oryzomyines broadly resemble those found in other rodents and primates, although a direct comparison between this study and others is complicated by the different approaches to measurement and by the fact that prior studies generally did not consider the possibility of modules spanning cranium and mandible. Despite these caveats, several studies have found patterns of integration resembling those seen in these oryzomyines. For example, Zelditch et al. (1990) found support for both neurocranial and orofacial integration in four species of *Sigmodon*, in which orofacial integration was explained in terms of musculoskeletal or occlusive function. Similarly, Willmore et al. (2006) found higher integration in calvarial and squamosal regions in a random-bred laboratory mouse strain (CV1), contrasting relatively low integration of the facial skeleton. Additionally, significant integration has been found within neurocranial, orbital (i.e., squamosal/frontal/maxilla), and oral (including the palatal process of the palatine) regions in tamarins (Cheverud 1995) and macaques (Cheverud 1982), although nasal integration was not found in the former group. However, integration of only the facial region is reported for Neotropical sakis (Marroig et al. 2004), and quantitative trait locus mapping (QTL) suggests that the calvarium and rostrum constitute two individual modules in mice. Support for the latter pattern, however, is weakened by the limited number of morphometric variables sampled in that study, which exclude cranial variables critical for making the distinction between these results and those shown herein.

The model that best fits the oryzomyine data, and which also appears broadly consistent with that seen in other rodents as well as primates, was originally derived from the phenotype of TGFβ2-null mice (Sandford et al. 1997). *Tgfβ2* is a growth/differentiation factor from the Bone Morphogenetic Protein family, which has a role in skeletal patterning and chondrogenesis (Sandford et al., 1997). It is not clear why this factor should be the best predictor of covariation in natural populations, although *Tgfβ2* might be a regulatory component of a functionally relevant module. Other genetic correlates for a recurrent variational module, as discussed above, are muscle regulatory genes, which, when knocked-out (Rot-Nikcevic et al. 2007) affect the same regions that appear to be integrated in natural populations. Other studies have found that population and geographic variation in cranial components can be traced to the modular effect of a single regulator, most notably, regulatory variation in *Bmp4* (Abzhanov et al. 2004; Badyaev et al. 2008), which also belongs to the family of bone morphogenetic protein genes. It is therefore possible that the pattern of craniomandibular integration found in this study is influenced, at least partly by a *Tgfβ2*-dependent regulatory network.

Most of the cranial regions spanned by this best-supported model are, in fact, functionally linked to masticatory activity, including the mandibular attachment sites of the masseter (see Fig. II.3.13), cranial and mandibular attachments of the temporalis (Fig. II.3.12), as well as other elements (i.e., parietal, squamosal, frontal) presumably loaded by these muscles based on data from other mammals (Herring and Teng 2000). Although a functional hypothesis for the observed pattern of craniomandibular integration would be consistent with a posterior-cranial module as detected in this study, it is not, as discussed above, consistent with a proximal-mandibular module.

Irrespective of the mechanisms integrating the proximal-half of the mandible, present results indicate that such a module exists. This is consistent with most quantitative-genetic studies of the mandible, which distinguish a distal (i.e., alveoli) and a proximal (i.e., mandibular processes) module (e.g., Cheverud et al. 1997; Mezey et al. 2000; Ehrich et al. 2003; Klingenberg et al. 2003, 2004). While these results do not contradict the proximal-mandibular module supported by cranio-mandibular data in oryzomyines, none of these studies have analyzed the patterns of pleiotropic interactions

between cranium and mandible, suggesting that a proximo-distal model of mandible modularity may be an incomplete model, and therefore difficult to interpret in functional or developmental terms. Due to differences in anatomical coverage among studies, it is difficult to determine whether QTL-based results are consistent with the other, more complex patterns of proximo-distal mandibular integration supported herein and by Zelditch et al. (2008, 2009). Although QTL studies routinely show pleiotropic interactions across the proximo-distal axis (see Kenney-Hunt et al. 2008 for a recent review), it would be necessary for such analyses to test alternative and more complex models of spatial distribution of pleiotropic effects in order to produce a result comparable to those presented herein.

Comparative analysis of intraspecific patterns of modularity

Interspecific comparisons suggest a higher than expected congruence between patterns of modularity and co-diversity, in which the dominant multidimensional aspect of intraspecific covariation is also the main axis of interspecific differences in mean shape. Furthermore, the congruence among these within- and among-species patterns is enhanced by the fact that the species with the most divergent shapes are also the ones with the most divergent patterns of modularity. This relationship, however, applies only to crania, the region for which the most divergence is actually observed. Congruence between intraspecific and interspecific covariation is expected for allometric data (Lande 1979; Klingenberg 1996) but not necessarily for allometry-free data. It is difficult to explain why intraspecific variation should so closely match among-species disparity except in terms of intrinsic constraints. This suggests that the conserved modules detected for craniomandibular, and cranial data in particular, may constrain the dimensions in which these species have evolved.

These constraints, however, are not absolute. Evidence for them is found in the first principal component of shape (after excluding the two highly divergent species). This component accounts for approximately 40% of the disparity and it describes a pattern of shape divergence that resembles the intraspecific pattern of modularity. However, this axis is dominated by differences among only four species. The remaining three are differentiated mostly by PC2 (5%), which appear unrelated to either the

consensus or any supported pattern of intraspecific modularity. The presence of dimensions of disparity that cannot be explained in terms of intraspecific modularity but that account for a substantially lower proportion of disparity is also consistent with the hypotheses of developmental constraints on cranial divergence in this group.

A different argument for the influence of constraints on evolutionary divergence can be made for the mandible. In this case, interspecific data support two distinct patterns of modularity, suggesting that divergence is at least partially independent between cranium and mandible. The first is the pattern associating mandible and cranium, the second is intrinsic to the mandible. As previously discussed, integration within the proximal mandible is seen at both levels. When the mandible is treated as part of the skull, it is the distal part that contributes most to disparity. However, when treated as an isolated structure, it is the proximal half that dominates. Congruence between the mandible-specific disparity and the intraspecific pattern of modularity suggests constraints on mandible diversification. Several other studies have found that the proximal mandible makes a disproportionally greater contribution to disparity in rodents (e.g., Atchley et al. 1992; Duarte et al. 2000; Monteiro and dos Reis 2005), but this is not as compelling evidence for constraint as is the observed similarity between patterns of interspecific co-disparity and of intraspecific modularity.

Sampled species	*N*
Holochilus chacarius	60
Melanomys caliginosus	48
Microryzomys minutus	67
Nectomys squamipes	70
Oligoryzomys nigripes	54
Oryzomys couesi	48
Oryzomys palustris	67
Oryzomys xantheolus	44
Sigmodontomys alfari	30

Table II.1. List of oryzomyine species and sample sizes (*N*) used in this study.

Species	Category for comparison[1]	Lateral cranium		Ventral cranium		Mandible	
		Angle (in radians)	*P*-value	Angle (in radians)	*P*-value	Angle (in radians)	*P*-value
H. chacarius[2]	*Geographical origin*:						
	• Chaco vs. Villa Hayes Prov.	3.315	0.029	2.896	0.741	2.967	0.774
	• Chaco Prov. vs. Rio Paraguay	3.463	0.116	3.306	0.209	2.505	0.703
	• Villa Hayes Prov. Vs. Río Paraguay	3.125	0.590	3.149	0.065	2.290	0.853
	Sex (M vs. F)	4.439	0.802	4.290	0.047	3.995	0.453
	Date of collection (1978-79 vs. 1986-88)	4.203	0.526	3.853	0.203	4.058	0.016
M. caliginosus[3]	Sex (M vs. F)	2.990	0.915	3.160	0.463	2.656	0.766
M. minutus[3]	Sex (M vs. F)	3.408	0.812	3.285	0.773	2.920	0.792
N. squamipes[4]	Sex (M vs. F)	4.442	0.687	4.346	0.132	3.702	0.849
	Date of collection[6] (1969-73 vs. 1973-75)	4.631	0.444	4.489	0.043	4.019	0.671
O. nigripes[2]	Sex (M vs. F)	4.678	0.895	4.379	0.616	4.180	0.924
O. couesi[2]	Sex (M vs. F)	4.372	0.390	4.126	0.277	3.939	0.845
O. palustris[2]	Sex (M vs. F)	5.036	0.090	4.552	0.244	4.182	0.811
O. xantheolus[5]	*Geographical origin*:						
	• Lambayeque vs. Piura Prov.	2.341	0.914	2.412	0.594	2.536	0.104
	• Lambayeque vs. Tombes Prov.	2.434	0.674	2.316	0.876	2.282	0.755
	• Piura vs. Tombes Prov.	4.287	0.178	4.124	0.066	3.737	0.504
	Sex (M vs. F)	4.625	0.261	4.023	0.788	4.171	0.151
S. alfari[2]	*Geographical origin*:						
	• Cana vs. Cerro Azul	3.332	0.042	2.943	0.822	2.952	0.328
	• Cana vs. Tacarcuna	3.090	0.855	3.209	0.034	2.780	0.409
	• Cerro Azul vs. Tacarcuna	3.269	0.294	3.161	0.240	3.020	0.107
	Sex (M vs. F)	3.464	0.021	3.077	0.116	2.923	0.962
	Date of collection (1912 vs. 1955-59)	3.733	0.348	3.658	0.136	3.600	0.894

Table II.2. Tests of homogeneity of samples included in this study. Samples were compared using the angles between the subspaces occupied by each sample category. *P*-values correspond to the null hypothesis that observed angles are no larger than expected from two random partitions of the sample. Magnitude of angle is a function of the dimensionality of the space compared (e.g., an angle of $\pi/2$ radians indicates geometrical independency only for R=2 dimensions). [1]See Appendix B for further details; [2]Compare at α=0.0102; [3]Compare at α=0.05; [4]Compare at α=0.0253; [5]Compare at α=0.0127; [6]Partitioning of *N. squamipes* specimens by collection date done at the longest interval (in months) between consecutive collections.

Gene	Module (Figure)	Reference
Egfr	II.4.3	Miettinen et al. (1999)
Fgf-3	II.4.8	Mansour et al. (1993)
Chordin	II.4.8	Bachiller et al. (2000)
Fgf-2	II.4.9	Montero et al. (2000)
Fgfr2	II.4.9-II.4.11	Perlyn et al. (2006)
Fgfr3	II.4.9-II.4.11	Wang et al. (1999)
PdgfαR	II.4.19	Soriano (1997)
Shh	II.4.19	Jeong et al. (2004)
Fgf-8	II.4.23	Trumpp et al. (1999)
Dlx-2	II.4.23	Qiu et al. (1995)
ET-1	II.4.52	Kurihara et al. (2004)
Tgfβ2	II.4.53	Sanford et al. (1997)
Tgfβ3	II.4.54	Proetzel et al. (1995)
Bmp1	II.4.55	Suzuki et al. (1996)
Noggin	II.4.55	Warren et al. (2003)
Msx2	II.4.55	Jabs et al. (1993)
Alx4	II.4.55	Antonopoulou et al. (2004)
Cart1	II.4.55	Zhao et al. (1996)
Bmp7	II.4.56	Luo et al. (1995)
Activin-βA	II.4.57	Matzuk et al. (1995)
Noggin+Chordin	II.4.58	Bachiller et al. (2000); Stottmann et al. (2001)
Ski	II.4.59	Berk et al. (1997)
RARα + RARγ	II.4.60	Lohnes et al. (1994)
Ihh	II.4.61	Young et al. (2006)
Gli2	II.4.62	Mo et al. (1997)
Gli3	II.4.63	Johnson (1967; Schimmang et al. (1992)
Wnt-1 + Wnt-3a	II.4.64	Ikeya et al. (1997)
Wnt-5a	II.4.65	Yamaguchi et al. (1999)
Dlx-1	II.4.66	Qiu et al. (1997)
Dlx-5	II.4.67	Acampora et al. (1999)
dHAND	II.4.68	Yaganisawa et al. (2003)
Hoxa1	II.4.69	Barrow and Capecchi (1999)
Hoxa2	II.4.70	Rijli et al. (1993; Barrow and Capecchi (1999)
Msx1	II.4.71	Satokata and Maas (1994)
Bapx1	II.4.72	Tribioli and Lufkin (1999)
Pax2	II.4.73	Torres et al. (1996)
Pax6	II.4.74	Kaufman et al. (1995)
Pax7	II.4.75	Mansouri et al. (1996)
Pax9	II.4.76	Peters et al. (1998)
Prx1	II.4.77	Martin et al. (1995)
Gsc	II.4.78	Yamada et al. (1995)
Otx2	II.4.79	Matsuo et al. (1995)
Ptx1	II.4.80	Lanctôt et al. (1999)
Pitx2	II.4.81	Lu et al. (1999)
Pbx1	II.4.82	Selleri et al. (2001)
Mfh1	II.4.83	Winnier et al. (1997)
Mf1	II.4.84	Kume et al. (1998)

Table II.3. List of secreted and transcription factors used to build hypotheses of "mutational targets" tested in this study. Hypothesized modules are designed based on the expectation that knocking out a listed gene under a controlled background generates a covariance pattern that is similar to the effect (i.e., anatomical target) of the mutation. Modules were drawn to match illustrations (in some cases, verbal descriptions) of mutational effects provided in the given references.

Model	Component modules
$\mathbf{H_0}$	$\{M_1\}$
$\mathbf{H_1}$	$\{M_{11}\}\{M_9\}\{M_{10}\}$
$\mathbf{H_2}$	$\{M_{13}\}\{M_{12}\}\{M_{14}\}\{M_{15}\}$
$\mathbf{H_3}$	$\{M_{16}\}$
$\mathbf{H_4}$	$\{M_6\}\{M_2\}\{M_7\}\{M_9\}\{M_4\}\{M_8\}$
$\mathbf{H_5}$	$\{M_6\}\{M_2\}\{M_7\}\{M_9\}\{M_{17}\}\{M_8\}$
$\mathbf{H_6}$	$\{M_6\}\{M_3\}\{M_7\}\{M_9\}\{M_4\}\{M_8\}$
$\mathbf{H_7}$	$\{M_6\}\{M_3\}\{M_7\}\{M_9\}\{M_{17}\}\{M_8\}$
$\mathbf{H_8}$	$\{M_6\}\{M_5\}\{M_7\}\{M_9\}\{M_4\}\{M_8\}$
$\mathbf{H_9}$	$\{M_6\}\{M_5\}\{M_7\}\{M_9\}\{M_{17}\}\{M_8\}$
$\mathbf{H_{10}}$	$\{M_6\}\{M_2\}\{M_7\}\{M_9\}\{M_4\}\{M_{13}\}\{M_{12}\}\{M_{14}\}\{M_{15}\}\{M_8\}$
$\mathbf{H_{11}}$	$\{M_6\}\{M_2\}\{M_7\}\{M_9\}\{M_{17}\}\{M_{13}\}\{M_{12}\}\{M_{14}\}\{M_{15}\}\{M_8\}$
$\mathbf{H_{12}}$	$\{M_6\}\{M_3\}\{M_7\}\{M_9\}\{M_4\}\{M_{13}\}\{M_{12}\}\{M_{14}\}\{M_{15}\}\{M_8\}$
$\mathbf{H_{13}}$	$\{M_6\}\{M_3\}\{M_7\}\{M_9\}\{M_{17}\}\{M_{13}\}\{M_{12}\}\{M_{14}\}\{M_{15}\}\{M_8\}$
$\mathbf{H_{14}}$	$\{M_6\}\{M_5\}\{M_7\}\{M_9\}\{M_4\}\{M_{13}\}\{M_{12}\}\{M_{14}\}\{M_{15}\}\{M_8\}$
$\mathbf{H_{15}}$	$\{M_6\}\{M_5\}\{M_7\}\{M_9\}\{M_{17}\}\{M_{13}\}\{M_{12}\}\{M_{14}\}\{M_{15}\}\{M_8\}$
$\mathbf{H_{16}}$	$\{M_6\}\{M_2\}\{M_7\}\{M_9\}\{M_4\}\{M_{16}\}\{M_8\}$
$\mathbf{H_{17}}$	$\{M_6\}\{M_2\}\{M_7\}\{M_9\}\{M_{17}\}\{M_{16}\}\{M_8\}$
$\mathbf{H_{18}}$	$\{M_6\}\{M_3\}\{M_7\}\{M_9\}\{M_4\}\{M_{16}\}\{M_8\}$
$\mathbf{H_{19}}$	$\{M_6\}\{M_3\}\{M_7\}\{M_9\}\{M_{17}\}\{M_{16}\}\{M_8\}$
$\mathbf{H_{20}}$	$\{M_6\}\{M_5\}\{M_7\}\{M_9\}\{M_4\}\{M_{16}\}\{M_8\}$
$\mathbf{H_{21}}$	$\{M_6\}\{M_5\}\{M_7\}\{M_9\}\{M_{17}\}\{M_{16}\}\{M_8\}$
$\mathbf{H_{22}}$	$\{M_{18}\}$
$\mathbf{H_{23}}$	$\{M_{19}\}$
$\mathbf{H_{24}}$	$\{M_{19}\}\{M_{18}\}$
$\mathbf{H_{25}}$	$\{M_{21}\}\{M_{20}\}$
$\mathbf{H_{26}}$	$\{M_{21}\}\{M_{20}\}\{M_{22}\}$
$\mathbf{H_{27}}$	$\{M_{23}\}$
$\mathbf{H_{28}}$	$\{M_{23}\}\{M_9\}$
$\mathbf{H_{29}}$	$\{M_6\}\{M_{23}\}\{M_9\}\{M_8\}$
$\mathbf{H_{30}}$	$\{M_6\}\{M_{23}\}\{M_{18}\}\{M_8\}$
$\mathbf{H_{31}}$	$\{M_{27}\}\{M_{24}\}\{M_{25}\}\{M_{26}\}\{M_{28}\}\{M_{29}\}$
$\mathbf{H_{32}}$	$\{M_{44}\}\{M_{43}\}\{M_{42}\}\{M_{45}\}\{M_{39}\}\{M_{41}\}\{M_{40}\}\{M_{31}\}\{M_{35}\}$ $\{M_{32}\}\{M_{37}\}\{M_{38}\}\{M_{36}\}\{M_{47}\}\{M_{46}\}\{M_{48}\}\{M_{50}\}\{M_{49}\}$ $\{M_{51}\}\{M_{34}\}\{M_{33}\}\{M_{30}\}$

Model	Component modules
$\mathbf{H_{33}}$	$\{M_{52}\}$
$\mathbf{H_{34}}$	$\{M_{53}\}$
$\mathbf{H_{35}}$	$\{M_{54}\}$
$\mathbf{H_{36}}$	$\{M_{55}\}$
$\mathbf{H_{37}}$	$\{M_{56}\}$
$\mathbf{H_{38}}$	$\{M_{57}\}$
$\mathbf{H_{39}}$	$\{M_{58}\}$
$\mathbf{H_{40}}$	$\{M_{59}\}$
$\mathbf{H_{41}}$	$\{M_{60}\}$
$\mathbf{H_{42}}$	$\{M_{61}\}$
$\mathbf{H_{43}}$	$\{M_{62}\}$
$\mathbf{H_{44}}$	$\{M_{63}\}$
$\mathbf{H_{45}}$	$\{M_{64}\}$
$\mathbf{H_{46}}$	$\{M_{65}\}$
$\mathbf{H_{47}}$	$\{M_{66}\}$
$\mathbf{H_{48}}$	$\{M_{67}\}$
$\mathbf{H_{49}}$	$\{M_{68}\}$
$\mathbf{H_{50}}$	$\{M_{69}\}$
$\mathbf{H_{51}}$	$\{M_{70}\}$
$\mathbf{H_{52}}$	$\{M_{71}\}$
$\mathbf{H_{53}}$	$\{M_{72}\}$
$\mathbf{H_{54}}$	$\{M_{73}\}$
$\mathbf{H_{55}}$	$\{M_{74}\}$
$\mathbf{H_{56}}$	$\{M_{75}\}$
$\mathbf{H_{57}}$	$\{M_{76}\}$
$\mathbf{H_{58}}$	$\{M_{77}\}$
$\mathbf{H_{59}}$	$\{M_{78}\}$
$\mathbf{H_{60}}$	$\{M_{79}\}$
$\mathbf{H_{61}}$	$\{M_{80}\}$
$\mathbf{H_{62}}$	$\{M_{81}\}$
$\mathbf{H_{63}}$	$\{M_{82}\}$
$\mathbf{H_{64}}$	$\{M_{83}\}$
$\mathbf{H_{65}}$	$\{M_{84}\}$

Table II.4. Models used in initial tests. Module numbers refer to numbers in Figure II.3 (i.e., $M_{\#}$ = Fig. II.3.#)

Species: Views	Best ranked models	Jackknife Support[1]	γ* (95% CI)
Holochilus chacarius:			
Cranium + mandible	Heuristic	100%	0.570 (0.565- 0.586)
	$\{M_{11}\}\{M_{18}\}$	0%	0.613 (0.605- 0.628)
Cranium	Heuristic	100%	0.540 (0.534- 0.562)
	$\{M_{11}\}\{M_{18}\}$	0%	0.633 (0.629- 0.648)
Mandible	Heuristic	100%	0.332 (0.324- 0.356)
	$\{M_{46}\}\{M_{47}\}\{M_{48}\}\{M_{77}\}$	0%	0.411 (0.400- 0.431)
Melanomys caliginosus:			
Cranium + mandible	Heuristic	100%	0.466 (0.459- 0.480)
	$\{M_{53}\}$ (H_{34})	0%	0.575 (0.565- 0.586)
	$\{M_{53}\}\{M_{6}\}$	0%	0.575 (0.566- 0.587)
Cranium	Heuristic	100%	0.508 (0.496- 0.532)
	$\{M_{53}\}$ (H_{34})	0%	0.615 (0.601- 0.628)
Mandible	Heuristic	100%	0.363 (0.352- 0.381)
	$\{M_{46}\}\{M_{48}\}\{M_{77}\}$	0%	0.403 (0.391- 0.425)
	$\{M_{16}\}$ (H_3) = $\{M_{53}\}$ (H_{34}) = $\{M_{80}\}$ (H_{61})	0%	0.423 (0.408- 0.439)
	$\{M_{5}\}$ $\{M_{16}\}$ (H_{20})	0%	0.425 (0.413- 0.439)
	$\{M_{46}\}\{M_{47}\}\{M_{48}\}\{M_{49}\}\{M_{50}\}\{M_{51}\}$	0%	0.425 (0.419- 0.444)
	(H_{32})	0%	0.430 (0.419- 0.453)
	$\{M_{5}\}\{M_{12}\}\{M_{13}\}\{M_{14}\}\{M_{15}\}$ (H_{14})	0%	0.431 (0.420- 0.454)
	$\{M_{12}\}\{M_{13}\}\{M_{14}\}\{M_{15}\}$ (H_2)		

Table II.5. Best supported models for each species. Given are the percentage of jackknife sub-samples in which each model was the best supported, the measure of model fit (γ*) and its 95% confidence interval (P = 1.0 in all listed cases, based on 1,000 Monte Carlo replicates). Suboptimal models shown are those whose γ* CI overlaps the CI of the most supported model-combination model. Ranks are based on the set comprising 66 models (H_0-H_{65}) plus the best-supported combination of their individual modules, plus a heuristic model obtaining by iteratively changing the boundaries of the latter. Jackknife support and 95% CI based on 500 jackknife sub-samples. [1]Note that this is the proportion of replicates in which a model ranks first. In most of these tests, the listed models rank in their noted positions in 100% of the replicates (e.g., in H. chacarius, in the cranial + mandible data set, model $\{M_{11}\}\{M_{18}\}$ ranks 0% first, but 100% second).

Species: Views	Best ranked models	Jackknife Support[1]	γ* (95% CI)
Microryzomys minutus:			
Cranium + mandible	Heuristic	100%	0.494 (0.485- 0.506)
	$\{M_{53}\}\{M_6\}$	0%	0.584 (0.576- 0.598)
	$\{M_{53}\}$ (H_{34})	0%	0.593 (0.581- 0.607)
Cranium	Heuristic	100%	0.503 (0.494- 0.519)
	$\{M_{53}\}$ (H_{34})	0%	0.597 (0.585- 0.611)
Mandible	Heuristic	100%	0.254 (0.246- 0.282)
	$\{M_{47}\}\{M_{48}\}\{M_{49}\}\{M_{50}\}\{M_{51}\}$	0%	0.306 (0.298- 0.334)
	$\{M_{46}\}\{M_{47}\}\{M_{48}\}\{M_{49}\}\{M_{50}\}\{M_{51}\}$	0%	0.315 (0.307- 0.342)
	(H_{32}) $\{M_{12}\}\{M_{13}\}\{M_{14}\}\{M_{15}\}$ (H_2)	0%	0.339 (0.328- 0.367)
	$\{M_5\}\{M_{12}\}\{M_{13}\}\{M_{14}\}\{M_{15}\}$ (H_{14})	0%	0.342 (0.332- 0.368)
Nectomys squamipes:			
Cranium + mandible	Heuristic	100%	0.486 (0.476- 0.499)
	$\{M_{53}\}\{M_6\}$	0%	0.606 (0.599- 0.616)
	$\{M_{53}\}$ (H_{34})	0%	0.619 (0.610- 0.630)
Cranium	Heuristic	100%	0.501 (0.491- 0.523)
	$\{M_{79}\}$ (H_{60})	0%	0.627 (0.613- 0.643)
Mandible	Heuristic	100%	0.375 (0.364- 0.389)
	$\{M_{16}\}\{M_{46}\}\{$ $M_{47}\}$	0%	0.386 (0.375- 0.401)
	$\{M_{46}\}\{M_{47}\}\{M_{48}\}\{M_{49}\}\{M_{50}\}\{M_{51}\}$ (H_{32})	0%	0.392 (0.386- 0.412)
Oligoryzomys nigripes:			
Cranium + mandible	Heuristic	100%	0.460 (0.452- 0.467)
	$\{M_{53}\}\{M_6\}$	0%	0.564 (0.555- 0.575)
	$\{M_{53}\}$ (H_{34})	0%	0.567 (0.557- 0.579)
Cranium	Heuristic	100%	0.502 (0.494- 0.514)
	$\{M_{53}\}$ (H_{34})	0%	0.622 (0.608- 0.634)
Mandible	Heuristic	100%	0.296 (0.291- 0.307)
	$\{M_{46}\}\{M_{48}\}\{M_{77}\}$	0%	0.354 (0.346- 0.372)
	$\{M_{46}\}\{M_{47}\}\{M_{48}\}\{M_{49}\}\{M_{50}\}\{M_{51}\}$	0%	0.369 (0.361- 0.389)
	(H_{32}) $\{M_5\}\{M_{12}\}\{M_{13}\}\{M_{14}\}\{M_{15}\}$ (H_{14})	0%	0.371 (0.358- 0.390)
	$\{M_{12}\}\{M_{13}\}\{M_{14}\}\{M_{15}\}$ (H_2)	0%	0.375 (0.360- 0.397)

Table II.5. Continued.

Species: Views	Best ranked models	Jackknife Support[1]	γ* (95% CI)
Oryzomys couesi:			
Cranium + mandible	Heuristic	100%	0.515 (0.505- 0.525)
	{M_{53}} (H_{34})	0%	0.589 (0.579- 0.602)
	{M_{53}}{M_6}	0%	0.589 (0.580- 0.603)
Cranium	Heuristic	100%	0.494 (0.482- 0.505)
	{M_{53}} (H_{34})	0%	0.611 (0.597- 0.620)
Mandible	Heuristic	100%	0.289 (0.279- 0.302)
	{M_{12}}{M_{13}}{M_{15}}	0%	0.420 (0.406- 0.446)
	{M_{12}}{M_{13}}{M_{14}}{M_{15}} (H_2)	0%	0.429 (0.416- 0.455)
	{M_5}{M_{12}}{M_{13}}{M_{14}}{M_{15}} (H_{14})	0%	0.437 (0.425- 0.462)
	{M_{16}} (H_3) = {M_{53}} (H_{34}) = {M_{80}} (H_{61})	0%	0.460 (0.435- 0.485)
Oryzomys palustris:			
Cranium + mandible	Heuristic	100%	0.480 (0.473- 0.487)
	{M_{53}}{M_6}	0%	0.579 (0.571- 0.592)
	{M_{53}} (H_{34})	0%	0.581 (0.572- 0.594)
Cranium	Heuristic	100%	0.489 (0.480- 0.504)
	{M_{53}} (H_{34})	0%	0.594 (0.583- 0.614)
	{M_{79}} (H_{60})	0%	0.623 (0.605- 0.645)
Mandible	Heuristic	100%	0.356 (0.347- 0.376)
	{M_{46}}{M_{48}}{M_{77}}	0%	0.409 (0.404- 0.427)
	{M_{46}}{M_{47}}{M_{48}}{M_{49}}{M_{50}}{M_{51}}	0%	0.425 (0.420- 0.441)
	(H_{32}) {M_5}{M_{12}}{M_{13}}{M_{14}}{M_{15}} (H_{14})	0%	0.435 (0.427- 0.453)

Table II.5. Continued.

Species: Views	Best ranked models	Jackknife Support[1]	γ* (95% CI)
Oryzomys xantheolus:			
Cranium + mandible	Heuristic	100%	0.519 (0.512- 0.529)
	{M_{53}}{M_6}	0%	0.646 (0.635- 0.657)
	{M_{53}} (H_{34})	0%	0.652 (0.638- 0.663)
Cranium	Heuristic	100%	0.533 (0.520- 0.552)
	{M_{53}} (H_{34})	0%	0.688 (0.675- 0.703)
	{M_{18}}{M_{19}} (H_{24})	0%	0.691 (0.681- 0.702)
	{M_{19}} (H_{23})	0%	0.698 (0.684- 0.708)
	{M_{79}} (H_{60})	0%	0.698 (0.686- 0.709)
	{M_{63}} (H_{44})	0%	0.713 (0.697- 0.737)
	{M_{77}} (H_{58})	0%	0.714 (0.698- 0.728)
Mandible	Heuristic	100%	0.345 (0.337- 0.363)
	{M_5}{M_{48}}{M_{77}}	0%	0.412 (0.404- 0.433)
	{M_5} {M_{16}} (H_{20})	0%	0.434 (0.420- 0.451)
	{M_{16}} (H_3) = {M_{53}} (H_{34}) = {M_{80}} (H_{61})	0%	0.436 (0.419- 0.458)
	{M_{46}}{M_{47}}{M_{48}}{M_{49}}{M_{50}}{M_{51}} (H_{32})	0%	0.437 (0.431- 0.455)
Sigmodontomys alfari:			
Cranium + mandible	Heuristic	100%	0.520 (0.511- 0.529)
	{M_{19}} (H_{23})	0%	0.628 (0.617- 0.639)
	{M_{53}} (H_{34})	0%	0.629 (0.610- 0.647)
	{M_{18}}{M_{19}} (H_{24})	0%	0.639 (0.633- 0.648)
	{M_{77}} (H_{58})	0%	0.640 (0.622- 0.657)
Cranium	Heuristic	100%	0.540 (0.531- 0.557)
	{M_{19}} {M_{28}}	0%	0.581 (0.566- 0.600)
	{M_{19}} (H_{23})	0%	0.583 (0.567- 0.602)
Mandible	Heuristic	100%	0.298 (0.286- 0.325)
	{M_{46}}{M_{48}}{M_{77}}	0%	0.378 (0.370- 0.403)
	{M_{16}} (H_3) = {M_{53}} (H_{34}) = {M_{80}} (H_{61})	0%	0.401 (0.382- 0.445)
	{M_5} {M_{16}} (H_{20})	0%	0.409 (0.396- 0.442)

Table II.5. Continued.

Species	Module									
	Molar alveolus	**Incisor alveolus**	**Tooth-bearing**	**Ramus**	**Masseter-bearing**	**Muscle-bearing**	**Coronoid**	**Angular**	**Condyloid**	**All processes**
H. chacarius	**Yes**	**Yes**	-	**Yes**	-	-	-	-	-	**Yes**
M. caliginosus	**Yes**	Yes	Yes	**Yes**	Yes	Yes	Yes	Yes	Yes	**Yes**
M. minutus	Yes	**Yes**	Yes	Yes	Yes	-	**Yes**	**Yes**	**Yes**	-
N. squamipes	**Yes**	**Yes**	-	Yes	-	**Yes**	Yes	Yes	Yes	-
O. nigripes	**Yes**	Yes	Yes	**Yes**	Yes	-	Yes	Yes	Yes	**Yes**
O. couesi	-	-	Yes	-	**Yes**	Yes	**Yes**	Yes	**Yes**	-
O. palustris	**Yes**	Yes	Yes	**Yes**	Yes	-	Yes	Yes	Yes	**Yes**
O. xantheolus	Yes	Yes	**Yes**	**Yes**	-	Yes	Yes	Yes	Yes	**Yes**
S. alfari	Yes	-	Yes	**Yes**	-	Yes	-	-	-	**Yes**

Table II.6. List of a priori modules of the mandible supported by each species. Modules included in best-supported models are highlighted in boldface. Note that some modules are nested within others: "Tooth-bearing" module spans molar and incisor alveoli; "Muscle-bearing" module spans all processes, "masseter-bearing" module, and the ramus; "masseter-bearing" module spans the ramus and angular process; "all processes" spans the coronoid, angular, and condyloid processes. Data extracted from Figures II.5-II.21.

Species	Partial disparity (x1000) (in sq. Procrustes units)	Percent of total disparity
H. chacarius	0.715	19.87%
M. caliginosus	0.420	11.68%
M. minutus	0.368	10.24%
N. squamipes	0.311	8.65%
O. nigripes	0.239	6.65%
O. couesi	0.297	8.24%
O. palustris	0.377	10.47%
O. xantheolus	0.284	7.89%
S. alfari	0.587	16.31%

Table II.7. Partial disparities contributed by each species to the total disparity among mean shapes of nine species of oryzomyines included in this study. Computations based on craniomandibular data set. Percent value of total disparity is shown. Total disparity of the group equals 0.0036 squared Procrustes units.

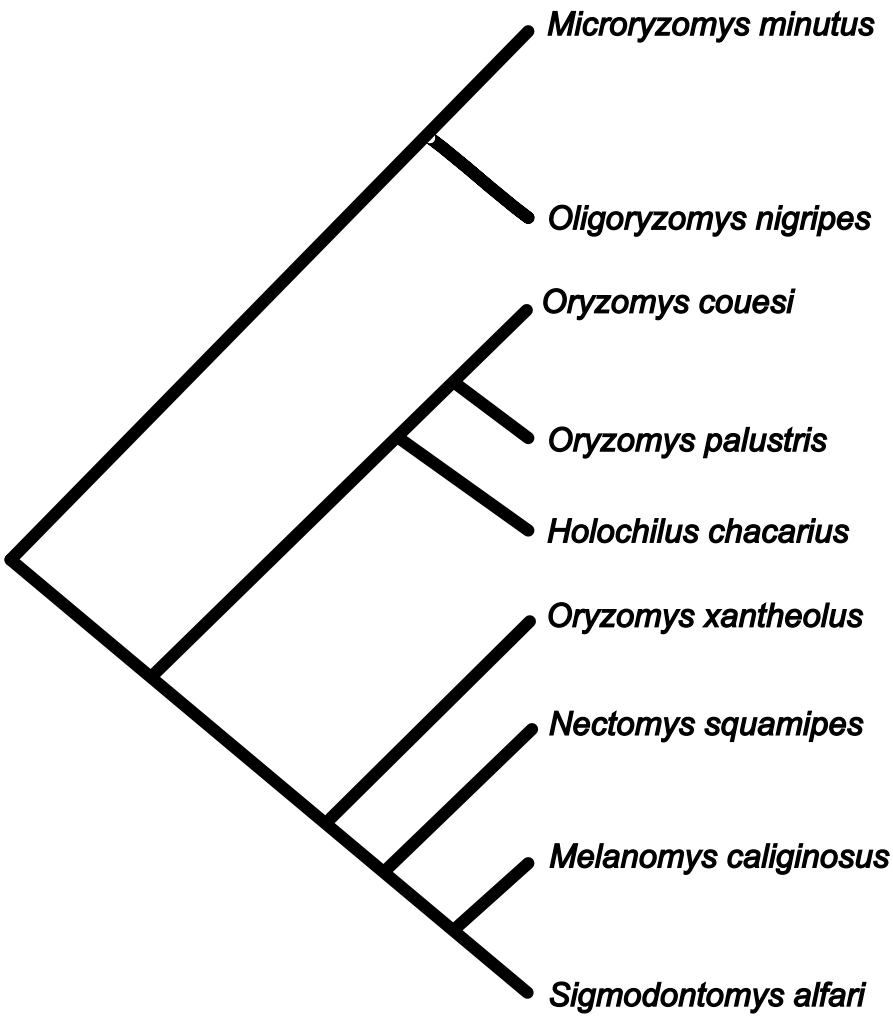

Figure II.1. Phylogenetic relationships among species included in this study. Modified from Weksler (2006).

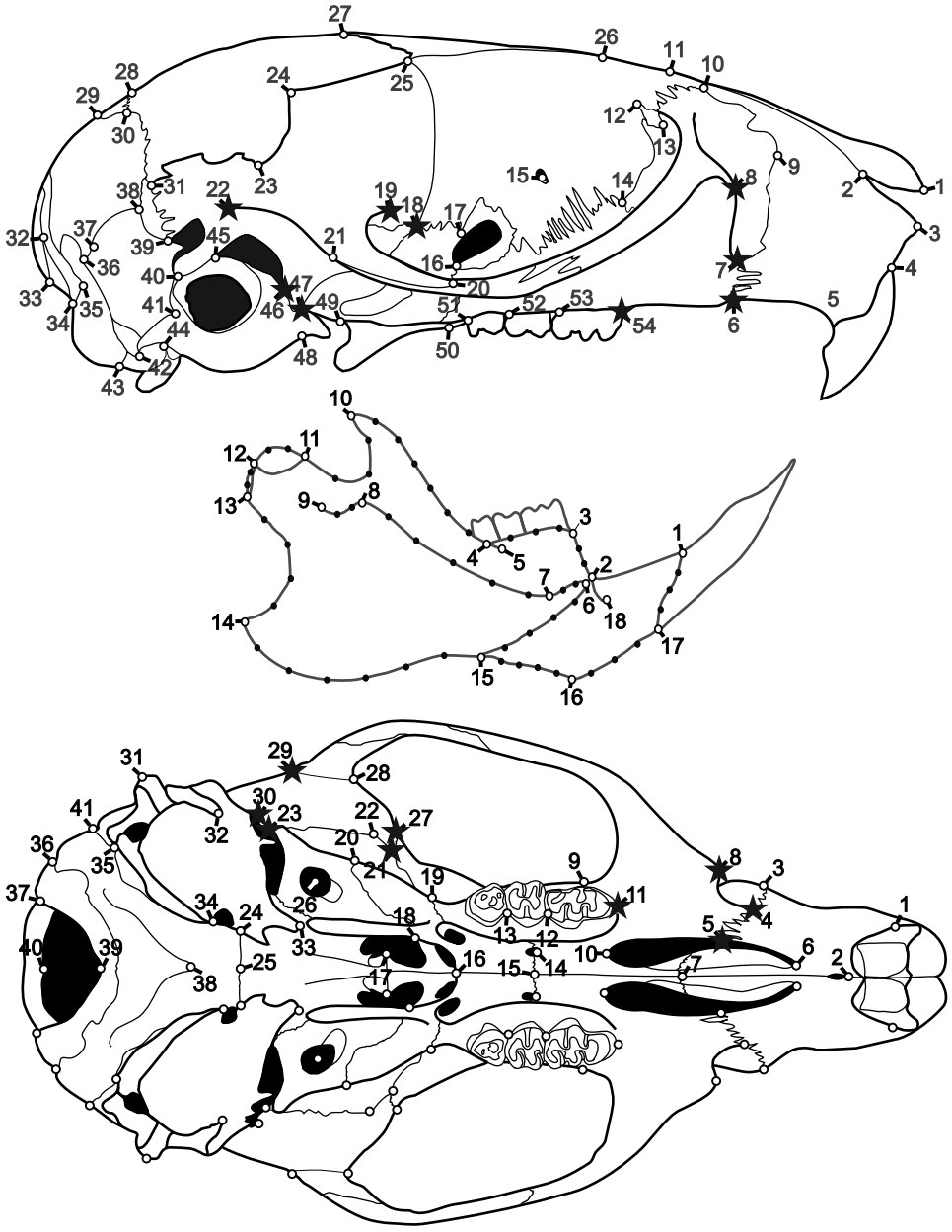

Figure II.2. Diagrammatic representation of the lateral (top), mandible (middle), and ventral (bottom) views of the skull analyzed in this study. Landmarks are indicated as open circles, semi-landmarks of the mandible are indicated as closed circles. Stars in lateral and ventral views represent common landmarks across views; these landmarks are treated as part of the same module to construct craniomandibular and cranial data sets.

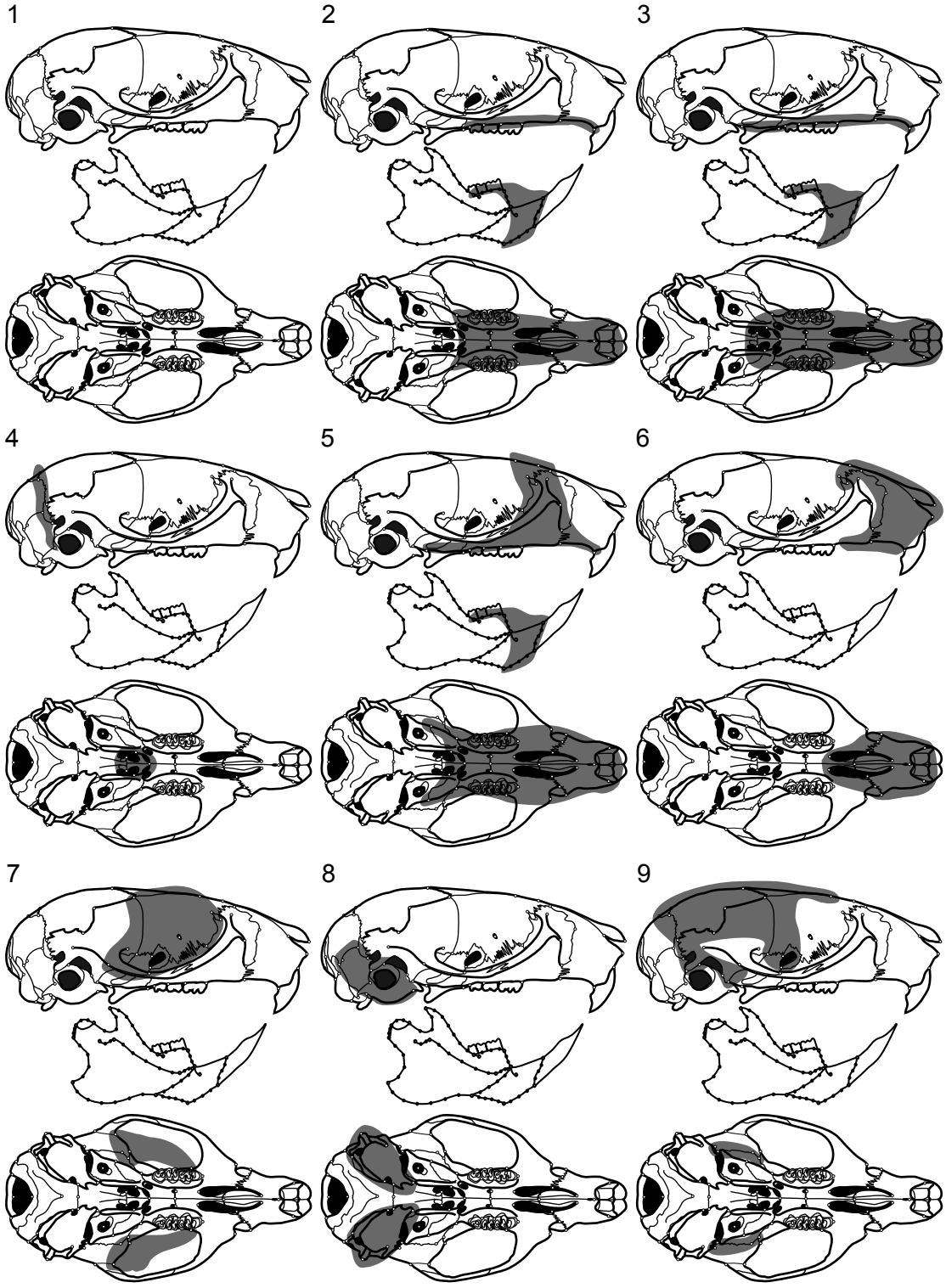

Figure II.3. Modules used to define hypotheses of modularity. Each module is shown in grey (one module per set of diagrams). Each module comprises a lateral-cranial, mandibular, and ventral-cranial component. Module numbers are referenced in the text either as Fig. II.3.# or as M#.

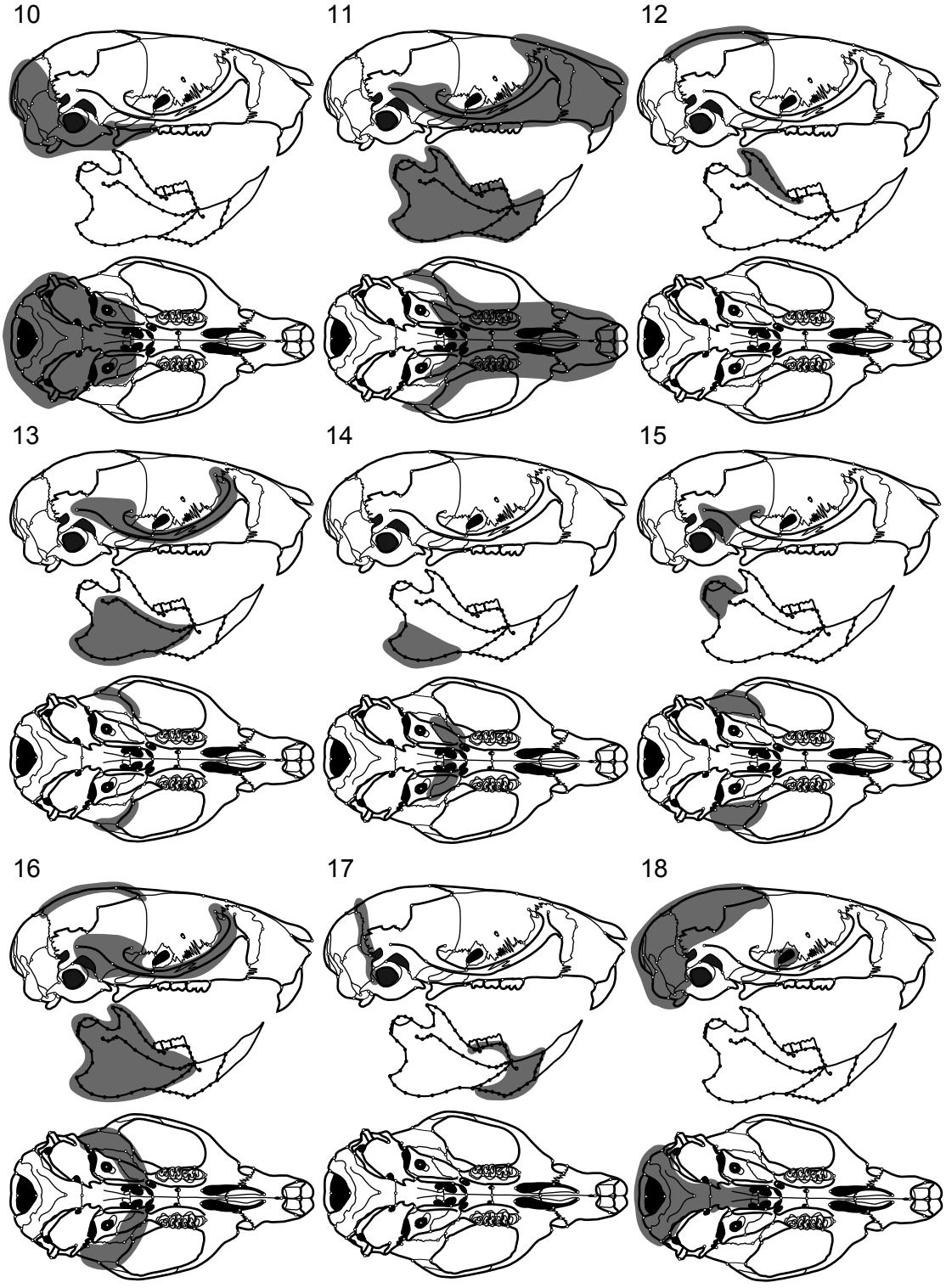

Figure II.3. Continued.

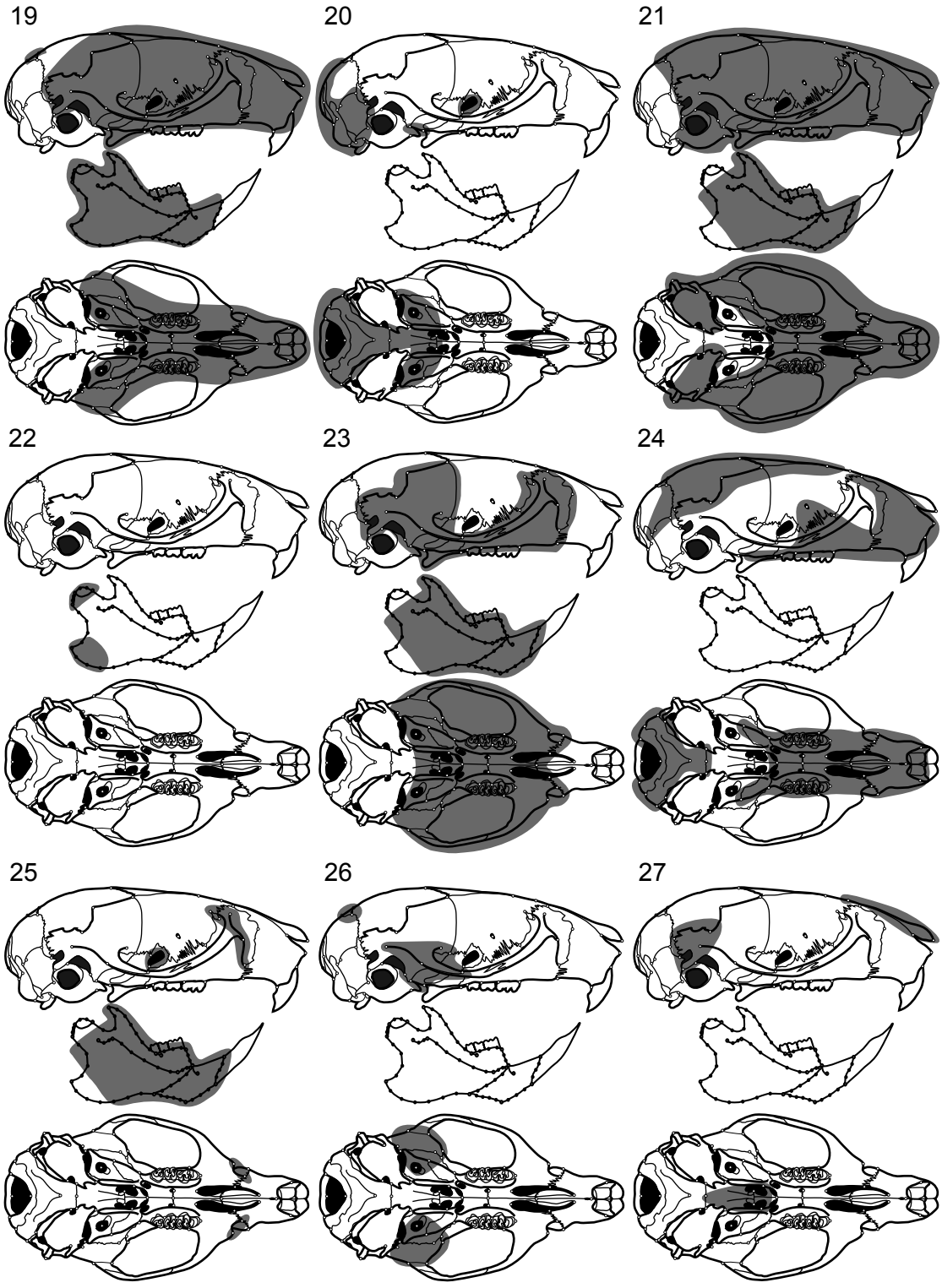

Figure II.3. Continued.

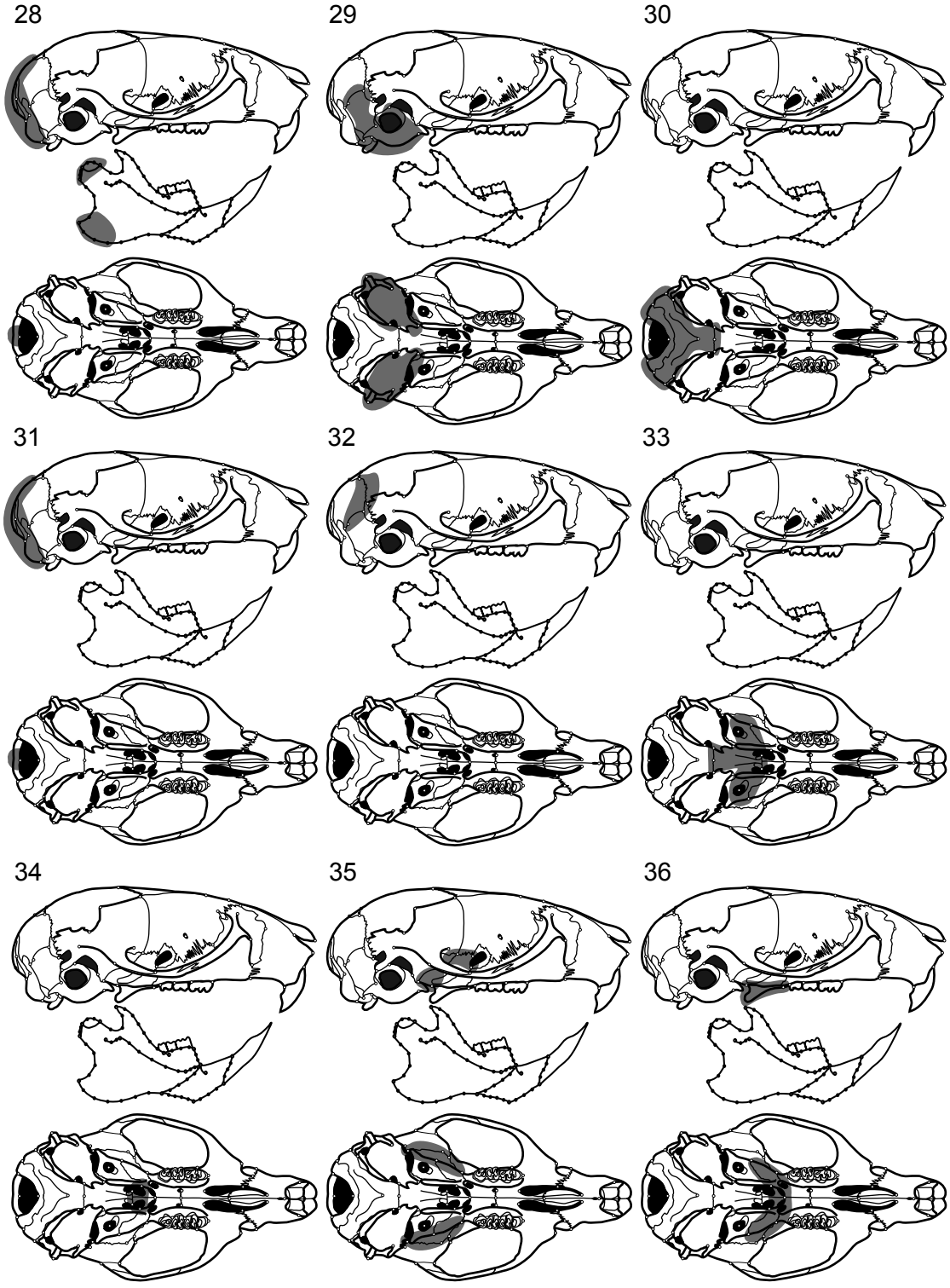

Figure II.3. Continued.

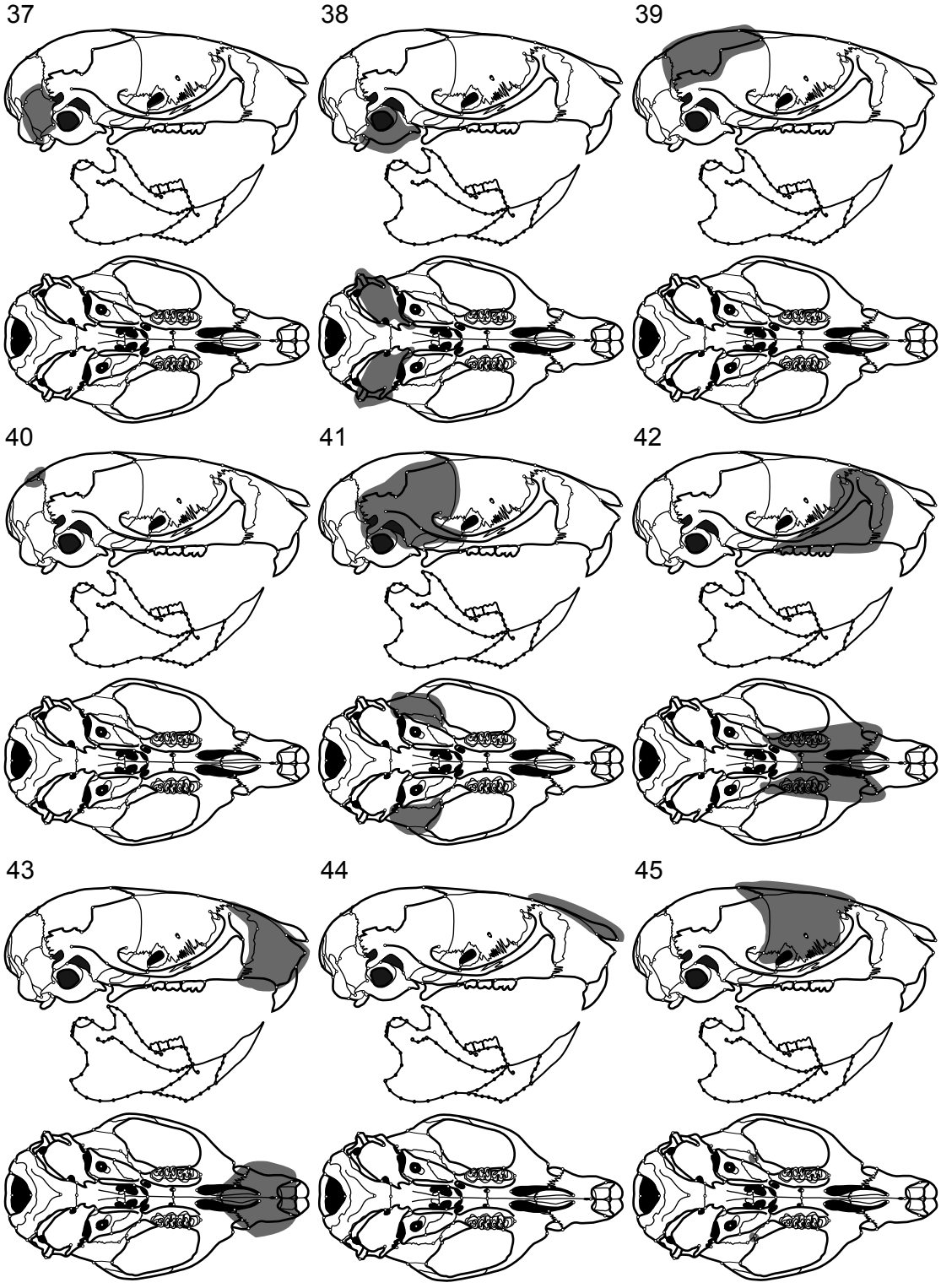

Figure II.3. Continued.

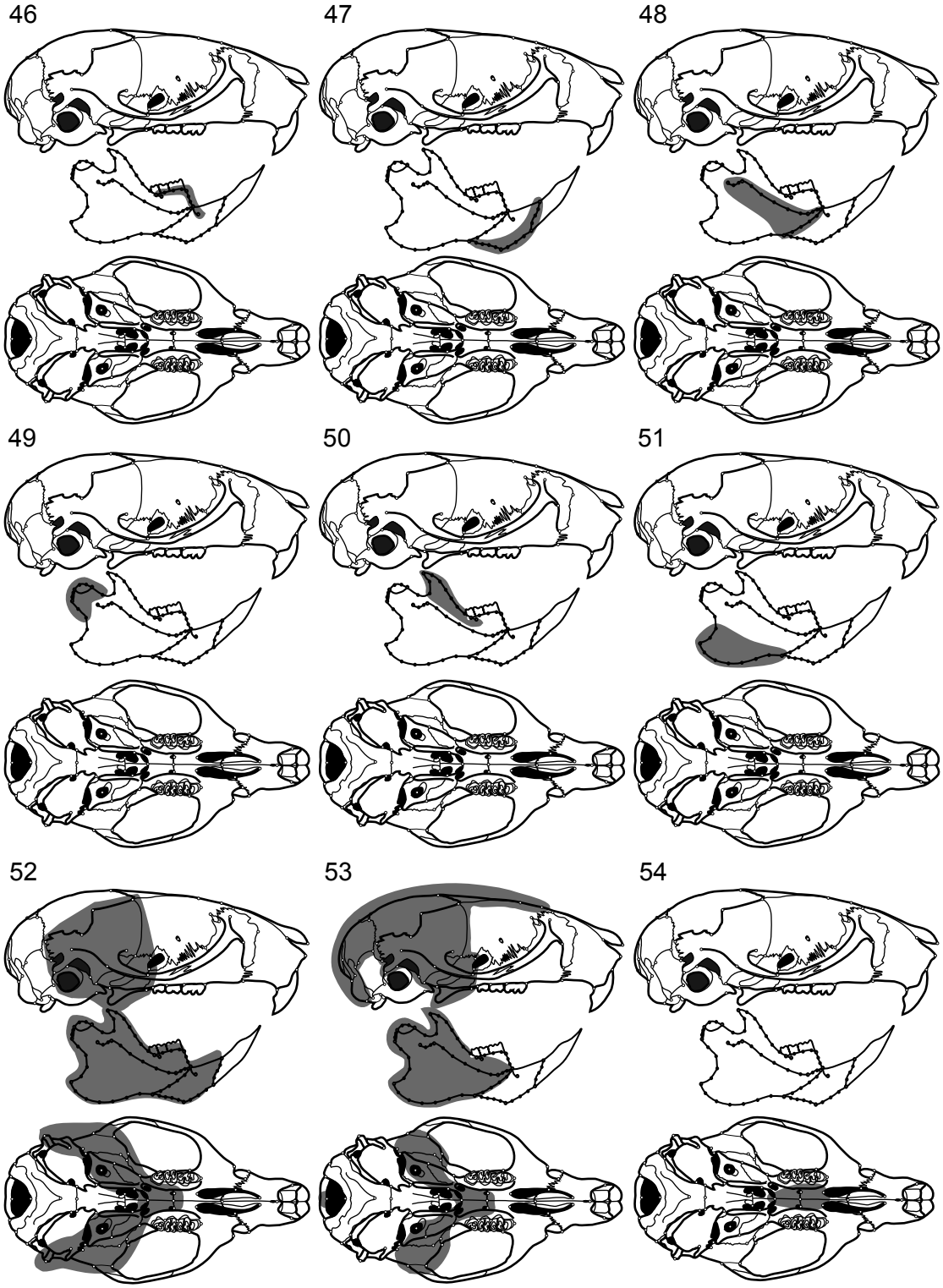

Figure II.3. Continued.

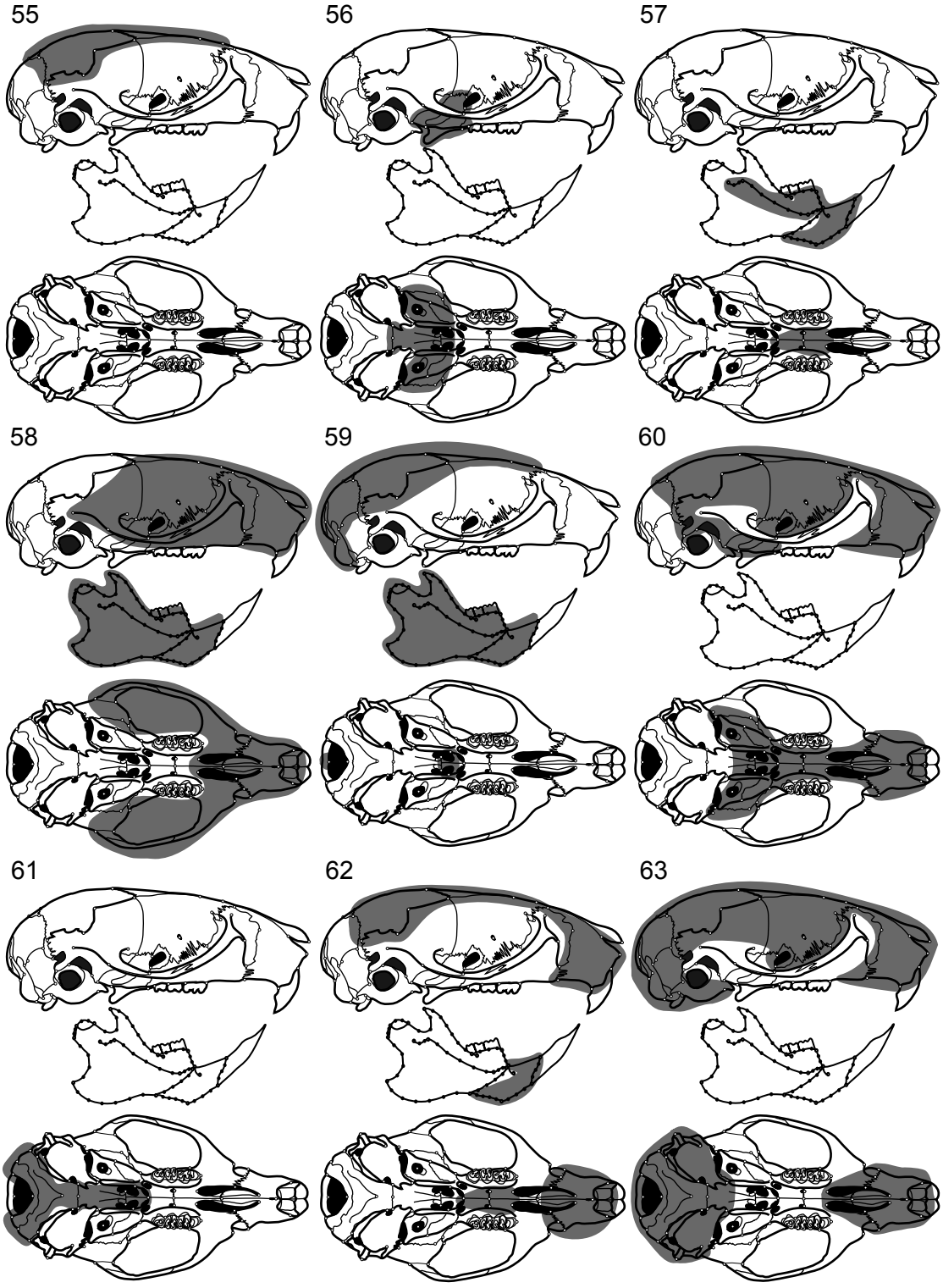

Figure II.3. Continued.

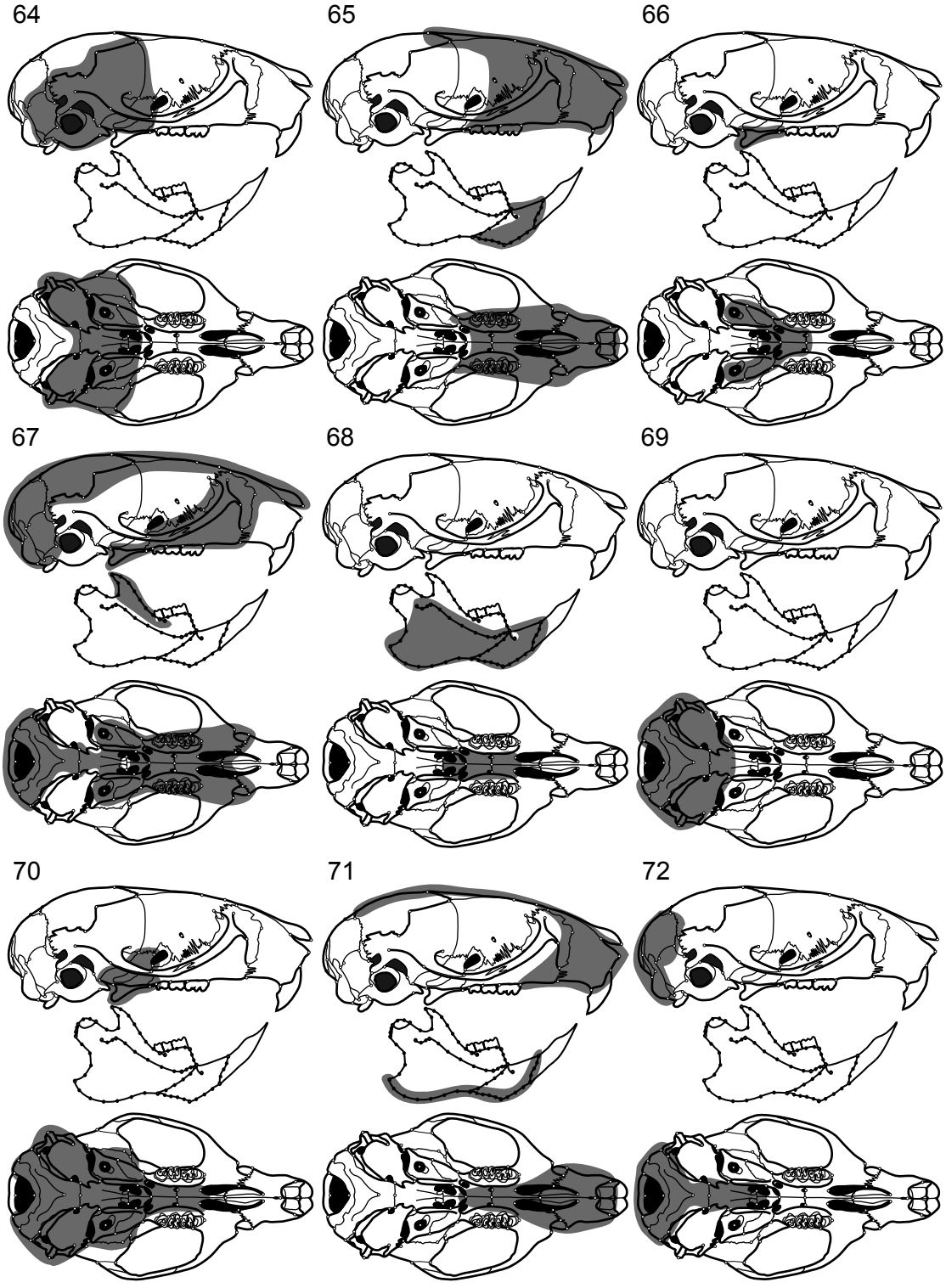

Figure II.3. Continued.

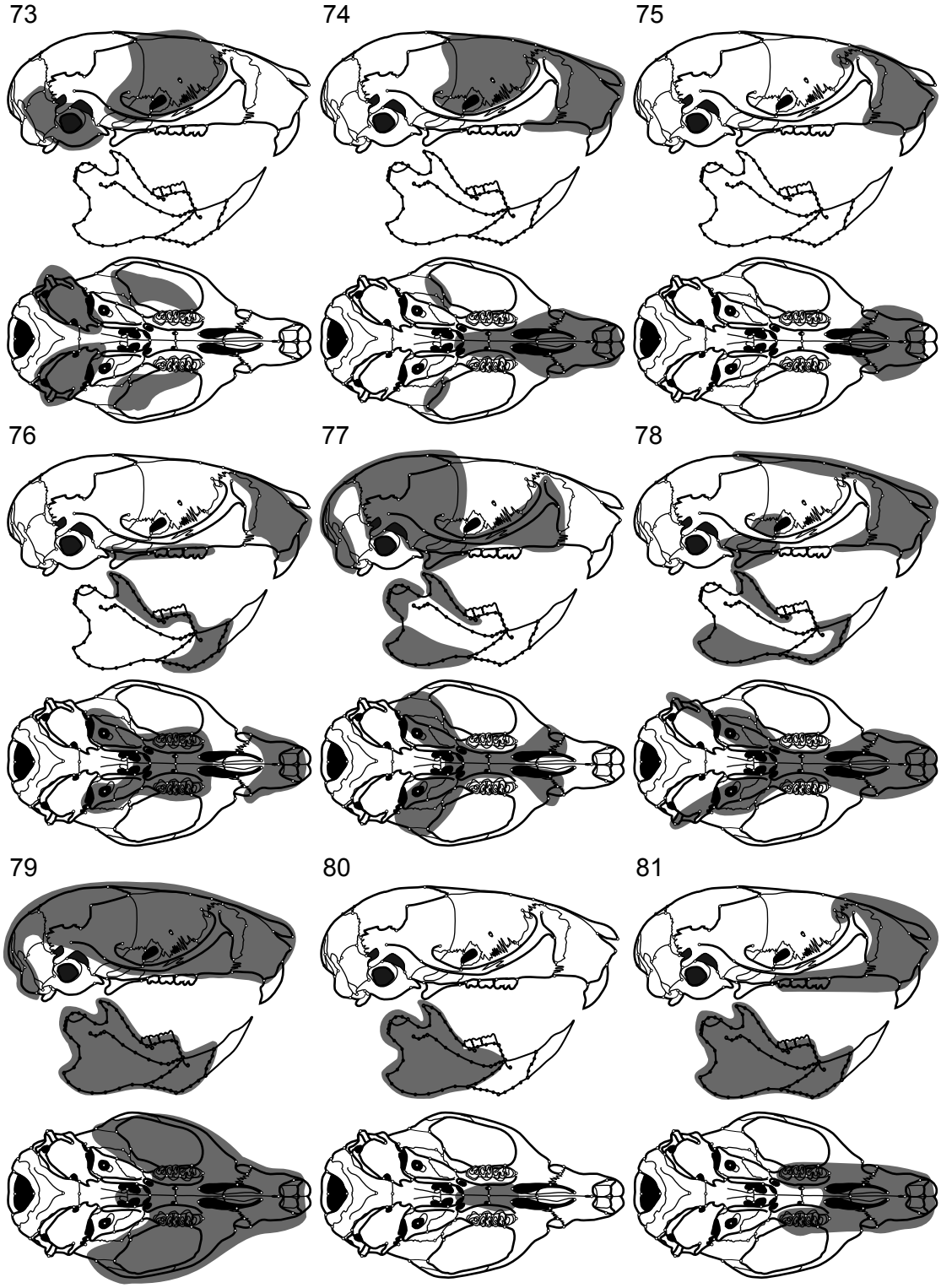

Figure II.3. Continued.

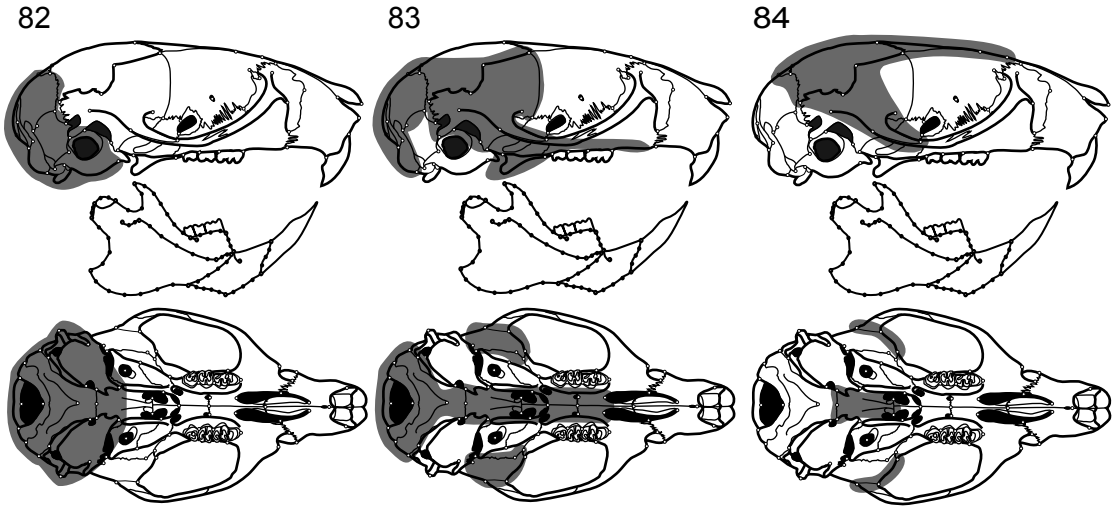

Figure II.3. Continued.

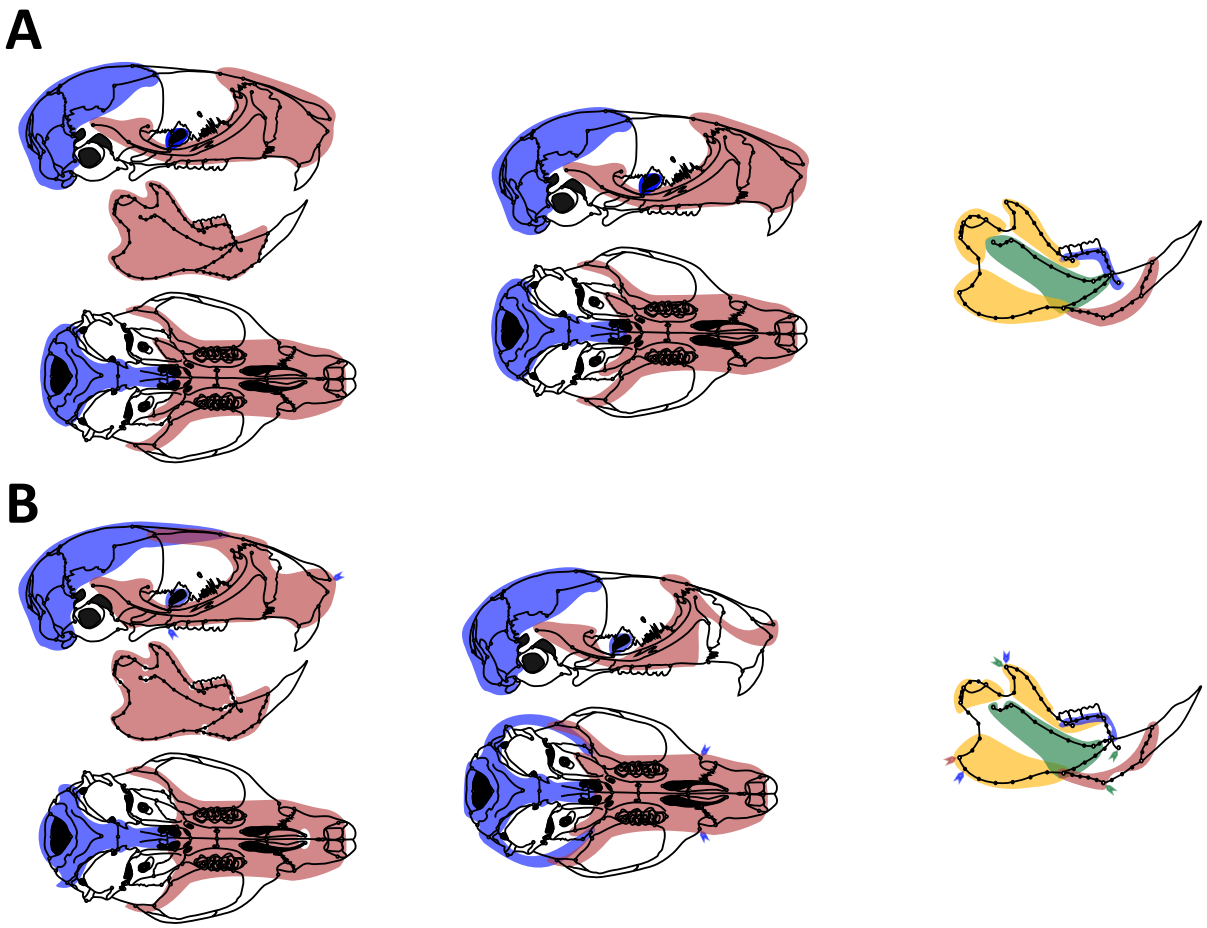

Figure II.4. Most-highly supported models for *Holochilus chacarius*. A, best-supported models among a priori models and combinations of their modules. B, model found after a heuristic search for improved models over those in A. Each color represents a module. Colored arrows in heuristic models indicate that the indicated landmark belongs to the module of the same color. Craniomandibular, cranial, and mandibular data sets were tested independently (i.e., meaning of colors is not shared across data sets).

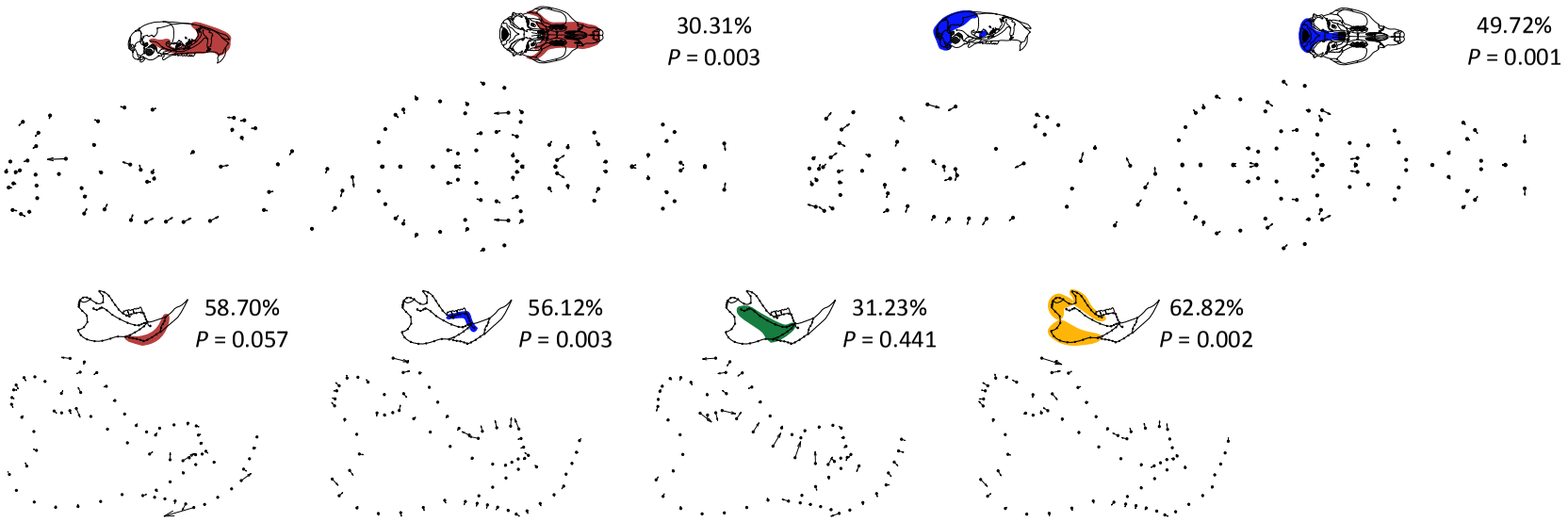

Figure II.5. Part-whole PLS analysis based on best-supported modules for *Holochilus chacarius* for cranial and mandibular data sets. Each set of diagrams includes a colored representation of the module being regressed onto the whole structure, a deformation plot, and two statistics. PLS analyses are based on entire modules; deformation graphs correspond to projections of individual views onto first PLS axis. Statistics show the percentage of squared covariance between part and whole explained by the depicted vector, and the *P*-value of this percentage for the null hypothesis that this value could be produced by chance. Non-significant values may indicate lack of association between part and whole or that the part-whole association cannot be appropriately represented by one dimension.

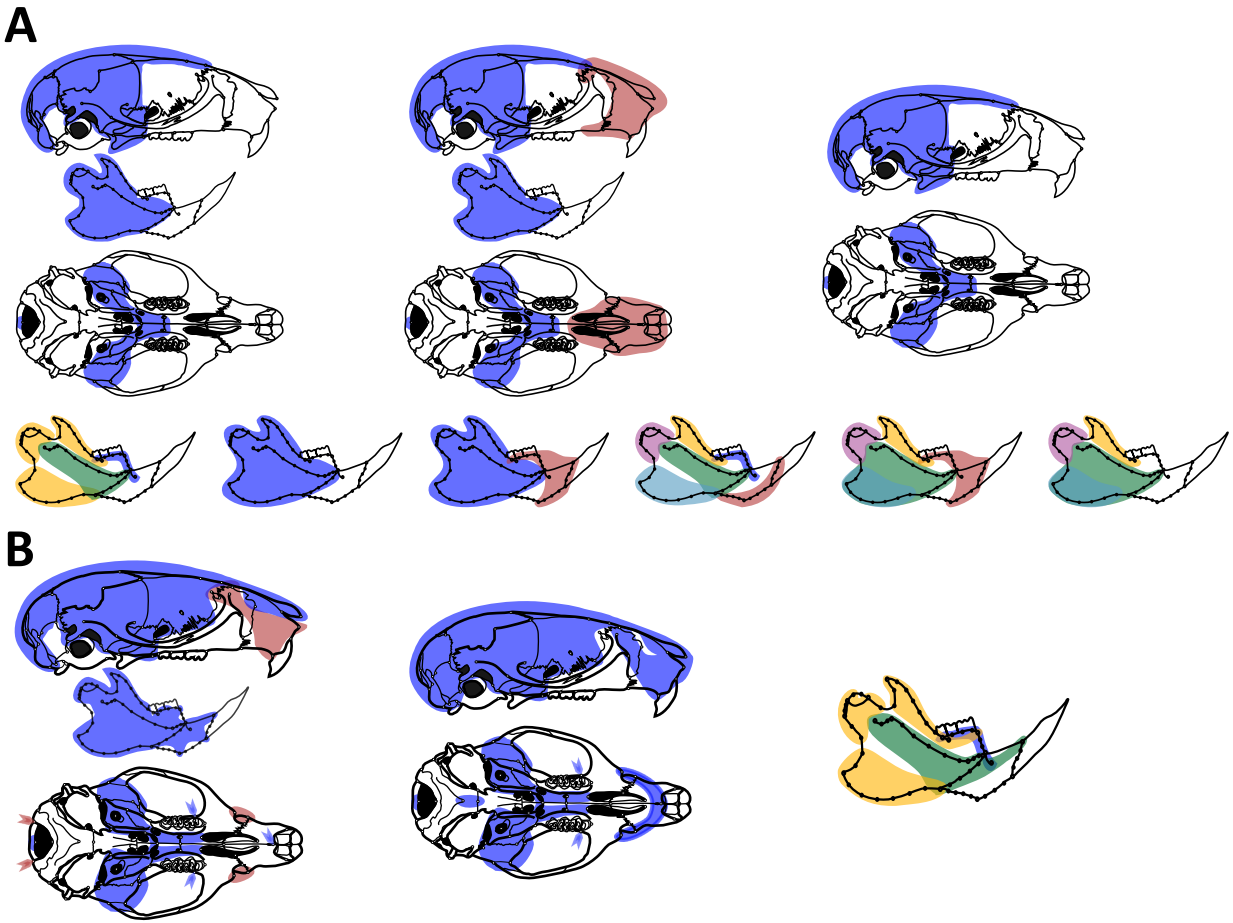

Figure II.6. Most-highly supported models for *Melanomys caliginosus*. A, best-supported models among a priori models and combinations of their modules. B, model found after a heuristic search for improved models over those in A. Each color represents a module. Colored arrows in heuristic models indicate that the indicated landmark belongs to the module of the same color. Craniomandibular, cranial, and mandibular data sets were tested independently (i.e., meaning of colors is not shared across data sets).

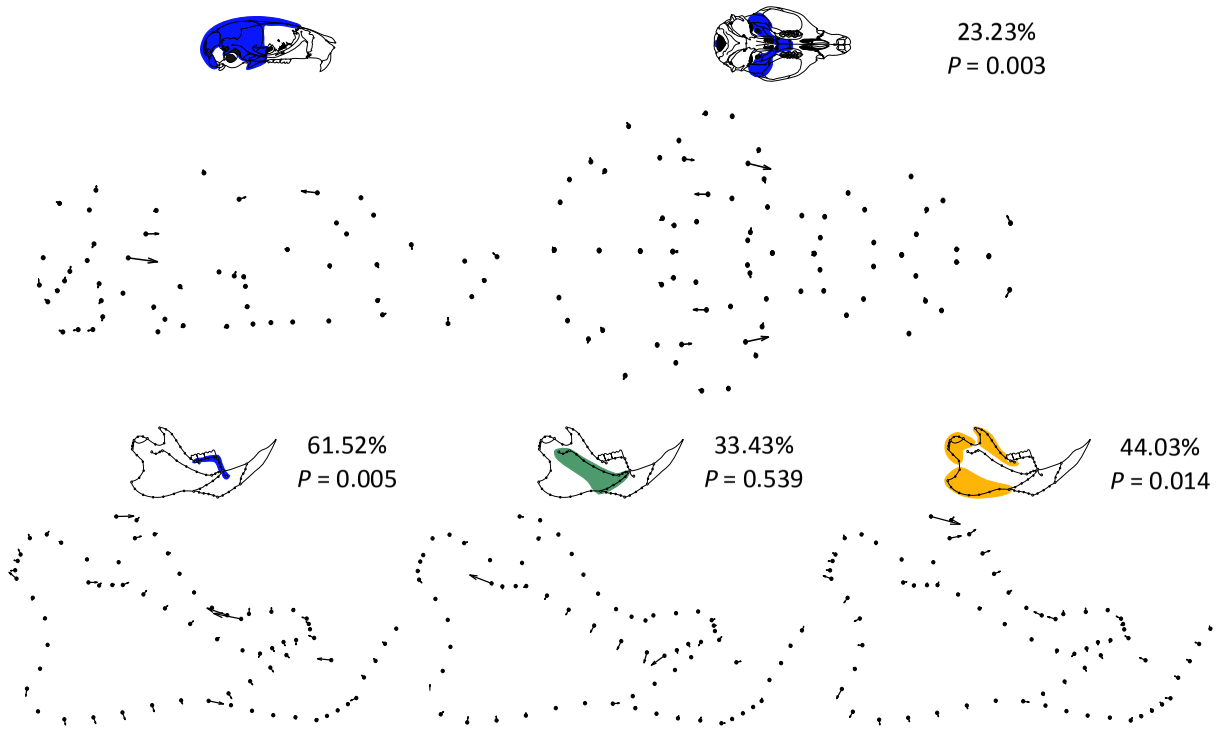

Figure II.7. Part-whole PLS analysis based on best-supported modules for *Melanomys caliginosus* for cranial and mandibular data sets. Each set of diagrams includes a colored representation of the module being regressed onto the whole structure, a deformation plot, and two statistics. PLS analyses are based on entire modules; deformation graphs correspond to projections of individual views onto first PLS axis. Statistics show the percentage of squared covariance between part and whole explained by the depicted vector, and the *P*-value of this percentage for the null hypothesis that this value could be produced by chance. Non-significant values may indicate lack of association between part and whole or that the part-whole association cannot be appropriately represented by one dimension.

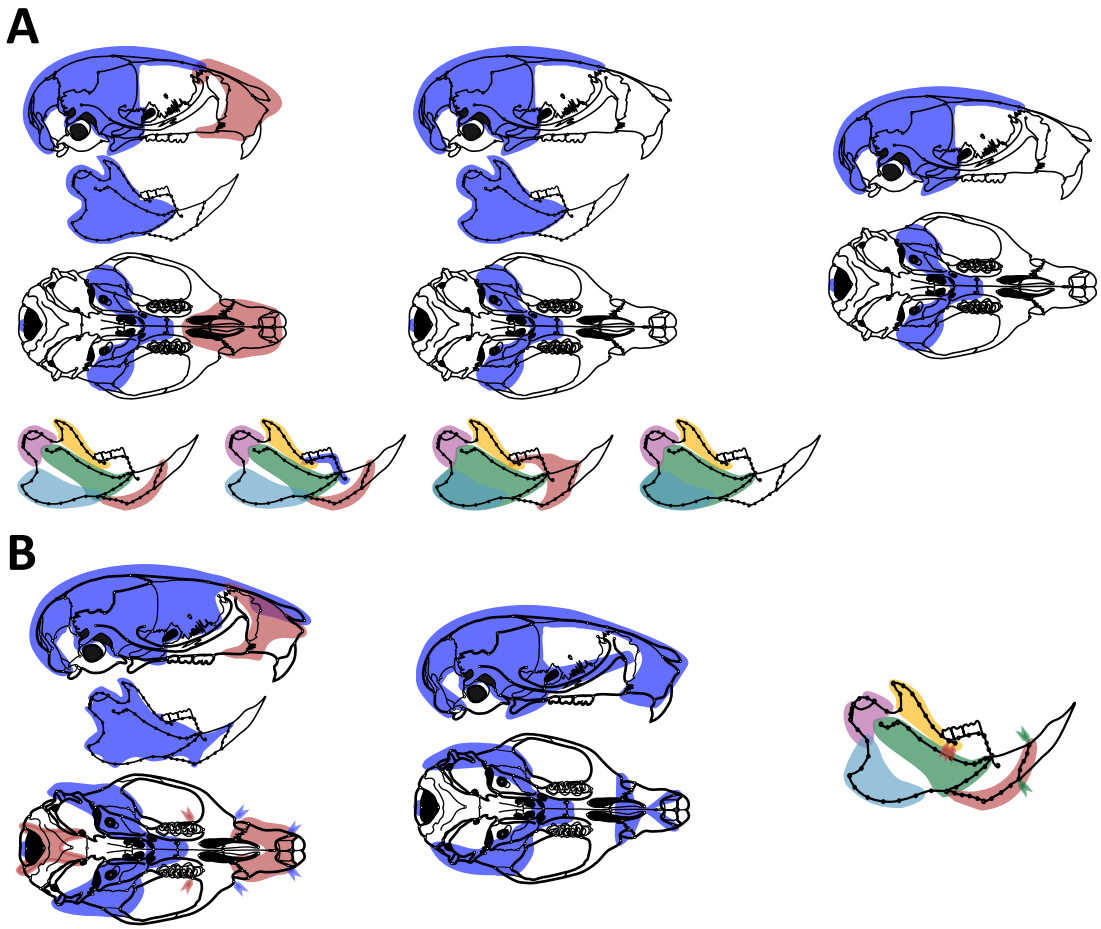

Figure II.8. Most-highly supported models for *Microryzomys minutus*. A, best-supported models among a priori models and combinations of their modules. B, model found after a heuristic search for improved models over those in A. Each color represents a module. Colored arrows in heuristic models indicate that the indicated landmark belongs to the module of the same color. Craniomandibular, cranial, and mandibular data sets were tested independently (i.e., meaning of colors is not shared across data sets).

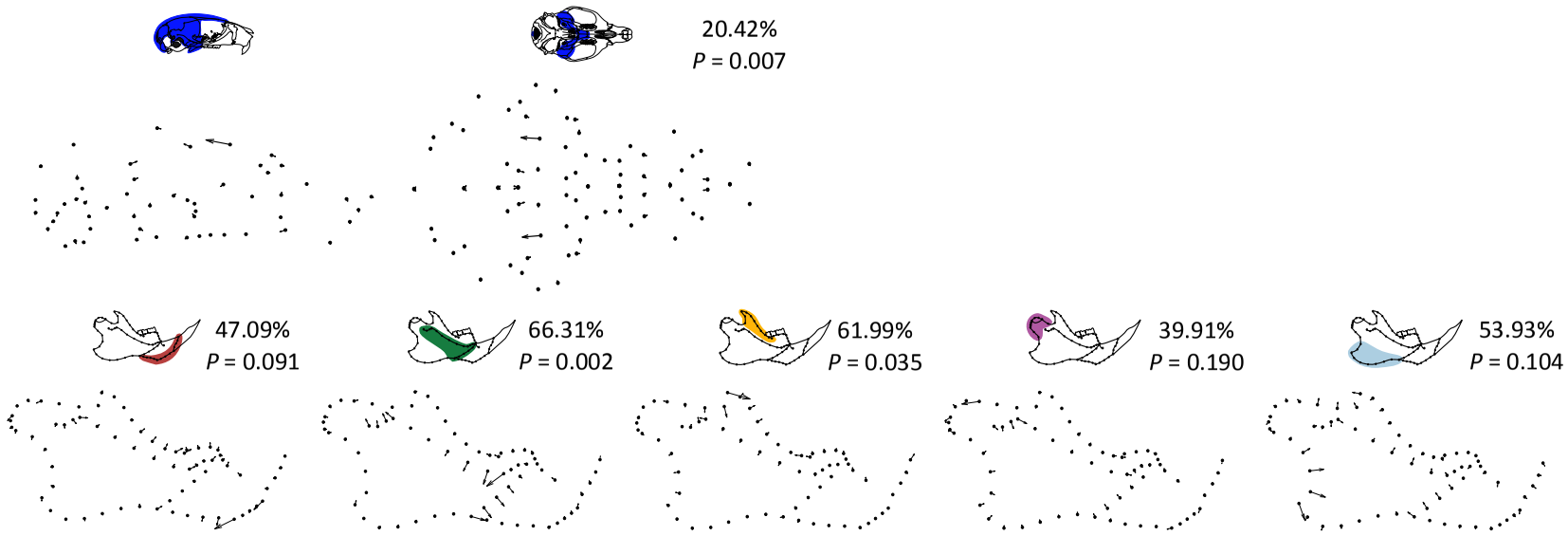

Figure II.9. Part-whole PLS analysis based on best-supported modules for *Microryzomys minutus* for cranial and mandibular data sets. Each set of diagrams includes a colored representation of the module being regressed onto the whole structure, a deformation plot, and two statistics. PLS analyses are based on entire modules; deformation graphs correspond to projections of individual views onto first PLS axis. Statistics show the percentage of squared covariance between part and whole explained by the depicted vector, and the *P*-value of this percentage for the null hypothesis that this value could be produced by chance. Non-significant values may indicate lack of association between part and whole or that the part-whole association cannot be appropriately represented by one dimension.

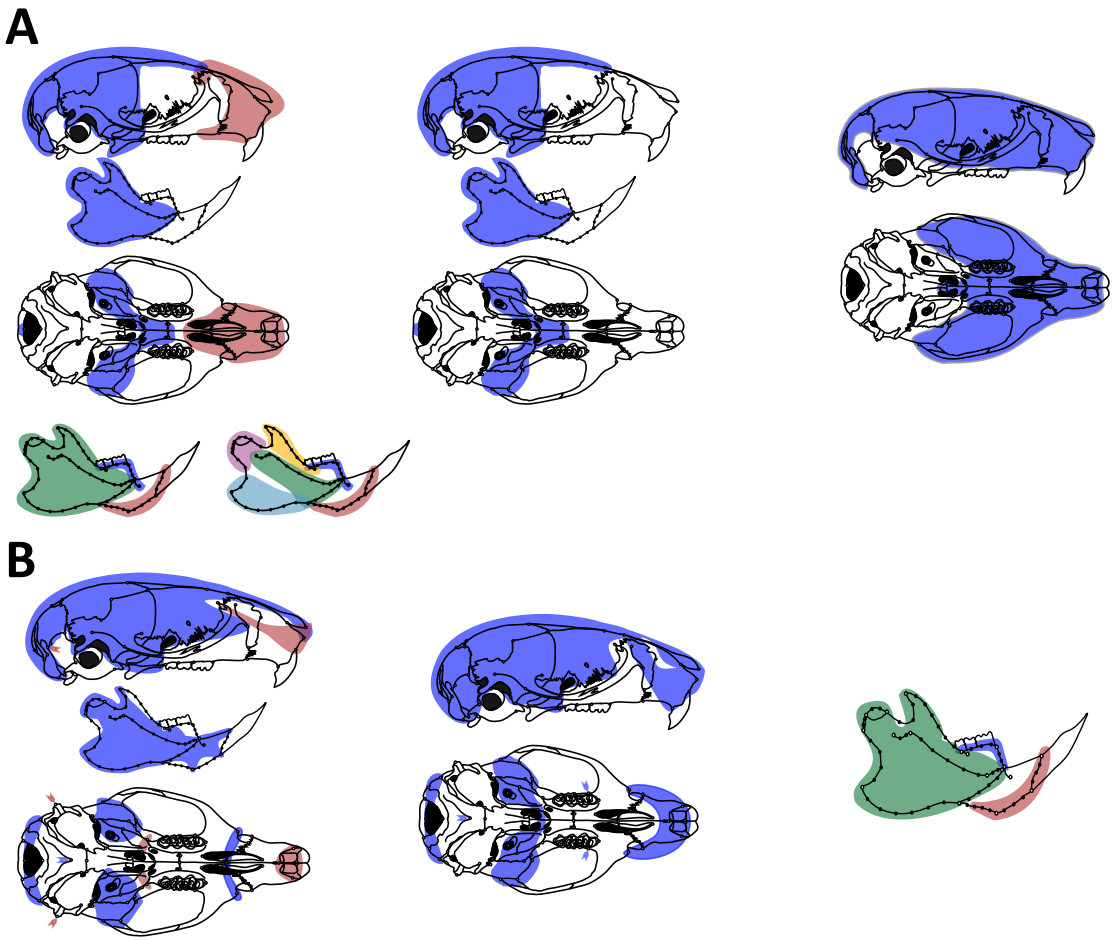

Figure II.10. Most-highly supported models for *Nectomys squamipes*. A, best-supported models among a priori models and combinations of their modules. B, model found after a heuristic search for improved models over those in A. Each color represents a module. Colored arrows in heuristic models indicate that the indicated landmark belongs to the module of the same color. Craniomandibular, cranial, and mandibular data sets were tested independently (i.e., meaning of colors is not shared across data sets).

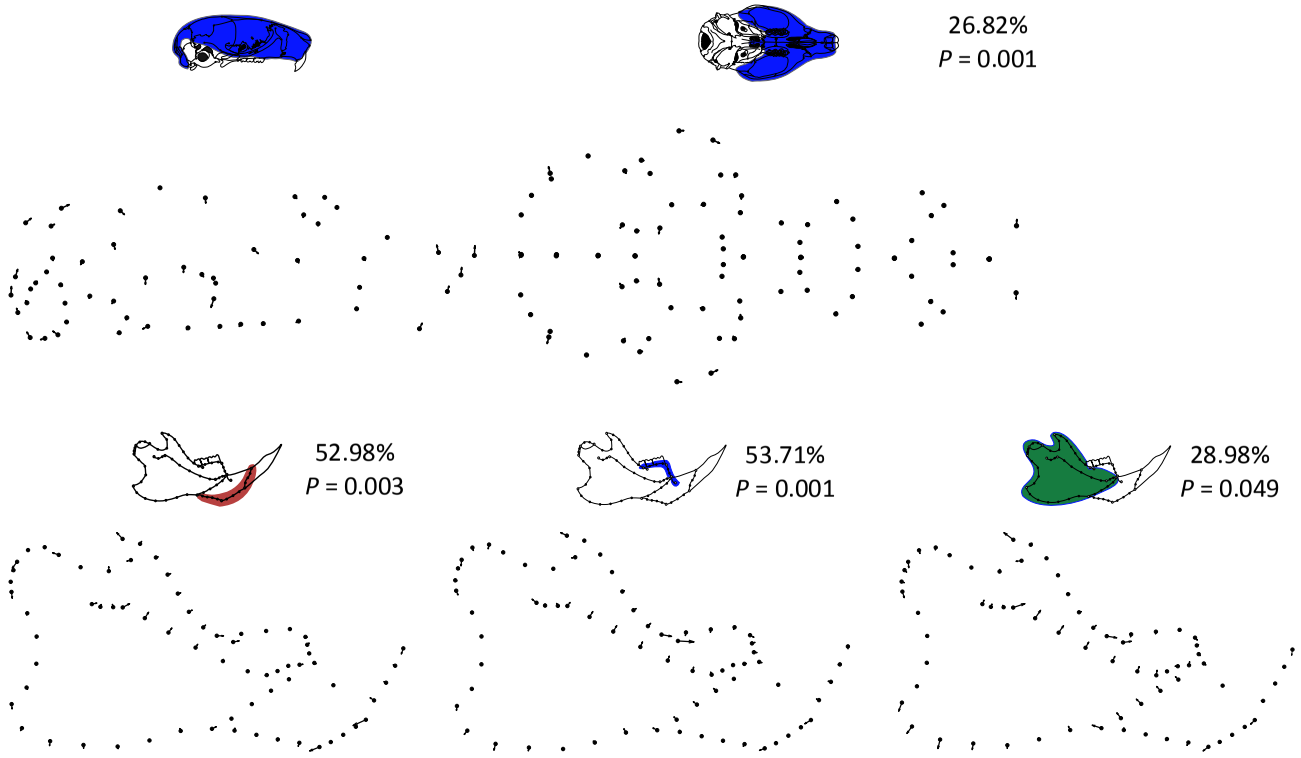

Figure II.11. Part-whole PLS analysis based on best-supported modules for *Nectomys squamipes* for cranial and mandibular data sets. Each set of diagrams includes a colored representation of the module being regressed onto the whole structure, a deformation plot, and two statistics. PLS analyses are based on entire modules; deformation graphs correspond to projections of individual views onto first PLS axis. Statistics show the percentage of squared covariance between part and whole explained by the depicted vector, and the *P*-value of this percentage for the null hypothesis that this value could be produced by chance. Non-significant values may indicate lack of association between part and whole or that the part-whole association cannot be appropriately represented by one dimension.

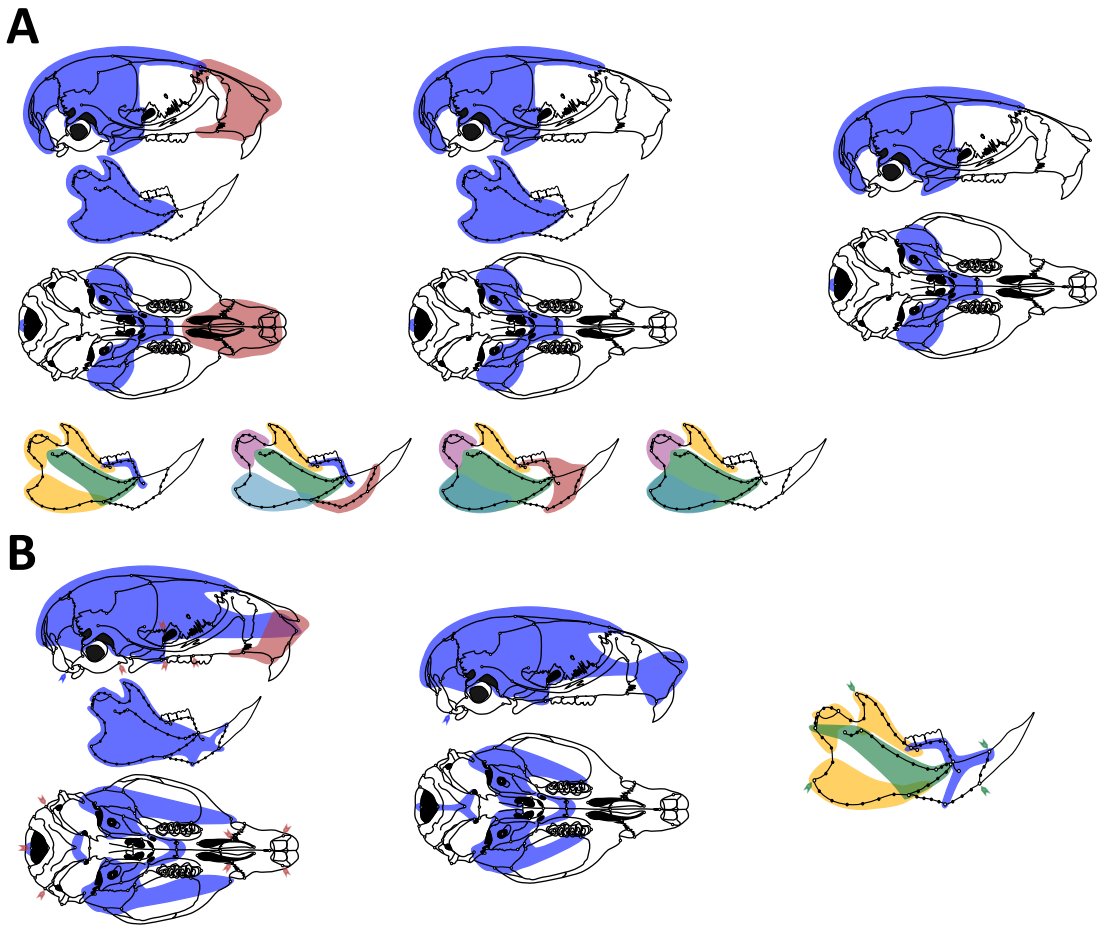

Figure II.12. Most-highly supported models for *Oligoryzomys nigripes*. A, best-supported models among a priori models and combinations of their modules. B, model found after a heuristic search for improved models over those in A. Each color represents a module. Colored arrows in heuristic models indicate that the indicated landmark belongs to the module of the same color. Craniomandibular, cranial, and mandibular data sets were tested independently (i.e., meaning of colors is not shared across data sets).

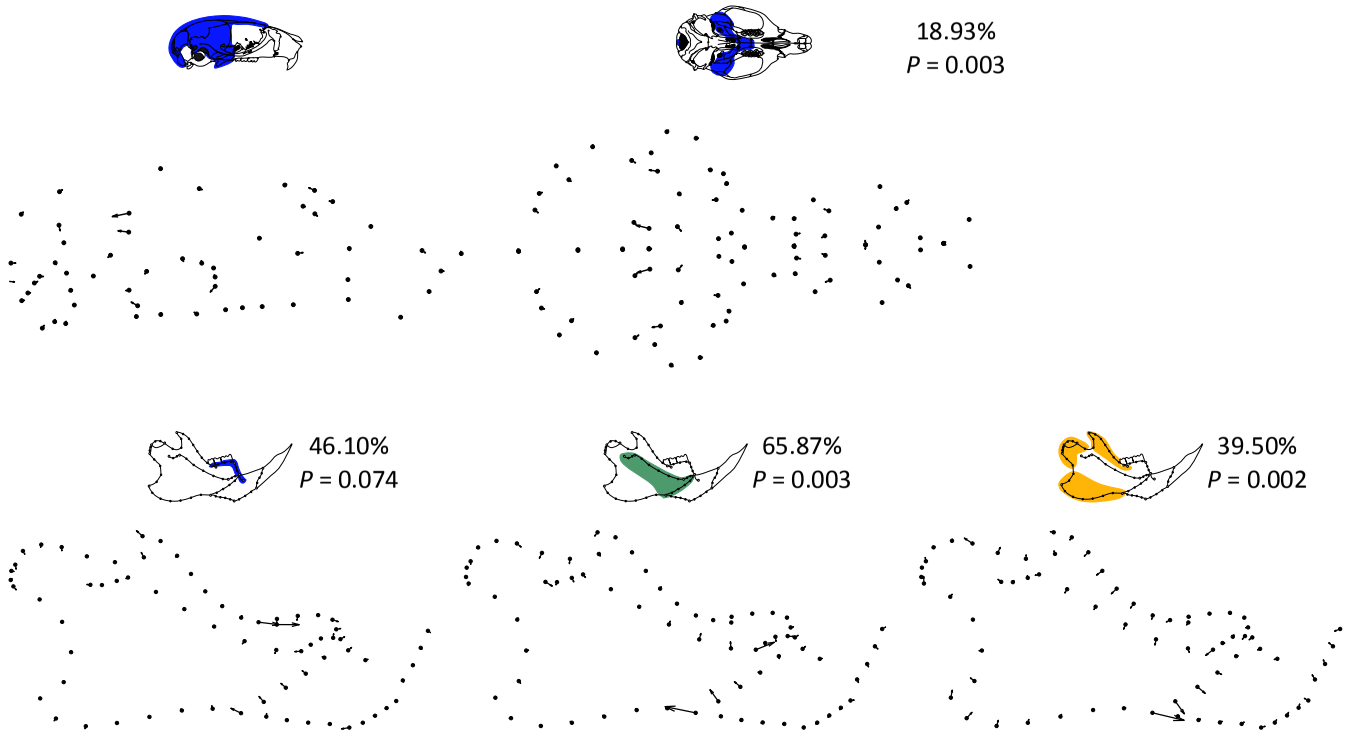

Figure II.13. Part-whole PLS analysis based on best-supported modules for *Oligoryzomys nigripes* for cranial and mandibular data sets. Each set of diagrams includes a colored representation of the module being regressed onto the whole structure, a deformation plot, and two statistics. PLS analyses are based on entire modules; deformation graphs correspond to projections of individual views onto first PLS axis. Statistics show the percentage of squared covariance between part and whole explained by the depicted vector, and the *P*-value of this percentage for the null hypothesis that this value could be produced by chance. Non-significant values may indicate lack of association between part and whole or that the part-whole association cannot be appropriately represented by one dimension.

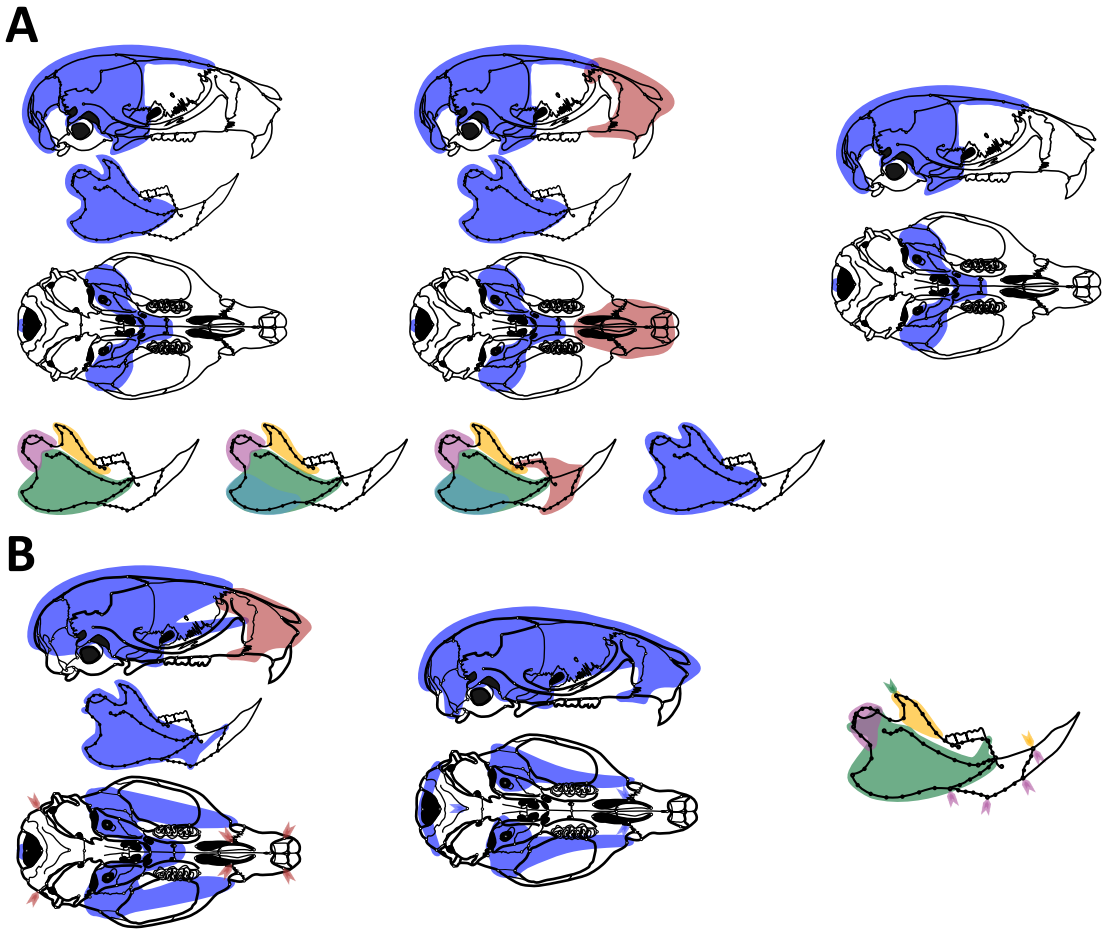

Figure II.14. Most-highly supported models for *Oryzomys couesi*. A, best-supported models among a priori models and combinations of their modules. B, model found after a heuristic search for improved models over those in A. Each color represents a module. Colored arrows in heuristic models indicate that the indicated landmark belongs to the module of the same color. Craniomandibular, cranial, and mandibular data sets were tested independently (i.e., meaning of colors is not shared across data sets).

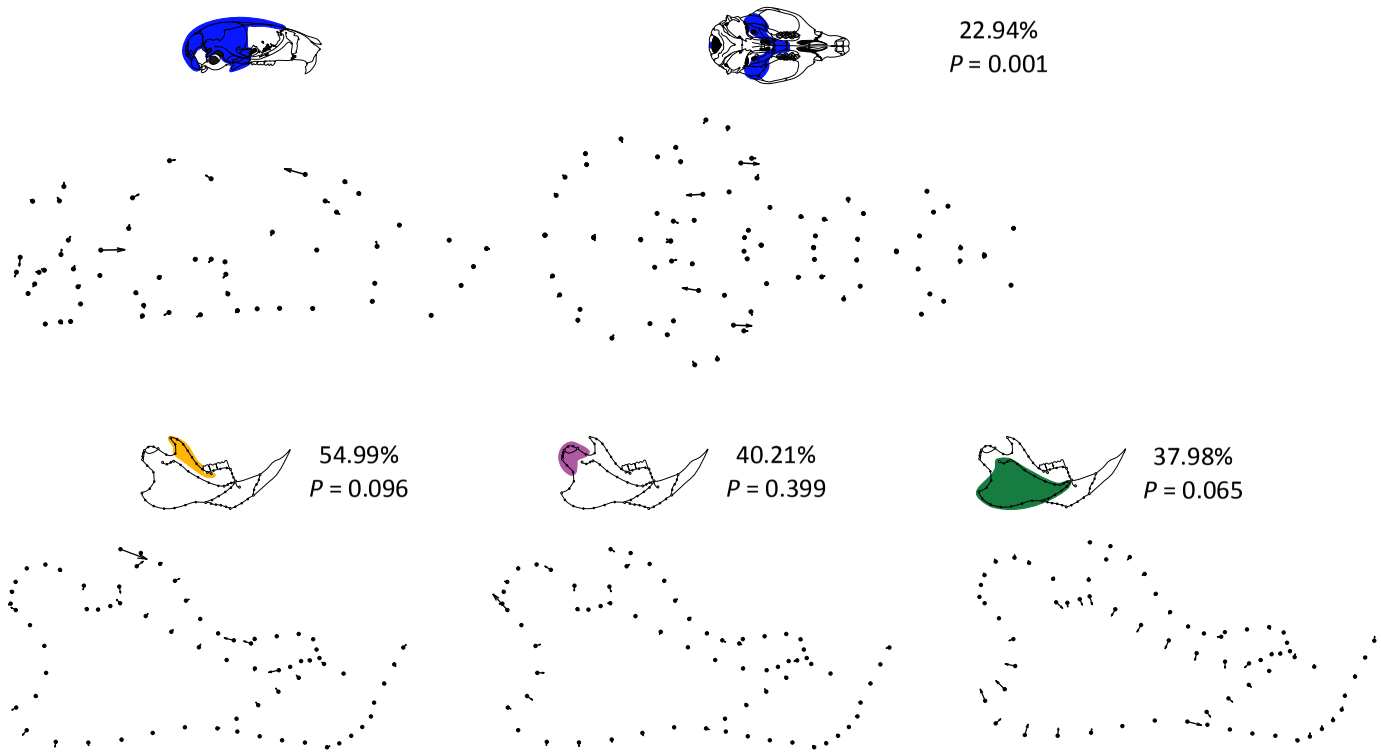

Figure II.15. Part-whole PLS analysis based on best-supported modules for *Oryzomys couesi* for cranial and mandibular data sets. Each set of diagrams includes a colored representation of the module being regressed onto the whole structure, a deformation plot, and two statistics. PLS analyses are based on entire modules; deformation graphs correspond to projections of individual views onto first PLS axis. Statistics show the percentage of squared covariance between part and whole explained by the depicted vector, and the *P*-value of this percentage for the null hypothesis that this value could be produced by chance. Non-significant values may indicate lack of association between part and whole or that the part-whole association cannot be appropriately represented by one dimension.

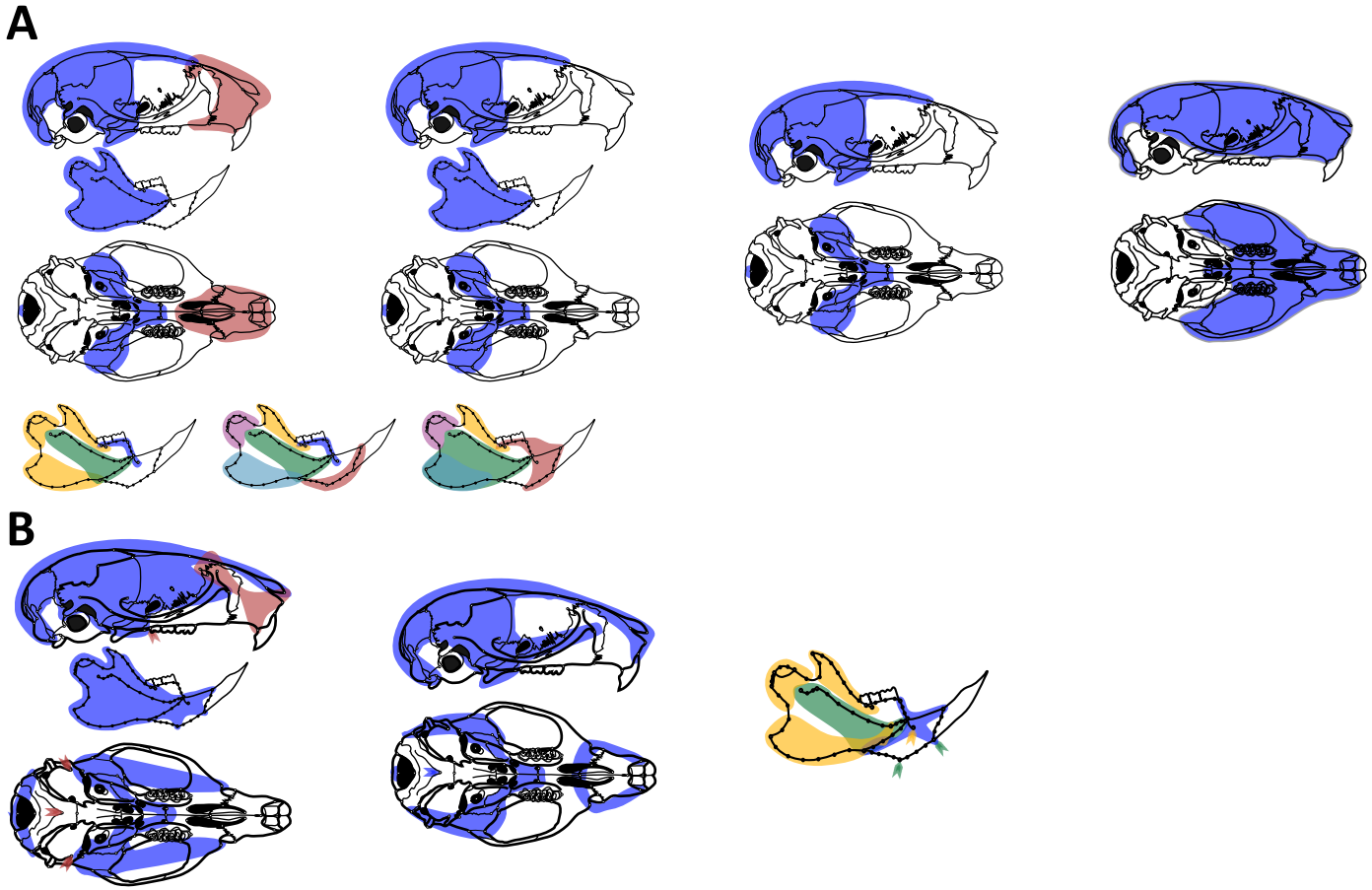

Figure II.16. Most-highly supported models for *Oryzomys palustris*. A, best-supported models among a priori models and combinations of their modules. B, model found after a heuristic search for improved models over those in A. Each color represents a module. Colored arrows in heuristic models indicate that the indicated landmark belongs to the module of the same color. Craniomandibular, cranial, and mandibular data sets were tested independently (i.e., meaning of colors is not shared across data sets).

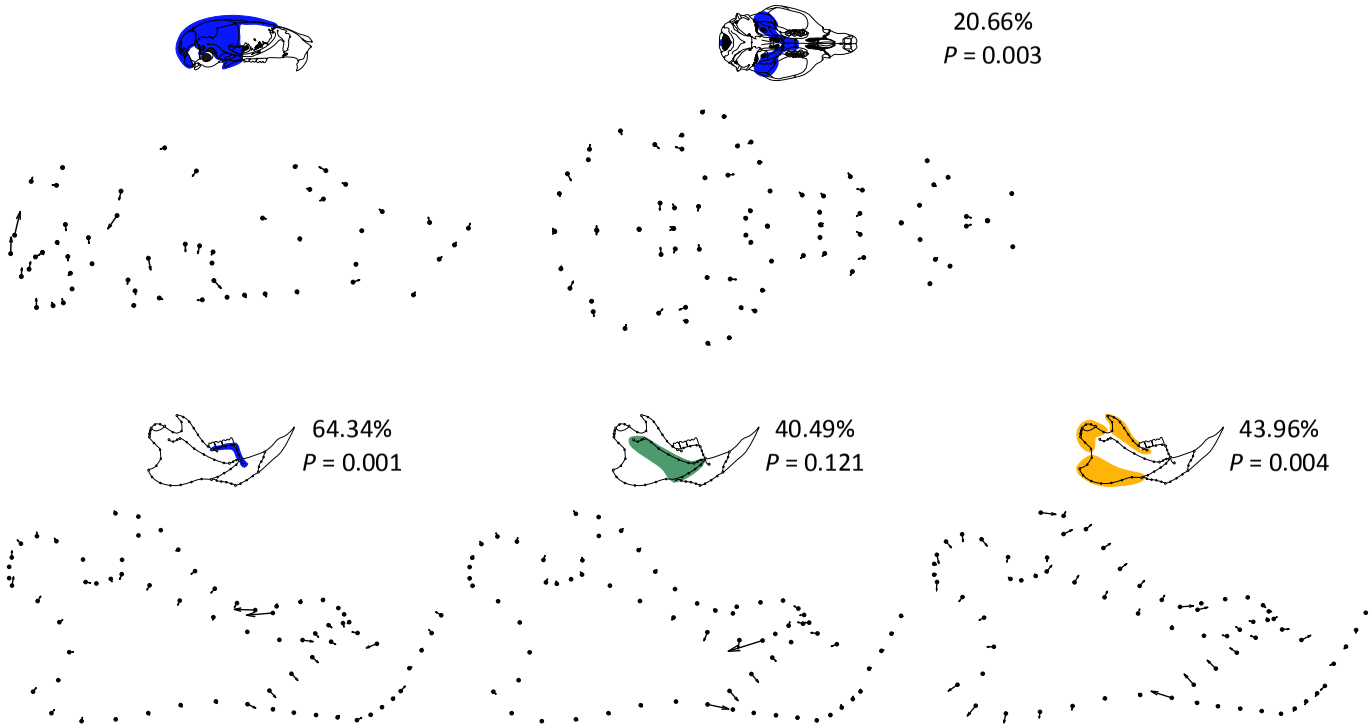

Figure II.17. Part-whole PLS analysis based on best-supported modules for *Oryzomys palustris* for cranial and mandibular data sets. Each set of diagrams includes a colored representation of the module being regressed onto the whole structure, a deformation plot, and two statistics. PLS analyses are based on entire modules; deformation graphs correspond to projections of individual views onto first PLS axis. Statistics show the percentage of squared covariance between part and whole explained by the depicted vector, and the *P*-value of this percentage for the null hypothesis that this value could be produced by chance. Non-significant values may indicate lack of association between part and whole or that the part-whole association cannot be appropriately represented by one dimension.

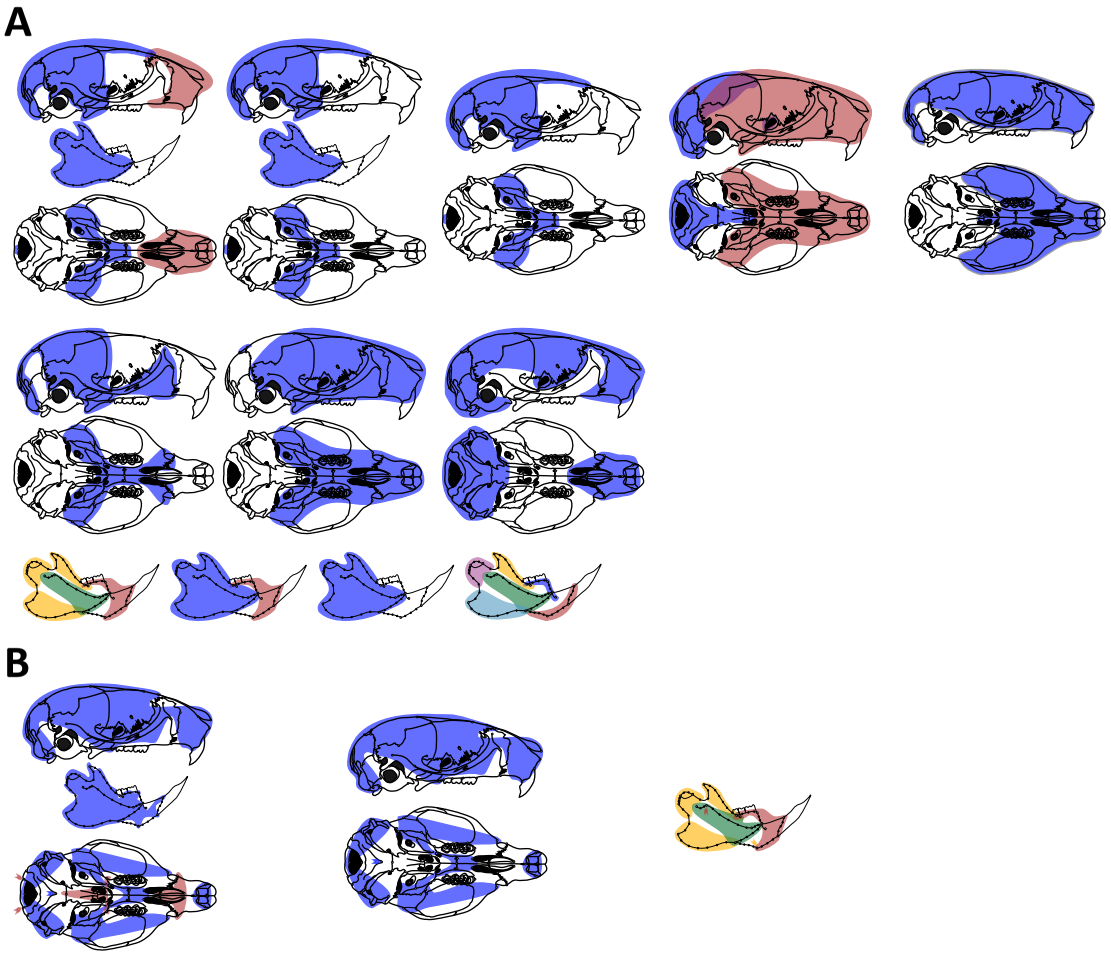

Figure II.18. Most-highly supported models for *Oryzomys xantheolus*. A, best-supported models among a priori models and combinations of their modules. B, model found after a heuristic search for improved models over those in A. Each color represents a module. Colored arrows in heuristic models indicate that the indicated landmark belongs to the module of the same color. Craniomandibular, cranial, and mandibular data sets were tested independently (i.e., meaning of colors is not shared across data sets).

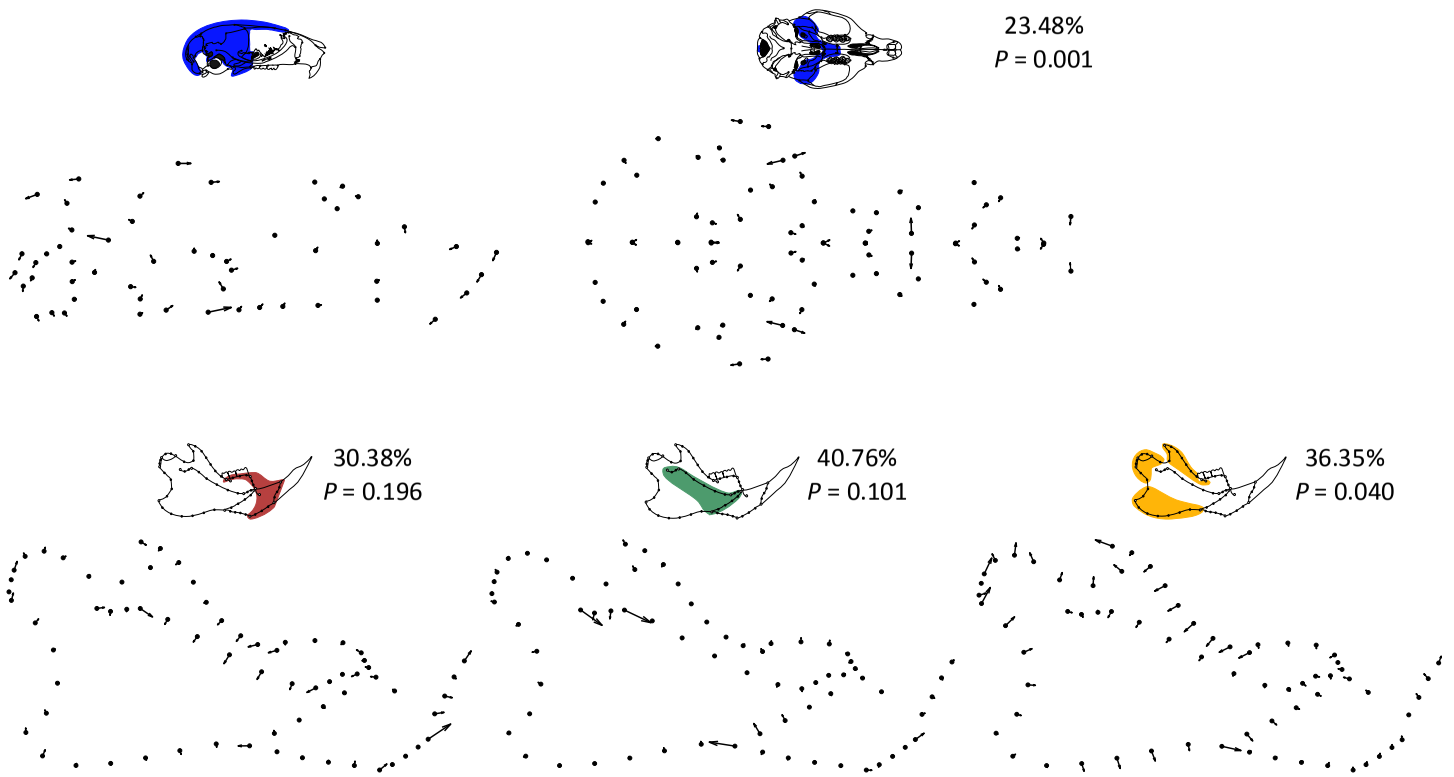

Figure II.19. Part-whole PLS analysis based on best-supported modules for *Oryzomys xantheolus* for cranial and mandibular data sets. Each set of diagrams includes a colored representation of the module being regressed onto the whole structure, a deformation plot, and two statistics. PLS analyses are based on entire modules; deformation graphs correspond to projections of individual views onto first PLS axis. Statistics show the percentage of squared covariance between part and whole explained by the depicted vector, and the *P*-value of this percentage for the null hypothesis that this value could be produced by chance. Non-significant values may indicate lack of association between part and whole or that the part-whole association cannot be appropriately represented by one dimension.

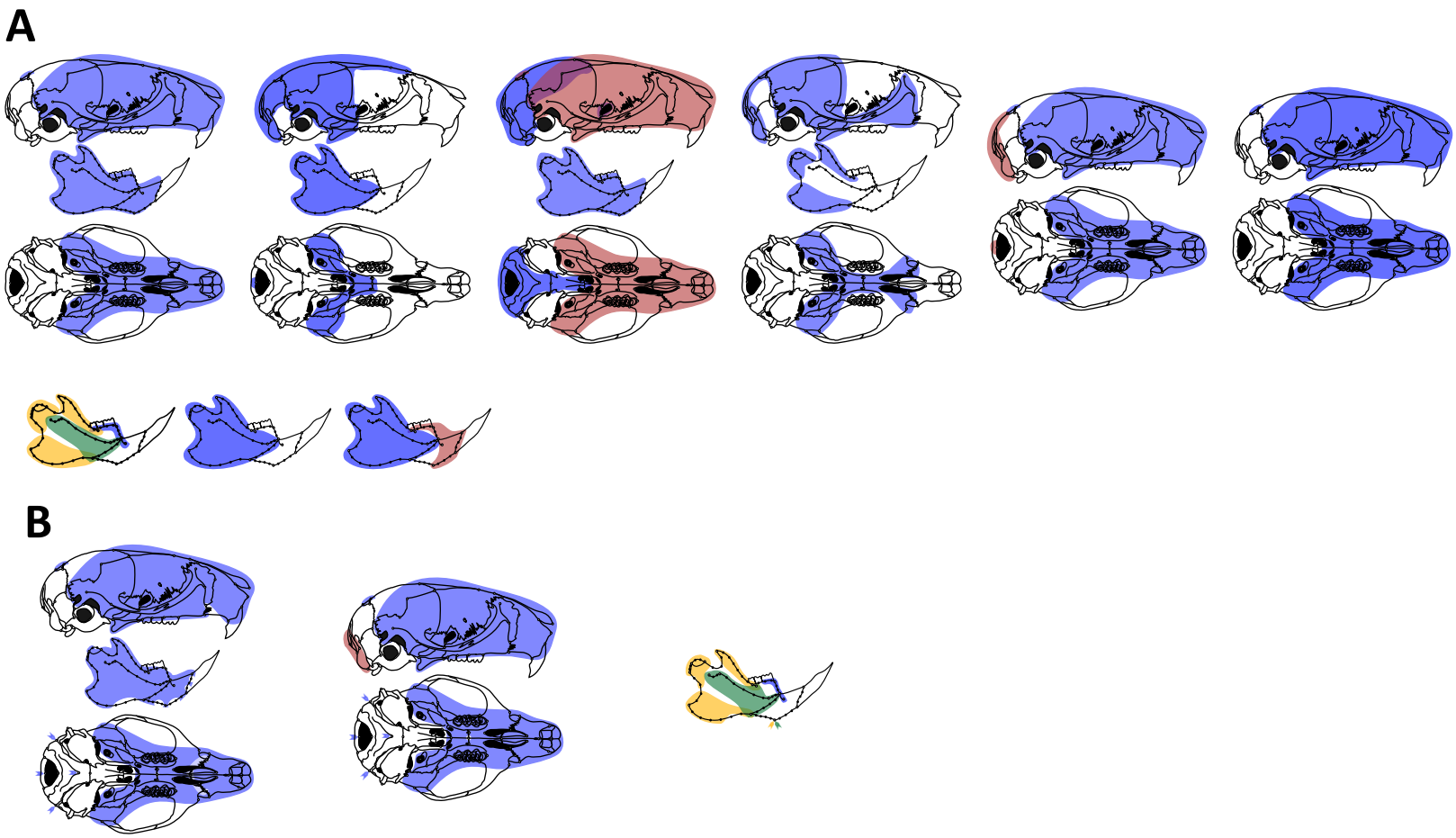

Figure II.20. Most-highly supported models for *Sigmodontomys alfari*. A, best-supported models among a priori models and combinations of their modules. B, model found after a heuristic search for improved models over those in A. Each color represents a module. Colored arrows in heuristic models indicate that the indicated landmark belongs to the module of the same color. Craniomandibular, cranial, and mandibular data sets were tested independently (i.e., meaning of colors is not shared across data sets).

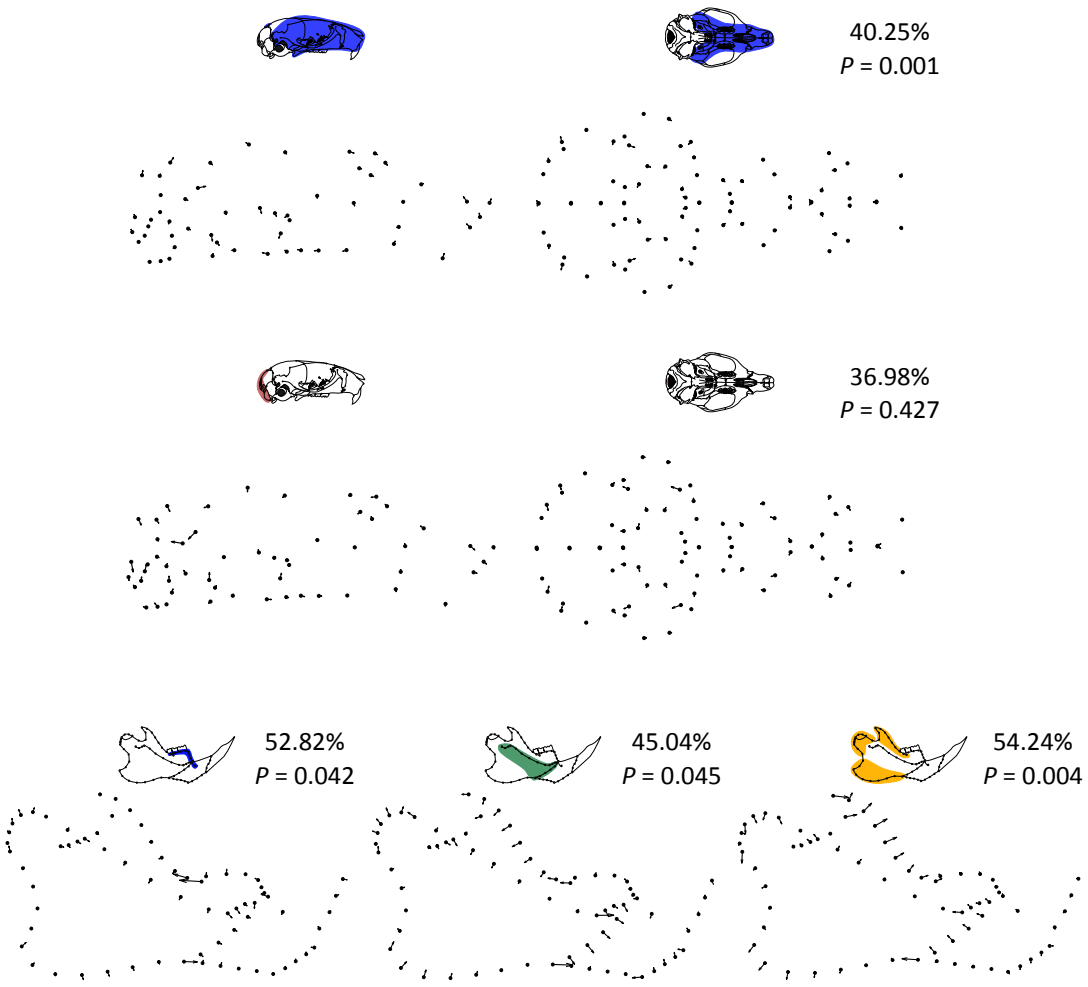

Figure II.21. Part-whole PLS analysis based on best-supported modules for *Sigmodontomys alfari* for cranial and mandibular data sets. Each set of diagrams includes a colored representation of the module being regressed onto the whole structure, a deformation plot, and two statistics. PLS analyses are based on entire modules; deformation graphs correspond to projections of individual views onto first PLS axis. Statistics show the percentage of squared covariance between part and whole explained by the depicted vector, and the *P*-value of this percentage for the null hypothesis that this value could be produced by chance. Non-significant values may indicate lack of association between part and whole or that the part-whole association cannot be appropriately represented by one dimension.

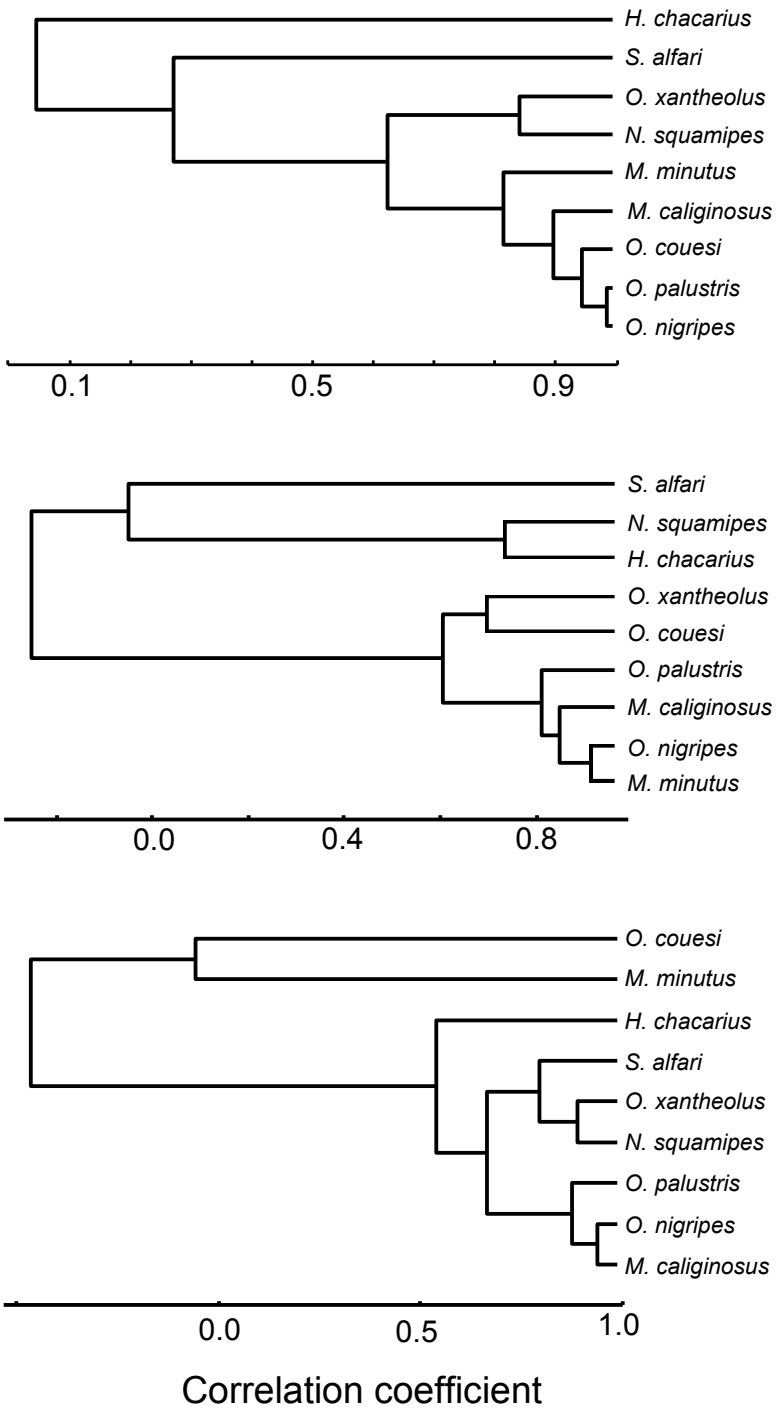

Figure II.22. Dendrograms showing similarity of oryzomyine species in model space. Top: craniomandibular data; middle: cranium data; bottom: mandible data. Distances were calculated as 1 - correlation coefficient. Data correspond to vectors of the 100 best models (according to γ^* values) for each species.

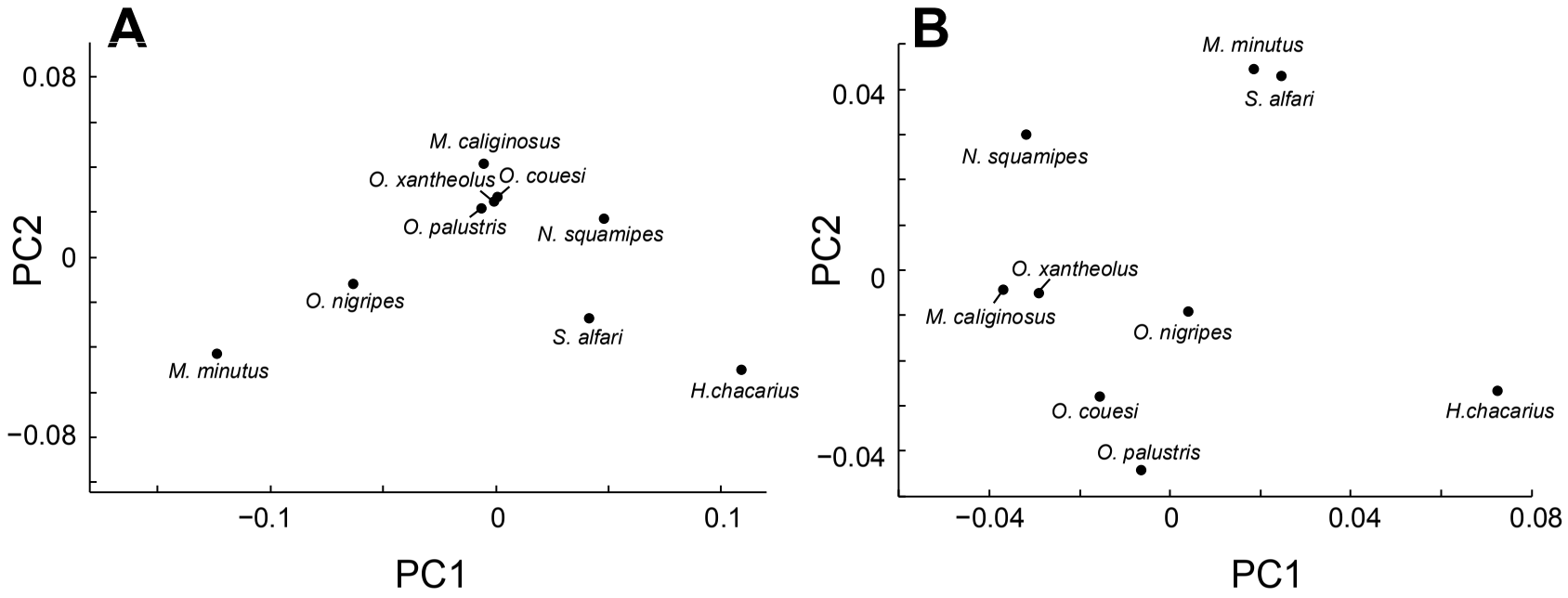

Figure II.23. Principal component analyses of mean shapes of craniomandibular data from nine species of oryzomyines. A, PCs computed from shape data that has been standardized within species only (PC1 = 77%, PC2 = 0.3% of total disparity); B, PCs computed from shape data that has been standardized to remove both intra- and interspecific allometry (PC1 = 19%, PC2 = 10% of total disparity).

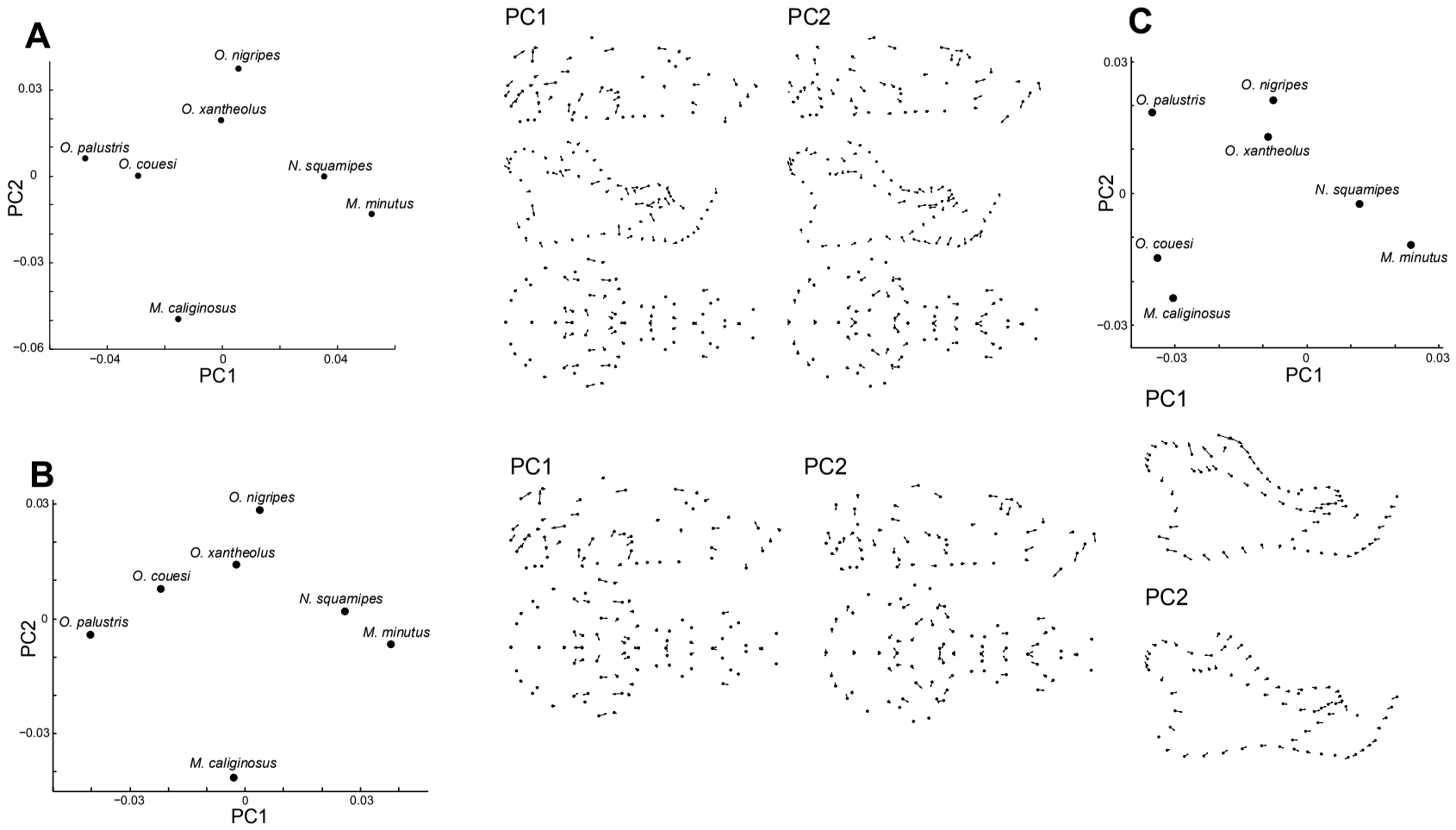

Figure II.24. Principal component analyses of mean shapes of skull shape data from seven species of oryzomyines. Species are the most homogenous, least divergent of those included in this study. A, scores and implied shape deformations for PC1 and PC2 of craniomandibular data (PC1 = 41.0%, PC2 = 5.6% of total disparity); B, cranial data (PC1 = 37.7%, PC2 = 7.4% of total disparity); C, mandibular data (PC1 = 44.5%, PC2 = 5.2% of total disparity). All deformations have been multiplied x2 to enhance visibility.

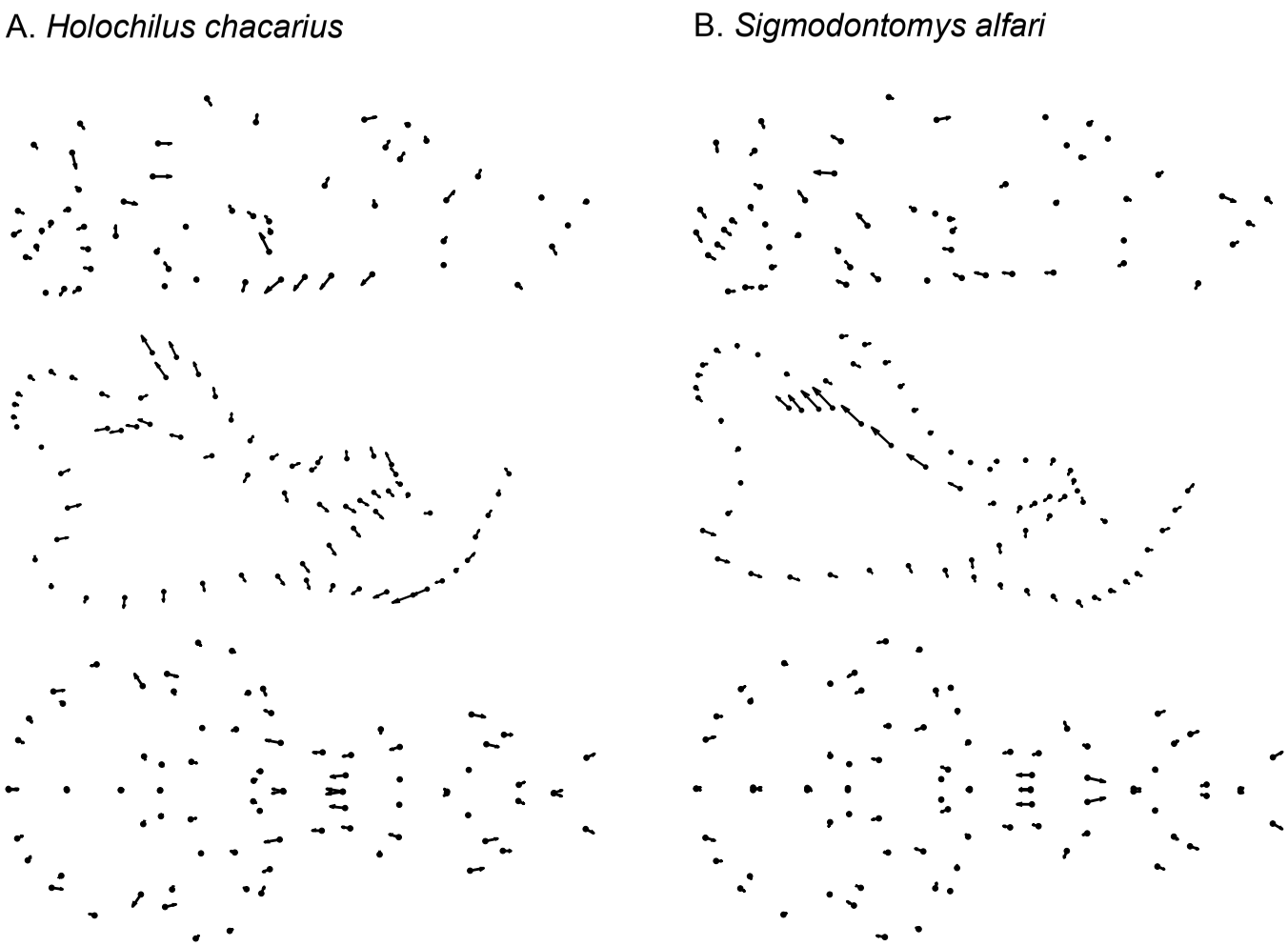

Figure II.25. Difference between (A) *H. chacarius* and (B) *S. alfari* and the mean of other seven oryzomyine species, computed after superimposing each pair of means using ordinary Procrustes superimposition.

APPENDICES

Appendix A

Photographs of typical specimens of the nine oryzomyine species included in this study.

1. *Holochilus chacarius*

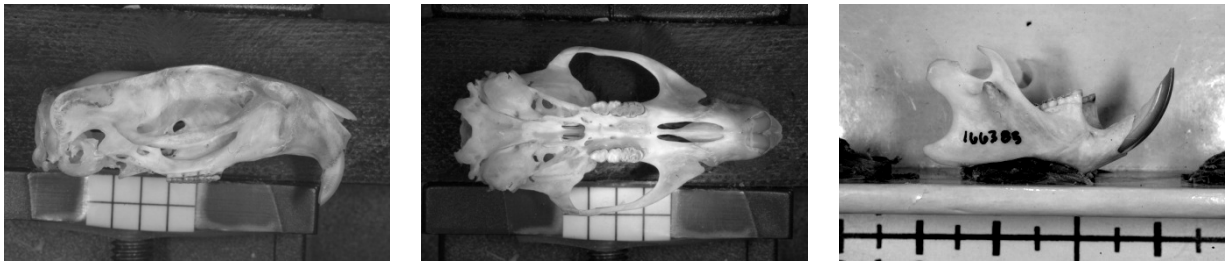

2. *Melanomys caliginosus*

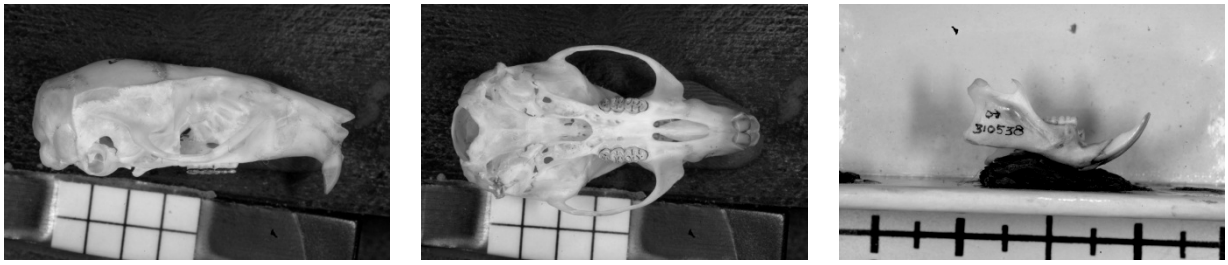

3. *Microryzomys minutus*

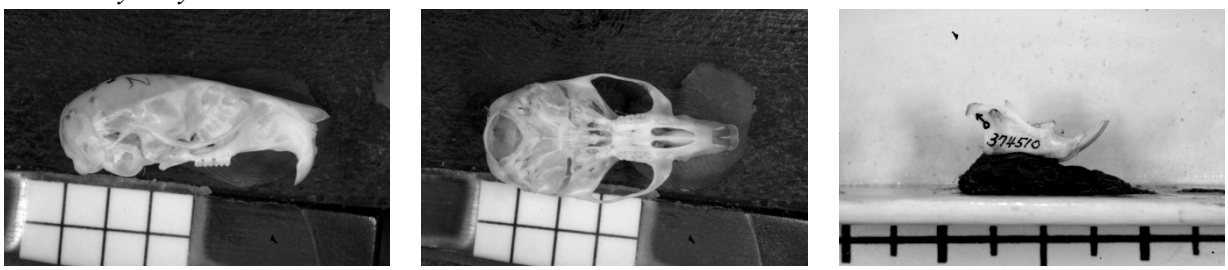

4. *Nectomys squamipes*

5. *Oligoryzomys nigripes*



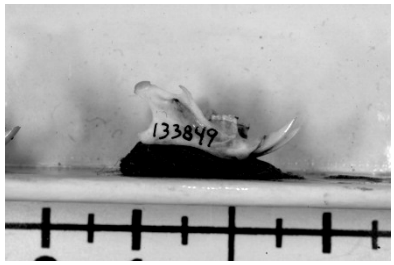

6. *Oryzomys couesi*


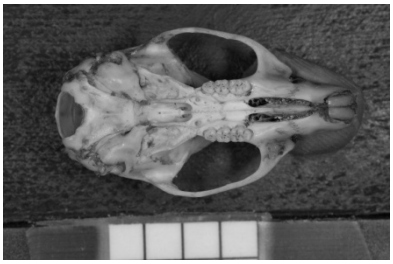


7. *Oryzomys palustris*

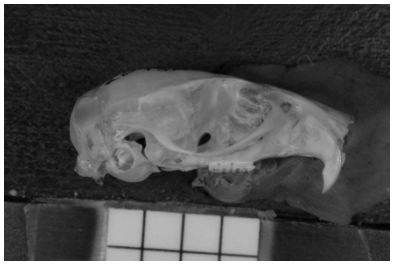
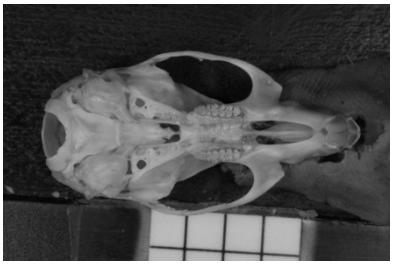


8. *Oryzomys xantheolus*


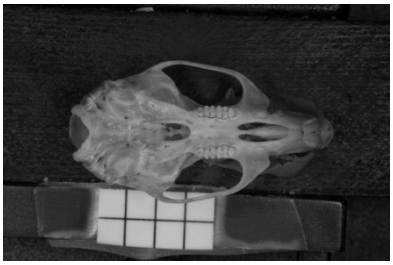
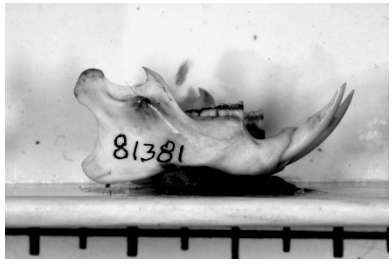

9. *Sigmodontomys alfari*

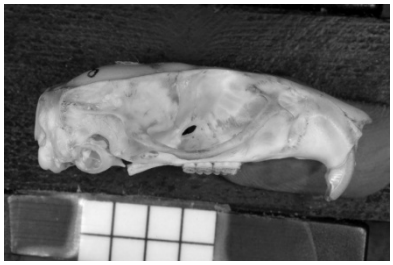

Appendix B

Detailed list of specimens sampled for this study, indicating localities of origin and sampling date.

Holochilus chacarius:

Origin: Presidente Hayes, Paraguay. Collection: University of Michigan (UMMZ):

Captured Jul. 1978-Aug. 1979: 125997, 125999, 126000, 126001, 126002, 126003, 126004, 126074, 126075, 126076, 126077, 126078, 133971, 133972, 133973, 133974, 133975, 133976, 133977, 133978, 133979, 133980, 137137, 137138; **captured Sep.-Oct. 1986**: 165990, 165991, 165992, 165993, 166149, 166150, 166176, 166197, 166198, 166199, 166200, 166202, 166203, 166204, 166208, 166209, 166234, 166235, 166236, 166237, 166238, 166239, 166260, 166325, 166326, 166327, 166328, 166329, 166330, 166331, 166332, 166333, 166334, 166335, 166686; **captured Oct. 1988**:166385, 166387, 166388, 166389, 166690.

Melanomys caliginosus:

Origin: Cerro Azul, Panama. Collection: Smithsonian Institution (USNM):
Captured Jan.-Apr. 1956: 305674, 306926, 302487, 302488, 302490, 302491, 302678, 302679, 302680, 302682, 302683, 303096; **captured Jun. 1957:** 303098, 303099, 303100, 305666, 305667, 305668, 305669, 305670; **captured Jan.-Aug. 1958:** 305671, 305672, 305673, 306927, 306928, 306929, 306930, 306931, 306932, 306933, 306934, 306935, 306936, 306937, 306938, 306940, 306941, 306942, 306943, 306945, 306946, 306947, 306948, 310533, 310534, 310535, 310537, 310538, 310539, 310540, 310541, 310542.

Microryzomys minutus:

Origin: Tabay, Mérida, Venezuela. Collection: Smithsonian Institution (USNM):
Captured Mar.-Apr. 1966: 374364, 374365, 374366, 374369, 374371, 374372, 374375, 374377, 374380, 374381, 374382, 374386, 374387, 374390, 374396, 374398, 374403, 374406, 374410, 374419, 374421, 374422, 374423, 374424, 374425, 374431, 374434, 374435, 374436, 374441, 374443, 374446, 374448, 374453, 374454, 374455, 374456, 374460, 374461, 374462, 374463, 374465, 374467, 374468, 374473, 374474, 374475, 374480, 374481, 374484, 374486, 374489, 374490, 374492, 374493, 374494, 374502, 374503, 374508, 374509, 374510, 374511, 387891, 387893, 387894, 387895, 387897, 387899, 387901.

Nectomys squamipes:

Origin: Varjao, São Paulo, Brazil. Collection: Smithsonian Institution (USNM).

Captured Aug.-Dec. 1969: 460525, 460527, 460528, 460529, 460530, 484187, 484188, 484189, 484190, 484191, 484192, 484193, 484194, 484195, 484196, 484198, 484199; **captured Feb.-Dec. 1970:** 484200, 484202, 484203, 484204, 484205, 484206, 484207, 484208, 484209, 484210; **captured Jan.-Dec. 1971:** 484211, 484213, 484214, 484215, 484216, 485058, 485059, 485060, 485064, 485065, 485066, 485067; **captured Mar.-Dec. 1972**: 462065, 462066, 485069, 485071, 485068, 485070, 485073; **captured Dec. 1973**: 462067, 462071; **captured May-Dec. 1974**: 462072, 462073, 542970, 542971, 542972, 542973, 542974, 542975, 542976, 542977, 542978, 542979, 542980, 542982, 542983, 542984, 542985, 542986, 542987, 542988; **captured Jan.-Sep. 1975:** 542989, 542990, 542991, 542993, 542994, 542995, 542996, 542997, 542998.

Oligoryzomys nigripes:

Origin: Ybycui N.P., Paraguari, Paraguay. Collection: University of Michigan (UMMZ):
Captured Jun. 1979: 133839, 133840, 133841, 133842, 133843, 133844, 133845, 133846, 133847, 133849, 133850, 133851, 133852, 133853, 133854, 133855, 133856, 133857, 133858, 133859, 133860, 133861, 133862, 133863, 133864, 133865, 133866, 133867, 133868, 133869, 133870, 133871, 133873, 133874, 133875, 133876, 133879, 133880, 133881, 133882, 133883, 133884, 133885, 134356, 134357, 137041, 137042, 137043, 137044, 137046, 137047, 137048, 137049, 137050, 137052, 137053, 137054, 137055, 137056, 137059, 137565.

Oryzomys couesi:

Origin: Uaxactun, Peten, Guatemala. Collection: University of Michigan (UMMZ):
Captured Mar.-May 1931: 63187, 63188, 63189, 63190, 63191, 63192, 63193, 63194, 63195, 63196, 63197, 63198, 63199, 63201, 63202, 63203, 63204, 63206, 63207, 63208, 63209, 63210, 63211, 63212, 63213, 63214, 63215, 63216, 63217, 63218, 63219, 63220, 63221, 63223, 63224, 63226, 63227, 63228, 63229, 63230, 63231, 63232, 63233, 63235, 63244, 63245, 63246, 63247, 63248, 63249, 63251, 63252, 63253, 63254, 63255, 63256, 63257, 63259, 63260, 63261, 63263, 63265, 63266, 63267.

Origin: Veracruz, Mexico. Collection: University of Michigan (UMMZ):
Captured Jan. 1946: 89901, 89907, 89908, 89909, 89910, 89911, 89912, 89913, 89914, 89915, 89916, 89917, 89918, 89919, 89920, 89921, 89922, 89923.

Oryzomys palustris:

Origin: Cameron Parish, Louisiana, USA. Collection: Louisiana State University (LSUMZ):
Captured Feb.-Mar. 1986: 28913, 28921, 28922, 28923, 28924, 28925, 28926, 28930, 28931, 28932, 28934, 28939, 28940, 28946, 28947, 28948, 28950, 28953, 28954, 28955, 28956, 28957, 28964, 28965, 28966, 28967, 28968, 28972, 28973, 28974, 28975, 28976, 28981, 28982, 28983, 28984, 28985, 28987, 28988, 28989, 28990, 28991, 28993, 28994, 28995, 28996, 28997, 29001, 29002, 29003, 29004, 29005, 29006, 29008, 29014, 29016,

29017, 29018, 29019, 29020, 29021, 29035, 29036, 29037, 29357, 29358, 29359, 29361, 29363, 29364.

Oryzomys xantheolus:

Origin: Ancash, Peru. Collection: Field Museum (FMNH):
Captured Mar. 1954: 81381, 81382.

Origin: Lambayeque, Peru. Collection: Field Museum (FMNH):
Captured Mar.-Apr. 1954: 81383, 81384, 81385, 81386, 81387, 81388.

Origin: Piura, Peru. Collection: Field Museum (FMNH):
Captured Apr.-Jun. 1954: 81389, 81390, 81391, 81392, 81393, 81394, 81395, 81397, 81398, 81399, 81400, 81401, 81402, 81403, 81404, 81405, 81406, 81407, 81431.

Origin: Tumbes, Peru. Collection: Field Museum (FMNH):
Captured Jul. 1954: 81408, 81409, 81410, 81411, 81412, 81413, 81414, 81415, 81416, 81417, 81418, 81419, 81420, 81421, 81422, 81423, 81424, 81425, 81426, 81427, 81428, 81429, 81430.

Sigmodontomys alfari:

Origin: Cana, Panama. Collection: Smithsonian Institution (USNM):
Captured Mar. 1912: 178622, 178623, 178624, 178625, 178626, 178628, 178629, 178630, 178631, 178632, 178633, 178634, 178635, 178636, 178637, 178639, 178640, 178641, 178977.

Origin: Cerro Azul, Panama. Collection: Smithsonian Institution (USNM):
Captured Mar. 1955: 302492; **Captured Jun. 1957**: 305717; **Captured Jan.-Oct. 1958**: 306963, 306964, 306965, 306966, 306967, 306969, 310597; **Captured Feb. 1960**: 314582.

Origin: Darien, Panama. Collection: Smithsonian Institution (USNM):
Captured Feb.-Mar. 1959: 310585, 310586, 310587, 310588, 310589, 310590, 310591, 310593, 310595, 310596.

BIBLIOGRAPHY

Abzhanov, A., M. Protas, B. R. Grant, P. R. Grant, and C. J. Tabin. 2004. *Bmp4* and morphological variation of beaks in Darwin's finches. Science 305:1462-1465.
Acampora, D., G. R. Merlo, L. Paleari, B. Zerega, M. P. Postiglione, S. Mantero, E. Bober, O. Barbieri, A. Simeone, and G. Levi. 1999. Craniofacial, vestibular and bone defects in mice lacking the Distal-less-related gene *Dlx5*. Development 126:3795-3809.
Alberch, P. 1980. Ontogenesis and morphological diversification. American Zoologist 20:653-668.
Albertson, R. C., J. T. Streelman, T. D. Kocher, and P. C. Yelick. 2005. Integration and evolution of the cichlid mandible: The molecular basis of alternate feeding strategies. Proceedings of the National Academy of Sciences of the United States of America 102:16287-16292.
Antonopoulou, I., L. A. Mavrogiannis, A. O. M. Wilkie, and G. M. Morriss-Kay. 2004. *Alx4* and *Msx2* play phenotypically similar and additive roles in skull vault differentiation. Journal of Anatomy 204:487-499.
Armbruster, W. S., V. S. Di Stilio, J. D. Tuxill, T. C. Flores, and J. L. V. Runk. 1999. Covariance and decoupling of floral and vegetative traits in nine neotropical plants: A re-evaluation of Berg's correlation-pleiades concept. American Journal of Botany 86:39-55.
Armbruster, W. S., and K. E. Schwaegerle. 1996. Causes of covariation of phenotypic traits among populations. Journal of Evolutionary Biology 9:261-276.
Arnold, S. J. 1992. Constraints on phenotypic evolution. American Naturalist 140:S85-S107.
Arnold, S. J., M. E. Pfrender, and A. G. Jones. 2001. The adaptive landscape as a conceptual bridge between micro- and macroevolution. Genetica 112:9-32.
Atchley, W. R., D. E. Cowley, C. Vogl, and T. McLellan. 1992. Evolutionary divergence, shape change, and genetic correlation structure in the rodent mandible. Systematic Biology 41:196-221.
Atchley, W. R., and B. K. Hall. 1991. A model for development and evolution of complex morphological structures. Biological Reviews of the Cambridge Philosophical Society 66:101-157.
Avis, V. 1961. Significance of angle of mandible: an experimental and comparative study. American Journal of Physical Anthropology 19:55-61.
Bachiller, D., J. Klingensmith, C. Kemp, J. A. Belo, R. M. Anderson, S. R. May, J. A. McMahon, A. P. McMahon, R. M. Harland, J. Rossant, and E. M. De Robertis. 2000. The organizer factors Chordin and Noggin are required for mouse forebrain development. Nature 403:658-661.
Badyaev, A. V., and G. E. Hill. 2000. The evolution of sexual dimorphism in the house finch. I. Population divergence in morphological covariance structure. Evolution 54:1784-1794.
Badyaev, A. V., R. L. Young, K. P. Oh, and C. Addison. 2008. Evolution on a local scale: Developmental, functional, and genetic bases of divergence in bill form and associated changes in song structure between adjacent habitats. Evolution 62:1951-1964.
Baer, M. J. 1954. Patterns of growth of the skull as revealed by vital staining. Human Biology 26:80-126.

Baer, M. J., Bosma, J. F., and Ackerman, J. L. 1983. The Postnatal Development of the Rat Skull. Univ. of Michigan Press, Ann Arbor, Mich.
Baker, C. V. H., and M. Bronner-Fraser. 1997. The origins of the neural crest. Part I: Embryonic induction. Mechanisms of Development 69:3-11.
Barrow, J. R., and M. R. Capecchi. 1999. Compensatory defects associated with mutations in *Hoxa1* restore normal palatogenesis to *Hoxa2* mutants. Development 126:5011-5026.
Beldade, P., K. Koops, and P. M. Brakefield. 2002. Modularity, individuality, and evo-devo in butterfly wings. Proceedings of the National Academy of Sciences of the United States of America 99:14262-14267.
Berg, R. L. 1960. The ecological significance of correlation pleiades. Evolution 14:171-180.
Berk, M., S. Y. Desai, H. C. Heyman, and C. Colmenares. 1997. Mice lacking the *ski* proto-oncogene have defects in neurulation, craniofacial patterning, and skeletal muscle development. Genes & Development 11:2029-2039.
Björk, A. 1969. Prediction of mandibular growth rotation. American Journal of Orthodontics 55:585-599.
Björk, A., and V. Skieller. 1972. Facial development and tooth eruption - implant study at age of puberty. American Journal of Orthodontics 62:339-383.
Blows, M., and B. Walsh. 2009. Spherical Cows Grazing in Flatland: Constraints to Selection and Adaptation. Pp. 83-101 *in* J. van der Werf, H.-U. Graser, and R. Frankham, eds. Adaptation and fitness in animal populations: Evolutionary and breeding perspectives on genetic resource management. Springer, Dordrecht, The Netherlands.
Bolker, J. A. 2000. Modularity in development and why it matters to evo-devo. American Zoologist 40:770-776.
Bookstein, F. L. 1986. The elements of latent variable models: a cautionary lecture. Pp. 203-229 *in* M. E. Lamb, A. L. Brown, and B. Rogoff, eds. Advances in developmental psychology, vol. 4. Lawrence Erlbaum, New Jersey.
Bookstein, F. L. 1991. Morphometric tools for landmark data. Cambridge Univ. Press, New York.
Bookstein, F. L. 1997. Landmark methods for forms without landmarks: morphometrics of group differences in outline shape. Medical Image Analysis 1:225-243.
Bookstein, F. L., P. Gunz, P. Mitteroecker, H. Prossinger, K. Schaefer, and H. Seidler. 2003. Cranial integration in Homo: singular warps analysis of the midsagittal plane in ontogeny and evolution. Journal of Human Evolution 44:167-187.
Bosma, J. F. 1963. Maturation of function of oral and pharyngeal region. American Journal of Orthodontics and Dentofacial Orthopedics 49:94-104.
Boughner, J. C., and B. Hallgrímsson. 2008. Biological spacetime and the temporal integration of functional modules: A case study of dento-gnathic developmental timing. Developmental Dynamics 237:1-17.
Brennan, M., and O. Antonyshyn. 1996. The effects of temporalis muscle manipulation on skull growth: An experimental study. Plastic and Reconstructive Surgery 97:13-24.
Bruner, E., and M. Ripani. 2008. A quantitative and descriptive approach to morphological variation of the endocranial base in modern humans. American

Journal of Physical Anthropology 137:30-40.
Bürger, R. 1986. Constraints for the evolution of functionally coupled characters: a nonlinear analysis of a phenotypic model. Evolution 40:182-193.
Carleton, M. D. 1973. A survey of gross stomach morphology in new-world cricetinae rodentia muroidea with comments on functional interpretations. Miscellaneous Publications of the Museum of Zoology of the Univ. of Michigan 146:1-43.
Caumul, R., and P. D. Polly. 2005. Phylogenetic and environmental components of morphological variation: Skull, mandible, and molar shape in marmots (Marmota, Rodentia). Evolution 59:2460-2472.
Carroll, S. B., Grenier, J. K., and Weatherbee, S. D. 2004. From DNA to diversity: Molecular genetics and the evolution of animal design. Blackwell, Malden, Massachussetts.
Chai, Y., X. B. Jiang, Y. Ito, P. Bringas, J. Han, D. H. Rowitch, P. Soriano, A. P. McMahon, and H. M. Sucov. 2000. Fate of the mammalian cranial neural crest during tooth and mandibular morphogenesis. Development 127:1671-1679.
Chernoff B., and P. M. Magwene, 1999. Morphological integration: Forty years later (Afterword). Pp. 319-353 *in*: E. C. Olson and R. L. Miller. Morphological Integration. Univ. Chicago Press, Chicago, Illinois.
Cheverud, J. M. 1982. Phenotypic, genetic, and environmental morphological integration in the cranium. Evolution 36:499-516.
Cheverud, J. M. 1989. A comparative analysis of morphological variation patterns in the papionins. Evolution 43:1737-1747.
Cheverud, J. M. 1995. Morphological integration in the saddle-back tamarin (*Saguinus fuscicollis*) cranium. American Naturalist 145:63-89.
Cheverud, J. M. 1996. Developmental integration and the evolution of pleiotropy. American Zoologist 36:44-50.
Cheverud, J. M. 2004. Modular pleiotropic effects of quantitative trait loci on morphological traits. Pp. 132-153 *in* G. Schlosser and G. P. Wagner, eds. Modularity in development and evolution. Univ. Chicago Press, Chicago, Illinois.
Cheverud, J. M., S. E. Hartman, J. T. Richtsmeier, and W. R. Atchley. 1991. A quantitative genetic analysis of localized morphology in mandibles of inbred mice using finite-element scaling analysis. Journal of Craniofacial Genetics and Developmental Biology 11:122-137.
Cheverud, J. M., E. J. Routman, and D. J. Irschick. 1997. Pleiotropic effects of individual gene loci on mandibular morphology. Evolution 51:2006-2016.
Couly, G. F., P. M. Coltey, and N. M. Ledouarin. 1993. The triple origin of skull in higher vertebrates: A study in quail-chick chimeras. Development 117:409-429.
Cowley, D. E., and W. R. Atchley. 1990. Development and quantitative genetics of correlation structure among body parts of *Drosophila melanogaster*. American Naturalist 135:242-268.
Cowley, D. E., and W. R. Atchley. 1992. Quantitative genetic models for development, epigenetic selection, and phenotypic evolution. Evolution 46:495-518.
de Beer, G. 1985. The development of the vertebrate skull. Univ. Chicago Press, Chicago, Illinois.
De Celis, J. F. 2004. The Notch signaling module. Pp. 81-100 *in* G. Schlosser and G. P. Wagner, eds. Modularity in development and evolution. Univ. Chicago Press,

Chicago, Illinois.
de Visser, J., J. Hermisson, G. P. Wagner, L. A. Meyers, H. C. Bagheri, J. L. Blanchard, L. Chao, J. M. Cheverud, S. F. Elena, W. Fontana, G. Gibson, T. F. Hansen, D. Krakauer, R. C. Lewontin, C. Ofria, S. H. Rice, G. von Dassow, A. Wagner, and M. C. Whitlock. 2003. Evolution and detection of genetic robustness. Evolution 57:1959-1972.
Debat, V., P. Alibert, P. David, E. Paradis, and J. C. Auffray. 2000. Independence between developmental stability and canalization in the skull of the house mouse. Proceedings of the Royal Society of London Series B: Biological Sciences 267:423-430.
Depew, M. J., J. K. Liu, J. E. Long, R. Presley, J. J. Meneses, R. A. Pedersen, and J. L. R. Rubenstein. 1999. *Dlx5* regulates regional development of the branchial arches and sensory capsules. Development 126:3831-3846.
Depew, M. J., A. S. Tucker, P. T. Sharpe. 2002a. Craniofacial development. Pp. 421-498 *in* J. Rossant and P. P. L. Tam, eds. Mouse development: Patterning, morphogenesis, and organogenesis. Academic Press, San Diego, California.
Depew, M. J., T. Lufkin, and J. L. R. Rubenstein. 2002b. Specification of jaw subdivisions by *Dlx* genes. Science 298:381-385.
Dietz, E. J. 1983. Permutation tests for association between two distance matrices. Systematic Zoology 32:21-26.
Dixon, A. D. 1997a. Prenatal development of the facial skeleton. Pp. 59-97 *in* A. D. Dixon, D. A. N. Hoyte, and O. Rönning, eds. Fundamentals of craniofacial growth. CRC Press, Boca Raton, Florida.
Dixon, A. D. 1997b. Muscles, soft tissues, and craniofacial growth. Pp. 443-462 *in* A. D. Dixon, D. A. N. Hoyte, and O. Rönning, eds. Fundamentals of craniofacial growth. CRC Press, Boca Raton, Florida.
Dixon, A. D., D. A. N. Hoyte, and O. Rönning. 1997. Fundamentals of craniofacial growth. CRC Press, Boca Raton, Florida.
Dryden, I. L., and K. V. Mardia. 1998. Statistical shape analysis. Wiley, New York, New York.
Duarte, L. C., L. R. Monteiro, F. J. von Zuben, and S. F. dos Reis. 2000. Variation in mandible shape in *Thrichomys apereoides* (Mammalia : Rodentia): Geometric analysis of a complex morphological structure. Systematic Biology 49:563-578.
Dworkin, I. 2005. A study of canalization and developmental stability in the sternopleural bristle system of *Drosophila melanogaster*. Evolution 59:1500-1509.
Ehrich, T. H., T. T. Vaughn, S. Koreishi, R. B. Linsey, L. S. Pletscher, and J. M. Cheverud. 2003. Pleiotropic effects on mandibular morphology I. Developmental morphological integration and differential dominance. Journal of Experimental Zoology Part B: Molecular and Developmental Evolution 296:58-79.
Fornell, C., and F. L. Bookstein. 1982. Two structural equation models: LISREL and PLS applied to consumer exit-voice theory. Journal of Marketing Research 19:440-452.
Frankino, W. A., B. J. Zwaan, D. L. Stern, and P. M. Brakefield. 2007. Internal and external constraints in the evolution of morphological allometries in a butterfly. Evolution 61:2958-2970.
Gerhart, J., and M. Kirschner. 1997. Cells, embryos, and evolution: Toward a cellular and

developmental understanding of phenotypic variation and evolutionary adaptability. Blackwell, Malden, Massachussetts.
Guabloche, A., M. Arana, and O. E. Ramirez. 2002. Diet and gross gastric morphology of *Oryzomys xantheolus* (Sigmodontinae, Rodentia) in a Peruvian loma. Mammalia 66:405-411.
Hall, B. K. 2003. Unlocking the black box between genotype and phenotype: Cell condensations as morphogenetic (modular) units. Biology & Philosophy 18:219-247.
Hall, B. K., and T. Miyake. 2000. All for one and one for all: condensations and the initiation of skeletal development. Bioessays 22:138-147.
Hallgrímsson, B., J. J. Y. Brown, A. F. Ford-Hutchinson, H. D. Sheets, M. L. Zelditch, and F. R. Jirik. 2006. The brachymorph mouse and the developmental-genetic basis for canalization and morphological integration. Evolution and Development 8:61-73.
Hallgrímsson, B., and B. K. Hall. 2005. Variation and variability: Central concepts in biology. Pp. 1-7 *in* B. Hallgrímsson and B. K. Hall, eds. Variation: A central concept in biology. Academic Press, Burlington, Massachusetts.
Hallgrímsson, B., D. E. Lieberman, N. M. Young, T. Parsons, and S. Wat. 2007. Evolution of covariance in the mammalian skull. Pp. 284:164-190 *in* Novartis Foundation, eds. Tinkering: The microevolution of development. Wiley, Chichester, UK.
Hallgrímsson, B., K. Willmore, and B. K. Hall. 2002. Canalization, developmental stability, and morphological integration in primate limbs. Yearbook of Physical Anthropology 45:131-158.
Hansen, T. F. 2003. Is modularity necessary for evolvability? Remarks on the relationship between pleiotropy and evolvability. Biosystems 69:83-94.
Hansen, T. F. 2006. The evolution of genetic architecture. Annual Review of Ecology Evolution and Systematics 37:123-157.
Hansen, T. F., W. S. Armbruster, M. L. Carlson, and C. Pélabon. 2003. Evolvability and genetic constraint in *Dalechampia* blossoms: Genetic correlations and conditional evolvability. Journal of Experimental Zoology Part B: Molecular And Developmental Evolution 296:23-39.
Hansen, T. F., and D. Houle. 2008. Measuring and comparing evolvability and constraint in multivariate characters. Journal of Evolutionary Biology 21:1201-1219.
Henrique, D., J. Adam, A. Myat, A. Chitnis, J. Lewis, and D. Ishhorowicz. 1995. Expression of a *Delta* homolog in prospective neurons in the chick. Nature 375:787-790.
Herring, S. W. 1993. Epigenetic and functional influences on skull growth. Pp. 153-206 *in* J. Hanken and B. K. Hall, eds. The Skull, vol. 1: Development. Univ. Chicago Press, Chicago, Illinois.
Herring, S. W., and S. Y. Teng. 2000. Strain in the braincase and its sutures during function. American Journal of Physical Anthropology 112:575-593.
Hershkovitz, P. 1944. A systematic review of the Neotropical water rats of the genus *Nectomys* (Cricetinae). Miscellaneous Publications of the Museum of Zoology of the Univ. Michigan 58:1-107.
Hinton, R. J. 1990. Myotomy of the lateral pterygoid muscle and condylar cartilage

growth. European Journal of Orthodontics 12:370-379.
Hohl, T. H. 1983. Masticatory muscle transposition in primates: Effects on craniofacial growth. Journal of Maxillofacial Surgery 11:149-156.
Houle, D. 1991. Genetic covariance of fitness correlates - what genetic correlations are made of and why it matters. Evolution 45:630-648.
Hoyte, D. A. N. 1971. Mechanisms of growth in cranial vault and base. Journal of Dental Research 50:1447-1461.
Hoyte, D. A. N. 1997a. Growth of the orbit. Pp. 225-255 *in* A. D. Dixon, D. A. N. Hoyte, and O. Rönning, eds. Fundamentals of craniofacial growth. CRC Press, Boca Raton, Florida.
Hoyte, D. A. N. 1997b. Growth of the cranial base. Pp. 257-333 *in* A. D. Dixon, D. A. N. Hoyte, and O. Rönning, eds. Fundamentals of craniofacial growth. CRC Press, Boca Raton, Florida.
Hoyte, D. A. N., and D. H. Enlow. 1966. Wolff's law and problem of muscle attachment on resorptive surfaces of bone. American Journal of Physical Anthropology 24:205-213.
Huggare, J., and O. Rönning. 1997. Growth of the cranial vault. Pp. 363-387 *in* A. D. Dixon, D. A. N. Hoyte, and O. Rönning, eds. Fundamentals of craniofacial growth. CRC Press, Boca Raton, Florida.
Hunt, G., M. A. Bell, and M. P. Travis. 2008. Evolution toward a new adaptive optimum: Phenotypic evolution in a fossil stickleback lineage. Evolution 62:700-710.
Ikeya, M., S. M. K. Lee, J. E. Johnson, A. P. McMahon, and S. Takada. 1997. *Wnt* signalling required for expansion of neural crest and CNS progenitors. Nature 389:966-970.
Jabs, E. W., U. Muller, X. Li, L. Ma, W. Luo, I. S. Haworth, I. Klisak, R. Sparkes, M. L. Warman, J. B. Mulliken, M. L. Snead, and R. Maxson. 1993. A mutation in the homeodomain of the human *MSX2* gene in a family affected with autosomal dominant craniosynostosis. Cell 75:443-450.
Jeong, J. H., J. H. Mao, T. Tenzen, A. H. Kottmann, and A. P. McMahon. 2004. Hedgehog signaling in the neural crest cells regulates the patterning and growth of facial primordia. Genes & Development 18:937-951.
Jepsen, K., B. Hu, S. Tommasini, H. W. Courtland, C. Price, M. Cordova, and J. Nadeau. 2009. Phenotypic integration of skeletal traits during growth buffers genetic variants affecting the slenderness of femora in inbred mouse strains. Mammalian Genome 20:21-33.
Jernvall, J. 2000. Linking development with generation of novelty in mammalian teeth. Proceedings of the National Academy of Sciences of the United States of America 97:2641-2645.
Jiang, X. B., S. Iseki, R. E. Maxson, H. M. Sucov, and G. M. Morriss-Kay. 2002. Tissue origins and interactions in the mammalian skull vault. Developmental Biology 241:106-116.
Johnson, D. R. 1967. *Extra-toes*: a new mutant gene causing multiple abnormalities in mouse. Journal of Embryology and Experimental Morphology 17:543-581.
Jones, A. G., S. J. Arnold, and R. Borger. 2003. Stability of the G-matrix in a population experiencing pleiotropic mutation, stabilizing selection, and genetic drift. Evolution 57:1747-1760.

Jöreskog, K. G., and H. Wold. 1982. The ML and PLS techniques for modeling with latent variables: historical and comparative aspects. Pp. 263-270 *in* H. Wold and K. Jöreskog, eds. Systems under indirect observation: Causality, structure, prediction, vol. I. North-Holland, Amsterdam, The Netherlands.

Kantomaa, T., and B. K. Hall. 1988. Mechanism of adaptation in the mandibular condyle of the mouse: An organ-culture study. Acta Anatomica 132:114-119.

Kaufman, M. H., and J. Bard. 1999. The anatomical basis of mouse development. Academic Press, San Diego, California.

Kaufman, M. H., H.-H. Chang, and J. P. Shaw. 1995. Craniofacial abnormalities in homozygous *Small eye* (*Sey*/*Sey*) embryos and newborn mice. Journal of Anatomy 186:607-617.

Kenney-Hunt, J. P., B. Wang, E. A. Norgard, G. Fawcett, D. Falk, L. S. Pletscher, J. P. Jarvis, C. Roseman, J. Wolf, and J. M. Cheverud. 2008. Pleiotropic patterns of quantitative trait loci for 70 murine skeletal traits. Genetics 178:2275-2288.

Kirschner, M., and J. Gerhart. 1998. Evolvability. Proceedings of the National Academy of Sciences of the United States of America 95:8420-8427.

Klingenberg, C. P. 1996. Multivariate allometry. Pp. 23-49 *in* L. F. Marcus, M. Corti, A. Loy, G. J. P. Naylor, and D. E. Slice, eds. Advances in morphometrics. Plenum Press, New York, New York.

Klingenberg, C. P. 2005. Developmental constraints, modules, and evolvability. Pp. 219-247 *in* B. Hallgrímsson and B. K. Hall, eds. Variation: A central concept in biology. Academic Press, Burlington, Massachusetts.

Klingenberg, C. P. 2008. Morphological integration and developmental modularity. Annual Review of Ecology Evolution and Systematics 39:115-132.

Klingenberg, C. P., L. J. Leamy, and J. M. Cheverud. 2004. Integration and modularity of quantitative trait locus effects on geometric shape in the mouse mandible. Genetics 166:1909-1921.

Klingenberg, C. P., and G. S. McIntyre. 1998. Geometric morphometrics of developmental instability: Analyzing patterns of fluctuating asymmetry with Procrustes methods. Evolution 52:1363-1375.

Klingenberg, C. P., K. Mebus, and J. C. Auffray. 2003. Developmental integration in a complex morphological structure: how distinct are the modules in the mouse mandible? Evolution and Development 5:522-531.

Köntges, G., and A. Lumsden. 1996. Rhombencephalic neural crest segmentation is preserved throughout craniofacial ontogeny. Development 122:3229-3242.

Krzanowski, W. J. 2000. Principles of multivariate analysis: A user's perspective. Oxford Univ. Press, Oxford, UK.

Kume, T., K. Y. Deng, V. Winfrey, D. B. Gould, M. A. Walter, and B. L. M. Hogan. 1998. The Forkhead/Winged Helix gene *Mf1* is disrupted in the pleiotropic mouse mutation *congenital hydrocephalus*. Cell 93:985-996.

Kurihara, Y., H. Kurihara, H. Suzuki, T. Kodama, K. Maemura, R. Nagai, H. Oda, T. Kuwaki, W. H. Cao, N. Kamada, K. Jishage, Y. Ouchi, S. Azuma, Y. Toyoda, T. Ishikawa, M. Kumada, and Y. Yazaki. 1994. Elevated blood pressure and craniofacial abnormalities in mice deficient in endothelin-1. Nature 368:703-710.

Lanctôt, C., A. Moreau, M. Chamberland, M. L. Tremblay, and J. Drouin. 1999. Hindlimb patterning and mandible development require the *Ptx1* gene.

Development 126:1805-1810.
Lande, R. 1979. Quantitative genetic analysis of multivariate evolution, applied to brain-body size allometry. Evolution 33:402-416.
Lande, R., and S. J. Arnold. 1983. The measurement of selection on correlated characters. Evolution 37:1210-1226.
Leamy, L. J., E. J. Routman, and J. M. Cheverud. 1997. A search for quantitative trait loci affecting asymmetry of mandibular characters in mice. Evolution 51:957-969.
Leamy, L. J., E. J. Routman, and J. M. Cheverud. 1999. Quantitative trait loci for early- and late-developing skull characters in mice: A test of the genetic independence model of morphological integration. American Naturalist 153:201-214.
Lewontin, R. C. 1970. The units of selection. Annual Review of Ecology and Systematics, 1:1-18.
Lieberman, D. E., C. F. Ross, and M. J. Ravosa. 2000. The primate cranial base: Ontogeny, function, and integration. Yearbook of Physical Anthropology 43:117-169.
Lohnes, D., M. Mark, C. Mendelsohn, P. Dolle, A. Dierich, P. Gorry, A. Gansmuller, and P. Chambon. 1994. Function of the retinoic acid receptors (RARs) during development: (I) Craniofacial and skeletal abnormalities in Rar double mutants. Development 120:2723-2748.
Lu, M. F., C. Pressman, R. Dyer, R. L. Johnson, and J. F. Martin. 1999. Function of Rieger syndrome gene in left-right asymmetry and craniofacial development. Nature 401:276-278.
Luo, G., C. Hofmann, A. Bronckers, M. Sohocki, A. Bradley, and G. Karsenty. 1995. BMP-7 is an inducer of nephrogenesis, and is also required for eye development and skeletal patterning. Genes & Development 9:2808-2820.
Lynch, M., and B. Walsh. 1998. Genetics and Analysis of Quantitative Traits. Sinauer, Sunderland, Massachusetts.
Mackay, T. F. C. 2001. The genetic architecture of quantitative traits. Annual Review of Genetics 35:303-339.
Magwene, P. M. 2001. New tools for studying integration and modularity. Evolution 55:1734-1745.
Manly, B. F. J. 2006. Randomization, bootstrap and Monte Carlo methods in biology, 3rd ed. Chapman and Hall/CRC Press, Boca Raton, Florida.
Mansour, S. L., J. M. Goddard, and M. R. Capecchi. 1993. Mice homozygous for a targeted disruption of the protooncogene *int-2* have developmental defects in the tail and inner-ear. Development 117:13-28.
Mansouri, A., A. Stoykova, M. Torres, and P. Gruss. 1996. Dysgenesis of cephalic neural crest derivatives in *Pax7*$^{-/-}$ mutant mice. Development 122:831-838.
Markow, T. A. 1993. Developmental instability: Its origins and evolutionary implications. Kluwer, Amsterdam, The Netherlands.
Márquez, E. J. 2008. A statistical framework for testing modularity in multidimensional data. Evolution 62:2688-2708.
Marroig, G., and J. M. Cheverud. 2004. Cranial evolution in sakis (*Pithecia*, platyrrhini) I: Interspecific differentiation and allometric patterns. American Journal of Physical Anthropology 125:266-278.
Martin, J. F., A. Bradley, and E. N. Olson. 1995. The *paired*-like homeo box gene *MHox*

is required for early events of skeletogenesis in multiple lineages. Genes & Development 9:1237-1249.
Matsuo, I., S. Kuratani, C. Kimura, N. Takeda, and S. Aizawa. 1995. Mouse *Otx2* functions in the formation and patterning of rostral head. Genes & Development 9:2646-2658.
Matzuk, M. M., T. R. Kumar, A. Vassalli, J. R. Bickenbach, D. R. Roop, R. Jaenisch, and A. Bradley. 1995. Functional analysis of activins during mammalian development. Nature 374:354-356.
Maynard Smith, J., R. Burian, S. Kauffman, P. Alberch, J. Campbell, B. Goodwin, R. Lande, D. Raup, and L. Wolpert. 1985. Developmental constraints and evolution. Quarterly Review of Biology 60:265-287.
Mezey, J. G., J. M. Cheverud, and G. P. Wagner. 2000. Is the genotype-phenotype map modular? : A statistical approach using mouse quantitative trait loci data. Genetics 156:305-311.
Mezey, J. G., and D. Houle. 2003. Comparing G matrices: Are common principal components informative? Genetics 165:411-425.
Miettinen, P. J., J. R. Chin, L. Shum, H. C. Slavkin, C. F. Shuler, R. Derynck, and Z. Werb. 1999. Epidermal growth factor receptor function is necessary for normal craniofacial development and palate closure. Nature Genetics 22:69-73.
Mitteroecker, P., and F. Bookstein. 2007. The conceptual and statistical relationship between modularity and morphological integration. Systematic Biology 56:818-836.
Mitteroecker, P., and F. Bookstein. 2008. The evolutionary role of modularity and integration in the hominoid cranium. Evolution 62:943-958.
Mitteroecker, P., P. Gunz, M. Bernhard, K. Schaefer, and F. L. Bookstein. 2004. Comparison of cranial ontogenetic trajectories among great apes and humans. Journal of Human Evolution 46:679-697.
Mo, R., A. M. Freer, D. L. Zinyk, M. A. Crackower, J. Michaud, H. H. Q. Heng, K. W. Chik, X. M. Shi, L. C. Tsui, S. H. Cheng, A. L. Joyner, and C. C. Hui. 1997. Specific and redundant functions of *Gli2* and *Gli3* zinc finger genes in skeletal patterning and development. Development 124:113-123.
Monteiro, L. R., V. Bonato, and S. F. dos Reis. 2005. Evolutionary integration and morphological diversification in complex morphological structures: mandible shape divergence in spiny rats (Rodentia, Echimyidae). Evolution and Development 7:429-439.
Monteiro, L. R., and S. F. dos Reis. 2005. Morphological evolution in the mandible of spiny rats, genus *Trinomys* (Rodentia : Echimyidae). Journal of Zoological Systematics and Evolutionary Research 43:332-338.
Montero, A., Y. Okada, M. Tomita, M. Ito, H. Tsurukami, T. Nakamura, T. Doetschman, J. D. Coffin, and M. M. Hurley. 2000. Disruption of the *fibroblast growth factor-2* gene results in decreased bone mass and bone formation. Journal of Clinical Investigation 105:1085-1093.
Moore, W. J. 1981. The Mammalian Skull. Cambridge Univ. Press, Cambridge, Massachusetts.
Moss, M. L. 1968. A theoretical analysis of the functional matrix. Acta Biotheoretica 18:195-202.

Moss, M. L., M. A. Meehan, and L. Salentijn. 1972. Transformative and translative growth processes in neurocranial development of rat. Acta Anatomica 81:161-182.
Moss, M. L., and R. M. Rankow. 1968. Role of functional matrix in mandibular growth. Angle Orthodontist 38:95-103.
Moss, M. L., and L. Salentijn. 1969. Primary role of functional matrices in facial growth. American Journal of Orthodontics 55:566-577.
Moss, M. L., H. Vilmann, L. Mosssalentijn, K. Sen, H. M. Pucciarelli, and R. Skalak. 1987. Studies on orthocephalization: Growth behavior of the rat skull in the period 13-49 days as described by the finite element method. American Journal of Physical Anthropology 72:323-342.
Moss, M. L., and R. W. Young. 1960. Functional approach to craniology. American Journal of Physical Anthropology 18:281-292.
Müller, G. B., and G. P. Wagner. 1991. Novelty in evolution: Restructuring the concept. Annual Review of Ecology and Systematics 22:229-256.
Nemeschkal, H. L. 1999. Morphometric correlation patterns of adult birds (Fringillidae: Passeriformes and Columbiformes) mirror the expression of developmental control genes. Evolution 53:899-918.
Nijhout, H. F., and G. Davidowitz. 2003. Developmental perspectives on phenotypic variation, canalization, and fluctuating asymmetry. Pp. 3-13 *in* M. Polak, ed. Developmental instability: Causes and consequences. Oxford Univ. Press, New York, New York.
Nijhout, H. F., and D. J. Emlen. 1998. Competition among body parts in the development and evolution of insect morphology. Proceedings of the National Academy of Sciences of the United States of America 95:3685-3689.
Nilsson, A., J. Isgaard, A. Lindahl, A. Dahlstrom, A. Skottner, and O. G. P. Isaksson. 1986. Regulation by growth hormone of number of chondrocytes containing IGF-I in rat growth plate. Science 233:571-574.
Noden, D. M. 1978. Control of avian cephalic neural crest cytodifferentiation. I. Skeletal and connective tissues. Developmental Biology 67:296-312.
Olson, E. C., and R. L. Miller. 1958. Morphological integration. Univ. Chicago Press, Chicago, Illinois.
Pavlicev, M., J. P. Kenney-Hunt, E. A. Norgard, C. C. Roseman, J. B. Wolf, and J. M. Cheverud. 2008. Genetic variation in pleiotropy: Differential epistasis as a source of variation in the allometric relationship between long bone lengths and body weight. Evolution 62:199-213.
Peres-Neto, P. R., and D. A. Jackson. 2001. How well do multivariate data sets match? The advantages of a Procrustean superimposition approach over the Mantel test. Oecologia 129:169-178.
Perlyn, C. A., V. B. DeLeon, C. Babbs, D. Govier, L. Burell, T. Darvann, S. Kreiborg, and G. Morriss-Kay. 2006. The craniofacial phenotype of the Crouzon mouse: Analysis of a model for syndromic craniosynostosis using three-dimensional MicroCT. Cleft Palate-Craniofacial Journal 43:740-747.
Peters, H., A. Neubuser, K. Kratochwil, and R. Balling. 1998. *Pax9*-deficient mice lack pharyngeal pouch derivatives and teeth and exhibit craniofacial and limb abnormalities. Genes & Development 12:2735-2747.

Phillips, P. C., and S. J. Arnold. 1999. Hierarchical comparison of genetic variance-covariance matrices. I. Using the Flury hierarchy. Evolution 53:1506-1515.
Pigliucci, M. 2001. Phenotypic plasticity: Beyond nature and nurture. John Hopkins Univ. Press, Baltimore, Maryland.
Pigliucci, M., and K. A. Preston. 2004. Phenotypic integration: Studying the ecology and evolution of complex phenotypes. Oxford Univ. Press, New York, New York.
Pratt L. W. 1943. Experimental masseterectomy in the laboratory rat. Journal of Mammalogy 24:204-211.
Proetzel, G., S. A. Pawlowski, M. V. Wiles, M. Y. Yin, G. P. Boivin, P. N. Howles, J. X. Ding, M. W. J. Ferguson, and T. Doetschman. 1995. Transforming growth factor-β3 is required for secondary palate fusion. Nature Genetics 11:409-414.
Qiu, M. S., A. Bulfone, I. Ghattas, J. J. Meneses, L. Christensen, P. T. Sharpe, R. Presley, R. A. Pedersen, and J. L. R. Rubenstein. 1997. Role of the Dlx homeobox genes in proximodistal patterning of the branchial arches: Mutations of Dlx-1, Dlx-2, and Dlx-1 and -2 alter morphogenesis of proximal skeletal and soft tissue structures derived from the first and second arches. Developmental Biology 185:165-184.
Qiu, M. S., A. Bulfone, S. Martinez, J. J. Meneses, K. Shimamura, R. A. Pedersen, and J. L. R. Rubenstein. 1995. Null mutation of *Dlx-2* results in abnormal morphogenesis of proximal first and second branchial arch derivatives and abnormal differentiation in the forebrain. Genes & Development 9:2523-2538.
Raff, R. 1996. The shape of life: Genes, development, and the evolution of animal form. Univ. Chicago Press, Chicago, Illinois.
Réale, D., and D. A. Roff. 2003. Inbreeding, developmental stability, and canalization in the sand cricket *Gryllus firmus*. Evolution 57:597-605.
Riddle, R. D., R. L. Johnson, E. Laufer, and C. Tabin. 1993. *Sonic Hedgehog* mediates the polarizing activity of the ZPA. Cell 75:1401-1416.
Riedl, R. 1977. Systems-analytical approach to macro-evolutionary phenomena. Quarterly Review of Biology 52:351-370.
Rijli, F. M., M. Mark, S. Lakkaraju, A. Dierich, P. Dolle, and P. Chambon. 1993. A homeotic transformation is generated in the rostral branchial region of the head by disruption of *Hoxa-2*, which acts as a selector gene. Cell 75:1333-1349.
Rinker, G. C. 1954. The comparative myology of the mammalian genera *Sigmodon*, *Oryzomys*, *Neotoma*, and *Peromyscus* (Cricetinae), with remarks on their intergeneric relationships. Miscellaneous Publications of the Museum of Zoology of the Univ. Michigan. 83:1-165.
Riska, B. 1986. Some models for development, growth, and morphometric correlation. Evolution 40:1303-1311.
Richtsmeier, J. T., S. R. Lele, and T. M. Cole, III. 2005. Landmark morphometrics and the analysis of variation. Pp. 49-69 *in* B. Hallgrímsson and B. K. Hall, eds. Variation: A central concept in biology. Academic Press, Burlington, Massachusetts.
Rohlf, F. J. 2006. TpsDig2 software, ver. 2.10. State Univ. New York, Stony Brook.
Rohlf, F. J., and M. Corti. 2000. Use of two-block partial least-squares to study covariation in shape. Systematic Biology 49:740-753.
Rohlf, F. J., and D. Slice. 1990. Extensions of the Procrustes method for the optimal

superimposition of landmarks. Systematic Zoology 39:40-59.
Rot-Nikcevic, I., K. J. Downing, B. K. Hall, and B. Kablar. 2007. Development of the mouse mandibles and clavicles in the absence of skeletal myogenesis. Histology and Histopathology 22:51-60.
Roth, V. L. 1996. Cranial integration in the Sciuridae. American Zoologist 36:14-23.
Sanford, L. P., I. Ormsby, A. C. Gittenberger-de Groot, H. Sariola, R. Friedman, G. P. Boivin, E. L. Cardell, and T. Doetschman. 1997. TGFβ2 knockout mice have multiple developmental defects that are nonoverlapping with other TGFβ knockout phenotypes. Development 124:2659-2670.
Sarnat, B. G. 1997. Postnatal growth of the nasomaxillary complex. Pp. 205-224 *in* A. D. Dixon, D. A. N. Hoyte, and O. Rönning, eds. Fundamentals of craniofacial growth. CRC Press, Boca Raton, Florida.
Satokata, I., and R. Maas. 1994. *Msx1* deficient mice exhibit cleft palate and abnormalities of craniofacial and tooth development. Nature Genetics 6:348-356.
Schimmang, T., M. Lemaistre, A. Vortkamp, and U. Ruther. 1992. Expression of the zinc finger gene *Gli3* is affected in the morphogenetic mouse mutant *extra-toes* (*Xt*). Development 116:799-804.
Schluter, D. 1996. Adaptive radiation along genetic lines of least resistance. Evolution 50:1766-1774.
Schumacher, G.-H. 1997. Muscles, blood vessels, and craniofacial growth: some experimental approaches. Pp. 463-486 *in* A. D. Dixon, D. A. N. Hoyte, and O. Rönning, eds. Fundamentals of craniofacial growth. CRC Press, Boca Raton, Florida.
Seegmiller, R. E., and F. C. Fraser. 1977. Mandibular growth retardation as a cause of cleft palate in mice homozygous for chondrodysplasia gene. Journal of Embryology and Experimental Morphology 38:227-238.
Selleri, L., M. J. Depew, Y. Jacobs, S. K. Chanda, K. Y. Tsang, K. S. E. Cheah, J. L. R. Rubenstein, S. O'Gorman, and M. L. Cleary. 2001. Requirement for *Pbx1* in skeletal patterning and programming chondrocyte proliferation and differentiation. Development 128:3543-3557.
Sheets, H. D. 2002a. Semiland6 software. Canisius College, Buffalo, NY.
Sheets, H. D. 2002b. Standard6 software. Canisius College, Buffalo, NY.
Sinervo, B., and E. Svensson. 2002. Correlational selection and the evolution of genomic architecture. Heredity 89:329-338.
Soriano, P. 1997. The PDGFα receptor is required for neural crest cell development and for normal patterning of the somites. Development 124:2691-2700.
Steppan, S. J., P. C. Phillips, and D. Houle. 2002. Comparative quantitative genetics: evolution of the G matrix. Trends in Ecology and Evolution 17:320-327.
Stottmann, R. W., R. M. Anderson, and J. Klingensmith. 2001. The BMP antagonists Chordin and Noggin have essential but redundant roles in mouse mandibular outgrowth. Developmental Biology 240:457-473.
Suzuki, N., P. A. Labosky, Y. Furuta, L. Hargett, R. Dunn, A. B. Fogo, K. Takahara, D. M. P. Peters, D. S. Greenspan, and B. L. M. Hogan. 1996. Failure of ventral body wall closure in mouse embryos lacking a procollagen C-proteinase encoded by *Bmp1*, a mammalian gene related to *Drosophila tolloid*. Development 122:3587-3595.

The Mathworks, Inc. 2006. Matlab R2006a software. Natick, Massachusetts.
Thomas, T., H. Kurihara, H. Yamagishi, Y. Kurihara, Y. Yazaki, E. N. Olson, and D. Srivastava. 1998. A signaling cascade involving endothelin-1, dHAND and Msx1 regulates development of neural-crest-derived branchial arch mesenchyme. Development 125:3005-3014.
Torres, M. A., E. Gómez-Pardo, and P. Gruss. 1996. *Pax2* contributes to inner ear patterning and optic nerve trajectory. Development 122:3381-3391.
Tribioli, C., and T. Lufkin. 1999. The murine *Bapx1* homeobox gene plays a critical role in embryonic development of the axial skeleton and spleen. Development 126:5699-5711.
Trumpp, A., M. J. Depew, J. L. R. Rubenstein, J. M. Bishop, and G. R. Martin. 1999. Cre-mediated gene inactivation demonstrates that FGF8 is required for cell survival and patterning of the first branchial arch. Genes & Development 13:3136-3148.
Turelli, M. 1988. Phenotypic evolution, constant covariances, and the maintenance of additive variance. Evolution 42:1342-1347.
van der Klaauw, C. J. 1945. Size and position of the functional components of the skull. A contribution to the knowledge of the architecture of the skull, based on data in the literature. Archives Néerlandaises de Zoologie 9:1-576.
van Limborgh, J. 1982. Factors controlling skeletal morphogenesis. Progress in Clinical Biological Research 101:1-17.
Van Valen, L. 1965. The study of morphological integration. Evolution 19:347-349.
von Dassow, G., and E. Munro. 1999. Modularity in animal development and evolution: Elements of a conceptual framework for EvoDevo. Journal of Experimental Zoology 285:307-325.
Voss, R. S. 1988. Systematics and ecology of Ichthyomyine rodents (Muroidea): Patterns of morphological evolution in a small adaptive radiation. Bulletin of the American Museum of Natural History 188:259-493.
Waddington, C. H. 1942. Canalization of development and the inheritance of acquired characters. Nature 150:563-565.
Wagner, G. P. 1984. On the eigenvalue distribution of genetic and phenotypic dispersion matrices: Evidence for a nonrandom organization of quantitative character variation. Journal of Mathematical Biology 21:77-95.
Wagner, G. P. 1988. The influence of variation and of developmental constraints on the rate of multivariate phenotypic evolution. Journal of Evolutionary Biology 1:45-66.
Wagner, G. P., and L. Altenberg. 1996. Complex adaptations and the evolution of evolvability. Evolution 50:967-976.
Wagner, G. P., and J. G. Mezey. 2004. The role of genetic architecture constraints in the origin of variational modularity. Pp. 338-358 *in* G. Schlosser and G. P. Wagner, eds. Modularity in development and evolution. Univ. Chicago Press, Chicago, Illinois.
Wagner, G. P., and B. Y. Misof. 1993. How can a character be developmentally constrained despite variation in developmental pathways. Journal of Evolutionary Biology 6:449-455.
Wagner, G. P., M. Pavlicev, and J. M. Cheverud. 2007. The road to modularity. Nature

Reviews Genetics 8:921-931.
Walker, J. A. 2000. Ability of geometric morphometric methods to estimate a known covariance matrix. Systematic Biology 49:686-696.
Walker, J. A. 2007. A general model of functional constraints on phenotypic evolution. American Naturalist 170:681-689.
Wang, Y. C., M. K. Spatz, K. Kannan, H. Hayk, A. Avivi, M. Gorivodsky, M. Pines, A. Yayon, P. Lonai, and D. Givol. 1999. A mouse model for achondroplasia produced by targeting fibroblast growth factor receptor 3. Proceedings of the National Academy of Sciences of the United States of America 96:4455-4460.
Warren, S. M., L. J. Brunet, R. M. Harland, A. N. Economides, and M. T. Longaker. 2003. The BMP antagonist noggin regulates cranial suture fusion. Nature 422:625-629.
Washburn, S. L. 1947. The relation of the temporal muscle to the form of the skull. Anatomical Record 99:239-248.
Weksler, M. 2003. Phylogeny of Neotropical oryzomyine rodents (Muridae : Sigmodontinae) based on the nuclear IRBP exon. Molecular Phylogenetics and Evolution 29:331-349.
Weksler, M. 2006. Phylogenetic relationships of oryzomine rodents (Muroidea : Sigmodontinae): separate and combined analyses of morphological and molecular data. Bulletin of the American Museum of Natural History 296:1-149.
West-Eberhard, M. J. 2003. Developmental plasticity and evolution. Oxford Univ. Press, New York, New York.
Wieslander, L., and L., Tandläkare. 1963. Effect of orthodontic treatment on concurrent development of craniofacial complex. American Journal of Orthodontics and Dentofacial Orthopedics 49:15-27.
Willmore, K. E., L. Leamy, and B. Hallgrimsson. 2006. Effects of developmental and functional interactions on mouse cranial variability through late ontogeny. Evolution and Development 8:550-567.
Winnier, G. E., L. Hargett, and B. L. M. Hogan. 1997. The winged helix transcription factor *MFH1* is required for proliferation and patterning of paraxial mesoderm in the mouse embryo. Genes & Development 11:926-940.
Whittaker, J. 1990. Graphical models in applied multivariate statistics. Wiley, New York, New York.
Wold, H. 1966. Nonlinear estimation by iterative least square procedures. Pp. 411-444 *in* F. N. David, ed. Research papers in statistics. Wiley, New York, New York.
Wolf, J. B., L. J. Leamy, E. J. Routman, and J. M. Cheverud. 2005. Epistatic pleiotropy and the genetic architecture of covariation within early- and late-developing skull trait complexes in mice. Genetics 171:683-694.
Wolf, J. B., D. Pomp, E. J. Eisen, J. M. Cheverud, and L. J. Leamy. 2006. The contribution of epistatic pleiotropy to the genetic architecture of covariation among polygenic traits in mice. Evolution and Development 8:468-476.
Wright, S. 1932. General, group and special size factors. Genetics 17:0603-0619.
Yamada, G., A. Mansouri, M. Torres, E. T. Stuart, M. Blum, M. Schultz, E. M. Derobertis, and P. Gruss. 1995. Targeted mutation of the murine *goosecoid* gene results in craniofacial defects and neonatal death. Development 121:2917-2922.
Yamaguchi, T. P., A. Bradley, A. P. McMahon, and S. Jones. 1999. A *Wnt5a* pathway

underlies outgrowth of multiple structures in the vertebrate embryo. Development 126:1211-1223.
Yoshida, T., P. Vivatbutsiri, G. Morriss-Kay, Y. Saga, and S. Iseki. 2008. Cell lineage in mammalian craniofacial mesenchyme. Mechanisms of Development 125:797-808.
Young, B., N. Minugh-Purvis, T. Shimo, B. St-Jacques, M. Iwamoto, M. Enomoto-Iwamoto, E. Koyama, and M. Pacifici. 2006. Indian and sonic hedgehogs regulate synchondrosis growth plate and cranial base development and function. Developmental Biology 299:272-282.
Young, R. L., and A. V. Badyaev. 2006. Evolutionary persistence of phenotypic integration: Influence of developmental and functional relationships on complex trait evolution. Evolution 60:1291-1299.
Young, R. L., and A. V. Badyaev. 2007. Evolution of ontogeny: linking epigenetic remodeling and genetic adaptation in skeletal structures. Integrative and Comparative Biology 47:234-244.
Zelditch, M. L. 1987. Evaluating models of developmental integration in the laboratory rat using confirmatory factor analysis. Systematic Zoology 36:368-380.
Zelditch, M. L. 2005. Developmental regulation of variability. Pp. 249-276 *in* B. Hallgrímsson and B. K. Hall, eds. Variation: A central concept in biology. Academic Press, Burlington, Massachusetts.
Zelditch, M. L., F. L. Bookstein, and B. L. Lundrigan. 1992. Ontogeny of integrated skull growth in the cotton rat *Sigmodon fulviventer*. Evolution 46:1164-1180.
Zelditch, M. L., and A. C. Carmichael. 1989. Ontogenetic variation in patterns of developmental and functional integration in skulls of *Sigmodon fulviventer*. Evolution 43:814-824.
Zelditch, M. L., J. Mezey, H. D. Sheets, B. L. Lundrigan, and T. Garland. 2006. Developmental regulation of skull morphology II: Ontogenetic dynamics of covariance. Evolution and Development 8:46-60.
Zelditch, M. L., H. D. Sheets, and W. L. Fink. 2003. The ontogenetic dynamics of shape disparity. Paleobiology 29:139-156.
Zelditch, M. L., D. O. Straney, D. L. Swiderski, and A. C. Carmichael. 1990. Variation in developmental constraints in *Sigmodon*. Evolution 44:1738-1747.
Zelditch, M. L., A. R. Wood, R. M. Bonett, and D. L. Swiderski. 2008. Modularity of the rodent mandible: Integrating bones, muscles, and teeth. Evolution and Development 10:756-768.
Zelditch, M. L., A. R. Wood, and D. L. Swiderski. 2009. Building developmental integration into functional systems: Function-induced integration of mandibular shape. Evolutionary Biology 36:71-87.
Zeng, Z. B. 1988. Long-term correlated response, interpopulation covariation, and interspecific allometry. Evolution 42:363-374.
Zhao, Q., R. R. Behringer, and B. de Crombrugghe. 1996. Prenatal folic acid treatment suppresses acrania and meroanencephaly in mice mutant for the *Cart1* homeobox gene. Nature Genetics 13:275-283.